Author:
Rodrigues Ferreira, Joana

Title:
The influence of sulfurization and burial history on melanin chemistry during fossilization

The influence of sulfurization and burial history on melanin chemistry during fossilization

Joana Isabel Rodrigues Ferreira

A dissertation submitted to the University of Bristol in accordance with the requirements for award of the degree of Master of Science by Research in the Faculty of Science

School of Earth Sciences

November 2018

Word count:
21373

ABSTRACT

Melanin is the most common pigment in vertebrates with two main forms, black melanin (eumelanin) and rufous red melanin (pheomelanin). This pigment is known to preserve chemically over geological time scales, over 100s of millions of years, allowing the reconstruction of aspects of integumentary colouration of fossils to be done. However, the chemical changes that eumelanin incurs during fossilization, including occasional secondary incorporation of sulfur, are still not fully understood. This has the potential of introducing a level of uncertainty in colour reconstructions.

In this project, I aim to investigate the influence of geothermal gradients and the depositional environment (with focus on the presence of sulfur species) on the chemical structure of eumelanin. This was done by analysing a comprehensive collection of fossil cephalopod ink, straddling a wide spectrum of ages (20 – 300 million years), locations, and burial history. For comparison, freshly extracted ink was artificially matured under different conditions (temperature and pressure) as well as with different sulfur species (elemental sulfur and a source of sulfide) to compare its chemistry with sulfur bearing pheomelanin. Samples were analysed with ToF-SIMS and FTIR, and comparatively analysed multivariate framework (PCA).

The PCA plots of the ToF-SIMS data verifies that maturation history has the greatest influence on eumelanin alteration. Comparative PCA analysis of FTIR data were used here for the first time on melanin and shows great promise for evaluating chemical alterations during fossilization in concordance with ToF-SIMS. FTIR elucidates the specific alteration of progressive dehydration and loss of carboxyl groups with increasing temperature. Lastly, artificially matured melanin with sulfur species yields thiophenes, but no moieties diagnostic of pheomelanin (thiazines/thiazoles).

ACKNOWLEDGMENTS

For my blue-eyed boys, Avô and Alex.
You are loved. You are missed.

I would like to start by expressing my uttermost gratitude to Dr Jakob Vinther for his infinite patience with me. I have been extremely lucky to have his guidance, encouragement and enthusiasm through the development of this project.

This project would have not been possible without all the members from the most diverse universities and institutions, from sending fossil samples to carrying out experiments. From the University of Bristol, Dr Sally Hobson, Dr Richard Brooker, Dr Ian Bull, and Mr. Fiann Smithwick. From the Newcastle University, Dr Geoff Abbott and team with a special word of thanks to Dr Ian Fletcher and the NEXUS team, for welcoming me twice in their laboratory. I assure you that, all things considered, I hold very fond memories of Newcastle and my time there.

I would like to thank the lovely people in the Oxfam shop in Corsham, for the kindness of accepting me as part of your community and for all the support. To our official boss Malcolm and to the one that's actually in charge, Eileen, a special thank you for never doubting my capabilities in seeing this through, even if I can't even make a "proper cup of tea". To my long-time Viseu friends, specially to Filipa Lagoas and Hugo Silva, for being by my side all these years, for always welcoming me home and for making me laugh the hardest. To my best friend, Nânci Winke who is always ready on the other side of the phone to hear about my crazy day and for whom I am grateful every day for finding her way into my life. Life would be boring without you and I hope you have forgiven me for turning into the Dark Side (a.k.a. The Earth Sciences Department).

I would like to thank my big, crazy, loving family. Being one of the youngest is a lot easier with all of you to follow as an example. My grandparents, my foundation stones, Gracinda e Celestino for making this dream possible, I thank from the bottom of my heart. To my parents, Felismina e António João, *obrigada por sempre me incentivarem a tomar as minhas próprias decisões e por me ensinarem que existem valores mais altos dos que os obtidos numa pauta. Por me ensinarem a erguer a cabeça e continuar a caminhar em frente independentemente dos obstáculos que possam aparecer.*

My dear sister, to thank you for everything you have done for me is impossible, and it demands more pages than this work could possibly hold. You are the best sister in the whole of the nine worlds and you'll always have the better half of my heart with you.

I declare that the work in this dissertation was carried out in accordance with the requirements of the University's *Regulations and Code of Practice for Research Degree Programmes* and that it has not been submitted for any other academic award. Except where indicated by specific reference in the text, the work is the candidate's own work. Work done in collaboration with, or with the assistance of, others, is indicated as such. Any views expressed in the dissertation are those of the author.

SIGNED:  DATE: 30 November 2018

TABLE OF CONTENTS

1. INTRODUCTION 1

1.1. Molecular biochemistry and biomarkers 1

1.2. Kerogen and biomolecular sulfurization 6

1.3. Cephalopod evolution and the emergence of the ink sac 9

1.3.1. Cephalopod evolution 9

1.3.2. Coleoids and the emergence of the ink sac 9

1.3.3. Ammonoids and the debated presence of an ink sac 10

1.3.4. Composition of cephalopod ink 11

1.4. Melanin molecules and their functions 12

1.4.1. Allomelanins 12

1.4.2. Neuromelanin 13

1.4.3. Eumelanin and pheomelanin 14

1.4.4. Melanosomes 16

1.5. Colouration and fossil melanin 18

1.6. Diagenetic incorporation of sulfur with implications for colour reconstructions 21

1.7. Objectives 22

2. TECHNIQUES 24

2.1. Artificial maturation 24

2.2. ToF-SIMS 26

2.3. ATR-FTIR 27

3. METHODS 28

3.1. Fresh samples 28

3.2. Artificial maturation 30

3.3. Fossil samples (location and age) 33

3.4. ToF-SIMS 37

3.5. ATR-FTIR 38

4. RESULTS/DISCUSSION 39

4.1. ToF-SIMS 39

4.1.1. PCA analysis with Colleary et al. (2015) dataset 41

4.1.1.1. Inorganics presence and their influence in PCA interpretation 41
4.1.1.2. Excluded sample (TMP 2013.036.0005) 41
4.1.1.3. Artificially matured samples 42
4.1.1.4. Fossil samples 44
4.1.2. PCA analysis of eumelanin samples 46
4.1.2.1. Artificially matured samples 46
4.1.2.2. Fossil samples and thermal maturity 48
4.1.2.3. PC1 relation with thermal maturity 50
4.2. FTIR 52
4.2.1. Peak identification and relative absorbance 52
4.2.1.1. Matured melanin without sulfur species 52
4.2.1.2. Matured melanin with sulfur species 53
4.2.1.3. Fossil samples 55
4.2.2. PCA analysis of FTIR data 56
4.2.2.1. PC1 relation with thermal maturity 56
4.2.2.2. Correlation between PC1 and thermal maturity 58
4.2.2.3. PC2 and inorganic signal 58
5. CONCLUSION 60
REFERENCES 62
SUPPLEMENTARY INFORMATION 72

LIST OF TABLES

Table 1: Bond dissociation energies. 2
Table 2: Solutions used in melanin extraction via enzymatic method 28
Table 3: Artificially matured samples experimental conditions. 32
Table 4: Fossil samples information on location, age, and taxonomy. 35
Table 5: Maturity level of the fossil locations. 49
Table 6: Relevant FTIR peaks for melanin study (wavelength in cm-1) 55

LIST OF FIGURES

Figure 1: Diagenetic alterations of chlorophyll *a* 4
Figure 2: Dissimilatory sulfate reduction pathway 6
Figure 3: Diagenetic alteration of thiolanes and thianes into thiophenes and benzothiophenes 7
Figure 4: Representative chemical structures of eumelanin and pheomelanin 14
Figure 5: Simplified version of eumelanin and pheomelanin formation pathway 15
Figure 6: SEM images of eumelanosomes and chephalopod's melanin granules 17
Figure 7: Microraptor gui holotype specimen (IVPP V 13352) 19
Figure 8: Thiazines and thiazoles chemical structure 21
Figure 9: Magnified view of a capsule used for maturation experiments 30
Figure 10: TZM pressure vessel used in artificial maturation experiments 31
Figure 11: Fossil samples location map 33
Figure 12: ION-TOF 'TOF-SIMS IV – 200' 37
Figure 13: Perkin- Elmer Spectrum Two FT-IR Spectrometer 38
Figure 14: PCA analysis of ToF-SIMS data with Colleary et al. (2015) dataset 43
Figure 15: PCA loadings of Fig. 14 analysis 44
Figure 16: PCA analysis of eumelanin ToF-SIMS data 47
Figure 17: Correlation of PC1 values and thermal maturity level (ToF-SIMS eumelanin data). 50
Figure 18: FTIR absorption spectra of artificially matured samples without sulfur species 52
Figure 19: Possible diagentic transformation of eumelanin 53
Figure 20: FTIR absorption spectra of artificially matured samples with elemental sulfur 54
Figure 21: FTIR absorption spectra of artificially matured samples with sodium sulfide 54
Figure 22: FTIR absorption spectra of fossil samples from Lyme Regis and Strawberry Bank 55
Figure 23: Principal Component Analysis of FTIR data region from 1700 cm^{-1} to 600 cm^{-1}. and respective loadings 57
Figure 24: Correlation of PC1 values and thermal maturity level (PCA analysis of FTIR eumelanin data) 58

1. INTRODUCTION

1.1. Molecular biochemistry and biomarkers

Life as we know it exists under a myriad of forms and it covers all Earth. From unicellular microscopic life forms to the multicellular giants, such as the great blue whale and sequoia trees, life comes in all forms and sizes and inhabits every type of environment. From the great tropical forests that house countless species (Attenborough 1979) to the toxic sulfuric vents that for many years people thought they could not possibly house life (Rothschild & Mancinelli 2001), life forms seem to appear in every environment on Earth. Not only must we consider this, but we must also think about the sheer diversity of organisms found on the fossil record, and even then, only a fraction of organisms that once lived are preserved (Foote & Sepkoski 1999).

However, even though there is such a diversity in life forms, they all seem to share, at molecular level, a similarity in the way they are made up, a reflexion of their common evolutionary origin (Sadava et al. 2008). In general, carbon along with hydrogen, oxygen, and nitrogen are responsible for 99% of cell mass in organisms. Contributions of other elements, for example, calcium, sodium, phosphor, and sulfur compose the remaining 1% (Nelson & Cox 2005). The way elements connect with one another creates different biomolecules, each with different properties, which in turn allows them to perform different tasks in the organisms. These building blocks of life are classically divided into four main classes according to their molecular structure: nucleic acids (DNA and RNA), proteins, carbohydrates, and lipids (Nelson & Cox 2005).

Works on petroleum in the 30's gave rise to the science of organic geochemistry, the chemical study of organic molecules in rocks. In 1936, Alfred Treibs discovered that porphyrins, derived from breakdown products of chlorophyll *a*, were present in petroleum (Treibs 1936). This finding inspired the search of other biomolecules in sediments, and eventually in fossils (Kvenvolden 2006). This way, fossils not only retain information about the organism they originate from at a macroscopic level, but the same also holds true at a molecular level.

The different underlying chemistries of molecules play a very important role in the molecular preservation process (Eglinton & Logan 1991; Briggs & Summons 2014). Atoms and functional groups within molecules are held together by different bonds and interactions, where covalent bonds are the most common. Each covalent bond has a different dissociation energy (the energy it takes to break this bond). Some bonds are stronger than others and these are more likely to withstand higher temperatures than weaker bonds (Table 1). For example, a common bond in biomolecules is a hydroxyl group connected to the main carbon skeleton. The interaction between the O-H is 470 kJ/mol while the interaction C-O is 352 kJ/mol (values from

(Nelson & Cox 2005)). This means that the C-O bond needs less energy to break than the O-H, reason why with increased maturation, molecules tend to initially lose the hydroxyl group, instead of breaking at the H-O bond. With increasing temperature other stronger bonds are also broken such as C=O bonds (712 kJ/mol).

Table 1: Bond dissociation energies. Each bond has a specific dissociation energy, which will influence their resistance to geothermal pressures (Values adapted from Nelson & Cox 2005).

BOND TYPE	DISSOCIATION ENERGY (kJ/mol)
C=O	712
C=C	611
O—H	470
H—H	435
S—H	339
C—O	352
C—C	348
S—S	214
C—S	260

Considering the atomic bonds that make up each group of biomolecules, a scale of overall resistance to breakdown can be made, from greater to weaker resistance: lipids-carbohydrates-proteins-nucleic acids (with DNA being more resistant than RNA) (Eglinton & Logan 1991; Briggs & Summons 2014). This means that lipids have greater chemical resistance to breakdown and overall a bigger potential of being preserved compared to DNA. However, chemistry is not the only factor to consider. Several factors come together to allow biomolecules to be preserved, identified and characterized. From the biological aspect of inhibiting the natural processes of decay and autolysis after organisms die, through the geological aspect of favourable depositional environments and diagenetic conditions (Parry et al. 2017; Curry 1990), and finishing with the time scale in study.

Hydrolysis and oxidative damage are the main sources of DNA damage (Lindahl 1993), affecting the DNA strand in two ways. Firstly, the phosphodiester bond between nucleotides can be broken, resulting in strand breakage into smaller pieces. Secondly, the glycosidic bond between sugar and base can also be affected, leading to depurination (loss of adenine or guanine) or the creation of miscoding bases (Cooke et al. 2003). Taking into consideration the

rate at which these reactions happen, DNA degrades on a very short time scale (Willerslev et al. 2004; Allentoft et al. 2012). However, when the amount of free water and oxygen is reduced, temperatures are low (polar ice and permafrost) (Orlando et al. 2013) or when DNA binds to a mineral matrix (Romanowski et al. 1991), this threshold can be pushed back about 1 million years.

If DNA is the carrier of life, proteins are the builders of life, constituting the second largest cell's component, after water (Nelson & Cox 2005). Although slightly more resistant than nucleic acids, proteins are still easily lost in diagenetic environments (Newman et al. 2016). Proteins' first line of defence is their structure. Some proteins have tertiary and quaternary structures, making the dissociation reactions begin on the functional groups on the outside of the main chain, protecting the main sequence of amino acids. However, the peptide bond (C-N dissociation energy 293 kJ/mol (Nelson & Cox 2005)) between amino acids is prone to hydrolysis (Bada 1991) leading to protein rupture into smaller peptides or free amino acids. Alterations at individual amino acid level may also take place, making it difficult to confidently trace altered proteins back to the organism they come from (Hendy et al. 2018). The same way as with DNA, the mineral matrix in which proteins are held, as well as being in an open or closed system, can also give them slightly more protection and enhance their preservation. For example, amino acids in the carbonate matrix of shells have been found to be more readily preserved than those present in a hydroxyapatite matrix in bones (Bada et al. 1999).

Carbohydrates are mostly used by organisms as an energy storage and consist of a molecular skeleton made of carbon, hydrogen, and oxygen. Monosaccharides only have a few carbons in their structure and are water soluble, so they are easily lost during biodegradation. Oligosaccharides are more complex carbohydrates, consisting of several monosaccharide units, connected by glycosidic bonds, with polysaccharides containing more than 20 monomers (Nelson & Cox 2005). Some polysaccharides are insoluble in water, making them more resistant to hydrolysis. Chitin, a derivative of glucose, is one of the constituents of arthropod (in association with proteins). The longevity of chitin in the fossil record depends on the cross-linking between chitin and proteins, making it more resistant to degradation as well as a favourable depositional environment, with inhibition of diagenetic alteration (Stankiewicz et al. 1997).

Following the principle that biomolecules can be preserved in sediments and fossils in such a state that their original molecules can still be identified (Alleon et al. 2017; Curry 1990), the term *biomarkers* appear. The term "biomarker" is used is to represent a marked difference between the biologically functional biomolecule and the geological equivalent that has suffered

alterations through diagenesis. Although no longer biologically functional, biomarkers retain the taxonomic specificity that allows them to be indicative of certain groups of organisms (Brocks & Pearson 2005).

Vanadyl petroporphyrin, for example, represents a biomarker of chlorophyll *a*, a photosynthetic pigment present in higher plants. When compared, chlorophyll a and vanadyl petroporphyrin present virtually the same structure, only the side chain in chlorophyll *a* has broken from the main structure, and the central magnesium ion has been replaced by a vanadyl ion (Curry 1990; Ekstrom et al. 1983). The detached chlorophyll *a* side chain, phytol, can also be preserved as an isoprenoid lipid under the form of phytanes and pristanes (Farrimond & Eglinton 1990; Blumer 1965; Simoneit 2004) (Fig. 1).

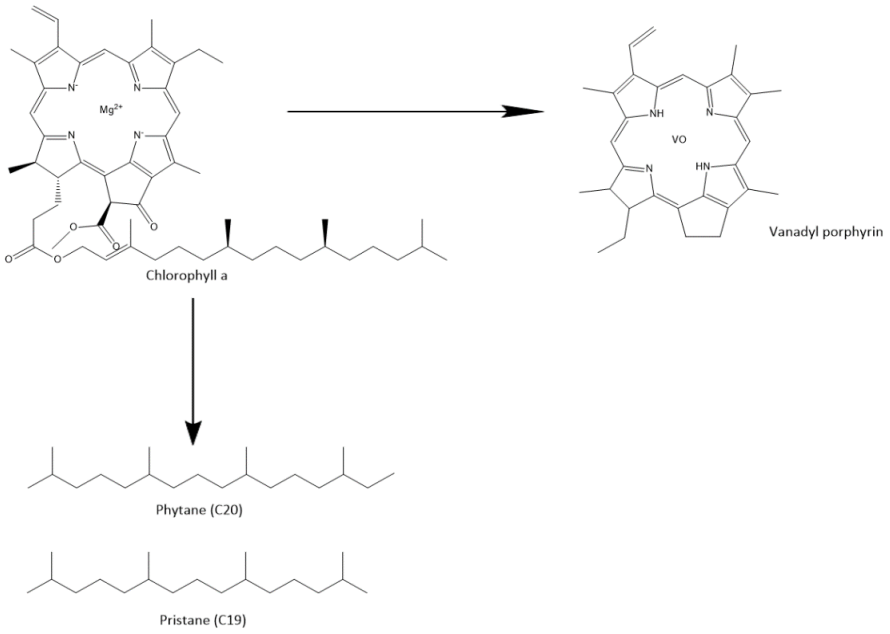

Figure 1: During diagenesis, the chlorophyll a molecule breaks down in two distinct parts that survive through time, serving as biomarkers. The side chain is transformed into phytanes and pristanes and the porphyrin ring suffers an alteration of the central ion from magnesium to a vanadyl ion. Adapted from Curry 1990.

However, the most informative class of biomarkers available in the rock record is lipids. Lipids perform several functions in organisms such as energy storage, cell signalling and are the main constituent in cell membranes. Defined by being insoluble in polar solvents (i.e. water), it is exactly this property that protects lipids from fast biodegradation. These molecules are the ones that survive diagenesis longest, and in such an unspoiled state that it is still possible to identify the original molecule (Newman et al. 2016) making them the most reliable biomarker. However, that does not make lipids entirely safe from alterations. Hydrogenation of double

bonds, aromatization, and loss of functional groups can still occur during diagenesis (Eglinton & Logan 1991) as well as isomeration, reduction (Newman et al. 2016), cyclization and further cross-linking (Farrimond & Eglinton 1990).

Sterols are a large group of molecules that have distinct functions in Eukarya (i.e. hormones and cell membrane fluidity). The combination of cholestane (C_{27}), ergostane (C_{28}) and stigmastane (C_{29}) have been useful in identifying early signs of eukaryotic life (Brocks et al. 2017) and early life phylogeny (Bobrovskiy et al. 2018). 24-isopropylcholestane (a C_{30} sterane that is the diagenetically altered form of 24-isopropylcholesterol) is a biomarker for the presence of demosponges (McCaffrey et al. 1994; Love et al. 2009). In truly exceptional cases, sterols can even be found in association with their diagenetic and catagenetic products (Melendez et al. 2013) allowing the degradation pathways to be inferred.

Bacterial hopanoids are constituents of bacterial cell walls and perform the same functions as steroids in eukaryotic cells, mainly cell membrane fluidity. These hopanoids are only found in bacterial cells walls and, after diagenesis, they transform into bacterialhopanoids (Farrimond & Eglinton 1990; Steele et al. 2001; Ourisson & Albrecht 1992), being, therefore, a biomarker for bacterial presence.

In this section, diagenetic alterations of biomolecules into biomarkers were explained in terms of bond breakage and loss of functional groups. However, as seen in porphyrin, elements from the surrounding sediments can be added to the structure of the precursor molecule (Curry 1990; Ekstrom et al. 1983), showing that the depositional environment also plays a role in the study of biomarkers.

1.2. Kerogen and biomolecular sulfurization

Kerogen is defined as a mixture of solid organic matter in sedimentary rocks, formed from biomolecules mainly from algae and higher terrestrial plants that survived biodegradation, making it the largest carbon deposit in the carbon cycle (Vandenbroucke & Largeau 2007). With time, these biomolecules can be chemically altered due to geothermal pressures, and eventually give rise to fossil fuels, petroleum, and natural gas (Tegelaar et al. 1989). Distinct types of kerogen are formed depending on the depositional setting, element composition, and the precursor organic matter.

Several techniques can be used to identify the type of organic matter present in kerogen and it's level of maturity, such as elemental analysis and Rock-Eval pyrolysis. During Rock-Eval pyrolysis, a sample is heated in a controlled manner, with several parameters being measured at different temperatures. The temperature at which the hydrocarbon generation reaches its maximum is identified as T_{max} (Killops & Killops 2005). T_{max} values between 415°C and 430°C indicate immature sediments, values between 430°C and 445°C indicate mature sediments, with values above 445°C indicating over-mature sediments (Killops & Killops 2005).

Overall, kerogen can contain from 0.1 to 6.0% of sulfur in its composition (Jasińska et al. 2012) a value that can surpass the expected value from the original biomass (around 1.0% of total biomass per organism) (Aizenshtat et al. 1995; Sievert et al. 2007). This difference between expected and measured values suggests an external source of sulfur, that was secondarily incorporated into the organic matter through geochemical processes during diagenesis (Francois 1987; Sinninghe Damsté et al. 1989) increasing the overall amount of sulfur in kerogen and sediments.

It is thought that the main source for the reactive sulfur comes from sulfate-reducing bacteria. These microorganisms, such as *Desulfovibrio* and *Desulfotomaculum* (Akagi 1995; Carbonero et al. 2012), decompose organic matter using it as a source of energy, but instead of using oxygen (O_2) as a terminal electron acceptor, in anoxic environments sulfur-reducing bacteria use inorganic sulfate (SO_4^{2-}). This process, known as dissimilatory sulfate reduction,

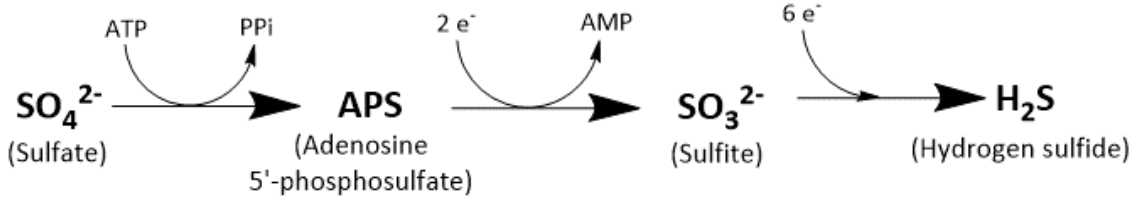

Figure 2: Dissimilatory sulfate reduction pathway performed by sulfate-reducing bacteria. In this type of anaerobic respiration, sulfate is used as a terminal electron acceptor instead of oxygen. Through a series of transformation, sulfate is reduced to hydrogen sulfide, a gas that easily diffuses through the sediments and reacts with organic matter, leading to secondary sulfurization of biomolecules. Adapted from Carbonero et al. 2012.

produces sulfide (S^{2-}) that can be protonated forming hydrogen sulfide (H_2S) that is released into the sediments (Fig. 2) (Akagi 1995; Carbonero et al. 2012). Hydrogen sulfide is a gas that can diffuse easily through the sediments and that can be oxidized, resulting in the formation of polysulfides (S_x^-) (Jasińska et al. 2012). These polysulfides are thought to be the main reactants responsible for the sulfur incorporation into functionalised organic compounds (Sinninghe Damsté et al. 1989; Aizenshtat et al. 1995; Kok et al. 2000; LaLonde 1990).

Sulfur is an extremely reactive element, with various states of oxidation and reduction (Greenwood & Earnshaw 1997). These characteristics, with the added variety of molecular geometries (i.e. linear, cyclic) that make up biomolecules, means there isn't a single pathway for sulfur incorporation into organic matter. Each biomolecule and each functional group interact differently with the reactive sulfur species and the mechanisms by which these reactions happen are still poorly understood (Aizenshtat et al. 1995; Vandenbroucke & Largeau 2007; Adam et al. 1998).

Sulfur becomes incorporated into organic matter under a relatively narrow range of temperatures and other environmental conditions. Sulfur-reducing bacteria only survive to temperatures up to 50°C, so these reactions occur in the near-surface sediments at low temperatures, or early-diagenesis (Vairavamurthy et al. 1995; Adam et al. 1998). This has also been proved by the increase of sulfur content with depth in sediments and in humic fractions as well as molecular studies (Vandenbroucke & Largeau 2007). Another factor responsible for the process of organic matter sulfurization is a low level of reactive iron in the environment (Eglington, 1992). Sulfur ions have a greater affinity for iron than organic matter, leading to the formation of iron sulphides and pyrite (Fe_2S) instead of organic matter sulfurization (Berner 1984) when large amounts of iron are present in the environment.

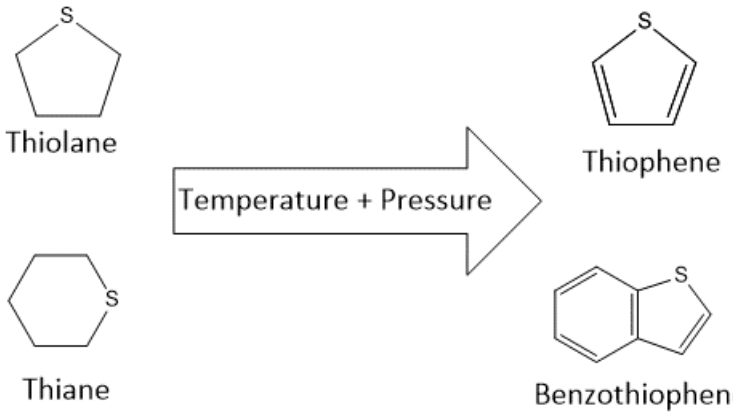

Figure 3: Thiophenes and benzothiophenes are commonly found in sulfurized kerogen. These molecules can have an organic origin from previously formed thiolanes and thianes that have undergone diagenetic alterations.

Posterior diagenetic transformations of the initially formed sulfur molecules can also happen. With increasing temperature and pressure, previously formed thiolanes and thianes can be stabilized into thiophenes and benzothiophenes, with the latter usually found in more mature sediments (Fig. 3) (Vandenbroucke & Largeau 2007; Aizenshtat et al. 1995; Sinninghe Damsté et al. 1990).

1.3. Cephalopod evolution and the emergence of the ink sac

1.3.1. Cephalopod evolution

Cephalopods' life story starts in the Early Cambrian (c.a. 530 Ma), in the divergence of the major classes of molluscs. Cephalopods' ancestors were monoplacophoran-like molluscs, and by the Late Cambrian, several cephalopod stem groups were rapidly evolving and diversifying, but still presented the characteristic body plan of other molluscs with the shell on top as well as having a forward locomotion (Kröger et al. 2011).

Extant cephalopods consist of two major groups: Nautiloidea and Coleoidea. Nautiloids are the only living cephalopods with an external shell while coleoids are characterized by the absence of an external shell. Coleoids are in turn divided into Decabrachia (squids and cuttlefish) and Octobrachia (octopuses and the vampire squid). Molecular clocks predict that nautiloids diverged from coleoids at the Silurian-Devonian boundary (c.a. 415 M.a) while Coleoidea seems to have diversified into Decabrachia and Octobrachia around the Early to Middle Permian (c.a. 276 Ma) (Kröger et al. 2011; Tanner et al. 2017). This is in accordance with the known fossil record.

Molecular clocks predict species divergence times by comparing the number of genetic differences between two organisms. Knowing the rate at which these changes happen, it is possible to work backwards to the time they shared the same code, or in other words, to their common ancestor (Kumar 2005; Bromham & Penny 2003). Although this technique has undergone several developments since its first proposal in the '60s, there are some aspects to consider with the use of molecular clocks to infer relationships between extinct organism.

The main drawback in using this methodology is the fact that organisms may not have a constant rate of genetic alterations (Kumar 2005; Bromham & Penny 2003). The use of "relaxed" clocks allows this rate variation to be accounted for in the statistical analysis, avoiding a strict model of genetic alteration (Kröger et al. 2011). Accurate methods of gene selection and statistical calibration with dated fossils also allow the divergence times obtained to be more precise.

1.3.2. Coleoids and the emergence of the ink sac

The characteristics that make coleoids stand out from the other molluscs is the fact they have internalised or lost their shell, and evolved an ink sac, camera eyes and chromatophores in their skin. The shell and the ink sac seem intimately connected. Ink sacs seem to have developed more or less simultaneously with shell internalisation, with the oldest known fossilized ink sacs

from the Early Carboniferous (Mapes et al. 2010; Sasaki et al. 2010). Shell reduction, or complete loss, allowed cephalopods to optimize their locomotion, allowing them to have a more efficient jet propulsion system (Kröger et al. 2011; Tanner et al. 2017). Cephalopod predatorial behaviour is not only extremely well known in extant animals, but the same behaviour has also been immortalized in their ancestors with some organisms being fossilized mid-hunt (Wilby et al. 2008).

Without the external shell to protect them, coleoids had to develop new ways of evading predators. Some developed venoms like the blue-ringed octopus *Hapalochlaena* spp. (Hwang et al. 1989). Others became masters of disguise with the development of specialised skin cells called chromatophores allowing octopuses and cuttlefish to change the texture and colour of their skin, camouflaging themselves efficiently in the surrounding environment from predators (Chiao et al. 2011). Still, when discovered in their trickery, they have one last defence mechanism: the release of ink. Coleoids have managed to couple their propulsion system with the ejection of dark ink, allowing a quick escape whilst obscuring the predators' vision at the same time. When the water clears, and the predator vision is once again unobstructed, they are already far away and out of harm's way (Derby 2007).

1.3.3. Ammonoids and the debated presence of an ink sac

When asked to name a fossil that is not a dinosaur, most people will say ammonite. These ammonoids once dominated the world oceans and their hard parts are commonly preserved in the fossil record, making them one of the prime fossils for stratigraphic correlation. Ammonoids are stem-coleoids, having diverged from the coleoid stem lineage in the Devonian (Kröger et al. 2011).

The presence of an ink sac in ammonoids has been a case of debate for the last 50 years (Klug & Lehmann 2015). Black bag-shaped structures, morphologically similar to ink sacs, have been reported in some specimens (Doguzhaeva et al. 2007) and their melanin-based chemistry is comparable to the ink found in extant cephalopods (Doguzhaeva et al. 2004).

However, ammonoid locomotion by shell pumping made them slow, unlike the jet propulsion system seen in other cephalopods. As an anti-predator mechanism, ink release works because coleoids are able to make a quick escape using the jet propulsion locomotion. Ammonoids, with their shell pumping mechanism, wouldn't be able to quickly escape, therefore making the production and release of ink unlikely in terms of energy costs/benefits (Naglik et al. 2015). The melanin signal, interpreted as ink, could be from other melanic organs in ammonoids

(Klug & Lehmann 2015) such as the black band, a dark band composed of conchiolin and melanin secreted on the inside of the aperture (Klug et al. 2007).

1.3.4. Composition of cephalopod ink

Cephalopod ink is a mixture of components dominated by melanin. The melanin is produced in the ink gland and stored in the ink sac. When ink is released, melanin is mixed with other component produced in the funnel organ, with the ejected ink being a mixture of melanin (approximately 15% of the total wet weight), mucus, and proteins as major constituents (Derby 2014).

1.4. Melanin molecules and their functions

"Melanins" is a broad term used to classify a group of phenolic based molecules found widespread in nature as well as similar laboratory-made molecules (Solano 2014). Melanins have been found in the most diverse groups, from most chordates to many groups of invertebrates including molluscs and arthropods as well as in plants, fungi, and bacteria (Edwards et al. 2014).

Different organisms found the most efficient way to produce melanins, meaning that there are similar molecules with the same basic characteristics and functions but formed from different precursors and with different structures and formation pathways. This makes them challenging to characterize, which is a reason why their structure is still ill-defined and poorly understood (D'Ischia et al. 2013).

Melanins are mostly well known for being the most commonly found pigment in animals, namely, skin, hairs, and feathers. Traditionally, animal colouration is categorized into concealment, communication, and regulation of physical processes (Caro 2005). However, colouration is not the only function melanins have in animals. Melanin confers photoprotection in organs such as eyes (Hu et al. 2008) and skin with its broadband light absorption spectrum, from the near infra-red (IR) to the ultraviolet (UV) radiation with up to 90% of the absorbed energy dissipated into heat (Nofsinger et al. 1999). Melanin also works as a free radical scavenger, acting as an antioxidant in internal organs such as the liver (Schiel et al. 1987; Rózanowska et al. 1999). Some studies also connect them to an increase in virulence in pathogenic bacteria (Bonser 1994; Plonka & Grabacka 2006) and it is also connected to antimicrobial activity (Mackintosh 2001).

Based on their precursor, final chemistry, and function, melanins are usually divided into four categories: Allomelanin, Neuromelanin, Eumelanin, and Pheomelanin.

1.4.1. Allomelanins

Allomelanins are a black to dark brown group of pigments mainly found in plants and also in some fungi. These melanins are grouped together due to the fact that they don't tend to have nitrogen present in their structure (Butler & Day 1998; Plonka & Grabacka 2006). Nitrogen is an essential element in plant metabolism, extremely important for their growth and one of the main constituents of chlorophyll, reason why is not used in melanin production. The main melanin precursor in plants is catechol or catecholic acids, generating catechol-melanin while in fungi the precursor tends to be hydroxylated naphthalene-derived molecules, creating DHN-melanin (Solano 2014). Fungal melanins are usually located in the cell walls opposed to

mammalian melanins that are usually located inside the cell in specialized organelles (Butler & Day 1998).

1.4.2. Neuromelanin

Neuromelanin is a complex insoluble pigment present in the human brain, especially in the dopaminergic neurons of the s*ubstancia nigra* and in the noradrenergic neurons of the *locus coeruleus* (Fedorow et al. 2005; Martin-Bastida et al. 2017). Derived from L-DOPA oxidative products (dopamine ($C_8H_{11}NO_2$) or noradrenaline ($C_8H_{11}NO_3$)), neuromelanin is, in fact, a mixture of eumelanin and pheomelanin molecules (Bush et al. 2006) but it isn't formed in melanosomes. Neuromelanin organelles are formed by an autophagic process that envelops the eumelanin and pheomelanin molecules with posterior fusion of the autophagic body with a lysosome (Engelen et al. 2012) and, through a maturation process, lipids and proteins are associated with the neuromelanin pigment (Zecca et al. 2000).

It is thought that neuromelanin formation and, subsequently, these organelles, is a cellular response to oxidative stress. Excessive amounts of cytosolic dopamine (and related reactive oxygen species) induces neuronal death. By consuming the excessive dopamine forming the stable neuromelanin and transporting it away from the cytosol, neurotoxicity is avoided (Mosharov et al. 2009). These organelles are not destroyed and instead get accumulated linearly in the brain areas above mentioned during development (Zecca et al. 2004) giving them their characteristic dark colouration. A secondary method of protection is the neuromelanin ability of chelating heavy transition metals such as iron, copper, and zinc, (Zecca et al. 2004) giving this molecule a high paramagnetic character (Sulzer et al. 2018).

The paramagnetic ability and specific location of neuromelanin have been proposed as a diagnosis method for Parkinson's Disease via Magnetic Resonance Imaging (MRI) (Sulzer et al. 2018). In broad terms, Parkinson's disease is a neurodegenerative condition characterized by the death of the melanic dopaminergic neurons. Currently, its diagnosis is only possible when the first motor symptoms are visible, which happens when approximately 30% of *substancia nigra* neurons are already lost, according to most studies (Cheng et al. 2010). MRI is able to detect a loss of neurons before symptoms start to show, leading to an early diagnosis and, consequently, an early symptomatic treatment that improves patients' long-term quality of life.

1.4.3. Eumelanin and pheomelanin

Eumelanin and pheomelanin are the most common forms of melanins in vertebrates. Due to their presence in human and mammalian skin and hair as well as in birds feathers, they were one of the first pigments to be recognized in ancient times and have been a subject of intensive studies (Simon & Peles 2010).

From the functional point of view, both eu- and pheomelanin have the same general photoprotective functions (Micillo et al. 2016), and both are usually found in association, within the same cellular structures (Ancans et al. 2001), also sharing the beginning of the formation pathway (Ito & Wakamatsu 2008).

However, from a chemical point of view, they have critical differences. Pheomelanin has sulfur incorporated in its structure, while natural eumelanin does not (Fig. 4). Eumelanin is a large polymer and insoluble in water. Its indole-based structure can absorb radiation across the visible spectrum as well as UV, giving it its black aspect. Pheomelanin, on the other hand, has a lower molecular weight and is soluble in alkaline solutions. Its red aspect comes from the lack of carbonyl groups (carbonyl groups absorb in the red wavelength, which means that a reduced amount of these functional groups will reflect the red wavelength, allowing us to perceive pheomelanin as having reddish tons) (McGraw 2006b).

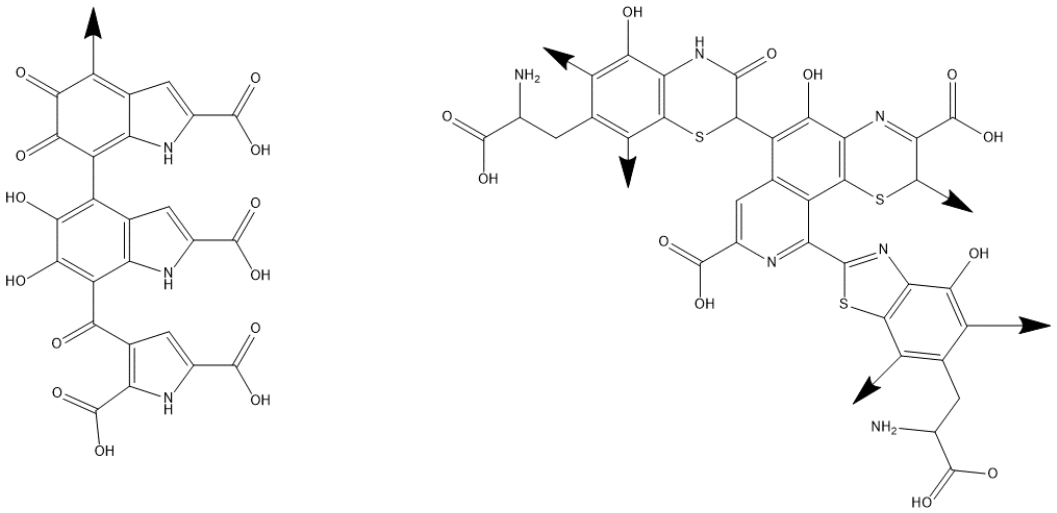

Figure 4: Representative chemical structures of eumelanin and pheomelanin. Adapted from Ito & Wakamatsu 2008.

Briefly, their formation pathway starts with L-tyrosine being oxidised into dopaquinone by tyrosinase, the point from which eumelanogenesis and pheomelanogenesis can progress independently (Fig. 5). If cysteine concentration in the system is above 0.13 µM, dopaquinone combines with cysteine, forming 5-*S*-cysteinyldopa and 2-*S*-cysteinyldopa. Sequentially, if the cysteinyldopa concentration reaches above 9 µM, it gets oxidized, forming benzothiazine units. The benzothiazine units can react between themselves or with some benzothiazine degradation products (i.e. benzothiazole and isoquinoline units), forming the pheomelanin structure (Ito 2003; Ito & Wakamatsu 2008; Prota et al. 1970; Wakamatsu et al. 2009; Simon et al. 2009).

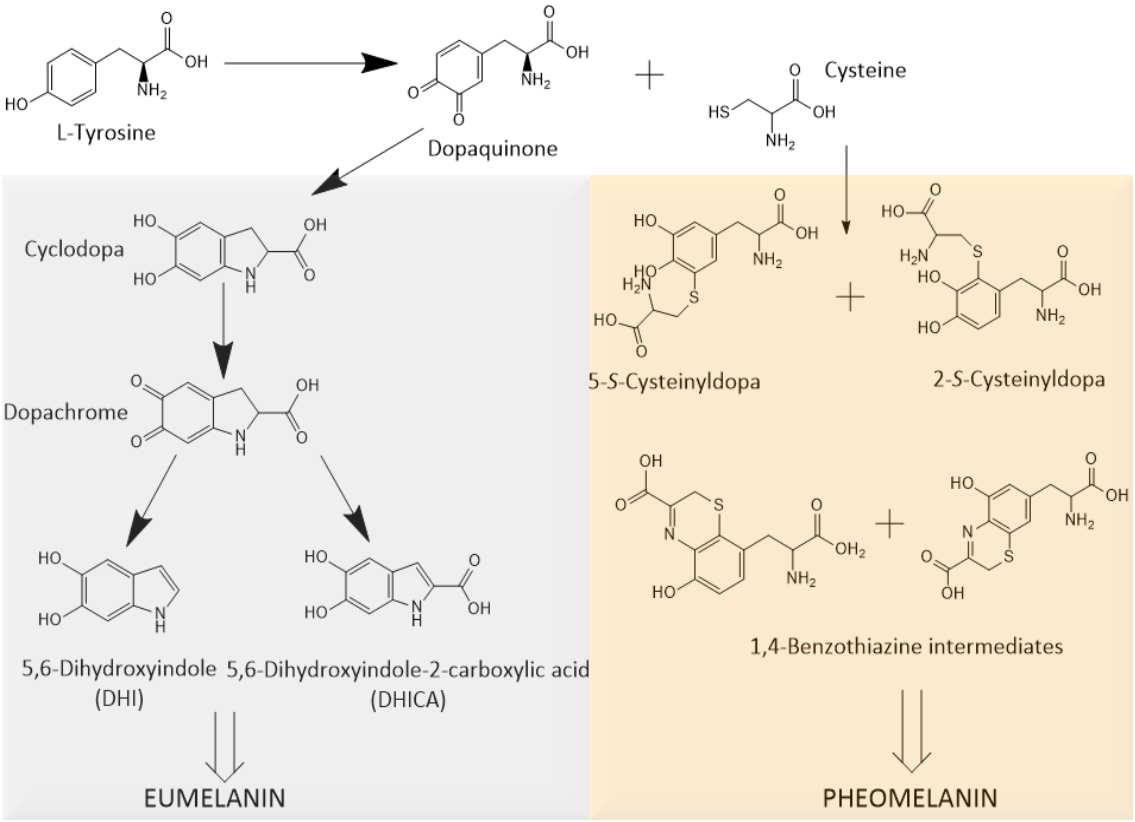

Figure 5: Simplified version of eumelanin and pheomelanin formation pathway, without the enzymes involved in each step. Adapted from Ito & Wakamatsu 2008.

Only when the cysteine is depleted or absent from the system, eumelanogenesis takes place. In eumelanogenesis, dopaquinone upon a reductive endocyclisation forms cyclodopa which in turn is rapidly oxidized to dopachrome. Dopachrome, in turn, can be converted into 5,6- dihydroxyindole (DHI) and 5,6- dihydroxyindole-2-carboxylic acid (DHICA), that are the basic building blocks of eumelanin (Raper 1927; Ito 2003; Ito & Wakamatsu 2008; Land & Riley 2000) along with pyrrole units derived from their peroxidative cleavage (Simon et al. 2009).

After the formation of DHI and DHICA, these two molecules will start to polymerize, forming oligomers. The ratio of DHI/DHICA changes depending on the melanin. *Sepia* melanin (extracted from *Sepia officinalis* ink) has around 75% DHICA-derived units to 20% DHI units, with the remaining 5% accounting for units in other oxidative states (Pezzella et al. 1997).

While DHI has a planar structure DHICA has a non-planar structure due to the presence of the carboxylic acid functional group. When polymerizing, DHI forms organized π-π stacking, while DHICA molecules tend to bundle together more randomly, due to the additional negative charge (Büngeler et al. 2017). The additional carboxylic acid functional group also confers these molecules different properties, with DHICA enhancing the molecular solubility and antioxidant properties while decreasing visible light absorption (Micillo et al. 2016).

1.4.4. Melanosomes

Eumelanin and pheomelanin production occurs in membrane-bound organelles called melanosomes. In the integumentary structures of mammals and birds, melanosomes are formed in highly dendritic specialized cells called melanocytes (Ancans et al. 2001). In cephalopods, these are produced in the ink gland (Schraermeyer 1994).

Integumentary melanosomes go through a series of stages until they reach the full matured stage when they are fully pigmented. Melanosome formation starts with a membrane-bound protein matrix. On the first and second formation stage, the premelanosome internal matrix undergoes a fibre rearrangement, forming a regular parallel pattern observable in SEM. Melanin gets deposited using the arranged fibres as a template. On the third stage, eumelanin continues to be deposited in the premelanosomes, resulting in a premelanosome darkening and thickening. On the fourth stage, they are fully melanized, and the internal structure of the melanosomes is no longer visible due to the accumulated melanin. (Marks & Seabra 2001; Slominski et al. 2004).

In cephalopods, namely *Sepia* sp., the melanosome formation follows a similar model. Pre-melanosomes, consisting of membrane-bound protein matrix formed in the Rough Endoplasmic Reticulum, fuse with coated vesicles containing tyrosinase and other enzymes formed in the Trans-Golgi Network. A maturation process happens with the formation of melanosomes. The major difference when compared with vertebrates melanosome formation, is that each melanosome forms several melanin granules, that will be released into the ink gland (Palumbo 2003; Schraermeyer 1994).

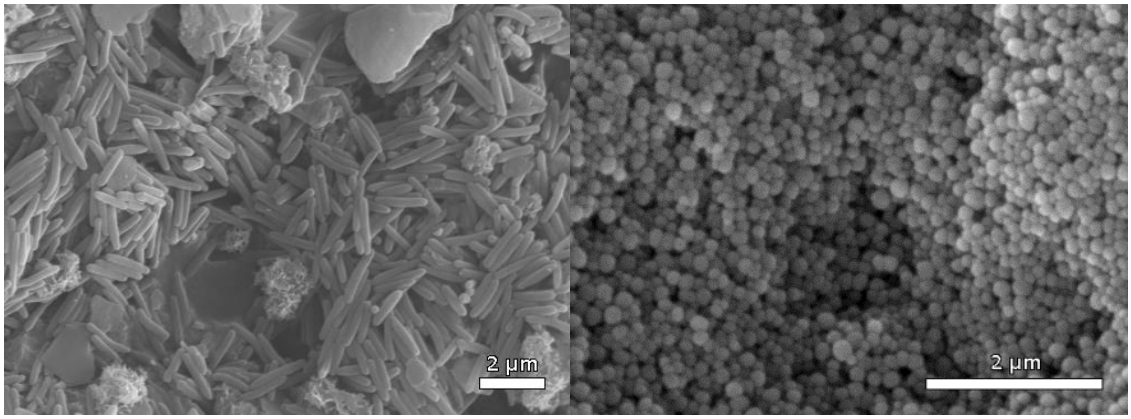

Figure 6: Scanning Electron Microscope (SEM) images of two distinct types of eumelanin bearing structures. A) Eumelanosomes extracted from crow feather. B) Melanin granules extracted from cephalopod ink.

Vertebrate eumelanosomes are usually elliptical shaped, with dimensions of around 900 nm x 350 nm (Liu et al. 2007), pheomelanosomes are usually round, with sizes of around 500 nm (Vinther 2015). *Sepia* melanin granules are round with dimensions around 150 nm (Liu & Simon 2003), although they contain pure eumelanin and not pheomelanin (Fig. 6).

1.5. Colouration and fossil melanin

Animal colouration is classically divided into three main functions: concealment (i.e. camouflage), communication (i.e. sexual selection and warning), and regulation of physical processes (i.e. patches around the eyes that can reduce glare) (Caro 2005; Cuthill et al. 2017). The main production mechanisms are pigments, structural colours, or a mixture of both (Shawkey & D'Alba 2017).

Pigments, such as melanin and carotenoids, absorb certain wavelengths of visible light. They can be produced endogenously by organisms, such as melanin or psittacofulvins (found in parrots) (Shawkey & D'Alba 2017), or obtained through diet, such as carotenoids (carotenoids are produced endogenously by algae, plants, and fungi) (McGraw 2006a). Structural colours come from the interaction of light at the interface of nanostructures with different reflective indexes (Parker 2000). This type of colouration method allows different colours to be observed depending on the angle of incidence of light, or viewing angle, the known iridescence of peacock feathers or hummingbirds necks (as seen in Cuthill et al. 2017).

Reconstructing the colour patterns of dinosaurs and other extinct animals used to be a combination of informed knowledge of the relationships that they hold with extant animals (extrapolating, we could assume that extinct animals would use integumentary colouration based on the same principles) and a bit of guesswork and input from the artists (Koepfer 2003). However, this has changed in recent years, with the discovery that melanin can fossilize.

In 2008, microbodies previously identified as bacteria (Davis & Briggs 1995) were reinterpreted as melanosomes (Vinther et al. 2008). These bodies matched in location, size, and spatial organization with melanosomes in extant species and further chemical analyses showed that their chemistry closely matched as well (Glass et al. 2012; Lindgren et al. 2014). More so, eumelanin and pheomelanin preserved their different chemistries, making them distinguishable. Time-of-Flight Secondary Ion Mass Spectrometry (ToF-SIMS) analysis shows a difference in eumelanin and pheomelanin spectra, with pheomelanin presenting characteristic peaks for sulfur-bearing moieties (Lindgren et al. 2014). Pyrolysis–Gas Chromatography-Mass Spectrometry (Py-GC/MS) analysis corroborates this chemical difference with the identification of benzothiazole and derivates from pheomelanin (Supplemental Information in Brown et al. 2017). This has allowed paleo artists to put another piece of information into the puzzle, with reconstructions getting more accurate, and giving information about how these animals interacted with their environment.

Microraptor (Li et al. 2012) (Fig. 7) was reconstructed as having an iridescent black plumage, meaning that they were diurnal animals since iridescence needs light to be observed.

Sinosauropteryx (Smithwick et al. 2017) and *Psittacosaurus* (Vinther et al. 2016) were both reconstructed in brown shades, in a patterning consistent for camouflage by countershading. Countershading is a patterning where the underside of the animal is lighter than the upper part, counterbalancing the natural way light falls on objects and animals, reducing its 3D aspect, and therefore making animals harder to detect (Rowland 2009). Different environments have different levels of illumination, and countershading patterns have evolved accordingly. *Psittacosaurus* patterning would be more suited to closed light environments (Vinther et al. c2016), while *Sinosauropteryx* would probably roam open habitats (Smithwick et al. 2017).

Figure 7: Microraptor gui holotype specimen (IVPP V 13352). This four winged feathered dinosaur exhibited an iridescent plumage (Li et al. 2012).

However, questions are still raised about the veracity of these studies (Negro et al. 2018). Some still hold alive the hypothesis that the first interpretation for these microscopic bodies is correct, and that they are bacteria (in-depth discussion in: Vinther 2015; Vinther 2016; Schweitzer et al. 2015). Others advise caution with interpreting any sulfur signal as pheomelanin since diagenetic incorporation of sulfur in soft tissues is known (McNamara et al. 2016; Glass et al. 2012; Glass et al. 2013). Another aspect to consider is that some of the melanin signal found could have come from internal organs and not exclusively from integumentary structures (McNamara et al. 2018).

Even at the most fundamental level, "*melanin remains an intensively studied but still mysterious and poorly understood group of pigments"* (Shawkey & D'Alba 2017). The diversity in melanin forms (as seen in section 1.4) and the fact that eumelanin and pheomelanin co-exist in most animals (McGraw 2006b) makes their study extremely complex. Eumelanin and

pheomelanin chemical structures are still ill-defined *in vivo* (D'Ischia et al. 2013) and the changes eumelanin suffers through diagenesis, from how its chemical structure gets altered to how it interacts with the sedimentary environment, is still mostly unknown.

1.6. Diagenetic incorporation of sulfur with implications for colour reconstructions

McNamara et al. (2016), while studying fossil frogs from Libros Gypsum Unit (Vallesian), Spain suggested that diagenetic incorporation of sulfur could enhance the preservation potential of melanin, in a process similar to what happens in other biomolecules. This sulfur incorporation into eumelanin was first seen by Glass et al. (2012) while studying fossil ink sacs from the Blue Lias Formation of Lyme Regis, Dorset, United Kingdom. Since extant cephalopod ink doesn't contain pheomelanin (as seen in section 1.3.2.), and eumelanin does not contain sulfur (Fig. 4), the sulfur signal identified by Glass et al. (2012) must have had an external origin.

Both locations, Libros and Lyme Regis, are known for having some sulfur in their environment, with Lyme Regis having a history of pyrite (Fe_2S) presence (Hallam 1960) and Libros having a history of gypsum ($CaSO_4 \cdot 2H_2O$) (Orti et al. 2003). Consequently, the sulfur from the surrounding environment could have reacted with the soft tissues producing the sulfur signal.

In both McNamara et al. (2016) and Glass et al. (2012) studies, only thiophene moieties were found when the fossils were subjected to Py-GC/MS. Thiophene moieties are a resulting product of both pheomelanin breakage and sulfur-rich eumelanin, as well as kerogen transformation reactions (as seen in Fig. 3). Thiophenes moieties tend to be one of the most stable and common forms of sulfur-containing compounds (Vandenbroucke & Largeau 2007), making them unusable as the main signal for pheomelanin identification. However, benzothiazole and benzothiazine units (cyclic molecules with sulfur and nitrogen) are not observed in sulfur-rich eumelanin, making high abundances of these molecules in soft tissues a strong indication of pheomelanin presence (Fig. 8) (Brown et al. 2017).

Still, a question arises: Is there any form of diagenetic incorporation of sulfur into the eumelanin molecule that could give rise to the same signal as pheomelanin, namely, the identification of thiazine/thiazole moieties, that could lead to a false positive for the presence of pheomelanin?

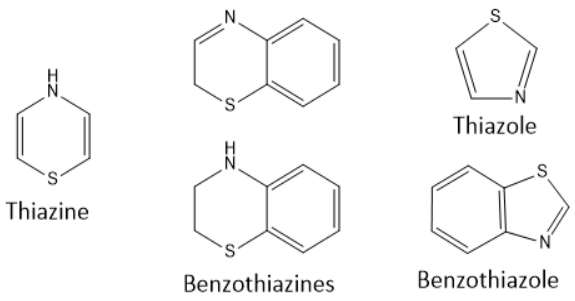

Figure 8: Thiazines and thiazoles molecules are the major building blocks of pheomelanin and are not observed in sulfurized eumelanin. When found in high abundances in original melanised tissues they are indicative of the presence of pheomelanin.

1.7. Objectives

Studying biomolecules and the changes they undergo during diagenesis can give us a glimpse of ancient life and their environments. The preservation of pigments in the fossil record, in particular, melanin, can give us a colour image of how past animals looked like. Reconstructing the colour patterns of ancient animals can elucidate how these animals interacted with their environment (i.e. if they roamed open spaces or closed light environments) (Smithwick et al. 2017; Vinther et al. 2016) as well as predator/prey interactions (Brown et al. 2017). Although several advances have been made in the last years in the emerging field of paleocolour (review in Vinther 2015a), there are still some aspects of melanin preservation that need further investigation.

An aspect that needs clarification is the effect of the geothermal gradient in the molecular chemistry of the eumelanin molecule. During diagenesis, molecules are transformed into more stable forms by losing their labile functional groups. Further cyclization and cross-linking can also occur with increasing temperatures (Aizenshtat et al. 1995). It is expected that eumelanin could have some of these processes happening, namely the loss of liable functional groups, however, the chemical changes that eumelanin incurs during fossilization are still not fully understood. It is also important to understand the main factors controlling its long-term preservation. Is melanin preservation related to its age or is the level of maturation the most determining effect in its preservation in a recognizable form?

To study the effects of diagenesis in the eumelanin molecule, purified cephalopod ink will be artificially matured under different sets of temperature/pressure. A broad collection of fossil ink sacs from different localities, diagenetic histories, and ages (ranging from the Carboniferous to the Cretaceous) will also be analysed through a range of chemical analysis.

Both pheomelanin and secondarily incorporated sulfur into eumelanin possess a sulfur signal when chemically analysed. Secondarily sulfurized eumelanin is known to produce thiophene moieties which are also common diagenetic products of sulfurized kerogen (Sinninghe Damsté & De Leeuw 1990). Thiophenes, although indicators of sulfur presence are not indicative of a specific biomolecule presence since they are common diagenetic products of several types of sulfurized molecules. However, high levels of thiazine and thiazole moieties have been used as indicators of pheomelanin presence in fossils (Brown et al. 2017; Dzierzęga-Lęcznar et al. 2012), since these moieties have not yet been found to be products of secondarily incorporated sulfur (Glass et al. 2012).

Although the presence of thiazine/thiazole moiteies seems to be a strong indicator of pheomelanin presence and not sulfurized eumelanin, it hasn't been tested if it is possible to have some form of incorporated sulfur into the eumelanin molecule that gives the same thiazine/thiazole moieties. Recurring to artificial maturation, eumelanin will be matured with sulfur species under several sets of temperature/pressure and chemically analysed to clarify this aspect.

The main aim of this project is to elucidate certain aspects of melanin chemistry that still raise some uncertainty in past colour reconstruction. By exploring the changes that eumelanin incurs with diagenesis, with a special focus in the incorporation of sulfur into its structure and its differences/similarities with pheomelanin, I aim to increase the current knowledge of fossilized melanin chemistry and consequently, contribute to make colour reconstructions more robust.

2. TECHNIQUES

2.1. Artificial maturation

Organism fossilization is a rare, complex phenomenon of chemical changes (Parry et al. 2017) with an interplay of different processes (e.g. decay, maturation and mineralization) (Purnell et al. 2018) happening through thousands or even millions of years, until the final result of a fossil. Each process has been studied individually in laboratory experiments to understand how each individually affects the organism (Briggs & McMahon 2016).

Maturation is defined as the effect of temperature and pressure in the preservation or loss of biomolecules, translated macroscopically in the preservation of tissues and anatomic features (Purnell et al. 2018). In artificial maturation experiments, the analogous biological material is subjected to a set of different pressures and temperatures allowing the replication, in the laboratory, of what happens in nature, with a further comparison to the fossil material.

The biggest obstacle to overcome in these experiments is time. Changes can happen in nature through millions of years so, to faithfully replicate this in a human time-scale, the maturation process needs to be accelerated. Following the Arrhenius principle (Arrhenius 1889), and assuming organic matter natural process of maturation follows a first-order kinetics reaction, time and temperature may be interchangeable. Exaggerated temperatures will compensate for the extensive amount of reaction time, making it possible to see comparable changes in a matter of days or even hours (Vandenbroucke & Largeau 2007).

Confined pyrolysis is the method that gives more comparable results to those observed in natural systems when compared with open systems (i.e. under an inert atmosphere) or other closed systems (such as glass vials) (Monthioux et al. 1985). Initially used in petroleum studies, it has been successfully applied to study biomolecules preservation, such as plant biomolecules (Gupta et al. 2007), arthropod cuticle (Gupta et al. 2006), melanin (Colleary et al. 2015) and keratin (Saitta et al. 2017).

In confined pyrolysis, a tube made of a non-reactive element (usually gold or palladium or an alloy of these two metals) is cut to the desired size, normally a few centimetres. One end of the tube is welded shut, allowing the sample to be loaded in. The free space at the end of the tube is flattened, ensuring the amount of dead volume is minimal and the remaining end is welded shut, creating a capsule. The desired maturation pressure controlled through hydrostatic external pressure and the oven temperature is adjusted as desired. Gold is a flexible metal, allowing the deflation or inflation of the capsule, according to the difference in pressure

between the inside and the outside of the capsule, ensuring the material stays at the same pressure as the pressurising medium (Monthioux et al. 1985).

Experiments in kerogen and oil cracking show that the most significant effect on confined pyrolysis artificial maturation is temperature and not pressure (Hill et al. 1996; Monthioux et al. 1985). However, pressure still has some effect on chemical development, especially at lower temperatures (e.g. the increase of viscosity) and still needs to be accounted for, to truthfully reproduce what happens in natural systems (Domine 1989; Michels et al. 1995).

Confined pyrolysis has the advantage of being a controllable environment. All the reaction products are the result of the reagents inserted in the capsule, and not from interactions with the outside environment (Gupta et al. 2007). However, this can also be a disadvantage. The primary reactions products may react with the sample or even between themselves, making the secondary reactions more severe than in natural environments, where these products would be allowed to escape through the sediment (Saitta, Kaye & Vinther. 2018).

2.2. ToF-SIMS

Time-of-Flight Secondary Ion Mass Spectrometry (ToF-SIMS) is a high-resolution analytical technique used to study the elemental and molecular composition of samples (Thiel & Sjövall 2011). In this technique, a high-energy ion beam (also denominated by primary ions) is directed onto a preselected small area of the sample. This impact results in the emission of secondary ions from the outermost layers of the sample surface. The secondary ions are then separated by mass in the ToF detector. Firstly, they are accelerated by an electrostatic field that gives them all the same kinetic energy, so that the time they take to reach the detector is based only on their masses, with heavier ions taking more time to reach the detector. This "flight time" can then be translated into a mass spectra of the sample surface (Vickerman 2001).

ToF-SIMS has been an extremely valuable technique in the chemical characterization of a variety of samples. Firstly used in inorganic and polymer studies, it has been effectively adapted to biological studies (Thiel & Sjövall 2011). Its main benefits are the small sample size needed (only around a few micrometres) and the fact that it allows for spatial resolution. Since the ion beam scans a preselected area of the sample, it allows the elemental detection *in situ*, something lost in other chemical techniques such as Py-GC/MS. However, it should be kept in mind that although not a macroscopically visible destructive analysis, ToF-SIMS is not without molecular damage. To have the secondary ions emission there needs to be a fragmentation of the molecule present on the sample (Thiel & Sjövall 2011).

A critical aspect when using ToF-SIMS is sample preparation. Since it is a surface analysis technique, any small contamination can be detected, influencing the results. The same way, samples with coarse topography can become an issue, because it will affect the ion's time of flight. This is observed in a decrease of the signal obtained from the sample and in the peak shape in the spectrum, creating artificial broad peaks and double peaks. Therefore, samples should be as flat as possible, without any rough surfaces, to allow a good signal and a reliable spectrum (Thiel & Sjövall 2011).

2.3. ATR-FTIR

Infrared spectrometry is a technique that exploits the fact that different chemical bonds absorb specific frequencies of infrared radiation. This infrared radiation is of lower energy than the dissociation energy (Table 1) so it doesn't break the bonds, it only makes them vibrate. A mid-infrared beam (400 - 4000 cm^{-1}) is emitted onto the sample and measured after interacting with the matter (Smith 2011). A graph of the transmitted frequencies is produced and by analysing which frequencies were absorbed, the different functional groups can be identified.

Chemical bonds can vibrate in different ways, either changing the length of the bond (stretching) or changing the angle (bending). Stretching between two functional groups can be symmetrical or asymmetrical. Changes in the angle can be between functional groups, between groups of functional groups, in-plane or between different planes. These are called vibrational modes and they depend on the overall number of atoms in the molecule and their configuration. Each vibrational mode has a specific energy, making the same bond have different energies, depending on the vibration happening (Sherman Hsu 1997).

In traditional Fourier Transform Infrared Spectroscopy (FTIR), solid samples need to be ground and mixed with a matrix (usually potassium bromide, KBr), to be analysed. This technique is time-consuming and it can be challenging to obtain a homogenous mixture of matrix and sample. The results obtained are also hard to reproduce because the previously used ratio of sample to the matrix can be hard to obtain (Smith 2011).

However, in Attenuated Total Reflection (ATR) mode, the sample is placed in direct contact with a high reflectance crystal, without being mixed in a matrix. An infrared beam is emitted onto the crystal where it will be reflected internally. When the beam reaches the top surface, it interacts with the sample surface (c.a 0.5 to 5 μm), with the different bonds of the sample absorbing certain wavelengths. The beam continues through the crystal until reaching the detector that identifies which wavebands have been absorbed by the sample. This information undergoes a mathematical Fourier transformation, in order to transform the raw data into a graph of absorbance in relation to the wavelength. This method removes reproducibility and homogeneity problems since the samples don't need previous preparation to be analysed (Smith 2011), except surface cleaning of contaminants.

3. METHODS

3.1. Fresh samples

The manufacture of synthetic melanins is dependent on specific monomers such as L-DOPA or tyrosine. Synthetic melanins present a different chemistry and morphology when compared with natural melanins (D'Alba & Shawkey 2019), making results obtained with synthetic melanins not comparable to the behaviour of natural melanin. It has long been accepted that melanin extracted from *Sepia officinalis* (known as *Sepia* melanin) is the most easily obtained and natural form of melanin and a reliable standard for melanin (Zeise et al. 1992). Melanin extracted from cephalopod ink sacs will serve as the standard for this study. Artificial maturations and posterior chemical analysis will also be performed in the purified ink.

Fresh squid ink sacs were previously collected and kept frozen in a 50 ml falcon tube until melanin extraction. Melanin extraction was done following the enzymatic extraction method by Liu et al. (2003) with some alterations. This method applies several proteinases and surfactants to break down all molecular components until all that remains is melanin (Table 2) instead of strong acid/base reactions. It has been proved that acid/base extraction of melanin destroys melanosomes and alters melanin chemistry (Liu et al. 2003; Ito 1986). In comparison, enzymatic extraction retains melanosome morphology and it doesn't affect melanin chemistry, resulting in the extraction of unaltered melanin (Liu et al. 2003; Colleary et al. 2015).

Table 2: Solutions used in melanin extraction via enzymatic method adapted from Liu et al. (2003) and Colleary et al. (2015). PBS - Phosphate-buffered saline buffer; DTT – Dithiothreitol; Papain and Proteinase K are broad spectrum proteases.

SOLUTIONS	CONCENTRATION
A	10 mg DTT powder per 1 ml PBS
B	100 mg DTT and 4 mg Proteinase K per 10 ml PBS
C	50 mg DTT and 10 mg Papain per 10 ml PBS
D	20 mg DTT and 4 mg Proteinase K per 10 ml PBS

To the ink sacs, 10ml of solution A was added, and it was left for 24 hours incubating at 37°C and 200 rpm in a shake incubator. The supernatant was then removed by centrifugation (10 min at 4226 rcf) and 10 ml solution B was added. The ink sacs were incubated for another 24 hours at 37°C, 200 rpm. After the removal of the supernatant, there were still remains of ink

sacs, and a clear pellet had not been formed. Therefore, another incubation with solution B was performed (5 ml, 24 hours, 37°C, 200 rpm). After the repetition of this step, the remains of ink sac had disappeared, and a clear pellet had been formed. The pellet was then washed 6 times, each time in 2 ml of deionized water, after which, 5 ml of solution C was added, and left in incubation for another 24 hours at 37°C, 200 rpm. After incubation, the pellet was washed 6 times with deionized water (2 ml) and left incubating in solution D (5 ml) for 24 hours at 37°C, 200 rpm. After the incubation period, the supernatant was removed and a 2% Triton X-100 solution (5 ml) was added and left stirring for 4 hours. The supernatant solution was then removed, and the pellet washed 10 times with deionized water. One last incubation at 37°C, 200 rpm for 24 hours with 5 ml of solution D was performed, after which the pellet was washed 3 times in ethanol.

Between these last washings with ethanol, a fine reflective sheen could be observed at the surface of the pellet, and during vortexing, typical surfactant bubbles were observed, visually indicating there were still traces of Triton X-100. This was chemically proved by analysis on ToF-SIMS (performed in Newcastle University by Professor Ian Fletcher), that showed the presence of surfactant residues. A series of further washings with deionized water were performed, but the Triton X-100 presence was still visually noticeable. Molluscs possess high levels of polysaccharides in their tissues (Wang et al. 2017) and it was thought that an interaction between the surfactant and polysaccharides could be happening (Pitha et al. 1979). The polysaccharide removal was performed following the Fang et al. (1992) protocol to remove polysaccharides from plant DNA extractions.

A 2.0 M solution of Tris-HCl-EDTA and NaCl was added to the pellet. After 4 washes of 5 ml, there were fewer signs of the reflective sheen and, during vortexing, there were fewer surfactant air bubbles. Further 5 final washes with deionized water and ethanol were performed. ToF-SIMS analysis was repeated, and it showed that the surfactant signal had been reduced to minimal levels with no effects in melanin chemistry. SEM imaging also showed that melanosome shape suffered no alterations. The purified melanin was then air dried and stored in the freezer.

3.2. Artificial maturation

The cephalopod purified melanin was artificially matured using the confined pyrolysis method (Monthioux et al. 1985). The melanin was subjected to three different sets of temperature and pressure (100 °C/100 bar; 200 °C/200 bar; 300 °C/300 bar) to recreate the mildest and the most extreme conditions that fossil melanin might have been subjected. Melanin has also been matured separately with two different sulfur species: elemental sulfur (S_8) and sodium sulfide hydrate ($Na_2S.xH_2O$) (Table 3).

The artificial maturation of melanin allows the study of the effects that different sets of temperature/pressure, i.e the different diagenetic histories, have on the chemical structure of eumelanin. The artificially matured eumelanin with sulfur species will be investigated in terms of sulfur incorporation in the eumelanin chemical structure and if these reactions produce pheomelanin-like moieties.

Elemental sulfur was used as a form of control, as it is the simplest form of sulfur, while $Na_2S.xH_2O$ was used as the most accurate representation of the natural processes of bacterial respiration. H_2S (the same product released by bacteria) is released when sodium sulfide reacts with water. In the confined space of the capsule and with the elevated temperatures and pressures it is expected that H_2S would react with the melanin, allowing, therefore, to study the diagenetic incorporation of sulfur into this molecule.

Artificial maturation was performed in the School of Earth Sciences of the University of Bristol, with the supervision of Dr Richard Brooker, following the confined pyrolysis method. 3 mm diameter gold tubes were used to create the maturation capsules. The tube was cut to a length of around 1 cm. One end was welded shut using a tungsten needle. The samples were loaded onto the tube (for weight see Table S1) and then the other end was shut, forming a

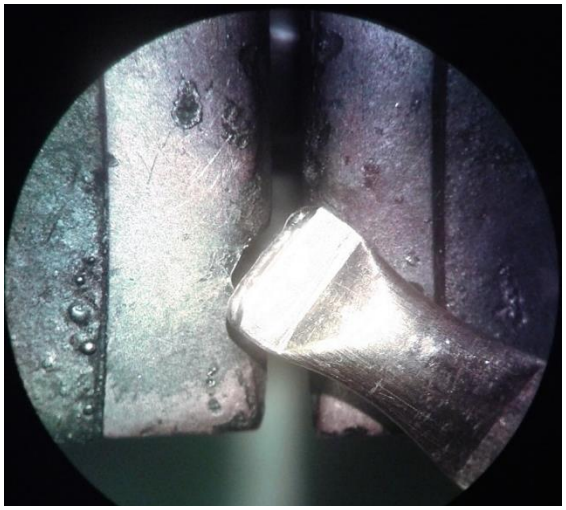

Figure 9: Magnified view of a capsule used for maturation experiments after wielding both ends. Capsule length around 1 cm.

capsule (Fig. 9). Capsules were loaded first with the sulfur material, then the melanin material to avoid combustion when welding shut the capsule.

A cold seal Titanium-Zirconium-Molybdenum-Alloy (TZM) pressure vessel (Fig. 10) was used to conduct the artificial maturation. In this equipment, the pressure vessel is fixed vertically on the end of a pressurization system. A vertical tube furnace is placed over the pressure vessel and heated to the required temperature. The sample is held at the correct place at the top of the pressuring vessel, the hot spot, by an internal support rod. The temperature increase will make the pressure fluctuate, so the pressure was adjusted according to the desired temperature until stable (around 30 minutes). After a 24-hour period, the samples were rapidly quenched, i.e. rapidly moved from the hot spot into the cold zone outside the furnace.

Figure 10: TZM (Titianium-Zirconium-Molybdenum-Alloy) pressure vessel used in artificial maturation experiments. Dr Richard Brooker laboratory at the Earth Sciences Department, University of Bristol.

To remove the samples from the capsule, both ends and one of the sides were cut using a wire cutter. The top part of the capsule was open with the help of a sterile scalpel blade and the contents were then tipped into an Eppendorf tube. Some material was lost due to it being stuck on the walls of the capsule. Effluents (the gases released during maturation that get trapped inside the capsule) were not analysed.

Table 3: Artificially matured samples experimental conditions. Null: Eumelanin only, no sulfur species; S_8: Elemental sulfur; $Na_2S.xH_2O$: Sodium sulfide; Pressure (P) in bar; Temperature (T) in °C. Samples number 9, 15 and 16 were matured for 42+ hours and were not analysed.

Sulfur species / **P/T (bar/°C)**	**Null**	**S_8**	**$Na_2S.xH_2O$**
100/100	7, 17	5	11, 12
200/200	1,2	3,4	13, 14
300/300	8, 10	6	18, 19

3.3. Fossil samples (location and age)

For the fossil analysis, a broad amount of fossil coleoid ink sacs were obtained, from diverse localities and ages (Fig. 11 and Table 4), ranging from the Carboniferous to the Cretaceous. In some cases, only the ink sac got preserved, without any soft tissue preservation that could indicate the specimens' taxonomy.

As discussed in section 1.3.3., it is still debated if ammonoids possessed an ink sac or not. Melanin traces have been found in the body chamber of several ammonites (Doguzhaeva et al. 2007, L. Doguzhaeva et al. 2004), however without conclusive presence of an ink sac (Klug & Lehmann 2015). The melanin presence could be explained as derived from other melanin-bearing organs (Klug & Lehmann 2015). While definite conclusion on the presence of an ink sac in ammonoids is not an objective of this work, the dark material will be submitted to the same chemical analysis as the fossil ink sacs and tested for melanin signal.

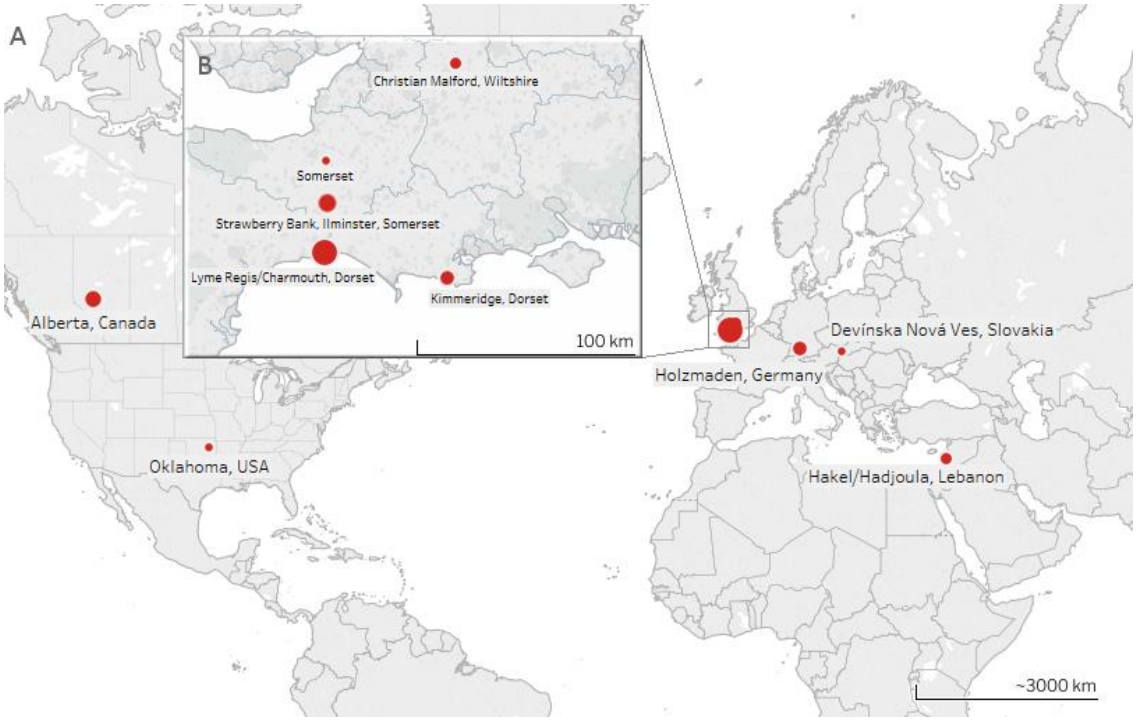

Figure 11: (A) Fossil samples location with mark size representing the number of samples from each location. United Kingdom (21 samples), Canada (4), Germany (3), Lebanon (2), USA, (1), and Slovakia (1). (B) Detailed map of United Kingdom localities. Charmouth and Lyme Regis (10 in total, computed as one location for clearer map reading), Strawberry Bank, Illminster (5), Kimmeridge (3), Christian Malford (2) and Somerset.

The fossil samples were gathered form a diversity of locations, reflecting different diagenetic histories, such as maturation degree and fossilization in different environments. The specimens also cover a large expanse of coleoid evolutionary history. The oldest sample (OK D-10) is from the Carboniferous. During this period, stem-coleoids were internalising their shells and going through the beginning of coleoid diversification (Kröger et al. 2011). The most recent sample is from the Upper Cretaceous, a time when coleoids were already diversified into Octobrachia and Decabrachia (Kröger et al. 2011; Tanner et al. 2017). From the analytical point of view, the large data set will ensure the chemical analysis is robust and assumption can be safely made.

Table 4: Fossil samples information on location, age, and taxonomy.

SAMPLE CODE	LOCATION	AGE	TAXONOMY
LR1	Lyme Regis, Dorset	Lower Jurassic	*Loligosepia*
LR2	Charmouth, Dorset	Lower Jurassic	Unidentified coleoid
LR3	Lyme Regis, Dorset	Lower Jurassic	Isolated ink sac
LR4	Charmouth, Dorset	Lower Jurassic; Obtusum Zone (upper Sinemurian)	Unidentified coleoid
LR5	Charmouth, Dorset	Lower Jurassic	Unidentified coleoid
LR6	Lyme Regis, Dorset	Lower Jurassic	Unidentified coleoid
LR7	Charmouth, Dorset	Lower Jurassic; Obtusum Zone (upper Sinemurian)	Unidentified coleoid
LR8	Lyme Regis/Charmouth, Dorset	Lower Jurassic	Unidentified coleoid
LR9	Lyme Regis/Charmouth, Dorset	Lower Jurassic	Unidentified coleoid
LR10	Lyme Regis/Charmouth, Dorset	Lower Jurassic, top of Blue Lias	Unidentified coleoid
K1	Kimmeridge, Dorset	Upper Jurassic	Ammonite
K1987	Kimmeridge, Dorset	Upper Jurassic	*Trachyteuthis*
K2	Kimmeridge, Dorset	Upper Jurassic	*Belemnoteuthis*
Leb1	Lebanon	Cretaceous	Coleoid in limestone
PRW 220	Christian Malford, Wiltshire	Middle Jurassic, Callovian	*Belemnoteuthis*
PRW 682	Christian Malford, Wiltshire	Middle Jurassic, Callovian	*Belemnoteuthis*
BRLSI M1224A	Strawberry Bank, Ilminster, Somerset	Lower Jurassic	*Loligosepia*
BRLSI M1225A	Strawberry Bank, Ilminster, Somerset	Lower Jurassic	*Loligosepia*
BRLSI M1227A	Strawberry Bank, Ilminster, Somerset	Lower Jurassic	*Loligosepia*
BRLSI M1228	Strawberry Bank, Ilminster, Somerset	Lower Jurassic	*Loligosepia*
BRLSI M1235A	Strawberry Bank, Ilminster, Somerset	Lower Jurassic	*Beloteuthis schubleri*
YPM 221211	Holzmaden, Germany	Lower Jurassic, Late Toarcian	Unidentified coleoid
YPM 221213	Holzmaden, Germany	Lower Jurassic, Late Toarcian	Unidentified coleoid
YPM 221214	Holzmaden, Germany	Lower Jurassic, Late Toarcian	Unidentified coleoid
OK D-10	Oklahoma, USA	Carboniferous	Unidentified coleoid

SAMPLE CODE	LOCATION	AGE	TAXONOMY
“Octopus”	Lebanon	Cretaceous	Unidentified octopod
SOM1	Watchet, Somerset	Jurassic	Unidentified coleoid
TMP 2013.036.0005	Ya Ha Tinda, Alberta, Canada	Lower Jurassic, Pleinsbachian	*Paraplesioteuthis* (Teuthida)
TMP 2013.036.0008	Ya Ha Tinda, Alberta, Canada	Lower Jurassic, Toarcian	Unindentified
TMP 2014.021.0058	Ya Ha Tinda, Alberta, Canada	Lower Jurassic, Toarcian	*Loligosepia*
TMP 2014.021.0059	Ya Ha Tinda, Alberta, Canada	Lower Jurassic, Toarcian	*Loligosepia*
SNM Z20058	Devínska Nová Ves, Slovakia	Upper Cretaceous	*Sepia juliebarborarum*

3.4. ToF-SIMS

ToF-SIMS analysis was carried out at the NEXUS facility of the Newcastle University by Professor Ian Fletcher.

No previous treatment was performed on the samples except for the TMP samples that were washed beforehand with a 1:1 solution of methanol and dichloromethane and the matured samples with $Na_2S.xH_2O$, that were analysed before and after washings with a mixture of deionized water and HCl, to ensure to total removal of Na_2S that didn't react. Most fossil samples were collected with the use of a sterile scalpel blade and sterile aluminium foil. However, some fossil samples were obtained from diverse sources and the collection methods used are unknown (namely the Canada and Slovakia samples).

All samples were mounted onto SEM stubs using double-sided copper tape. The stubs were then mounted onto a sample holder suitable for ToF-SIMS analysis.

The analysis was carried out in an ION-TOF 'TOF-SIMS IV – 200' instrument (ION-TOF GmbH, Münster, Germany) of single-stage reflectron design (Schwieters et al. 1991) (Fig. 12). Positive and negative ion static SIMS spectra were recorded from the upmost layer of the sample surface (ca. 1 nm) at room temperature using a Bi_3+ liquid metal ion gun, incident at 45° to the surface at 25 keV energy, operating in "bunched" mode for high mass resolution. The spatial resolution was limited by the primary ion beam diameter to ca. 4 µm. Raw data containing the secondary ions recorded at each pixel was acquired with a 128 × 128-pixel raster and a field of view of 50 µm × 50 µm.

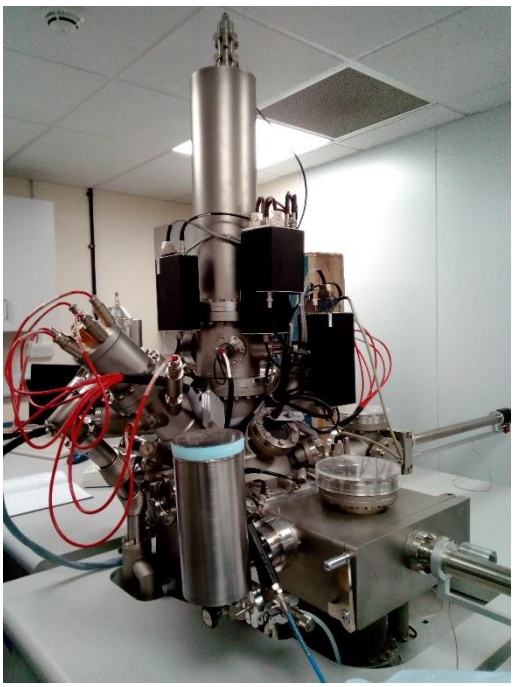

Figure 12: ION-TOF 'TOF-SIMS IV – 200' at NEXUS facility in Newcastle University.

A positive and three negative ion spectra were obtained per sample (except LR7, from which it wasn't possible to obtain any viable spectrum) using predesigned chemometrics for the specific melanin peaks (Lindgren et al. 2014). The area defined by each peak was converted into counts and the results exported into an EXCEL spreadsheet.

3.5. ATR-FTIR

Data were acquired using Perkin-Elmer Spectrum Two FT-IR Spectrometer (Fig. 13) located in the Teaching Laboratories in the Chemistry Department of the University of Bristol. The crystal and clamp were cleaned with isopropanol wipes before any data acquisition, and a background spectrum correction was performed. A background spectrum is a spectrum obtained without any sample placed in the crystal, therefore accounting for the environmental conditions (such as air) that would otherwise also show in the results. This background spectrum is subtracted from the final spectrum, ensuring that the results obtained correspond solely to the sample chemistry.

Samples were placed directly onto the crystal using a spatula. Enough material to cover the crystal (dimensions around 1 mm x 1 mm) was used. The sample was firmly secured in contact with the crystal using the integrated clamp. The force used was adjusted considering the spectrum seen on screen in preview mode.

For data acquisition, a range between (600 - 4000 cm^{-1}) was used with a 1 cm^{-1} resolution. The program was set on default to acquire 4 spectra per sample and compute them together making a mean spectrum. Equipment and utensils were cleaned with isopropanol wipes between samples to avoid cross-contamination.

Not all samples were analysed via FTIR due to sample availability. All artificially matured samples (Table 3) were analysed as well as the purified ink, serving as the eumelanin control. All samples from Holzmaden, Christian Malford, Strawberry Bank, and Ya Ha Tinda were analysed as well as SOM1. From the Lyme Regis/Charmouth samples, LR8 and LR10 were not analysed as well as Kimmeridge sample identified by K1. Samples identified by Leb1, OK D-10, “Octopus”, and DNM Z20058 were not analysed (Table 4).

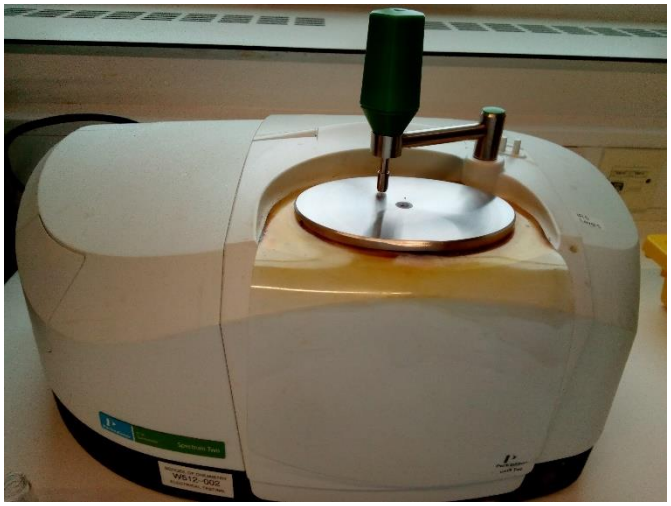

Figure 13: Perkin- Elmer Spectrum Two FT-IR Spectrometer. Chemistry Department at the University of Bristol.

4. RESULTS/DISCUSSION

4.1. ToF-SIMS

The most complete fossil melanin chemical analysis to this date has been performed by Colleary et al. (2015), where ToF-SIMS data of fossil and artificially matured samples have been analysed via Principal Component Analysis (PCA). By only analysing the characteristic melanin peaks using PCA (Lindgren et al. 2014), the ToF-SIMS spectra obtained from extant, fossil and artificially matured melanin can be differentiated. PCA is a multivariate statistical analysis used to identify relevant information in large and complex datasets. The relevant information from the data is extracted and expressed as a set of new orthogonal variables called principal components, compressing the size of the dataset (Abdi & Williams 2010). Data are plotted according to similarities, allowing patterns to be discerned (Cumpson et al. 2015; Naumann et al. 1988).

While PCA proves to be a valid statistical analysis to have a distribution pattern overview, it has its limitations. Adding new samples to original datasets can change the way PCA interprets the data due to newfound similarities or disparities between samples. There is also an inherent statistical bias that can come from sample size disparity. When large amounts of heterogeneous samples are being studied, the statistical analysis can overlook minor differences in the dataset in favour of the major differences. The small nuances in the dataset can be further analysed, either by reducing the datasets to homogenous samples or by using other statistical analysis (Parsons et al. 2009).

In the PCA analysis performed in Colleary et al. (2015), the main trend observed is a variation in fossil and artificially matured samples (PC1). The freshly extracted melanin and fossil melanin plot in opposite regions of the score plot. Artificially matured samples plot in an intermediate region between freshly extracted and fossil samples, with milder conditions (200 °C/ 250 bar) plotting closer to the fresh melanin while higher temperatures (250 °C/ 250 bar) plot closer to the fossil samples. However, within the fossil samples, PC1 explains the variability of taxonomy. The trend in PC2 is the chemical distinction between pheomelanin and eumelanin. Diagenetic history or geological age do not seem to be the more relevant factors of variance in the Colleary et al. (2015) dataset.

In this project, ToF-SIMS data interpretation via PCA was done using two separate datasets. Firstly, the newly acquired data (fossil cephalopods ink sacs and artificially matured samples with and without sulfur species) were added to the Colleary et al. (2015) original dataset and analysed. The main objective of this analysis is to study the overall sample distribution

pattern within the previously identified clusters (fresh, artificially matured, fossil, and negatives) and to identify outliers from these clusters. It is expected that the artificially matured samples plot with the previously matured samples while the fossil samples are expected to plot on the area occupied by the fossil samples. Samples plotting outside the correspondent clusters (or "categories") or within the negatives (non-melanin samples) will be identified as outliers and individually studied and interpreted. Since all fossil data added to the Colleary et al. (2015) data correspond to cephalopod ink sacs it is expected that these samples will plot next to previously analysed ink sacs, since taxonomy was one of the most relevant factors in the variance of Colleary data plot.

Secondly, the newly data acquired were plotted by themselves, thus removing taxonomic and melanin types variability, to study what other factors are important for melanin identification and preservation, including the impact of burial history and geological age. Another aspect that will be studied is the secondary incorporation of sulfur into the eumelanin molecule. PCA will allow to study if it is possible to see differences in the artificially matured samples chemistry compared with pure eumelanin, synthetic pheomelanin, and fossil eumelanin samples with naturally incorporated sulfur.

Keeping the previously used analysis methodology to avoid sampling bias, only one of the three ToF-SIMS negative ion spectra acquired per sample (or six spectra in some matured samples, accounting for replicates) was included in the PCA analysis. These were chosen based on the overall peak detection (the number of counts in each variable) and the relative intensity between known fossil melanin peaks (Lindgren et al. 2014). A synthetic pheomelanin spectrum (DOPA+Cysteinyl (1:1)) was also obtained, as well as a standard spectrum of eumelanin, obtained from the purified ink melanin. All fossil samples were included in the analysis except LR7 since no viable spectrum was obtained.

The counts of each characteristic melanin peaks (Lindgren et al. 2014, Colleary et al. 2015) were extracted from the negative ion ToF-SIMS spectra (Fig. S4-S50) using predesign chemometrics. Peak counts were normalized and mean-centred before statistical analysis. PCA was carried out using PAST software and posterior graph construction was performed in TABLEAU software.

4.1.1. PCA analysis with Colleary et al. (2015) dataset

4.1.1.1. Inorganics presence and their influence in PCA interpretation

ToF-SIMS is a surface analysis technique, where inorganic molecules, and topography greatly influence results (section 2.2). Contaminants derived from preparation and storage history of the samples, such as the use of consolidant or other chemicals can also influence the results obtained. Fossil ink sacs are known to have hydroxyapatite and calcite in association with melanin (Glass et al. 2012; Glass et al. 2013). Since only the negative ion spectra are used for PCA and the fact that melanin specific ions are extracted from the spectra, the presence of these ions don't seem to affect the melanin chemical analysis, the same way that gold coating doesn't seem to affect the results (Colleary et al. 2015).

The artificially matured samples with $Na_2S.xH_2O$ were presenting a strong inorganic signal upon analysis. One replicate of each experimental condition was washed with HCl and deionized water to remove unreacted sulfur (sample signal can be compared between replicates in Fig. S11-14 and S19-20) and reanalysed. The washings effectively reduced the inorganic signal, revealing a stronger melanin signal.

Samples matured with elemental sulfur were only analysed without cleaning of inorganics. In organic geochemistry, in bitumen and kerogen extractions, free sulfur is removed by reactions with activated copper (Kenig & Huc 1990; Hartgers et al. 1997; Scott et al. 2018), and it is possible that the same technique could be used to remove un-reacted elemental sulfur from these samples. Unfortunately, it wasn't possible to perform this technique as well as test the effects of copper in melanin. Melanin is known to chelate heavy metals, including copper (Wogelius et al. 2011), so tests would have to be run to analyse the influence of this metal in the melanin molecule before submitting the samples to this extraction. Results obtained and inferred from the artificially matured samples with elemental sulfur will be considered with caution.

4.1.1.2. Excluded sample (TMP 2013.036.0005)

In a first analysis, the newly analysed samples fit the maturation distribution of Colleary et al. (2015) data plot, with the exception of TMP 2013.036.0005 (Fig. S2). This sample appears in the opposite region of the cluster of fossil samples, near the fresh/matured samples, but not within any specific "category". During data acquisition, the ink sample spectrum showed a close resemblance with ethyl-cyanoacrylate, a constituent of common adhesives, known as "superglues". Adhesives and consolidates are sometimes used in fossil preparation and it has been shown that they can interfere with fossil chemical analysis (Saitta et al. 2018).

The presence of consolidant contamination in the sample surface was corroborated with the acquisition and comparison with the spectrum of a common consolidant (LOCTITE 401) (Fig. S1). Not only both spectra closely match in peak intensities and overall spectra pattern, when added to the PCA analysis (consolidant data treated for the specific melanin peaks) the two samples plot near each other in an isolated area of the plot. To avoid analysis bias from this clear outlier, this sample was excluded from the PCA analysis.

With clear outliers (TMP 2013.036.0005) excluded from the analysis, the samples analysed for this work and the Colleary et al. (2015) data were analysed through PCA (Fig. 14). Overall, most of the new samples fall within the expected area of the plot, in concordance with the Colleary et al. (2015) plot. The main sample variability explained by PC1 is difference between samples categories, while PC2 explains differences in melanin chemistry (eumelanin/pheomelanin).

4.1.1.3. Artificially matured samples

The new artificially matured samples fall next to the previously matured samples (Fig. 14) in an area distinct from the areas defined by the fossil samples. While the 100 °C/100 bar samples are completely within the area created by the fresh samples (represented in yellow), the 300 °C/300 bar samples (represented in dark orange) plot closer to the fossil samples in the PC1 axis, creating an apparent step-like "bridge" of increasing temperatures between the fresh and the fossil samples already observed in Colleary et al. (2015). This apparent progression of the level of maturation, from fresh to fossil, could be interpreted as the progressive changes that eumelanin molecule undergoes during diagenesis. The samples have had some chemical changes that make them chemically different from the fresh, non-matured melanin, but do not present the same chemistry as the fossil samples.

There could be two factors that explain why the most mature samples (300 °C/ 300 bar) do not overlap with the fossil samples. Firstly, here only maturation is being studied. There are other factors in the formation of fossils that could still account for the differences observed (such as environmental conditions or the influence of sediment in fossil chemistry). Secondly, while artificial maturation in gold-sealed capsules is the most adequate method for recreating natural maturation sequences, the confined space could trap some of the volatiles that would, in natural conditions, escape through the sediment. These volatiles can either reacts with the sample or adhere to the sample surface when the sample is rapidly quenched, creating artefacts in the analysed chemistry of the sample.

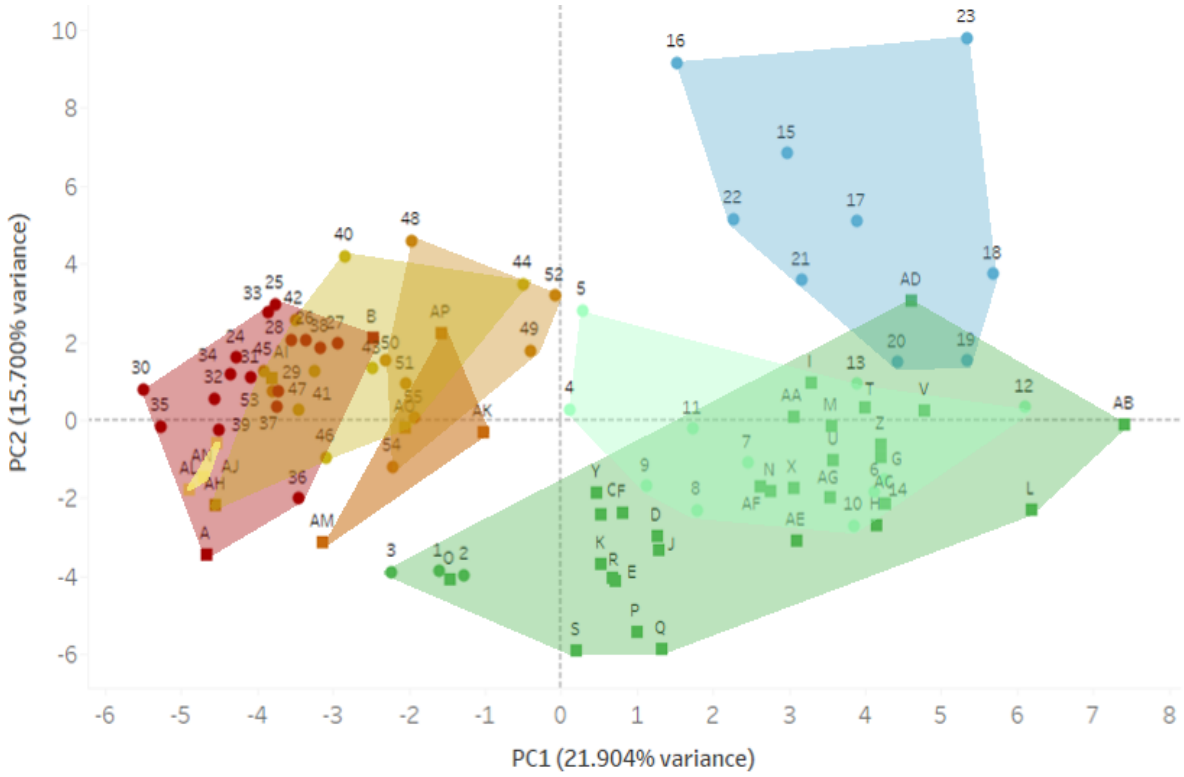

SYMBOL
- COLLEARY
- FERREIRA

COLOUR
- FRESH
- 100 °C/100 bar
- 200 °C/200 bar + 200 °C/250 bar
- 250 °C/250 bar
- 300°C/300 bar
- FOSSILS
- EUMELANIN FOSSILS
- NEGATIVES

Colleary dataset: Fossils: Ink sac, Lyme Regis (1), Cephalopods, Lebanon (2, 3), Isolated feather, Messel (4), Messelornis, Messel (5), Isolated feather, Fur Formation (6), Frogs, Messel (7, 8), Frogs, Mush Valley (9, 10), Tadpole, Enspel (11), Bats, Messel (12, 13), Cyclostome fish, Mazon Creek (14) **Negatives**: Recent oak leaf (15), Baker's yeast (16), Fossil angiosperm (17), Fossil *Sequoia* (18), Fossil leaf, Mush Valley (19), Rock matrix, Messel (20), Rock matrix, Mazon Creek (21), Rock matrix, Mush Valley (22), Carbon tape (23) **Fresh, 200°, 250°:** *Gallus gallus* (24, 40, 48), *Troglodytes aedon* (25, 49), *Anas platyrhynchos* (26, 41, 50), *Junco hyemalis* (27, 42, 51), *Columba livia* (28, 43, 52), *Dumetella carolinensis* (29, 44), *Gallus gallus* (30, 45, 53), *Corvus corone* (31, 46, 54), *Meleagris gallopavo* (32, 47, 55), *Pelophylax* kl. *esculentus* eye tissue (33, 34), *Pelophylax* kl. *esculentus* liver tissue (35), *Sepia officinalis* (36), *Columba livia* (37), *Columba livia* (38), *Pica pica* (39).

Ferreira dataset: Fresh: *Sepia officinalis* (A); Synthetic pheomelanin (B). **Matured:** 100 °C/100 bar (AL); 200 °C/200 bar (AH); 300 °C/300 bar (AM). **Matured with elemental sulfur:** 100 °C/100 bar (AJ); 200 °C/200 bar (AI); 300 °C/300 bar (AK). **Matured with sodium sulfide:** 100 °C /100 bar (AN); 200°C/200 bar (AO); 300 °C/300 bar (AP). **Fossils: Kimmeridge:** K1 (L); K1987 (M); K2 (N); **Lebanon:** Leb1 (O); "Octopus" (U); **Lyme Regis:** LR1 (C); LR2 (D); LR3 (E); LR4 (F); LR5 (G); LR6 (H); LR8 (I); LR9 (J); LR10 (K); **Strawberry Bank:** M1224A (P); M1225A (Q); M1227A (R); M1228 (S); M1235A (T); **Oklahoma:** OK D-10 (V); **Christian Malford:** PRW 220 (X); PRW 682 (Y); **Somerset:** SOM1 (Z); **Alberta:** TMP 2013.036.0008 (AA); TMP 2014.021.0058 (AB); TMP 2014.021.0059 (AC); **Slovakia:** SNM Z20058 (AD); **Holzmaden:** YPM 221211 (AE); YPM 221213 (AF); YPM 221214 (AG).

Figure 14: Principal component analysis of the negative secondary ions obtained from ToF-SIMS from fossil and artificially matured melanin samples. Spectra identified by numbers and circles previously used in Colleary et al. (2015). Spectra identified by letters and squares relative to samples analysed in this work. Information on the fossils can be found in Table 4 and Colleary et al. (2015) supplementary data Table S1.

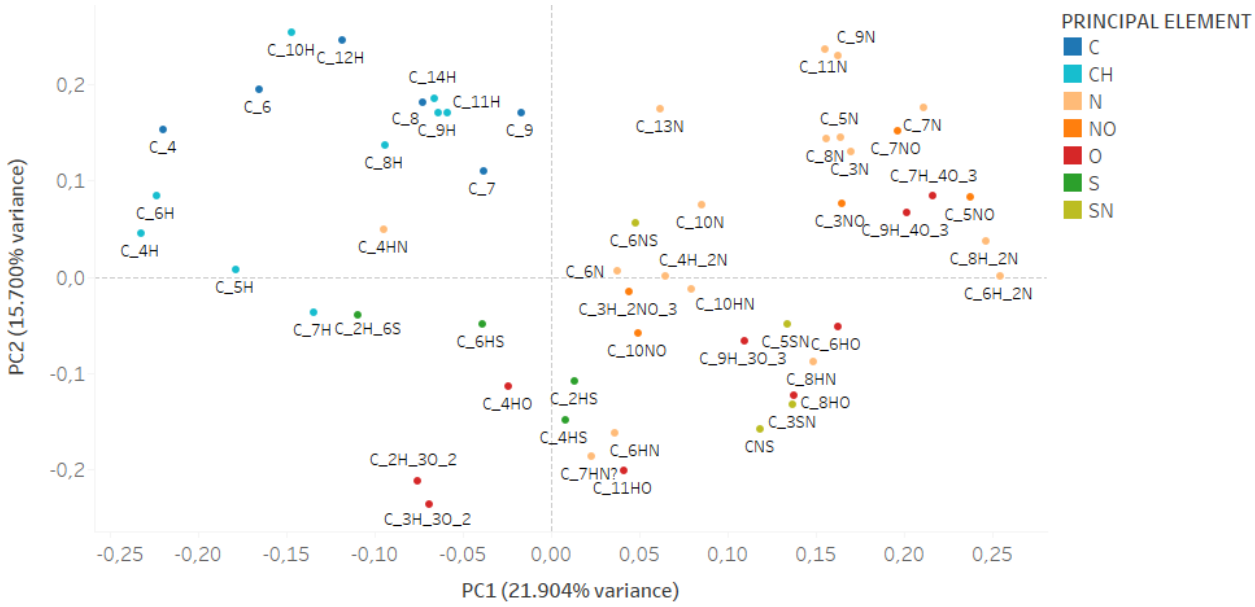

Figure 15: Loadings refer to the analysis at Fig. 14, with colours representing the major elemental contribution.

In the PC2 axis, the main trend from Colleary et al. (2015), namely a distribution by melanin type seems to be maintained. The newly analysed synthetic pheomelanin control sample (identified as B in Fig.14) plots in next to brown and grey samples analysed in Colleary et al. (2015) (such as sample number 27 and 50) and in a different region that the eumelanin sample (identified as A).

Artificially matured samples with sulfur species also plot in a distinct area from the eumelanin (A), closer to previously analysed pheomelanin samples with the exceptions being 100 °C /100 bar $Na_2S.H_2O$ (AN) and 100 °C /100 bar S_8 (AJ), which are closer to the non-sulfurized eumelanin samples (AH and AJ). This could mean that these conditions may be too mild for high-temperature dependent reactions to happen. Thiophenes and benzothiophenes, commonly found in diagenetic environments are known to be only formed in more mature environments (as seen in Fig. 3).

4.1.1.4. Fossil samples

The new cephalopod ink sacs do not plot next to the ones previously analysed (samples number 1 to 3) as expected, instead they overlap across the fossil samples, including fossil pheomelanin samples (Fig. 14). This shows that in this analysis, there are more factors than just taxonomy and melanin chemistry involved in the spreading on the data in the PC1 and PC2 axis.

An apparent plotting by location can be seen in some samples. Six of the nine samples from Lyme Regis plot together (C-F, J, and K). A Lebanon sample (O) plots next to cephalopod

ink sacs also from Lebanon (2, 3) from Colleary et al. (2015). Three of the five Strawberry Bank are also together (P, Q, and S). This could mean that there is a factor related with fossil location or age since most localities also present the same geological age, that could be influencing the distribution in PC1 and PC2 that needs further investigation.

Two samples that need to be analysed individually within the PCA and how they are being mapped are the Slovakia sample (identified as AD) and the purported melanin sample from an ammonoid (identified as L).

The Slovakia sample (AD) is mapped within the negative (non-melanin) area. SEM imaging obtained (Fig. S3) shows that this sample is constituted by melanin granules; however, there seems to be a layer of inorganic material that could be obscuring the melanin signal. Another factor to consider is the possibility of contaminants in the sample surface. The amount of material available for the ToF-SIMS analysis was minimal (sample size around 0.4 mm x 0.2 mm) so some contaminants from the copper tape may have been transferred to the sample when mounted onto the SEM stub for analysis.

The dark sample obtained from the ammonoid (L) is being mapped within the melanin samples and not within the negatives (non-melanin) samples or in a completely isolated area (such as TMP 2031.036.0005 in Fig. S2). This allows the inference that this sample has a valid melanin signal.

4.1.2. PCA analysis of eumelanin samples

To reduce the amount of variability within the samples (such as taxonomy and melanin chemistry), the newly obtained samples were analysed via PCA without any contribution from the Colleary et al. (2015) dataset (Fig. 16). This analysis will permit the study of the factors that are most relevant in the dataset composed by eumelanin fossil samples, eumelanin artificially matured with and without sulfur species and discern some plotting patterns observed in the previous analysis (Fig. 14).

4.1.2.1. Artificially matured samples

The artificially matured samples show the same trend in PC1 as in the previous plot (Fig. 14). The artificially matured samples, as well as the fresh samples (eumelanin and pheomelanin controls), are plotted in a distinct area from the fossil samples, without fossils and matured samples overlapping. The previously observed "step-like bridge" of increasing temperatures from the 100 °C/100 bar to the fossil samples is also seen along the PC1 axis. Within the fossil samples, the previously observed apparent plotting by location is still apparent and needs further scrutiny and interpretation.

The main trend described by PC2 in the artificially matured samples seems to be the presence of sulfur signal. Matured samples with sulfur species (AN, AJ, AI, AO, AP, and AK) are plotting in the positive PC2 axis with the synthetic pheomelanin, while matured eumelanin samples without sulfur species (AL, AH, and AM) plot in the negative side of PC2 with the *Sepia* eumelanin. Here, it is seen that there is a sulfur signal in both 100 °C/100 bar sulfur samples (AN and AJ) that was not noticeable in the previous plot (Fig. 14) since there was too much variability in the dataset for this to be considered a major difference. This could mean that these conditions, although too mild to produce significant changes in the eumelanin molecule (i.e the production of thiophenes and benzothiophenes), are still able to produce small alterations in the melanin chemistry.

Although the matured samples with sulfur species (AK, AP, and AO) seem to show a similar signal to synthetic pheomelanin (B), some aspects need to be clarified before conclusions are drawn. The PCA analysis could just be picking up the sulfur signal in the large dataset of mainly eumelanin and identify it as similar when compared with the large number of eumelanin samples without sulfur. When compared, the ToF-SIMS spectra of pheomelanin (Fig. S4) and AK, AP, and AO (Fig. S11, Fig. S18, and Fig. S20 respectively) show a great difference in overall patterning.

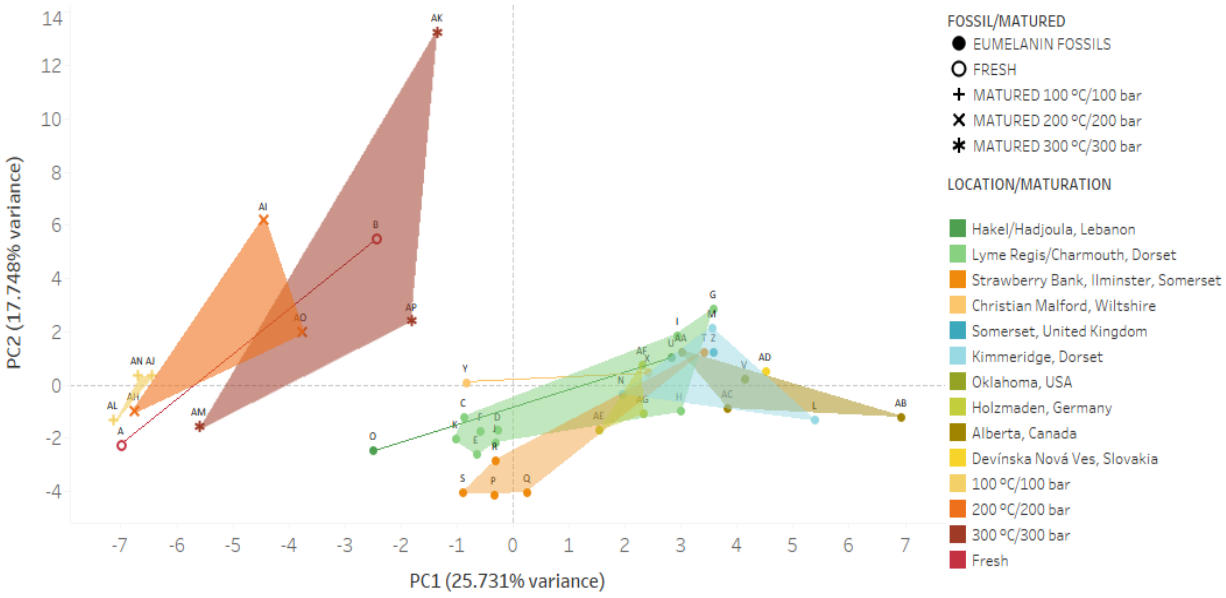

Fresh: *Sepia officinalis* (A); Synthetic pheomelanin (B). **Matured:** 100 °C/100 bar (AL); 200 °C/200 bar (AH); 300 °C/300 bar (AM). **Matured with elemental sulfur:** 100 °C/100 bar (AJ); 200 °C/200 bar (AI); 300 °C/300 bar (AK). **Matured with sodium sulfide:** 100 °C /100 bar (AN); 200°C/200 bar (AO); 300 °C/300 bar (AP). **Fossils: Kimmeridge:** K1 (L); K1987 (M); K2 (N); **Lebanon:** Leb1 (O); "Octopus" (U); **Lyme Regis:** LR1 (C); LR2 (D); LR3 (E); LR4 (F); LR5 (G); LR6 (H); LR8 (I); LR9 (J); LR10 (K); **Strawberry Bank:** M1224A (P); M1225A (Q); M1227A (R); M1228 (S); M1235A (T); **Oklahoma:** OK D-10 (V); **Christian Malford:** PRW 220 (X); PRW 682 (Y); **Somerset:** SOM1 (Z); **Alberta:** TMP 2013.036.0008 (AA); TMP 2014.021.0058 (AB); TMP 2014.021.0059 (AC); **Slovakia:** SNM Z20058 (AD); **Holzmaden:** YPM 221211 (AE); YPM 221213 (AF); YPM 221214 (AG).

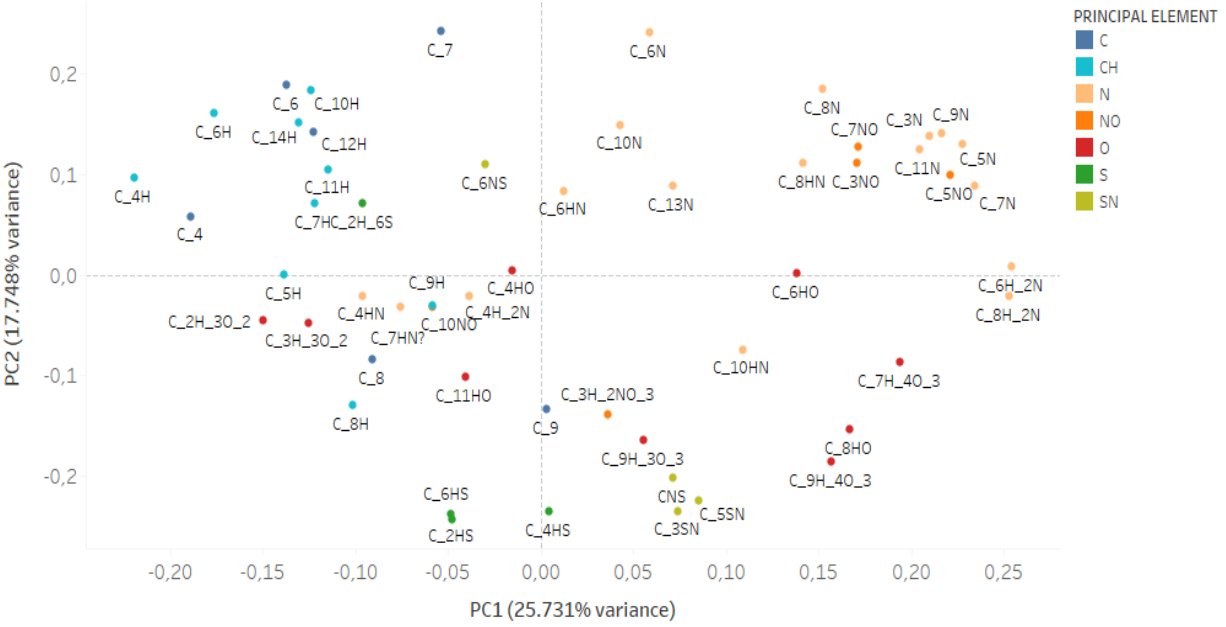

Figure 16: Principal component analysis of the negative secondary ions obtained from ToF-SIMS from fossil and artificially matured melanin samples. Above: Spectra identified by letters and squares relative to samples analysed in this work. Information on the fossils can be found in Table 4. Below: Loadings for this analysis, with colours representing the major elemental contribution.

Preliminary Py-GC/MS results of samples AO and AP (respectively 200 °C/200 bar and 300 °C/ 300 bar with $Na_2S.xH_2O$) (Fig. S95 and S96)) don't indicate any benzothiazine/benzothiazole units (indicative of pheomelanin presence), only thiophenes moieties, similar to diagenetic incorporated sulfur in fossil eumelanin (observed in sample C (Fig. S97) and Glass et al. (2012)). Another aspect to consider is the fact that the samples matured with elemental sulfur weren't cleaned before analysis so there could be non-reacted sulfur in the sample surface that could be influencing the results. Samples need to be cleaned of non-reacted sulfur and more samples need to be analysed before definitive conclusions can be drawn about the absence of pheomelanin markers.

4.1.2.2. Fossil samples and thermal maturity

Although a clear trend in PC2 in the fossil samples is not evident, there could be a sample plotting based on diagenetic sulfur content. Thiophenes moieties are found in preliminary Py-GC/MS results from sample identified as C (Fig. S97) although they are not found in the sample identified as G (Fig. S98) nor in artificially matured sample without sulfur species (sample identified as AM (300 °C/300 bar) (Fig. S94)). However, more pyrolysis results are needed before making further inferences as well as cleaning the artificially matured samples of non-reacted sulfur.

Some of the areas defined by the fossils are spread in the plot (Fig. 16), especially Lyme Regis and Strawberry Bank. However, six of the nine Lyme Regis samples analysed (C-F, K, and J), as well as four of the five samples from Strawberry Bank are mapped in a distinct area of the plot from Holzmaden (light brown area) or Kimmeridge (light blue). The two Lebanon samples are also spread, however in the previous analysis with the Colleary et al. (2015) data, other Lebanese samples plotted next to sample identified as O. This apparent plotting by fossil location, associated with the plotting of the artificially matured samples by increased geothermal conditions, could indicate that PC1 is plotting the data according to the level of thermal maturity, using T_{max} values as a proxy for maturity (Table 5). T_{max} values were described from the literature being, therefore, theoretical values and not experimentally obtained values. Literature for all sample locations describing thermal maturity could not be found.

Starting at the left side of the plot with the artificially matured samples plotting with slightly overlapping areas with increasing maturity (also seen in Colleary et al. (2015)), this trend

seems to follow on the fossil samples. Lyme Regis/Charmouth and Strawberry Bank fossils, that have gone through mild levels of thermal maturation (Lyme Regis T_{max} = 424 °C) plot in an intermediate area of the plot, while more thermally mature samples like Holzmaden (T_{max} = 435 °C) and Alberta, Canada (T_{max} = 436 to 447 °C) plot at the right side of the plot.

Table 5: Maturity level of the fossil locations based on Rock-Eval pyrolysis results. T_{max} refers to the temperature at which hydrocarbon generation reaches is maximum and is used as a proxy for organic matter maturity (415 °C -430 °C: immature; 430 °C -445 °C: matured; above 445 °C: over-mature) (Killops & Killops 2005). Not all fossil locations of the analysed fossils in this work are here referenced.

LOCATION	T_{MAX}	MATURITY LEVEL	REFERENCE
Christian Malford, UK	411 °C	Mild	Glass et al. 2012
Lyme Regis, UK	424 °C	Mild	Glass et al. 2012
Holzmaden, Germany	435 °C	Early mature	Glass et al. 2013; Prauss et al. 1991
Kimmeridge, UK	415 °C – 425 °C	Mild	Scotchman 1991
Slovakia	427 °C – 447 °C	Mild to Overmature	Janočko et al. 2006
Alberta, Canada	436 °C -447 °C	Mature to Overmature	Riediger 2002

The two samples that needed further scrutiny in the plot with Colleary et al. (2015) dataset, the sample from Slovakia (AD) and the melanin sample of an ammonoid (L) were also analysed in this plot.

The dark material found in the body chamber of an ammonoid, when plotted with the Colleary et al. (2015) dataset (Fig. 14), showed a mapping consistent with melanin signal. In this plot (Fig. 16), this sample plots in the right side of the plot, relatively close to other samples from the same location (Kimmeridge). The fact that it is not plotted in an isolated area of the map, and close to the other fossil eumelanin samples, further consolidates the conclusion that this sample is eumelanin.

The youngest sample analysed (Upper Cretaceous), coming from Slovakia (SNM Z20058 and identified in the plots as AD), is actually one of the most mature, with T_{max} ranging from mild to over-mature (427 to 447 °C). In this analysis (Fig. 16) it is plotted at the right side of the plot next to other highly matures samples (Alberta). This high level of maturity could explain why it was plotting in the negatives in the previous plot (Fig. 14), although here it is not plotted in an isolated area. Besides the possible contamination and matrix effect described before (section

4.1.1.3.), perhaps the sample has gone over the maturity level for melanin to be recognized in large heterogenous datasets (Fig. 14), therefore showing more resemblance to the negatives than with the melanin samples. Further analysis of melanin from high levels of maturity could help to pinpoint the highest level of maturity that melanin can withstand and still be recognizable. This, however, further increases the evidence for maturation being the defining factor in melanin survival in the fossil record, not age (Glass et al. 2013).

4.1.2.3. PC1 relation with thermal maturity

To test the apparent relation of PC1 with thermal maturity, PC1 values were plotted according to thermal maturity temperatures (T_{max}) (Fig. 17). Thermal maturity information couldn't be experimentally tested nor found in the literature for all the locations analysed in this work, making this analysis lacking in information for all samples analysed. Here only samples with theoretical T_{max} values were plotted corresponding to the samples from the locations described in Table 5.

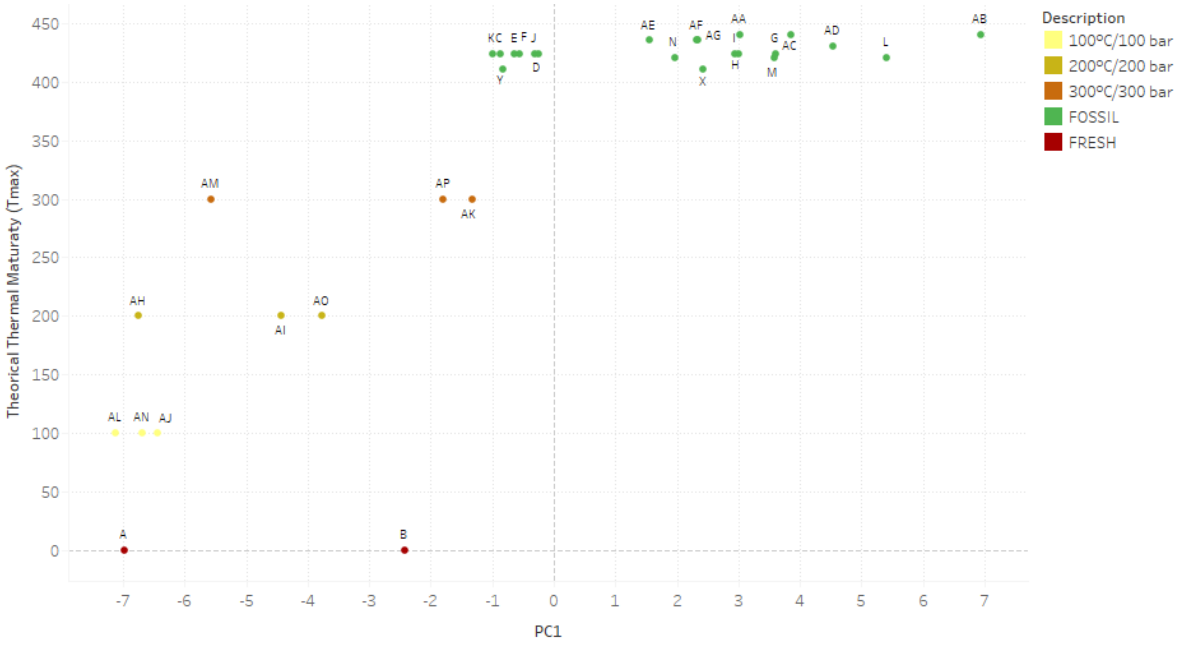

Figure 17: Correlation between PC1 values relative to PCA analysis of ToF-SIMS eumelanin data (R^2 =0.66273; p<0.0001). **Fresh:** Sepia officinalis (A); Synthetic pheomelanin (B). **Matured:** 100 °C/100 bar (AL); 200 °C/200 bar (AH); 300 °C/300 bar (AM). **Matured with elemental sulfur:** 100 °C/100 bar (AJ); 200 °C/200 bar (AI); 300 °C/300 bar (AK). **Matured with sodium sulfide:** 100 °C /100 bar (AN); 200°C/200 bar (AO); 300 °C/300 bar (AP). **Fossils: Kimmeridge:** K1 (L); K1987 (M); K2 (N); **Lebanon:** Leb1 (O); "Octopus" (U); **Lyme Regis:** LR1 (C); LR2 (D); LR3 (E); LR4 (F); LR5 (G); LR6 (H); LR8 (I); LR9 (J); LR10 (K); **Strawberry Bank:** M1224A (P); M1225A (Q); M1227A (R); M1228 (S); M1235A (T); **Oklahoma:** OK D-10 (V); **Christian Malford:** PRW 220 (X); PRW 682 (Y); **Somerset:** SOM1 (Z); **Alberta:** TMP 2013.036.0008 (AA); TMP 2014.021.0058 (AB); TMP 2014.021.0059 (AC); **Slovakia:** SNM Z20058 (AD); **Holzmaden:** YPM 221211 (AE); YPM 221213 (AF); YPM 221214 (AG).

This plot (Fig. 17) shows that there is some level of linear correlation between these two variables (R^2 = 0.66273; $p < 0.0001$). Although tentative, this analysis shows that the level of thermal maturity seems to be the principal component identified by PCA of the ToF-SIMS data. Since not all samples are plotted in this analysis, other statistical analysis or models (such as performing curve fitting) that could explain better the variability observed in PC1 were not performed in this work. Pheomelanin is an outlier in this analysis influencing the determination coefficient R^2. Experimentally obtained thermal levels of maturity should be obtained for these samples in future, making this correlation more robust.

4.2. FTIR

For a better understanding of the underlying chemical bonds present in the different maturation ranges, as well as the changes induced by secondary sulfurization, FTIR was performed. FTIR data were analysed not only quantitatively, by identifying and comparing which bonds change with maturation using the relative absorbance values, but also in a qualitative matter using PCA (Naumann et al. 1988; Bombalska et al. 2011). This approach will allow the data to be analysed and plotted based on the underlying chemical bonds (represented by specific absorbance peaks), and not the molecular fragments produced, as previously with ToF-SIMS. Studying the bond changes that occur with increasing temperatures in artificial maturation, allows for a better understanding of what happens to the molecular chemistry of eumelanin during diagenesis and how thermal maturity influences its preservation.

4.2.1. Peak identification and relative absorbance

4.2.1.1. Matured melanin without sulfur species

Analysis of the purified extant ink (used as standard eumelanin) (Fig. 18) shows a close resemblance with previously studied eumelanin (Glass et al. 2012; McNamara et al. 2016), with relevant peaks at 3262 cm^{-1} corresponding to hydroxyl (OH) stretching mode, 1566 cm^{-1} corresponding to carboxyl (C=O) stretch in indole quinone and 1339 cm^{-1} corresponding to in-plane bending modes of OH ± NH bonds. Another small peak at 1041 cm^{-1} can also be observed, corresponding to phosphate groups that could be chelated in the melanin, either from the original ink chemical composition or from the PBS buffer used during the extraction (section 3.1).

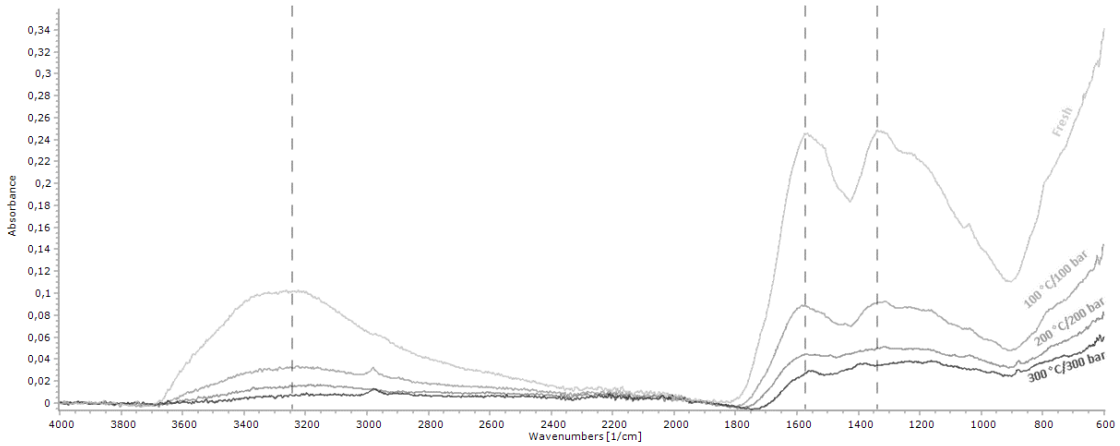

Figure 18: FTIR absorption spectra of artificially matured samples without sulfur species (Fresh and samples 2, 7, and 8). Vertical trace marks symbolize fresh melanin peaks.

The matured eumelanin without any sulfur species (Fig. 18) seems to undergo a progressive decrease in absorbance in the broad peak at 3500 cm^{-1} (OH stretching) with increasing temperature/pressure conditions. There is also an apparent loss of carboxyl groups, represented by a decrease in the absorbance in the CO peak (at approximately 1566 cm^{-1}). This decrease in absorbance with increasing temperatures is indicative of dehydration and decarboxylation, derived from the loss of hydroxyl and carboxylic functional groups (Fig 19). Hydroxyl and carboxylic groups are transformed in water and carbon dioxide molecules. Further bond breakages can lead to the fragmentation of the building blocks of eumelanin in indoles and pyrroles moieties, elements commonly found in Py-GC/MS studies of fossil eumelanin (Glass et al. 2012).

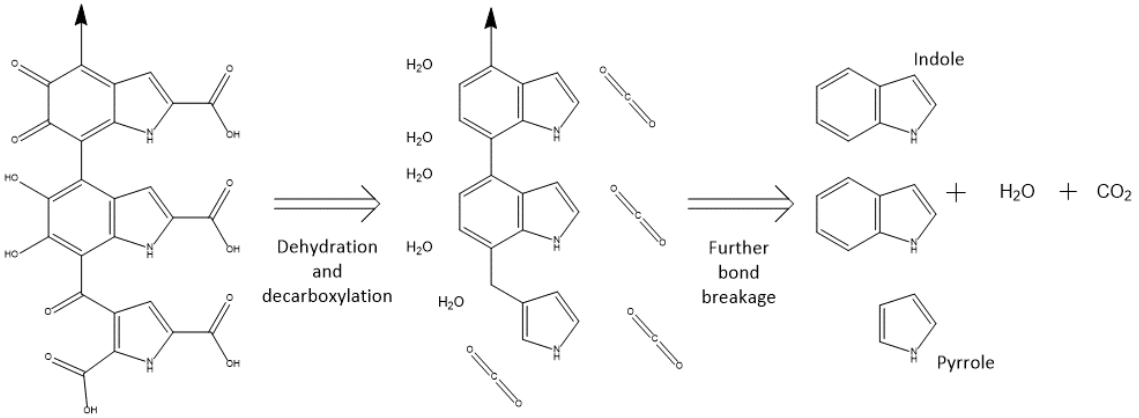

Figure 19: Possible eumelanin transformation seen in analytical pyrolysis. Increasing temperatures in maturation experiments lead to dehydration and decarboxylation with formation of water and carbon dioxide molecules.

4.2.1.2. Matured melanin with sulfur species

The samples matured with elemental sulfur seem to follow the same pattern as the samples matured without sulfur species (Fig. 20). The 100 °C/100 bar samples show a spectrum similar to the non-sulfurized counterpart, corroborating the assumption that these conditions are too mild for reactions to happen (section 4.1.1.3.). With increasing temperature, strong absorbance peaks appear between 1200-800 cm^{-1}, indicating that higher temperatures are inducing reactions that produce a different signal from eumelanin. However, the artificially matured samples with sulfur species (both elemental sulfur and sodium sulfide) were not cleaned before analysis. Therefore, at this stage, is not possible to confidently affirm that these reactions represent an organic signal (sulfur reacting with the eumelanin) or an inorganic signal (reactions happening only in the sulfur molecule).

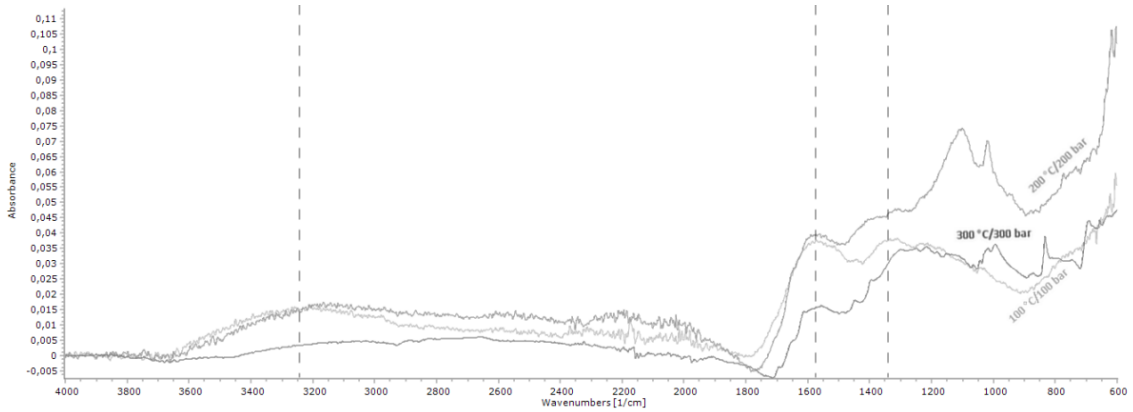

Figure 20: FTIR absorption spectra of artificially matured samples with elemental sulfur (Samples 3, 5, and 6). Vertical trace marks symbolize fresh melanin characteristic peaks. Samples not washed before analysis.

The presence of a strong inorganic signal from the non-reacted sulfur can be seen in the $Na_2S.H_2O$ samples (Fig. 21), where the melanin signal is completely obscured by the presence of sodium sulfide. The pyrolysis results of two samples matured with $Na_2S.H_2O$ show that there are thiophenes present in sample 13 (200 °C /200 bar) (Fig. S95) and 19 (300 °C/300 bar) (Fig. S96) allowing the assumption that the sulfur has reacted with carbon structures derived from the eumelanin during maturation. However, the conditions and processes behind the thiophenes formation can not be explained due to the strong presence of inorganic material interfering with the melanin signal.

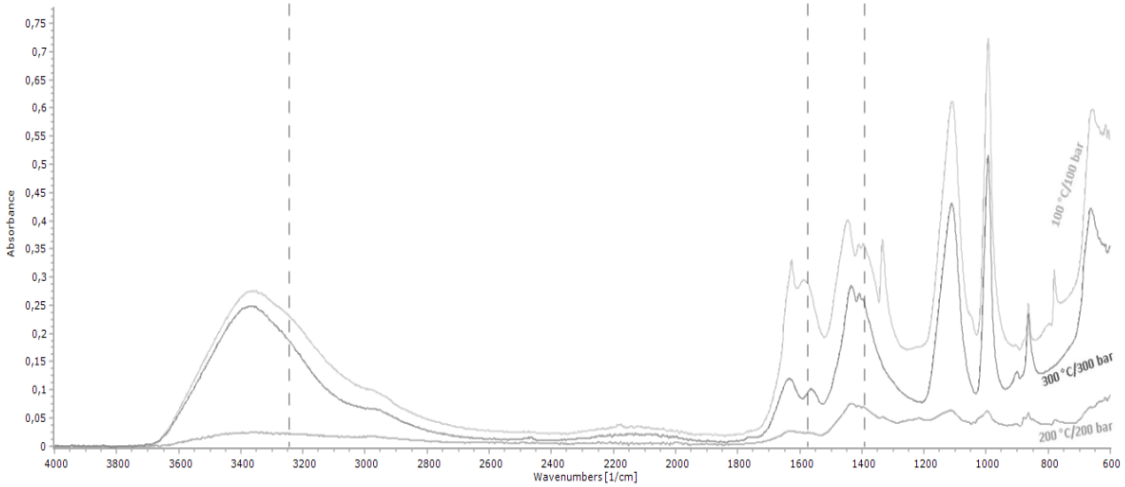

Figure 21: FTIR absorption spectra of artificially matured samples with sodium sulfide (Samples 11, 13, and 19). Vertical trace marks symbolize fresh melanin characteristic peaks. Samples not washed before analysis.

4.2.1.3. Fossil samples

FTIR analysis of the fossil samples shows an evident presence of hydroxyapatite and calcite in most samples (Fig. 22). Strong peaks at around 1796 cm^{-1}, 871 cm^{-1}, and 712 cm^{-1} are indicative of calcite presence while strong peaks at around 1035 cm^{-1}, 962 cm^{-1}, and 600 cm^{-1} are indicative of the presence of hydroxyapatite. These minerals are commonly associated with fossil cephalopod ink sacs, with hydroxyapatite being a common diagenetic product, while calcite probably originates from cephalopods' internal shells (Glass et al. 2012; Glass et al. 2013). Unequivocal peak identification is not possible due to the overlap of inorganic peaks derived from these minerals and possible organic peaks from diagenetic sulfurization (Table 6). Melanin characteristic peaks are also masked by the inorganic signal, making relative peak intensities unable to be determined.

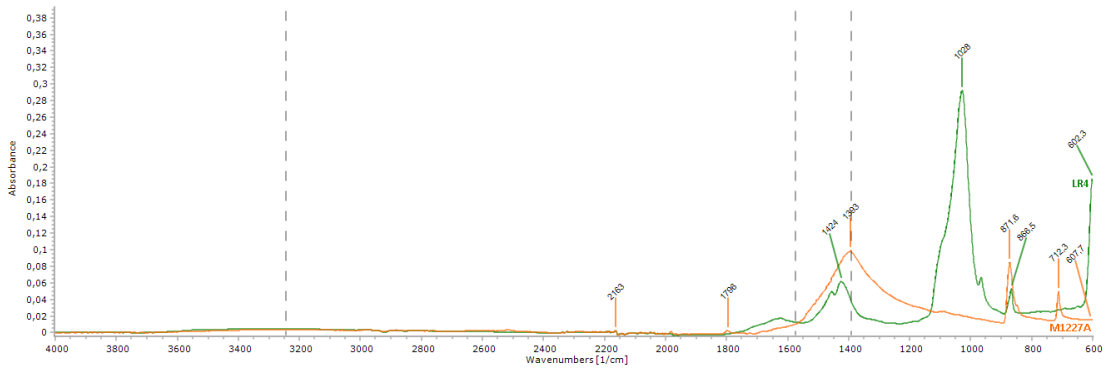

Figure 22: FTIR absorption spectra of fossil samples from Lyme Regis (LR4 (green)) and Strawberry Bank (M1227A (orange)). Major peaks for each sample identified by designated colour. Vertical trace marks symbolize fresh melanin characteristic peaks. LR4 shows the presence of characteristic hydroxyapatite peaks while M1227A shows the presence of calcite.

Table 6: Relevant FTIR peaks for melanin study (wavelength in cm^{-1}) with characteristic sulfur, hydroxyapatite, and calcite peaks highlighted. Melanin peaks information from (Glass et al. 2012); Sulfur peaks from (McNamara et al. 2016); Calcite peaks from NIST library (online); Hydroxyapatite(HA) peaks from (Mendes et al. 2012).

4000-3000	**2999-2000**	**1999-1000**	**999-560**
		1796 – $CaCO_3$	
3600 – 3200 – OH	2920 – CH	1710 – indole rings	962 - HA
	2926 – 2912 - lipids	1620 – 1605 (C=O)	
	2856 – 2840 - lipids	1428 – CH	876 – 871 – $CaCO_3$
		1426 –1404 – $CaCO_3$	780 –775 – CH
	2550 – SH (thiol)	1315 – 1290 – OH+-NH	716 – 712 – $CaCO_3$
	2533 – 2514 – CaCO3	1150 – C=S	635 – 630 – OH^- (HA)
		1106 – 1101 – HA	601 – 600 - HA
		1040 – CS ± CO	598 - CS
		1035 – HA	562 – 560 – HA

4.2.2. PCA analysis of FTIR data

4.2.2.1. PC1 relation with thermal maturity

Although most samples presented a strong inorganic signal (Fig. S53-93), PCA was still performed to assess the viability of using this method for melanin study. A method of analysing FTIR data could be by plotting only organic specific peaks (Wiemann et al. 2018) and study their variance. However, specific peaks could not be chosen for the analysis since their identification and relevance to the organic material signal could not be discerned from the inorganic signal.

Following previously used methodology (Bombalska et al. 2011; Naumann et al. 1988; Szymanska-Chargot & Zdunek 2013) a designated area of interest was chosen (1700 cm^{-1} to 600 cm^{-1}) with each individual wavelength acting as a variable. This range includes the specific melanin peaks (except OH bending at approximately 1560 cm^{-1} that is also characteristic of water presence) as well as sulfur, calcite and hydroxyapatite peaks, therefore providing a general picture of the samples' chemistry. It is also close to the area known as "fingerprint area" (1500 cm^{-1} to 500 cm^{-1}), an area usually used for molecular studies.

Since a whole area of the spectrum is being used instead of specific peaks, there is a high variability inherent to this analysis. In this case, each specific wavelength is a variable, amounting to 1100 variables (as can be seen in the loadings Fig. 23). Upon analysis, data from purified ink (standard eumelanin) and eumelanin artificially matured with sulfur species (both elemental sulfur and sodium sulfide) were excluded from the analysis due to plotting in extremely isolated areas of the plot, without any patterning or clustering. Pheomelanin, artificially matured samples with an identified strong inorganic signal of sulfur, as well as standard eumelanin completely pure of inorganic or any type of thermal maturation, add even more variability to the analysis. This makes the dataset extremely heterogeneous and with the high number of variables influencing the distribution in the axis, no discernible pattern can be observed. Values were analysed in transmittance (%), baseline corrected and mean-centred before PCA analysis, following the same methodology used for the ToF-SIMS analysis.

Even with the strong inorganic signal from hydroxyapatite and calcite, the PCA analysis of FTIR data (Fig. 23) seems to follow the same trends in sample plotting, producing similar patterns to those observed in the ToF-SIMS data analysis plots (Fig. 14 and 16). In this analysis (Fig. 23) PC1 seems to be distributing the samples according to maturation. Less mature fossil, such as Christian Malford (T_{max} = 411 °C) are plotted on the positive side of the PC1 axis, while more mature samples (Holzmaden (T_{max} = 435 °C) and Alberta (T_{max} = 436 °C – 447 °C)) are plotted on the negative side of the PC1 axis. Lyme Regis samples (T_{max} = 424 °C) are plotted in an

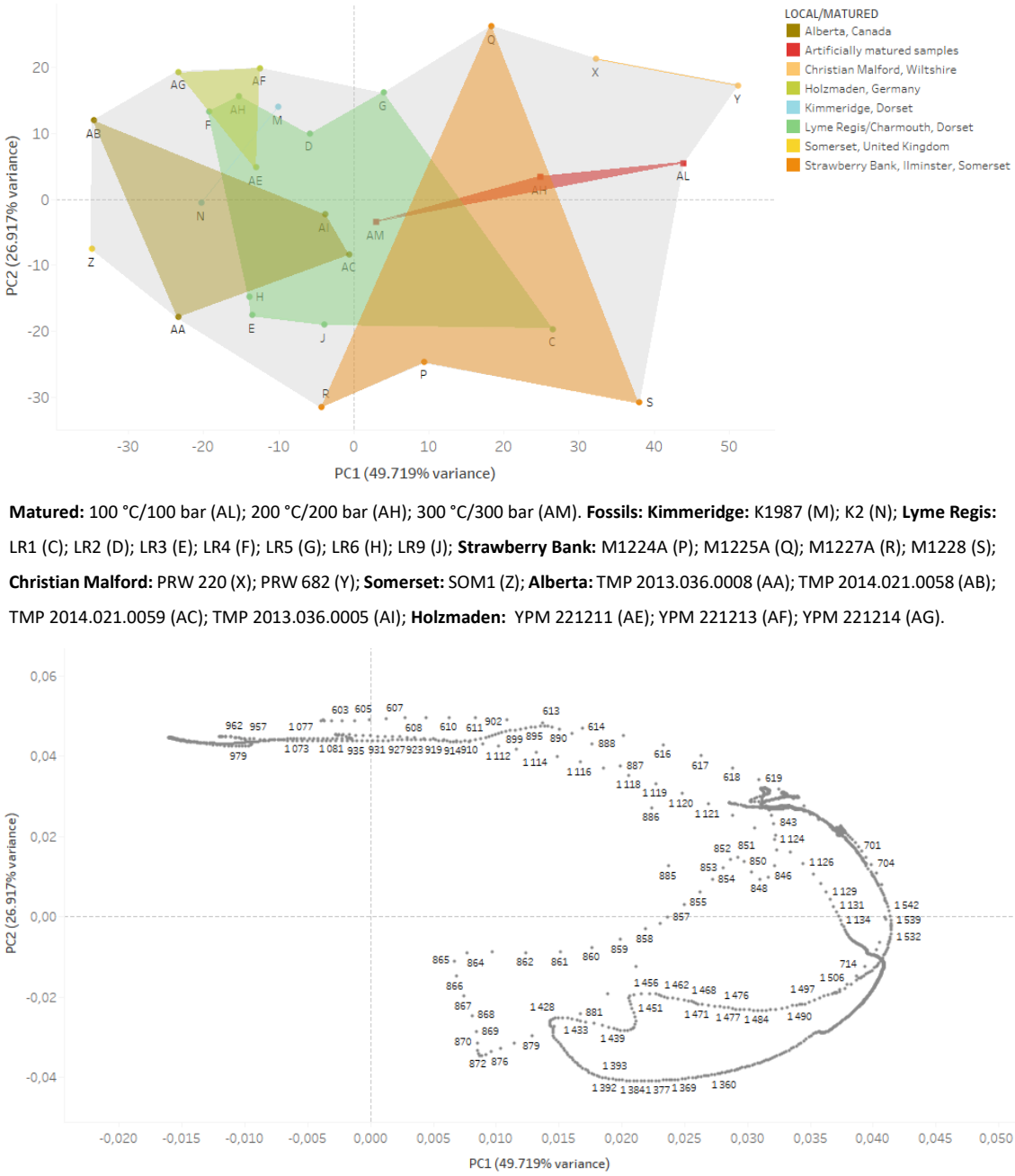

Matured: 100 °C/100 bar (AL); 200 °C/200 bar (AH); 300 °C/300 bar (AM). **Fossils: Kimmeridge:** K1987 (M); K2 (N); **Lyme Regis:** LR1 (C); LR2 (D); LR3 (E); LR4 (F); LR5 (G); LR6 (H); LR9 (J); **Strawberry Bank:** M1224A (P); M1225A (Q); M1227A (R); M1228 (S); **Christian Malford:** PRW 220 (X); PRW 682 (Y); **Somerset:** SOM1 (Z); **Alberta:** TMP 2013.036.0008 (AA); TMP 2014.021.0058 (AB); TMP 2014.021.0059 (AC); TMP 2013.036.0005 (AI); **Holzmaden:** YPM 221211 (AE); YPM 221213 (AF); YPM 221214 (AG).

Figure 23: Principal Component Analysis of FTIR data region from 1700 cm^{-1} to 600 cm^{-1}. Squares represent artificially matured samples. Circles indicate fossil samples. Above: Spectra identified by letters and squares relative to samples analysed in this work. Information on the fossils can be found in Table 4. Below: Loadings for this analysis. Since each specific wavelength acts as a variable, not all vectors are identified for reading purposes.

intermediate position. It is important to point out that these are theoretical values from literature (Table 5) and not experimentally validated. Artificially matured eumelanin samples seem to follow the same trend as fossils, with the less mature sample 100 °C/ 100 bar (AL) plotting furthest right while the more mature sample 300 °C/ 300 bar (AM) plots in an intermediate region of the plot. The sample matured at 200 °C/ 200 bar (AH) plots between AL and AM.

4.2.2.2. Correlation between PC1 and thermal maturity

As before (section 4.1.2.3.), PC1 values were plotted with thermal maturity values (Fig: 23). Here the relation between these two variables is not as visible as the one observed relative to ToF-SIMS results (R^2 = 0.582489; p > 0.0001), but it is still somewhat relevant. This analysis presents the same limitations of theoretical values and not experimentally analysed thermal maturity with the added inorganic signal.

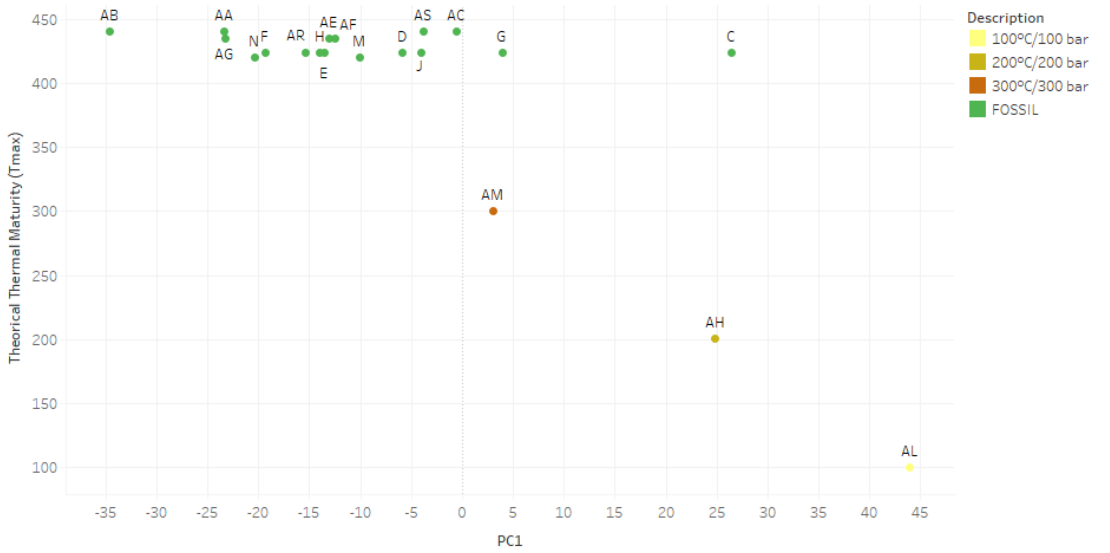

Figure 24: Correlation between PC1 values relative to PCA analysis of FTIR eumelanin data (R^2 =0.582489; p<0.0001). Matured: 100 °C/100 bar (AL); 200 °C/200 bar (AH); 300 °C/300 bar (AM). Fossils: Kimmeridge: K1987 (M); K2 (N); Lyme Regis: LR1 (C); LR2 (D); LR3 (E); LR4 (F); LR5 (G); LR6 (H); LR9 (J); Strawberry Bank: M1224A (P); M1225A (Q); M1227A (R); M1228 (S); Christian Malford: PRW 220 (X); PRW 682 (Y); Somerset: SOM1 (Z); Alberta: TMP 2013.036.0008 (AA); TMP 2014.021.0058 (AB); TMP 2014.021.0059 (AC); TMP 2013.036.0005 (AI); Holzmaden: YPM 221211 (AE); YPM 221213 (AF); YPM 221214 (AG).

4.2.2.3. PC2 and inorganic signal

The trend in PC2 seems to be related to the inorganic signal. Hydroxyapatite and calcite were identified in the fossil samples (Fig. S70-S93) (Table 6). Samples potentially rich in hydroxyapatite (are plotted on the positive PC2 axis, while samples potentially rich in calcite plot in the negative side. Artificially matured eumelanin samples show an intermediate position as well as samples with signals of both hydroxyapatite and calcite. However, it should be kept in mind that some sulfur peaks overlap with the hydroxyapatite signal, so there could be other components contributing to this separation that cannot be studied with the current data.

PCA analysis of FTIR data presents, a new methodology in fossil melanin study that can potentially give new insights to melanin chemistry. Submitting FTIR data to multivariate statistical analysis unveils information that is not obtainable by quantitative analysis. Although the analysis here presented is still heavily influenced by the strong inorganic signal, it seems able

to discern the samples level of maturation is concordance with the ToF-SIMS analysis of eumelanin samples (Fig. 16). Further data gathering on the remaining unanalysed samples, as well as treatment to remove the matrix and the inorganic signal from the artificially matured samples, should make this methodology more robust.

5. CONCLUSION

The aim of this project was to elucidate some aspects of fossil melanin that can introduce a certain level of uncertainty in reconstructions of integumentary colouration of fossils. Although the aims of this project are not totally fulfilled, the results here presented start to explain some of the chemical aspects of fossil eumelanin that are still elusive.

By a focused study of eumelanin from both the fossil record, the recent and with artificial maturation I am able to constrain the most significant factors in the fossilization of eumelanin. ToF-SIMS analysis by PCA of eumelanin samples (Fig. 16) shows that thermal maturity is more relevant for melanin survival through time than age (in concordance with (Glass et al. 2013)).

Preliminary Py-GC/MS results obtained from the artificially matured samples with sulfur species (S_8 and $Na_2S.H_2O$) indicate they do not have the same signal as pheomelanin. Hence, finding exceptional fossils with integument yielding significant moieties of benzothiazines and benzothiazoles is a strong indicator for preserved pheomelanin that cannot be conflated with diagenetic sulfurization (Brown et al. 2017). Removing this uncertainty is an important step in making colour reconstructions more robust. However, matured samples still need to be carefully cleaned of unreacted inorganics and reanalysed. Further Py-GC/MS tests, as well as a range of sulfur species maturations proportions, should also be investigated to assess the changes that stoichiometry can have on the final products.

An added control sample of eumelanin with sulfur species without any type of thermal maturation should also be added to the dataset. Here it is shown that low levels of thermal maturation (100 °C/100 bar) don't seem to induce significant diagenetic incorporation of sulfur in the eumelanin molecule. Samples matured at with sulfur species at these conditions plotted close to non-matured melanin in PCA analysis of ToF-SIMS data (Fig. 14 and Fig. 16) and FTIR quantitative analysis doesn't show significant changes compared to non-matured eumelanin (Fig. 20). Nonetheless, this control sample would make the study of secondary incorporation of sulfur in eumelanin less uncertain and should be incorporated in future studies.

Multivariable statistical analysis of FTIR data on fossil melanin is used, to my knowledge, for the first time for comparative analysis of fossil melanin, showing an apparent concordance with ToF-SIMS results. Both ToF-SIMS and FTIR data PCA analysis seems to show that maturation history plays an important role in the chemical survival of eumelanin. Correlations between PC1 values and T_{max} values of samples were obtained based in theoretical values (Table 5) of thermal maturity for some locations. There seems to be a confident correlation between PC1 and T_{max}

however, in future, thermal maturity levels of these samples should be experimentally obtained and new correlations with PC1 reinterpreted.

FTIR presents itself as a strong tool in conjunction with ToF-SIMS, as it directly illuminates the progressive dehydration and loss of labile functional carboxyl groups that takes place with increasing temperature during burial (Fig. 18). Based on my observations, I propose a molecular structure for fossil eumelanin (Fig. 19). Next steps will include the removal of the matrix and other inorganics, FTIR re-analysis after washing and acid treatment for more compelling analysis in PCA that may be more comparable to fossil evidence. In addition, peak re-analysis would give more information on the chemical changes suffered, such as bonds lost, and new bonds formed including bonds formed in the secondary incorporation of sulfur in the eumelanin molecule to further improve the schematic view of fossil eumelanin chemical structure.

This work stands as a step forward in the study of the chemical preservation of melanin in the fossil record, contributing with new information that could hopefully, one day, help in the discovery of the melanin biomarker.

REFERENCES

Abdi, H. & Williams, L.J., 2010. Principal component analysis. *Wiley Interdisciplinary Reviews: Computational Statistics*, 2(4), pp.433–459.

Adam, P., Philippe, E. & Albrecht, P., 1998. Photochemical Sulfurization of Sedimentary Organic Matter: A Widespread Process Occurring at Early Diagenesis in Natural Environments? *Geochimica et Cosmochimica Acta*, 62(2), pp.265–271.

Aizenshtat, Z. et al., 1995. Role of Sulfur in the Transformations of Sedimentary Organic Matter: A Mechanistic Overview. *Geochemical Transformations of Sedimentary Sulfur*, 612, pp.16–37.

Akagi, J.M., 1995. Respiratory Sulfate Reduction. In L. L. Barton, ed. *Sulfate-Reducing Bacteria*. Boston, MA: Springer US, pp. 89–111.

Allentoft, M.E. et al., 2012. The half-life of DNA in bone: measuring decay kinetics in 158 dated fossils. *Proceedings of the Royal Society B: Biological Sciences*, 279(1748), pp.4724–4733.

Alleon, J. et al., 2017. Organic molecular heterogeneities can withstand diagenesis. *Scientific Reports*, 7(1), p.1508.

Ancans, J. et al., 2001. Melanosomal pH Controls Rate of Melanogenesis, Eumelanin/Phaeomelanin Ratio and Melanosome Maturation in Melanocytes and Melanoma Cells. *Experimental Cell Research*, 268(1), pp.26–35.

Arrhenius, S., 1889. Über die Reaktionsgeschwindigkeit bei der Inversion von Rohrzucker durch Säuren. *Zeitschrift für Physikalische Chemie*, 4U(1).

Attenborough, D., 1979. *Life on Earth: A Natural History* 4th editio., Glasgow: William Collins & Sons.

Bada, J.L., 1991. Amino acid cosmogeochemistry. *Philosophical Transactions - Royal Society of London, B*, 333(1268), pp.349–358.

Bada, J.L., Wang, X.S. & Hamilton, H., 1999. Preservation of key biomolecules in the fossil record: current knowledge and future challenges. *Philosophical transactions of the Royal Society of London. Series B, Biological sciences*, 354(1379), pp.77-86; discussion 86-87.

Berner, R.A., 1984. Sedimentary pyrite formation: An update. *Geochimica et Cosmochimica Acta*, 48(4), pp.605–615.

Blumer, M., 1965. Organic Pigments: Their Long-Term Fate. *Science*, 149(3685), pp.722–726.

Bobrovskiy, I. et al., 2018. Ancient steroids establish the Ediacaran fossil Dickinsonia as one of the earliest animals. *Science*, 361(6408), pp.1246–1249.

Bombalska, A. et al., 2011. Classification of the biological material with use of FTIR spectroscopy and statistical analysis. *Spectrochimica Acta - Part A: Molecular and Biomolecular Spectroscopy*, 78(4), pp.1221–1226.

Bonser, R.H.C., 1994. Melanin and the abrasion resistance of feathers. *The Condor*, 97(2), pp.590–591.

Briggs, D.E.G. & McMahon, S., 2016. The role of experiments in investigating the taphonomy of exceptional preservation. *Palaeontology*, 59(1), pp.1–11.

Briggs, D.E.G. & Summons, R.E., 2014. Ancient biomolecules: Their origins, fossilization, and role in revealing the history of life. *BioEssays*, 36(5), pp.482–490.

Brocks, J.J. et al., 2017. The rise of algae in Cryogenian oceans and the emergence of animals. *Nature*, 548(7669), pp.578–581.

Brocks, J.J. & Pearson, A., 2005. Building the Biomarker Tree of Life. *Reviews in Mineralogy and Geochemistry*, 59(1), pp.233–258.

Bromham, L. & Penny, D., 2003. The modern molecular clock. *Nature Reviews Genetics*, 4(3), pp.216–224.

Brown, C.M. et al., 2017. An Exceptionally Preserved Three-Dimensional Armored Dinosaur Reveals Insights into Coloration and Cretaceous Predator-Prey Dynamics. *Current Biology*, pp.1–8.

Büngeler, A., Hämisch, B. & Strube, O., 2017. The Supramolecular Buildup of Eumelanin: Structures, Mechanisms, Controllability. *International Journal of Molecular Sciences*, 18(9), p.1901.

Bush, W.D. et al., 2006. The surface oxidation potential of human neuromelanin reveals a spherical architecture with a pheomelanin core and a eumelanin surface. *Proc Natl Acad Sci U S A*, 103(40), pp.14785–14789.

Butler, M.J. & Day, A.W., 1998. Fungal melanins: a review. *Canadian Journal of Microbiology*, 44(12), pp.1115–1136.

Carbonero, F. et al., 2012. Microbial pathways in colonic sulfur metabolism and links with health and disease. *Frontiers in Physiology*,

Caro, T., 2005. The Adaptive Significance of Coloration in Mammals. *BioScience*, 55(2), p.125.

Cheng, H.C., Ulane, C.M. & Burke, R.E., 2010. Clinical progression in Parkinson disease and the neurobiology of axons. *Annals of Neurology*, 67(6), pp.715–725.

Chiao, C.-C. et al., 2011. Hyperspectral imaging of cuttlefish camouflage indicates good color match in the eyes of fish predators. *Proceedings of the National Academy of Sciences*, 108(22), pp.9148–9153.

Colleary, C. et al., 2015. Chemical, experimental, and morphological evidence for diagenetically altered melanin in exceptionally preserved fossils. *Proceedings of the National Academy of Sciences*, 112(41), pp.12592–12597.

Cooke, M.S. et al., 2003. Oxidative DNA damage: mechanisms, mutation, and disease. *FASEB Journal*, 17(10), pp.1195–214.

Cumpson, P.J. et al., 2015. Multivariate analysis of extremely large ToFSIMS imaging datasets by a rapid PCA method. *Surface and Interface Analysis*, 47(10), pp.986–993.

Curry, G.B., 1990. Molecular Palaeontology. In D. E. G. Briggs & P. Crowther, eds. *Paleobiology: a synthesis*. Oxford: Blackwell Scientific Publications, pp. 95–100.

Cuthill, I.C. et al., 2017. The biology of color. *Science*, 357(6350).

D'Alba, L. & Shawkey, M.D., 2019. Melanosomes: Biogenesis, Properties, and Evolution of an Ancient Organelle. *Physiological Reviews*, 99(1), pp.1–19.

D'Ischia, M. et al., 2013. Melanins and melanogenesis: Methods, standards, protocols. *Pigment Cell and Melanoma Research*, 26(5), pp.616–633.

Davis, P.G. & Briggs, D.E.G., 1995. Fossilization of feathers. *Geology*, 23(9), pp.783–786.

Derby, C.D., 2014. Cephalopod ink: Production, chemistry, functions and applications. *Marine Drugs*, 12(5), pp.2700–2730.

Derby, C.D., 2007. Escape by inking and secreting: Marine molluscs avoid predators through a rich array of chemicals and mechanisms. *Biological Bulletin*, 213(3), pp.274–289.

Doguzhaeva, L., Mapes, R. & Mutvei, H., 2004. Occurrence of ink in Paleozoic and Mesozoic coleoids (Cephalopoda). *Mitt. Geol.-Paläont. Inst. Univ. Hamburg*, 88(January), pp.145–156.

Doguzhaeva, L.A. et al., 2007. The mantle, ink sac, ink, arm hooks and soft body debris associated with the shells in Late Triassic coleoid cephalopod *Phragmoteuthis* from the Austrian Alps. *Palaeoworld*, 16(4), pp.272–284.

Domine, F., 1989. Kinetics of hexane pyrolysis at very high pressures.. *Energy & Fuels*, 3(1), pp.89–96.

Dzierzęga-Lęcznar, A., Kurkiewicz, S. & Stępié, K., 2012. Detection and quantitation of a pheomelanin component in melanin pigments using pyrolysis-gas chromatography/tandem mass spectrometry system with multiple reaction monitoring mode. *Journal of Mass Spectrometry*, 47(2), pp.242–245.

Edwards, N.P., Manning, P.L. & Wogelius, R.A., 2014. Pigments through time. *Pigment Cell and Melanoma Research*, 27(5), pp.684–685.

Eglinton, G. & Logan, G. a, 1991. Molecular preservation. *Philosophical transactions of the Royal Society of London. Series B, Biological sciences*, 333(1268), pp.315-327; discussion 327-328.

Ekstrom, A. et al., 1983. Determination of the crystal structure of a petroporphyrin isolated from oil shale. *Nature*, 306(5939), pp.173–174.

Engelen, M. et al., 2012. Neuromelanins of Human Brain Have Soluble and Insoluble Components with Dolichols Attached to the Melanic Structure. *PLoS ONE*, 7(11).

Fang, G., Hammar, S. & Rebecca, R., 1992. A quick and inexpensive method for removing polyssaccharides from plant genomic DNA. *BioTechniques*, 13(1), pp.52–56.

Farrimond, P. & Eglinton, G., 1990. The Record of Organic Components and the Nature of Source Rocks. In D. E. G. Briggs & P. Crowther, eds. *Paleobiology: a synthesis*. Oxford: Blackwell Scientific Publications, pp. 217–222.

Fedorow, H. et al., 2005. Neuromelanin in human dopamine neurons: Comparison with peripheral melanins and relevance to Parkinson's disease. *Progress in Neurobiology*, 75(2), pp.109–124.

Foote, M. & Sepkoski, J.J., 1999. Absolute measures of the completeness of the fossil record. *Nature*, 398(6726), pp.415–417.

Francois, R., 1987. A study of sulfur enrichment in the humic fraction of marine-sediments during early diagenesis. *Geochimica et Cosmochimica Acta*, 51(1), pp.17–27.

Glass, K. et al., 2012. Direct chemical evidence for undegraded eumelanin pigment from the Jurassic period. *Pnas*, 109(26), pp.10218–10223.

Glass, K. et al., 2013. Impact of diagenesis and maturation on the survival of eumelanin in the fossil record. *Organic Geochemistry*, 64, pp.29–37.

Greenwood, N.N. & Earnshaw, A., 1997. 15. Sulphur. In *Chemistry of the Elements*. Oxford; Boston: Butterworth-Heinemann, pp. 645–746.

Gupta, N.S. et al., 2007. Experimental evidence for the formation of geomacromolecules from plant leaf lipids. *Organic Geochemistry*, 38(1), pp.28–36.

Gupta, N.S. et al., 2006. The organic preservation of fossil arthropods: an experimental study. *Proceedings. Biological sciences*, 273(1602), pp.2777–83.

Hallam, A., 1960. A Sedimentary and Faunal Study of the Blue Lias of Dorset and Glamorgan. *Philosophical Transactions of the Royal Society B: Biological Sciences*, 243(698), pp.1–44.

Hartgers, W. a. et al., 1997. Sulfur-binding in recent environments: II. Speciation of sulfur and iron and implications for the occurrence of organo-sulfur compounds. *Geochimica et Cosmochimica Acta*, 61(22), pp.4769–4788.

Hendy, J. et al., 2018. A guide to ancient protein studies. *Nature Ecology & Evolution 2018*, p.1.

Hill, R.J. et al., 1996. The Influence of Pressure on the Thermal Cracking of Oil. *Energy & Fuels*, 10(4), pp.873–882.

Hu, D.N., Simon, J.D. & Sarna, T., 2008. Role of ocular melanin in ophthalmic physiology and pathology. *Photochemistry and Photobiology*, 84(3), pp.639–644.

Hwang, D.F. et al., 1989. Tetrodotoxin-producing bacteria from the blue-ringed octopus Octopus maculosus. *Marine Biology*, 100(3), pp.327–332.

Ito, S., 2003. A Chemist's View of Melanogenesis. *Pigment Cell Research*, 16(3), pp.230–236.

Ito, S., 1986. Reexamination of the structure of eumelanin. *BBA - General Subjects*, 883(1), pp.155–161.

Ito, S. & Wakamatsu, K., 2008. Chemistry of mixed melanogenesis - Pivotal roles of dopaquinone. *Photochemistry and Photobiology*, 84(3), pp.582–592.

Janočko, J. et al., 2006. Geology and Hydrocarbon Resources of the Inner Western Carpathians, Slovakia, and Poland. *The Carpathians and Their Foreland: Geology and Hydrocarbon Researces: AAPG Memoir 84*, pp.569–603.

Jasińska, A., Burska, D. & Bolałek, J., 2012. Sulfur in the marine environment. *Oceanological and Hydrobiological Studies*, 41(2).

Kenig, F. & Huc, A.Y., 1990. Incorporation of Sulfur into Recent Organic Matter in a Carbonate Environment (Abu Dhabi, United Arab Emirates). *Geochemistry of Sulfur in Fossil Fuels*, 429(2), p.Washington, DC (US).

Killops, S. & Killops, V., 2005. *Introduction to Organic Geochemistry* 2nd editio., Blackwell Publishing.

Klug, C. et al., 2007. Ammonoid shell structures of primary organic composition. *Palaeontology*, 50(6), pp.1463–1478.

Klug, C. & Lehmann, J., 2015. Soft Part Anatomy of Ammonoids: Reconstructing the Animal Based on Exceptionally Preserved Specimens and Actualistic Comparisons. In C. Klug et al., eds. *Topics in Geobiology Volume 43: Ammonoid Paleobiology: From Anatomy to Ecology*. Springer, pp. 507–529.

Koepfer, D.L., 2003. Representation and Aesthetics in Paleo-Art: An Interview with John Gurche. *American Anthropologist*, 105(1), pp.146–148.

Kok, M.D., Schouten, S. & Sinninghe Damsté, J.S., 2000. Formation of insoluble, nonhydrolyzable, sulfur-rich macromolecules via incorporation of inorganic sulfur species into algal carbohydrates. *Geochimica et Cosmochimica Acta*, 64(15), pp.2689–2699.

Kröger, B., Vinther, J. & Fuchs, D., 2011. Cephalopod origin and evolution: A congruent picture emerging from

fossils, development and molecules: Extant cephalopods are younger than previously realised and were under major selection to become agile, shell-less predators. *BioEssays*, 33(8), pp.602–613.

Kumar, S., 2005. Molecular clocks: four decades of evolution. *Nature Reviews Genetics*, 6(8), pp.654–662.

Kvenvolden, K.A., 2006. Organic geochemistry - A retrospective of its first 70 years. *Organic Geochemistry*, 37(1), pp.1–11.

LaLonde, R.T., 1990. Polysulfide Reactions in the Formation of Organosulfur and Other Organic Compounds in the Geosphere. *Geochemistry of Sulfur in Fossil Fuels*, 426, pp.68–82.

Land, E.. & Riley, P.., 2000. Spontaneous Redox Reactions of Dopaquinone and the Balance between the Eumelanic and Phaeomelanic Pathways. *Pigment Cell Research*, 13(4), pp.273–277.

Li, Q. et al., 2012. Reconstruction of Microraptor and the Evolution of Iridescent Plumage. *Science*, 335(6073), pp.1215–1219.

Lindahl, T., 1993. Instability and decay of the primary structure of DNA. *Nature*, 362(6422), pp.709–715.

Lindgren, J. et al., 2014. Skin pigmentation provides evidence of convergent melanism in extinct marine reptiles. *Nature*, 506(7489), pp.484–8.

Liu, Y. et al., 2007. Comparison of Structural and Chemical Properties of Black and Red Human Hair Melanosomes. *Photochemistry and Photobiology*, 81(1), pp.135–144.

Liu, Y. et al., 2003. Comparison of the structural and physical properties of human hair eumelanin following enzymatic or acid/base extraction. *Pigment Cell Research*, 16(4), pp.355–365.

Liu, Y. & Simon, J.D., 2003. The Effect of Preparation Procedures on the Morphology of Melanin from the Ink Sac of Sepia officinalis. *Pigment Cell Research*, 16(1), pp.72–80.

Love, G.D. et al., 2009. Fossil steroids record the appearance of Demospongiae during the Cryogenian period. *Nature*, 457(7230), pp.718–721.

Mackintosh, J.A., 2001. The antimicrobial properties of melanocytes, melanosomes and melanin and the evolution of black skin. *Journal of Theoretical Biology*, 211(2), pp.101–113.

Mapes, R.H., Weller, E.A. & Doguzhaeva, L.A., 2010. Early Carboniferous (Late Namurian) coleoid cephalopods showing a tentacle with arm hooks and an ink sac from Montana , USA. , (September), pp.155–170.

Marks, M.S. & Seabra, M.C., 2001. The melanosome: membrane dynamics in black and white. *Nature reviews. Molecular cell biology*, 2(10), pp.738–48.

Martin-Bastida, A., Pietracupa, S. & Piccini, P., 2017. Neuromelanin in parkinsonian disorders: an update. *International Journal of Neuroscience*, 127(12), pp.1116–1123.

McCaffrey, M.A. et al., 1994. Paleoenvironmental implications of novel C30 steranes in Precambrian to Cenozoic Age petroleum and bitumen. *Geochimica et Cosmochimica Acta*, 58(1), pp.529–532.

McGraw, K.J., 2006a. Mechanisms of Carotenoid-Based Coloration. In G. E. Hill & K. J. McGraw, eds. *Bird Coloration: Mechanisms and Measurements Volume I*. Cambridge, Massachusetts; London, England: Harvard University Press, pp. 177–242.

McGraw, K.J., 2006b. Mechanisms of Melanin-Based Coloration. In G. E. Hill & K. J. McGraw, eds. *Bird Coloration: Mechanisms and Measurements Volume I*. Cambridge, Massachusetts; London, England:

Harvard University Press, pp. 243–294.

McNamara, M.E. et al., 2016. Fossilization of melanosomes via sulfurization. *Palaeontology*, 59(3), pp.337–350.

McNamara, M.E. et al., 2018. Non-integumentary melanosomes can bias reconstructions of the colours of fossil vertebrates. *Nature Communications*, 9(1).

Melendez, I., Grice, K. & Schwark, L., 2013. Exceptional preservation of Palaeozoic steroids in a diagenetic continuum. *Scientific Reports*, 3(1), p.2768.

Mendes, L.C., Ribeiro, G.L. & Marques, R.C., 2012. In situ Hydroxyapatite Synthesis: Influence of Collagen on Its Structural and Morphological Characteristic. *Materials Sciences and Applications*, 03(08), pp.580–586.

Michels, R. et al., 1995. Effects of effluents and water pressure on oil generation during confined pyrolysis and high-pressure hydrous pyrolysis. *Geochimica et Cosmochimica Acta*, 59(8), pp.1589–1604.

Micillo, R. et al., 2016. "Fifty shades" of black and red or how carboxyl groups fine tune eumelanin and pheomelanin properties. *International Journal of Molecular Sciences*, 17(5).

Monthioux, M., Landais, P. & Monin, J.-C., 1985. Comparison between natural and artificial maturation series of humic coals from the Mahakam delta, Indonesia. *Organic Geochemistry*, 8(4), pp.275–292.

Mosharov, E. V. et al., 2009. Interplay between Cytosolic Dopamine, Calcium, and α-Synuclein Causes Selective Death of Substantia Nigra Neurons. *Neuron*, 62(2), pp.218–229.

Naglik, C. et al., 2015. Ammonoid Locomotion. In C. Klug et al., eds. *Topics in Geobiology Volume 43: Ammonoid Paleobiology: From Anatomy to Ecology*. Springer, pp. 649–688.

Naumann, D. et al., 1988. The rapid differentiation and identification of pathogenic bacteria using Fourier transform infrared spectroscopic and multivariate statistical analysis. *Journal of Molecular Structure*, 174(C), pp.165–170.

Negro, J., Finlayson, C. & Galván, I., 2018. Melanins in Fossil Animals: Is It Possible to Infer Life History Traits from the Coloration of Extinct Species? *International Journal of Molecular Sciences*, 19(2), p.230.

Nelson, D. & Cox, M., 2005. *Lehninger principles of biochemistry (4th ed.)*,

Newman, D.K. et al., 2016. Cellular and Molecular Biological Approaches to Interpreting Ancient Biomarkers. *Annual Review of Earth and Planetary Sciences*, 44(1), pp.493–522.

Nofsinger, J.B., Forest, S.E. & Simon, J.D., 1999. Explanation for the Disparity among Absorption and Action Spectra of Eumelanin. *The Journal of Physical Chemistry B*, 103(51), pp.11428–11432.

Orlando, L. et al., 2013. Recalibrating equus evolution using the genome sequence of an early Middle Pleistocene horse. *Nature*, 499(7456), pp.74–78.

Orti, F., Rosell, L. & AnadON, P., 2003. Deep to shallow lacustrine evaporites in the Libros Gypsum (southern Teruel Basin, Miocene, NE Spain): an occurrence of pelletal gypsum rhythmites. *Sedimentology*, 50(2), pp.361–386.

Ourisson, G. & Albrecht, P., 1992. Hopanoids. 1. Geohopanoids: The Most Abundant Natural Products on Earth? *Accounts of Chemical Research*, 25(9), pp.398–402.

Palumbo, A., 2003. Melanogenesis in the ink gland of Sepia officinalis. *Pigment cell research / sponsored by*

the European Society for Pigment Cell Research and the International Pigment Cell Society, 16(5), pp.517–522.

Parker, A.R., 2000. 515 Million Years of Structural Colour. *Journal of Optics A: Pure and Applied Optics*, 2(6).

Parry, L.A. et al., 2017. Soft-Bodied Fossils Are Not Simply Rotten Carcasses - Toward a Holistic Understanding of Exceptional Fossil Preservation. *BioEssays*, 1700167, p.1700167.

Parsons, K.J., Cooper, W.J. & Albertson, R.C., 2009. Limits of principal components analysis for producing a common trait space: Implications for inferring selection, contingency, and chance in evolution. *PLoS ONE*, 4(11).

Pezzella, A. et al., 1997. An integrated approach to the structure of Sepia melanin. Evidence for a high proportion of degraded 5,6-dihydroxyindole-2-carboxylic acid units in the pigment backbone. *Tetrahedron*, 53(24), pp.8281–8286.

Pitha, J., Kociolek, K. & Caron, M.G., 1979. Detergents Linked to Polysaccharides: Preparation and Effects on Membranes and Cells. *European Journal of Biochemistry*, 94(1), pp.11–18.

Plonka, P.M. & Grabacka, M., 2006. Melanin synthesis in microorganisms - Biotechnological and medical aspects. *Acta Biochimica Polonica*, 53(3), pp.429–443.

Prauss, M., Ligouis, B. & Luterbacher, H., 1991. Organic matter and palynomorphs in the 'Posidonienschiefer' (Toarcian, Lower Jurassic) of southern Germany. *Geological Society, London, Special Publications*, 58(1), pp.335–351.

Prota, G. et al., 1970. New intermediates in phaeomelanogenesis in vitro. *Experientia*, 26(10), pp.1058–1059.

Purnell, M.A. et al., 2018. Experimental analysis of soft-tissue fossilization: opening the black box. *Palaeontology*, pp.1–7.

Raper, H.S., 1927. The Tyrosinase-tyrosine Reaction: Production from Tyrosine of 5: 6-Dihydroxyindole and 5: 6-Dihydroxyindole-2-carboxylic Acid-the Precursors of Melanin. *The Biochemical journal*, 21(1), pp.89–96.

Riediger, C.L., 2002. Hydrocarbon source rock potential and comments on correlation of the Lower Jurassic Poker Chip Shale, west-central Alberta. *Bulletin of Canadian Petroleum Geology*, 50(2), pp.263–276.

Romanowski, G., Lorenz, M.G. & Wackernagel, W., 1991. Adsorption of plasmid DNA to mineral surfaces and protection against DNase I. *Applied and Environmental Microbiology*, 57(4), pp.1057–1061.

Rothschild, L.J. & Mancinelli, R.L., 2001. Life in extreme environments. *Nature*, 409(6823), pp.1092–1101.

Rowland, H.M., 2009. From Abbott Thayer to the present day: What have we learned about the function of countershading? *Philosophical Transactions of the Royal Society B: Biological Sciences*, 364(1516), pp.519–527.

Rózanowska, M. et al., 1999. Free radical scavenging properties of melanin interaction of eu- and pheo-melanin models with reducing and oxidising radicals. *Free Radical Biology and Medicine*, 26(5–6), pp.518–525.

Sadava, D. et al., 2008. *Life: The Science of Biology* 8th editio., Sinauer Associates, Inc.

Saitta, E.T. et al., 2017. Low fossilization potential of keratin protein revealed by experimental taphonomy. *Palaeontology*, pp.1–10.

Saitta, E.T. et al., 2018. Preservation of feather fibers from the Late Cretaceous dinosaur Shuvuuia deserti raises concern about immunohistochemical analyses on fossils. *Organic Geochemistry*, 125(November), pp.142–151.

Saitta, E.T., Kaye, T.G. & Vinther, J., 2019. Sediment-encased maturation: a novel method for simulating diagenesis in organic fossil preservation S. Gabbott, ed. *Palaeontology*, 62(1), pp.135–150.

Sasaki, T., Shigeno, S. & Tanabe, K., 2010. *Anatomy of living Nautilus : Reevaluation of primitiveness and comparison with Coleoidea*,

Schiel, G. et al., 1987. Relationship between melanin content and superoxide dismutase (SOD) activity in the liver of various species of animals. *Cell Biochemistry and Function*, 5(2), pp.123–128.

Schraermeyer, U., 1994. Fine Structure of Melanogenesis in the Ink Sac of Sepia officinalis. *Pigment Cell Research*, 7(1), pp.52–60.

Schweitzer, M.H., Lindgren, J. & Moyer, A.E., 2015. Melanosomes and ancient coloration re-examined: A response to Vinther 2015. *BioEssays*, 37(11), pp.1174–1183.

Schwieters, J. et al., 1991. High mass resolution surface imaging with a time-of-flight secondary ion mass spectroscopy scanning microprobe. *Journal of Vacuum Science & Technology A: Vacuum, Surfaces, and Films*, 9(6), pp.2864–2871.

Scotchman, I.C., 1991. Kerogen facies and maturity of the Kimmeridge Clay Formation in southern and eastern England. *Marine and Petroleum Geology*, 8(3), pp.278–295.

Scott, A.C. et al., 2018. Heterogeneity of free and occluded bitumen in a natural maturity sequence from Oligocene Lake Enspel. *Geochimica et Cosmochimica Acta*, 245, pp.240–265.

Shawkey, M.D. & D'Alba, L., 2017. Interactions between colour-producing mechanisms and their effects on the integumentary colour palette. *Philosophical Transactions of the Royal Society B: Biological Sciences*, 372(1724).

Sherman Hsu, C.P., 1997. Infrared Spectroscopy. In F. A. Settle, ed. *Handbook of instrumental Techniques for Analytical Chemistry*. Upper Saddle River, New Jersey: Prentice Hall; Har/Cdr edition, pp. 247–284.

Sievert, S.M., Kiene, R.P. & Schulz-Vogt, H.N., 2007. The Sulfur Cycle. *Oceanography*, 20(June), pp.117–123.

Simon, J.D. et al., 2009. Current challenges in understanding melanogenesis: Bridging chemistry, biological control, morphology, and function. *Pigment Cell and Melanoma Research*, 22(5), pp.563–579.

Simon, J.D. & Peles, D.N., 2010. The Red and the Black. *Accounts of Chemical Research*, 43(11), pp.1452–1460.

Simoneit, B.R.T., 2004. Biomarkers (molecular fossils) as geochemical indicators of life. *Advances in Space Research*, 33(8), pp.1255–1261.

Sinninghe Damsté, J.S. et al., 1990. Characterization of Organically Bound Sulfur in High-Molecular-Weight, Sedimentary Organic Matter Using Flash Pyrolysis and Raney Ni Desulfurization. In *Geochemistry of Sulfur in Fossil Fuels*. pp. 486–528.

Sinninghe Damsté, J.S. et al., 1989. Quenching of labile functionalised lipids by inorganic sulphur species: Evidence for the formation of sedimentary organic sulphur compounds at the early stages of diagenesis. *Geochimica et Cosmochimica Acta*, 53(6), pp.1343–1355.

Sinninghe Damsté, J.S. & De Leeuw, J.W., 1990. Analysis, structure and geochemical significance of

organically-bound sulphur in the geosphere: State of the art and future research. *Organic Geochemistry*, 16(4–6), pp.1077–1101.

Slominski, A. et al., 2004. Melanin Pigmentation in Mammalian Skin and Its Hormonal Regulation. *Physiological Reviews*, 84(4), pp.1155–1228.

Smith, B.C., 2011. *Fundamentals of Tranform Infrared Fourier Spectroscopy* 2nd Editio., Boca Raton: CRC Press; Taylor & Francis Group.

Smithwick, F.M. et al., 2017. Countershading and Stripes in the Theropod Dinosaur Sinosauropteryx Reveal Heterogeneous Habitats in the Early Cretaceous Jehol Biota. *Current Biology*, 0(0), pp.1–7.

Solano, F., 2014. Melanins: Skin Pigments and Much More—Types, Structural Models, Biological Functions, and Formation Routes. *New Journal of Science*, 2014, pp.1–28.

Stankiewicz, B. et al., 1997. Preservation of Chitin in 25- million-year-old fossils. *Science*, 276(June), pp.1541–1543.

Steele, A. et al., 2001. Time of flight secondary ion mass spectrometry (ToFSIMS) of a number of hopanoids. *Organic Geochemistry*, 32(7), pp.905–911.

Sulzer, D. et al., 2018. Neuromelanin detection by magnetic resonance imaging (MRI) and its promise as a biomarker for Parkinson's disease. *npj Parkinson's Disease*, 4(1), p.11.

Szymanska-Chargot, M. & Zdunek, A., 2013. Use of FT-IR Spectra and PCA to the Bulk Characterization of Cell Wall Residues of Fruits and Vegetables Along a Fraction Process. *Food Biophysics*, 8(1), pp.29–42.

Tanner, A.R. et al., 2017. Molecular clocks indicate turnover and diversification of modern coleoid cephalopods during the Mesozoic Marine Revolution. *Proceedings of the Royal Society B: Biological Sciences*, 284(1850), p.20162818.

Tegelaar, E.W. et al., 1989. A reappraisal of kerogen formation. *Geochimica et Cosmochimica Acta*, 53(11), pp.3103–3106.

Thiel, V. & Sjövall, P., 2011. Using Time-of-Flight Secondary Ion Mass Spectrometry to Study Biomarkers. *Annual Review of Earth and Planetary Sciences*, 39(1), pp.125–156.

Treibs, A., 1936. Chlorophyll- und Haminderivate in organishen Mineralstoffen. *Angewandte Chemie*, 49(38), pp.682–686.

Vairavamurthy, M.A., Orr, W.L. & Manowitz, B., 1995. Geochemical Transformations of Sedimentary Sulfur. In M. A. Vairavamurthy et al., eds. *Geochemical Transformations of Sedimentary Sulfur*. ACS Symposium Series. Washington, DC: American Chemical Society, pp. 1–14.

Vandenbroucke, M. & Largeau, C., 2007. Kerogen origin, evolution and structure. *Organic Geochemistry*, 38(5), pp.719–833.

Vickerman, J.C., 2001. ToF-SIMS — An Overview. In J. C. Vickerman & D. Briggs, eds. *ToF-SIMS: Surface Analysis by Mass Spectrometry*. Chichester, UK: IM Publishers, pp. 1–40.

Vinther, J. et al., 2016. 3D Camouflage in an Ornithischian Dinosaur. *Current Biology*, 26(18), pp.2456–2462.

Vinther, J., 2015a. A guide to the field of palaeo colour: Melanin and other pigments can fossilise: Reconstructing colour patterns from ancient organisms can give new insights to ecology and behaviour. *BioEssays*, 37(6), pp.643–656.

Vinther, J., 2016. Fossil melanosomes or bacteria? A wealth of findings favours melanosomes. *BioEssays*, 38(3), pp.220–225.

Vinther, J., 2015b. SI 2015 (REVIEW)A guide to the field of palaeo colour.

Vinther, J. et al., 2008. The colour of fossil feathers. *Biology letters*, 4(July), pp.522–525.

Wakamatsu, K., Ohtara, K. & Ito, S., 2009. Chemical analysis of late stages of pheomelanogenesis: Conversion of dihydrobenzothiazine to a benzothiazole structure. *Pigment Cell and Melanoma Research*, 22(4), pp.474–486.

Wang, L.C. et al., 2017. Elaboration in type, primary structure, and bioactivity of polysaccharides derived from mollusks. *Critical Reviews in Food Science and Nutrition*, 8398, pp.1–24.

Wiemann, J. et al., 2018. Fossilization transforms vertebrate hard tissue proteins into N-heterocyclic polymers. *Nature Communications*, 9(1).

Wilby, P.R. et al., 2008. Preserving the unpreservable: a lost world rediscovered at Christian Malford, UK. *Geology Today*, 24(3), pp.95–98.

Willerslev, E., Hansen, A.J. & Poinar, H.N., 2004. Isolation of nucleic acids and cultures from fossil ice and permafrost. *Trends in Ecology and Evolution*, 19(3), pp.141–147.

Wogelius, R.A. et al., 2011. Trace metals as biomarkers for eumelanin pigment in the fossil record. *Science*, 333(6049), pp.1622–1626.

Zecca, L. et al., 2000. Interaction of human substantia nigra neuromelanin with lipids and peptides. *Journal of Neurochemistry*, 74(4), pp.1758–1765.

Zecca, L. et al., 2004. The role of iron and copper molecules in the neuronal vulnerability of locus coeruleus and substantia nigra during aging. *Proceedings of the National Academy of Sciences of the United States of America*, 101(26), pp.9843–9848.

Zeise, L., Murr, B.L. & Chedekel, M.R., 1992. Melanin Standard Method: Particle Description. *Pigment Cell Research*, 5(3), pp.132–142.

Supplementary Information

Table S1: Melanin and sulfur compounds weights used for the artificial maturations (in grams). Samples 9, 15, and 16 are strikethrough due not being used for further analysis. These samples suffered fluctuations in temperature and pressure during maturation, going beyond the experimental parameters. T -Temperature; P- Pressure; Ø – No sulfur species; S_8 – Elemental sulfur; $Na_2S.xH_2O$ – Sodium sulfide hydrate.

Sample number	Conditions (T/P) (°C/bar)	Sulfur conditions	Capsule weight	Capsule + Sulfur weight	Capsule + Sulfur + Melanin weight	After wielding	Final Melanin weight used	Final Sulfur weight used
1	200/200	Ø	0,6458		0,6543	0,6542	0,0085	
2	200/200	Ø	0,6061		0,6135	0,6131	0,0074	
3	200/200	S_8	0,5830	0,6022	0,6182	0,6128	0,0160	0,0192
4	200/200	S_8	0,6183	0,6386	0,6486	0,6483	0,0100	0,0203
5	100/100	S_8	0,6177	0,6378	0,6494	0,6491	0,0116	0,0201
6	300/300	S_8	0,5691	0,5895	0,5996	0,5993	0,0101	0,0204
7	100/100	Ø	0,5322		0,5422	0,5420	0,0100	
8	300/300	Ø	0,4860		0,4955	0,4953	0,0095	
~~**9**~~	~~100/100~~	~~Ø~~	~~0,4920~~		~~0,5045~~	~~0,5048~~	~~0,0125~~	
10	300/300	Ø	0,4883		0,4983	0,4981	0,0100	
11	100/100	$Na_2S.xH_2O$	0,6318	0,6437	0,6549	0,6541	0,0112	0,0119
12	100/100	$Na_2S.xH_2O$	0,5592	0,5676	0,5772	0,5765	0,0096	0,0084
13	200/200	$Na_2S.xH_2O$	0,5893	0,5989	0,6072	0,6070	0,0083	0,0096
14	200/200	$Na_2S.xH_2O$	0,5415	0,5527	0,5621	0,5614	0,0094	0,0112
~~**15**~~	~~300/300~~	~~$Na_2S.xH_2O$~~	~~0,5394~~	~~0,549~~	~~0,5581~~	~~0,5572~~	~~0,0091~~	~~0,0096~~
~~**16**~~	~~300/300~~	~~$Na_2S.xH_2O$~~	~~0,5834~~	~~0,5925~~	~~0,6002~~	~~0,5997~~	~~0,0077~~	~~0,0091~~
17	100/100	Ø	0,4120		0,4207	0,4202	0,0087	
18	300/300	$Na_2S.xH_2O$	0,4446	0,4538	0,4637	0,4632	0,0099	0,0092
19	300/300	$Na_2S.xH_2O$	0,4800	0,4908	0,4998	0,4998	0,0090	0,0108

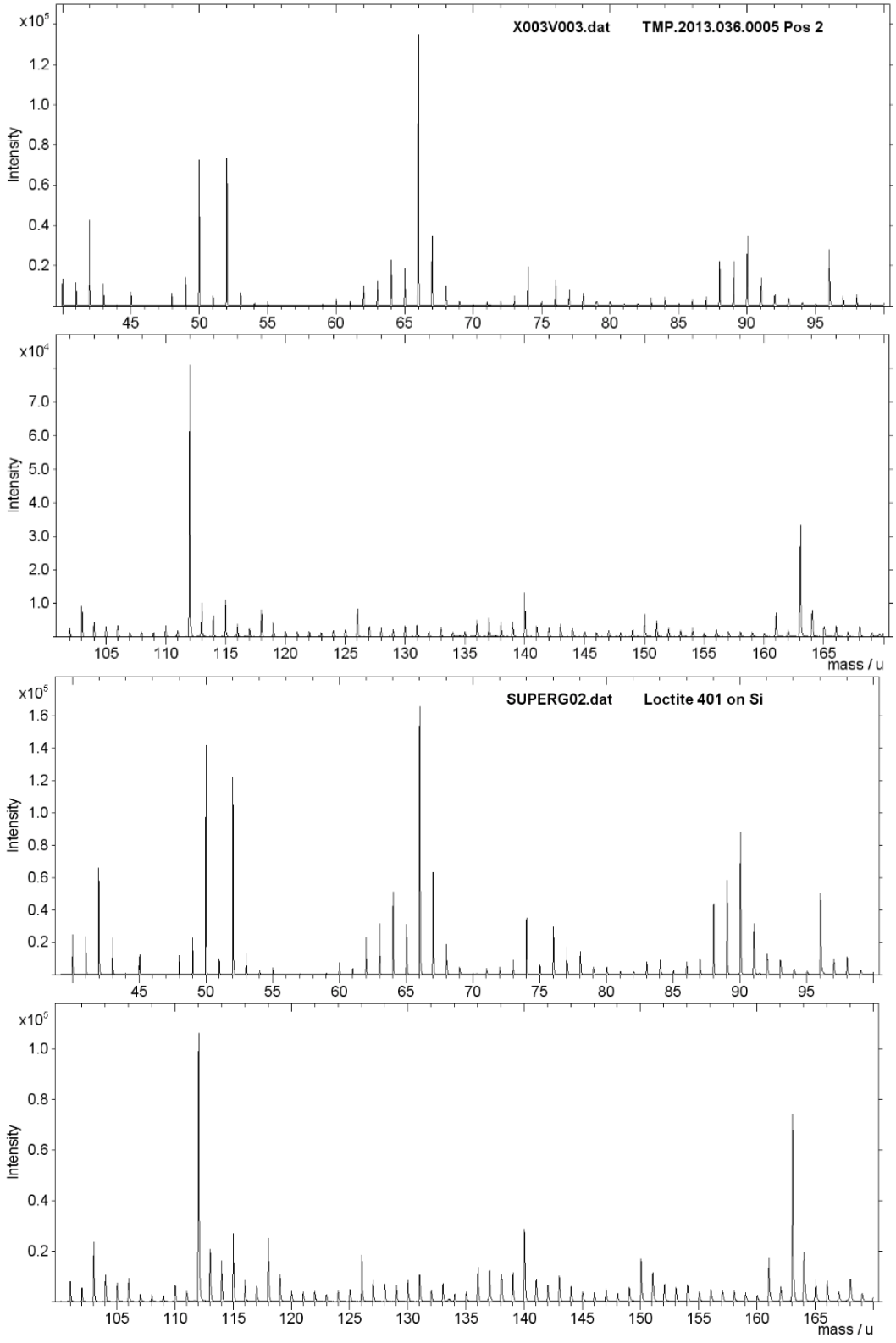

Figure S1: ToF-SIMS spectra comparison between a fossil sample from Ya Ha Tinda, Alberta, Canada (TMP.2013.036.0005) and common consolidant (LOCTITE 401). Spectra show a close resemblance in relative peak intensities, leading to the conclusion that the fossil sample surface was contaminated with consolidant.

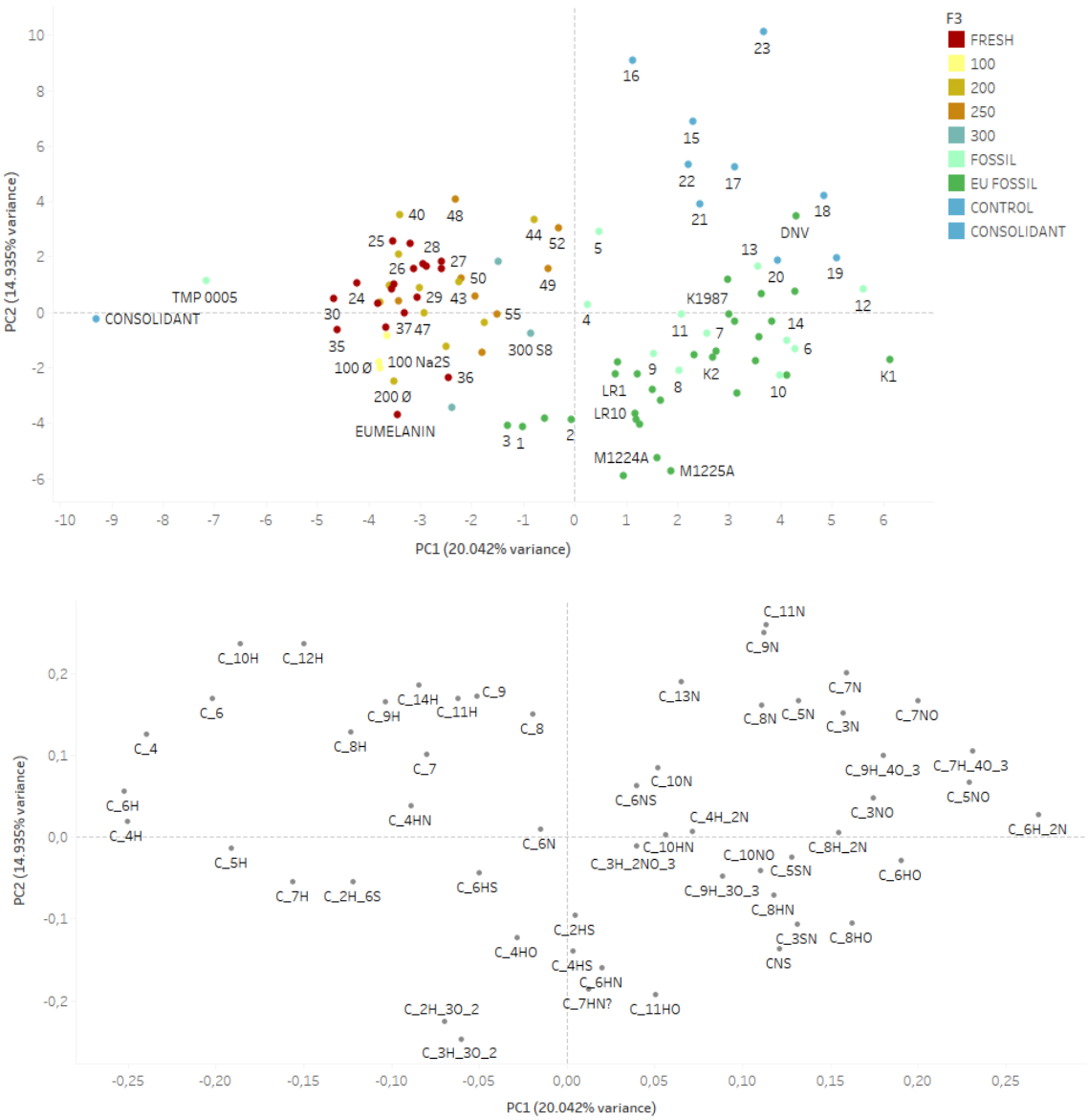

Figure S2: Principal Component Analysis plot of ToF-SIMS data. Above: Colleary et al. 2015 dataset and samples analysed in this work. Not all samples are identified for visibility purposes. Numbers correspond to Colleary samples (corresponding with the numbers used in Colleary et al. 2015). Other points references refer to fossils and matured samples analysed in this work. A clear separation of sample TMP 2013.036.0005 and consolidant from other samples corroborate the presence of contaminant in the sample surface (also seen in Figure S1). Below: Loadings for this analysis.

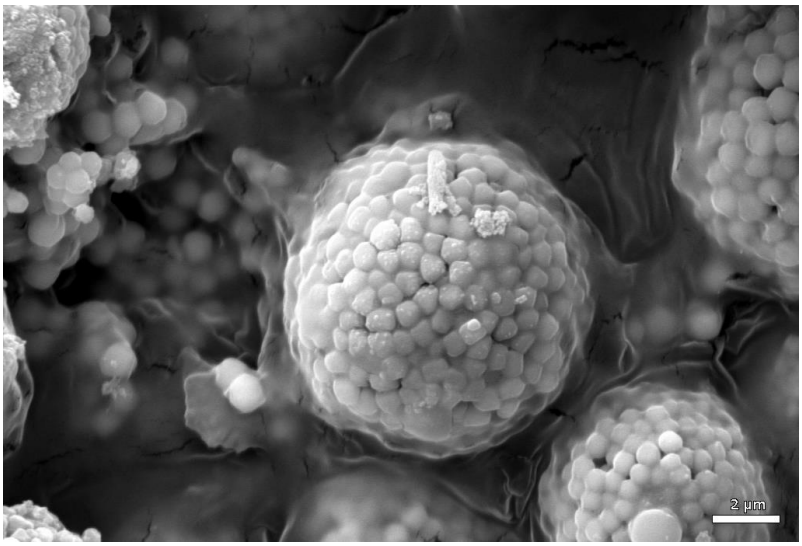

Figure S3: Scanning Electron Microscopy (SEM) image of sample DNM Z20058 showing melanin granules incased in an inorganic matrix.

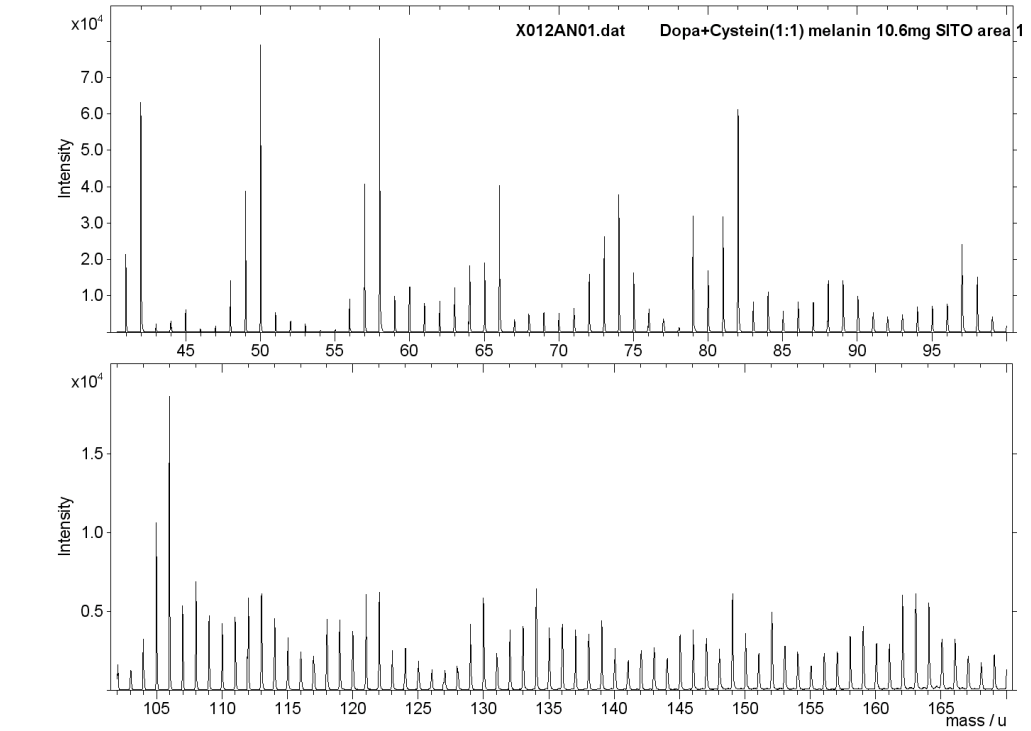

Figure S4: ToF-SIMS spectrum of synthetic pheomelanin.

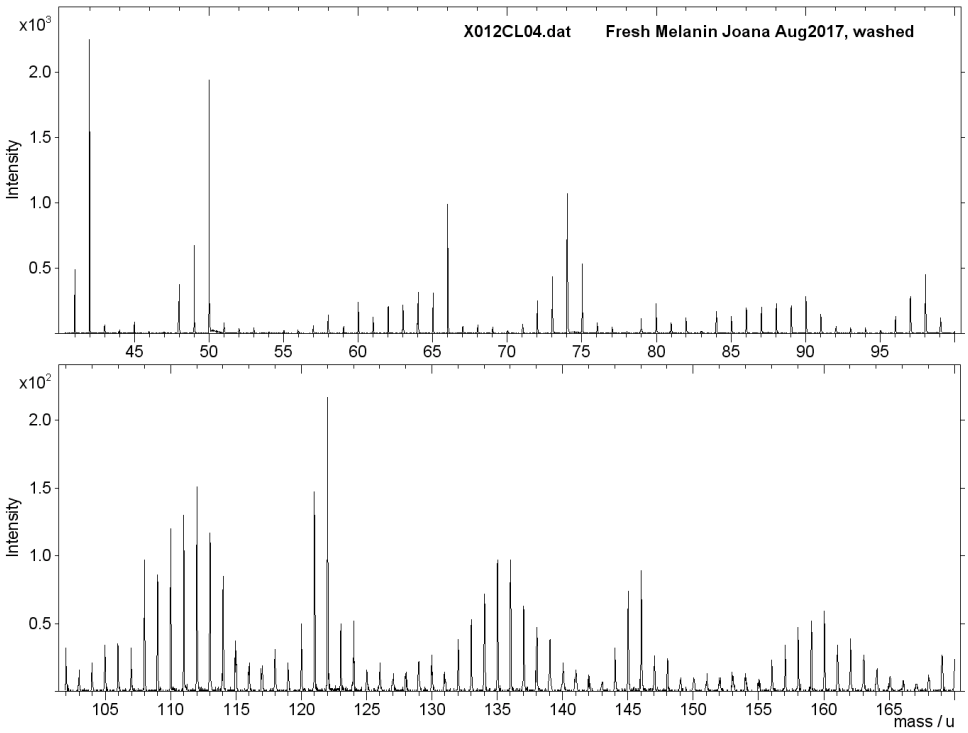

Figure S6: ToF-SIMS spectrum of purified cephalopod ink (Fresh) after washings to remove Triton X-100 surfactant signal.

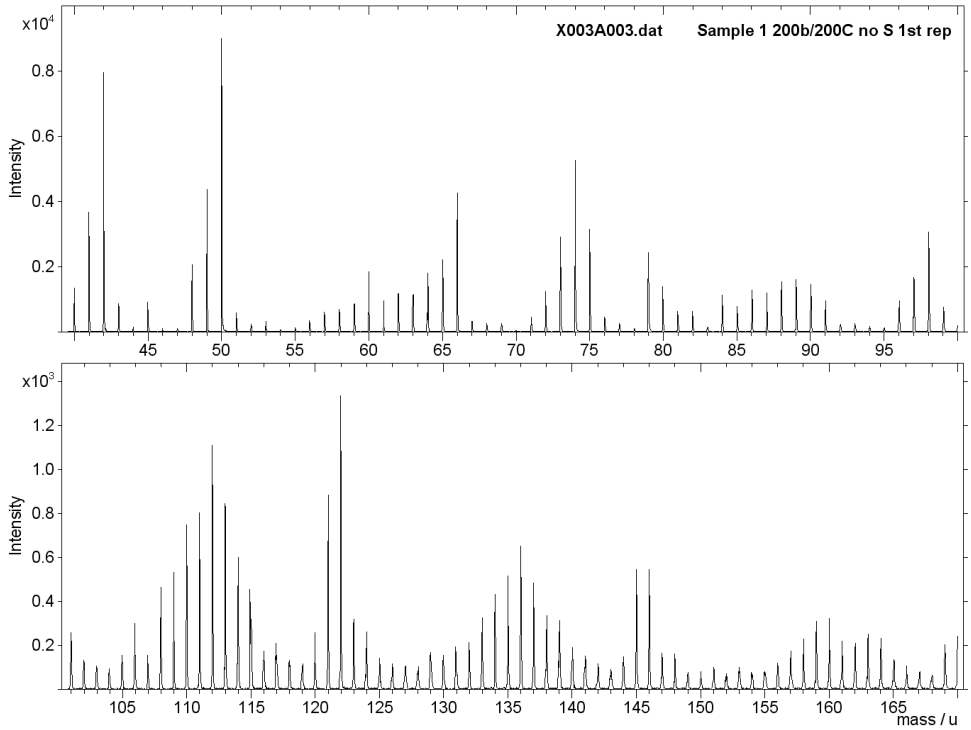

Figure S5: ToF-SIMS spectrum of sample 1 (200 °C/200 bar).

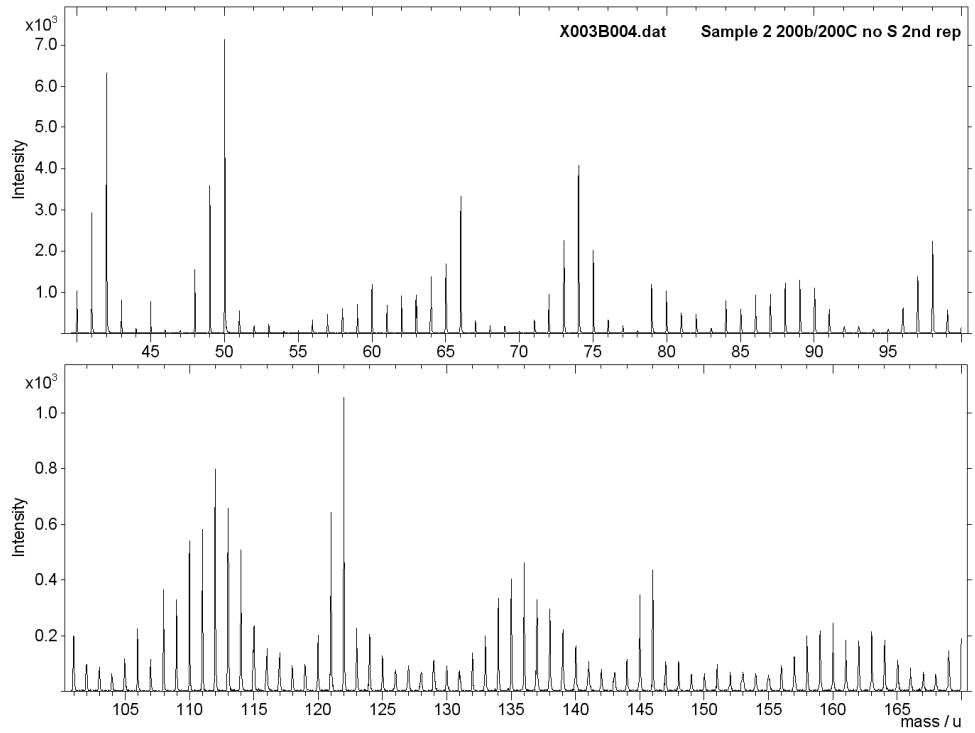

Figure S7: ToF-SIMS spectrum of sample 2 (200 °C/200 bar).

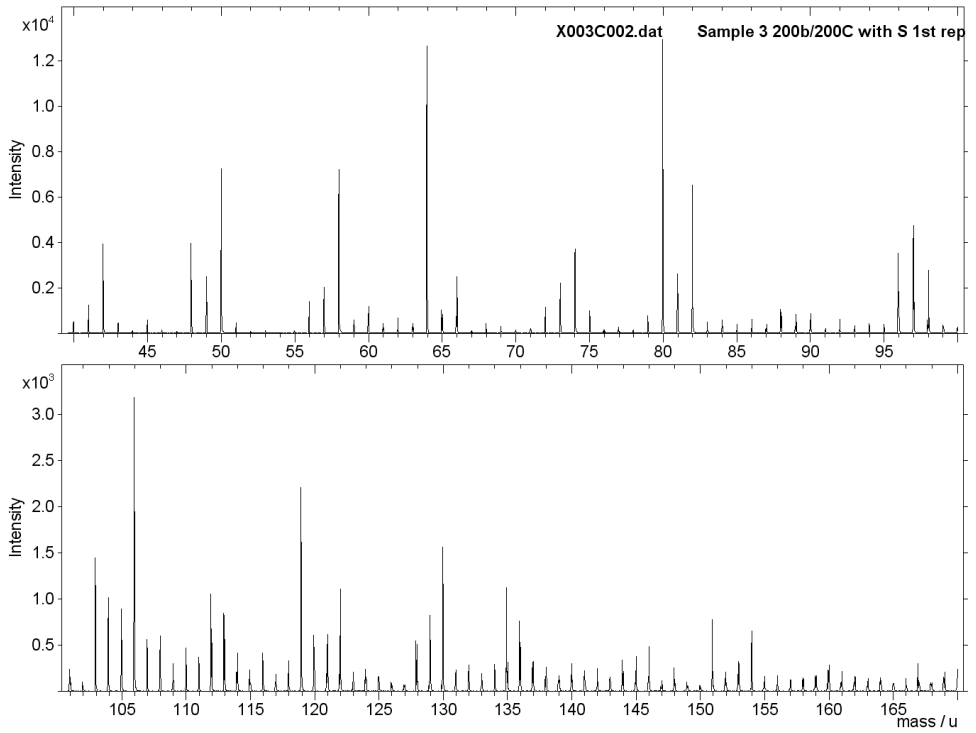

Figure S8: ToF-SIMS spectrum of sample 3 (200 °C/200 bar with S_8). Sample not washed before analysis.

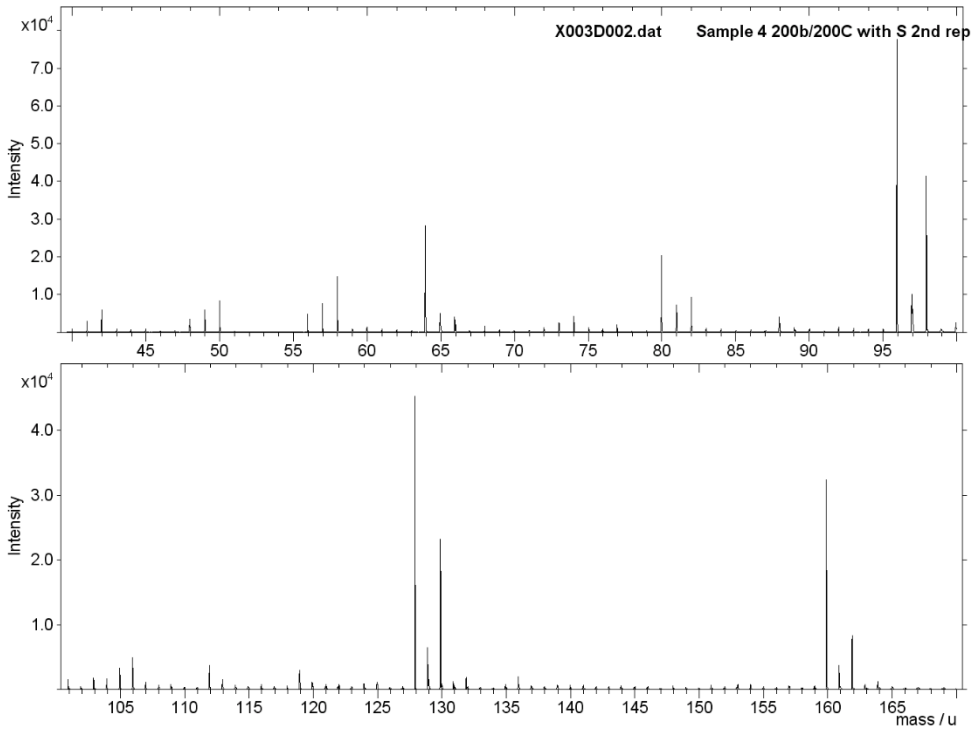

Figure S9: ToF-SIMS spectrum of sample 4 (200 °C/200 bar with S_8). Sample not washed before analysis.

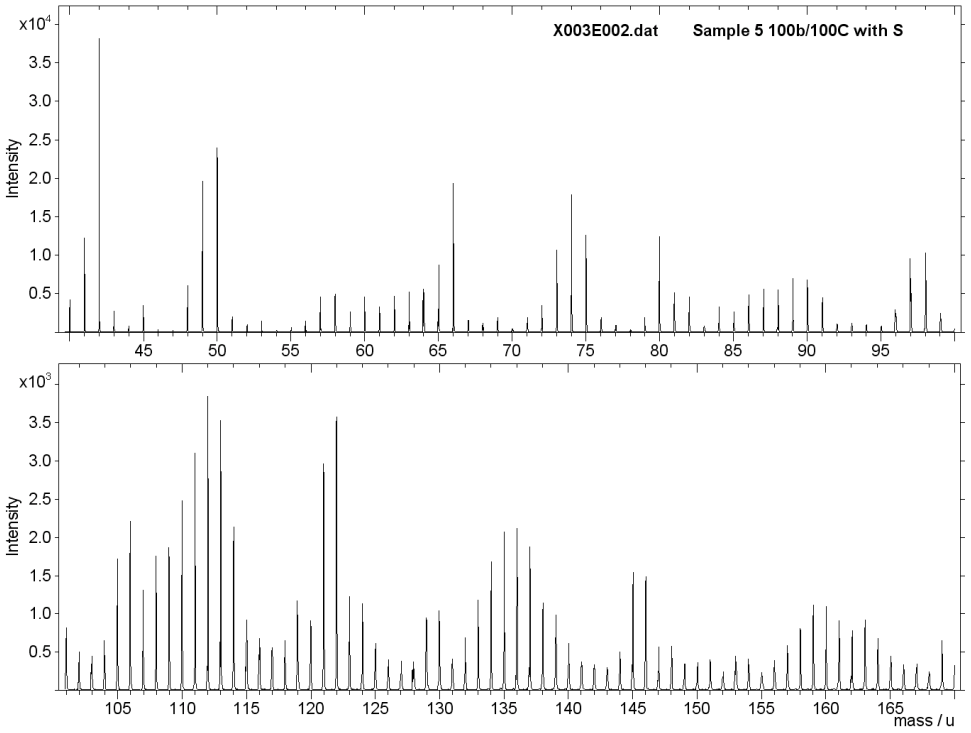

Figure S10: ToF-SIMS spectrum of sample 5 (100 °C/100 bar with S_8). Sample not washed before analysis.

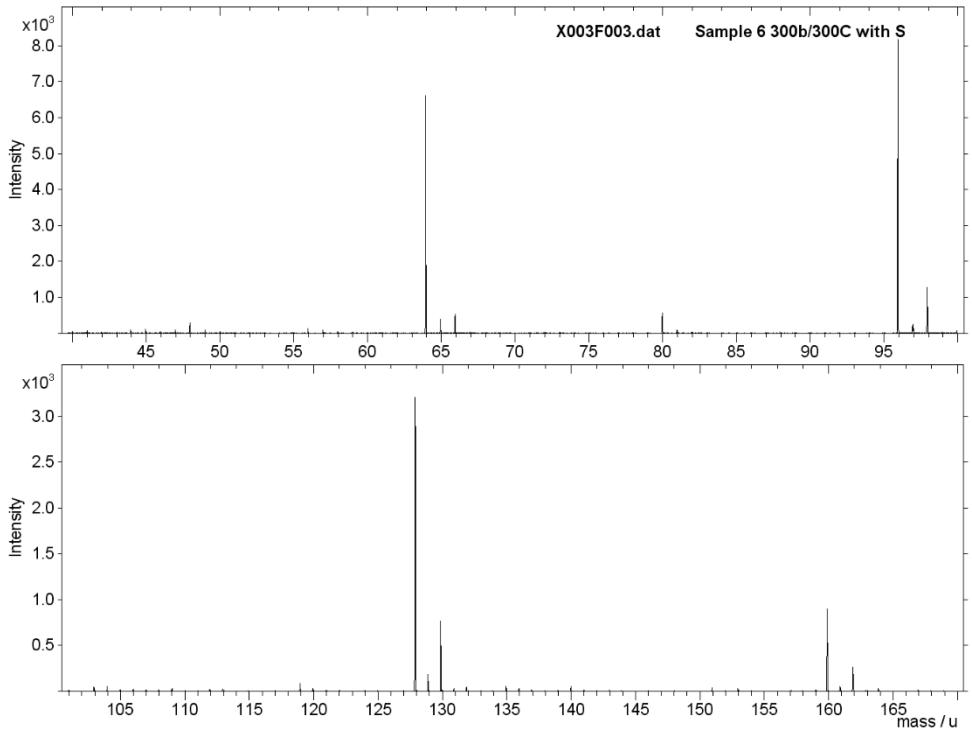

Figure S11: ToF-SIMS spectrum of sample 6 (300 °C/300 bar with S_8). Sample not washed before analysis.

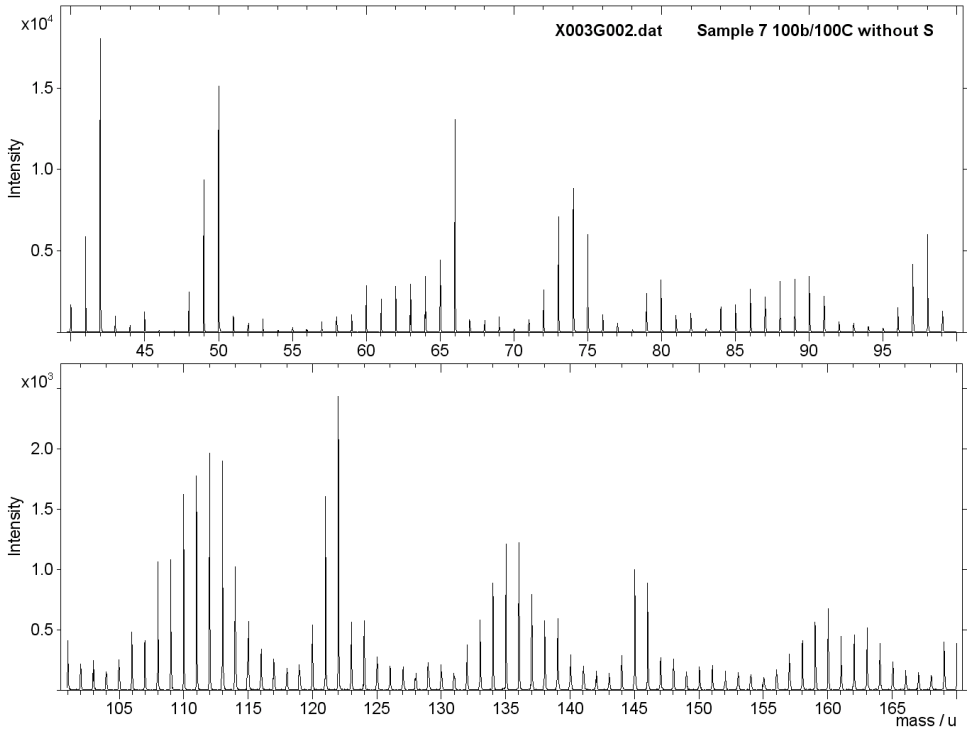

Figure S12: ToF-SIMS spectrum of sample 7 (100 °C/100 bar).

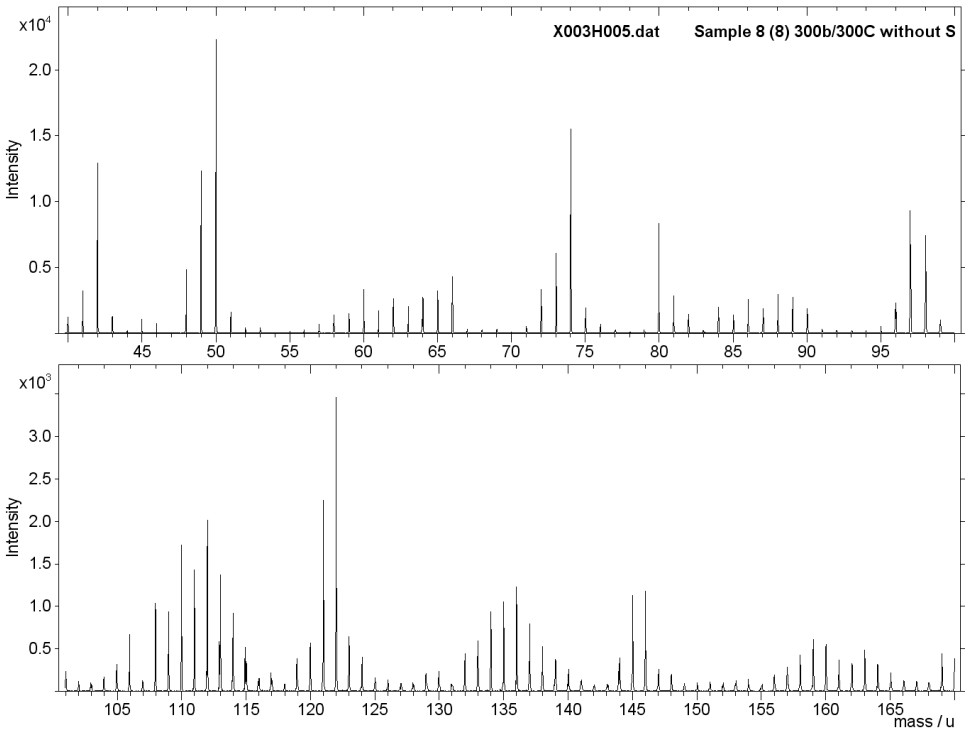

Figure S13 ToF-SIMS spectrum of sample 8 (300 °C/300 bar)

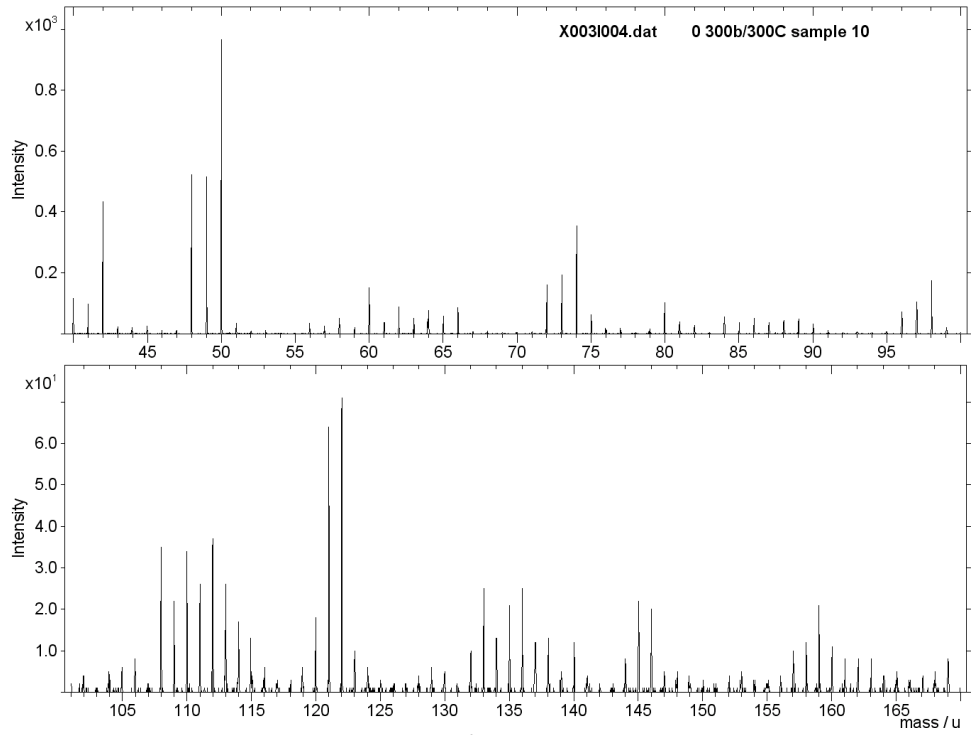

Figure S14: ToF-SIMS spectrum of sample 10 (300 °C/300 bar)

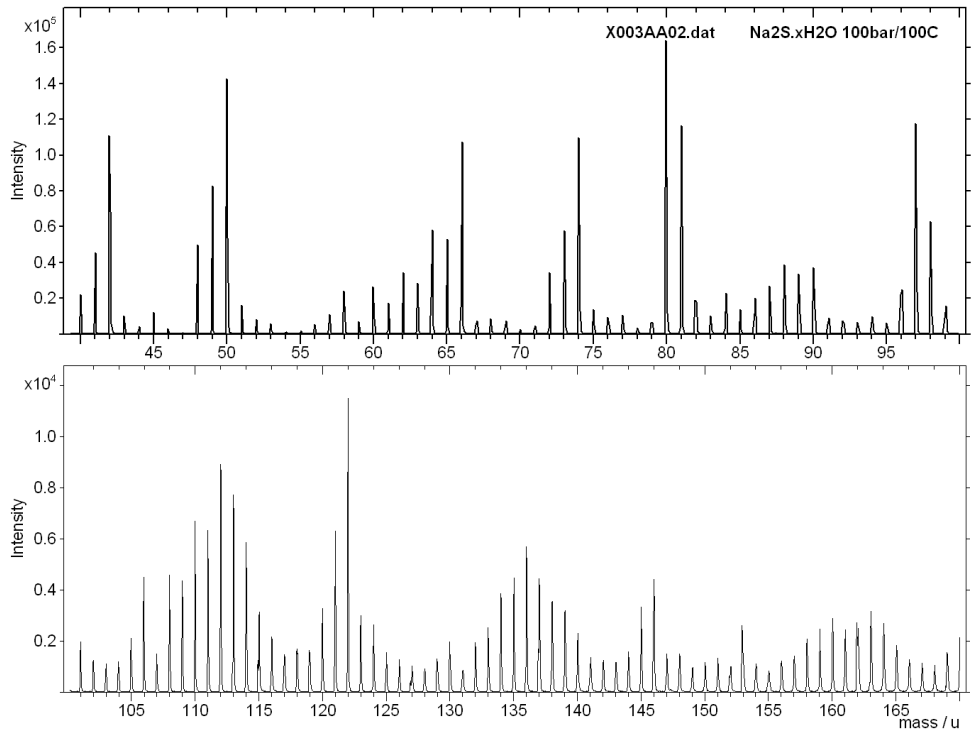

Figure S15: ToF-SIMS spectrum of sample 11 (100 °C/100 bar with Na2S.xH2O) after washings to remove unreacted sulfur.

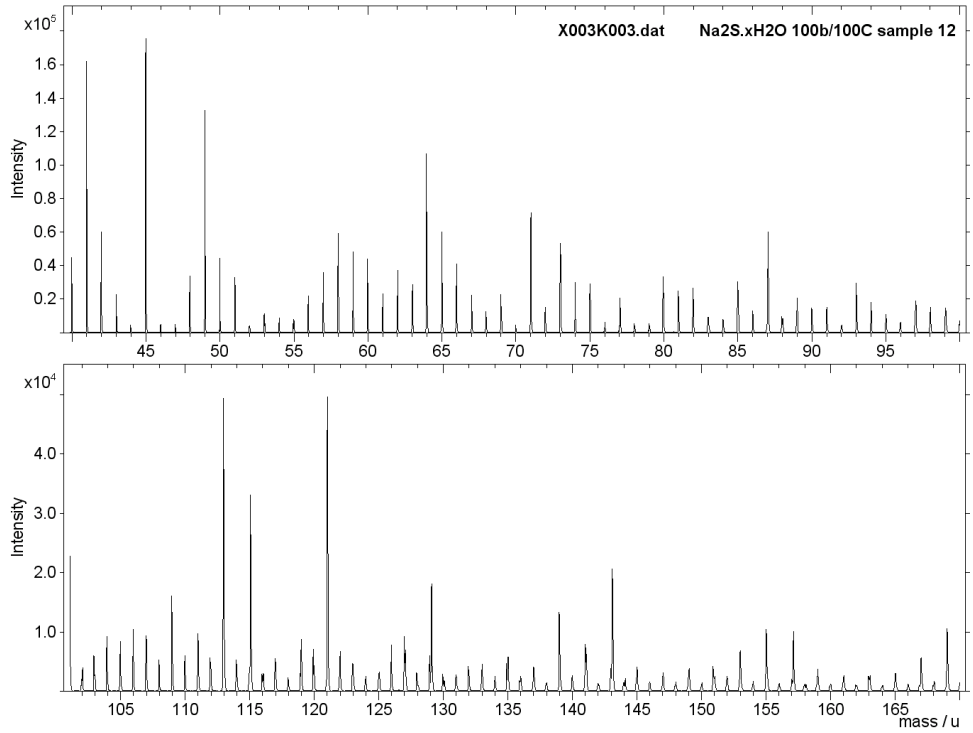

Figure S16: ToF-SIMS spectrum of sample 12 (100 °C/100 bar with Na2S.xH2O). This sample was not washed before analysis.

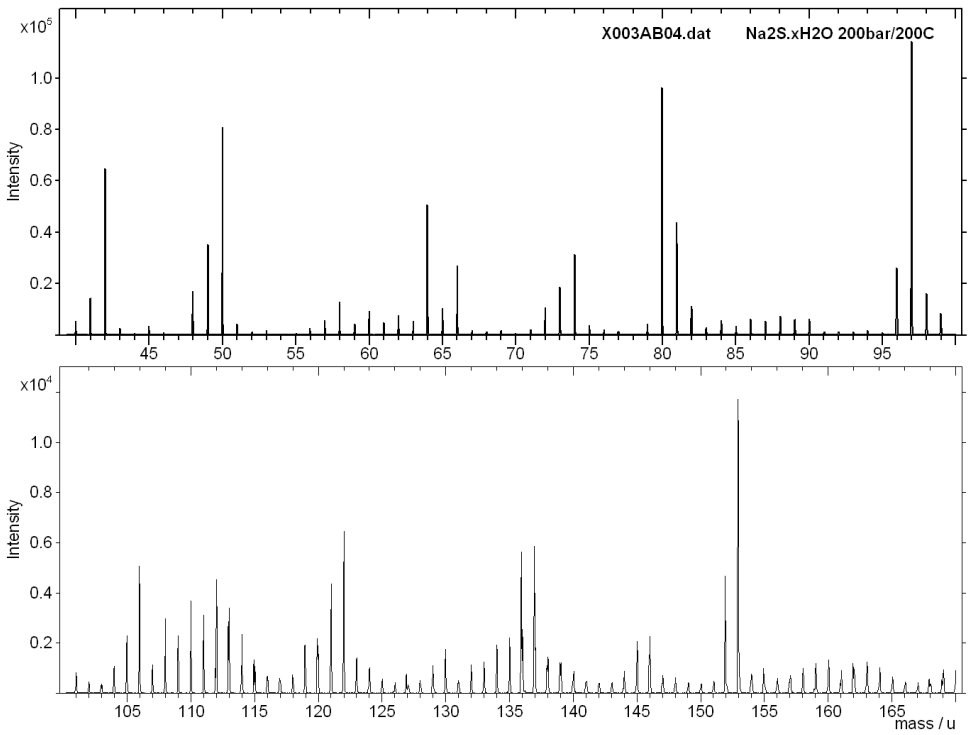

Figure S18: ToF-SIMS spectrum of sample 13 (200 °C/200 bar with $Na_2S.xH_2O$) after washings to remove unreacted sulfur.

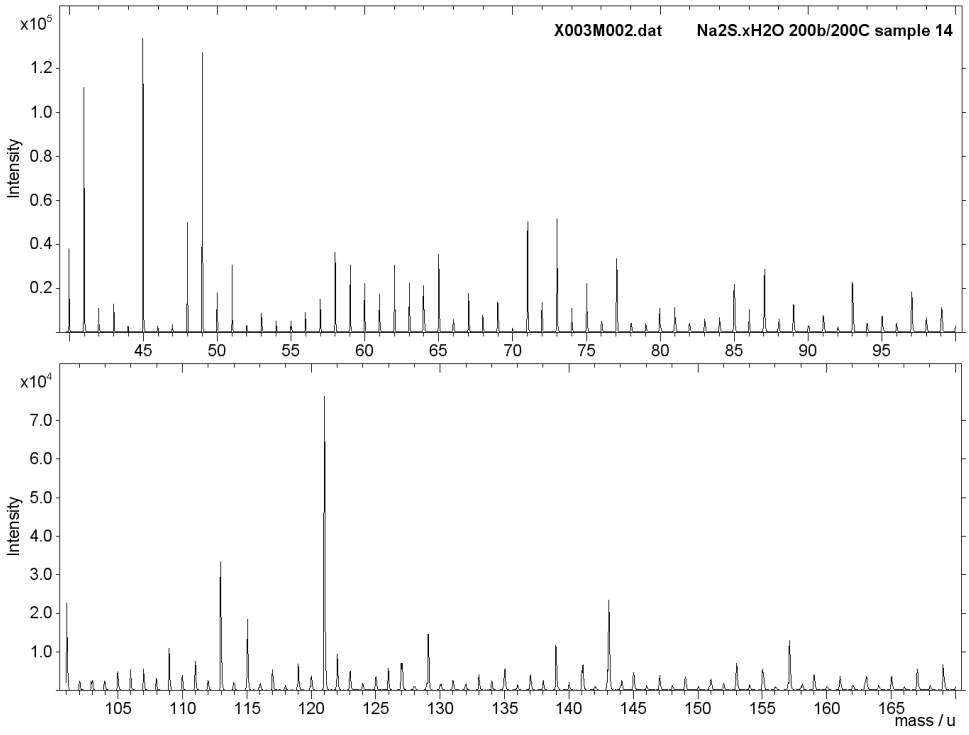

Figure S17: ToF-SIMS spectrum of sample 14 (200 °C/200 bar with Na2S.xH2O). This sample was not washed before analysis.

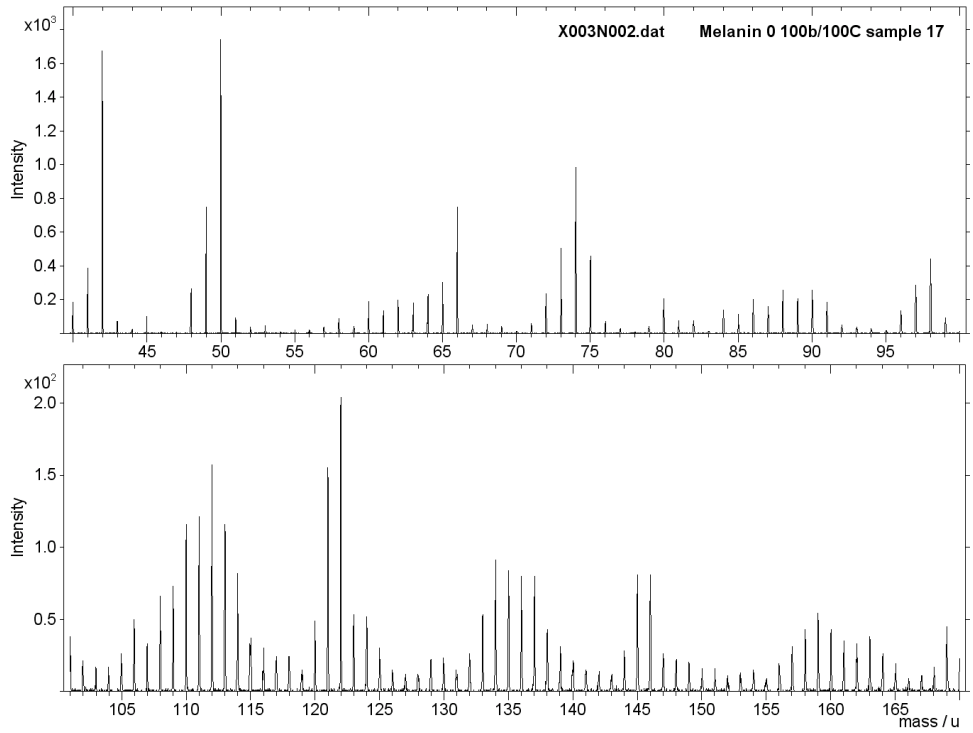

Figure S19: ToF-SIMS spectrum of sample 17 (100 °C/100 bar)

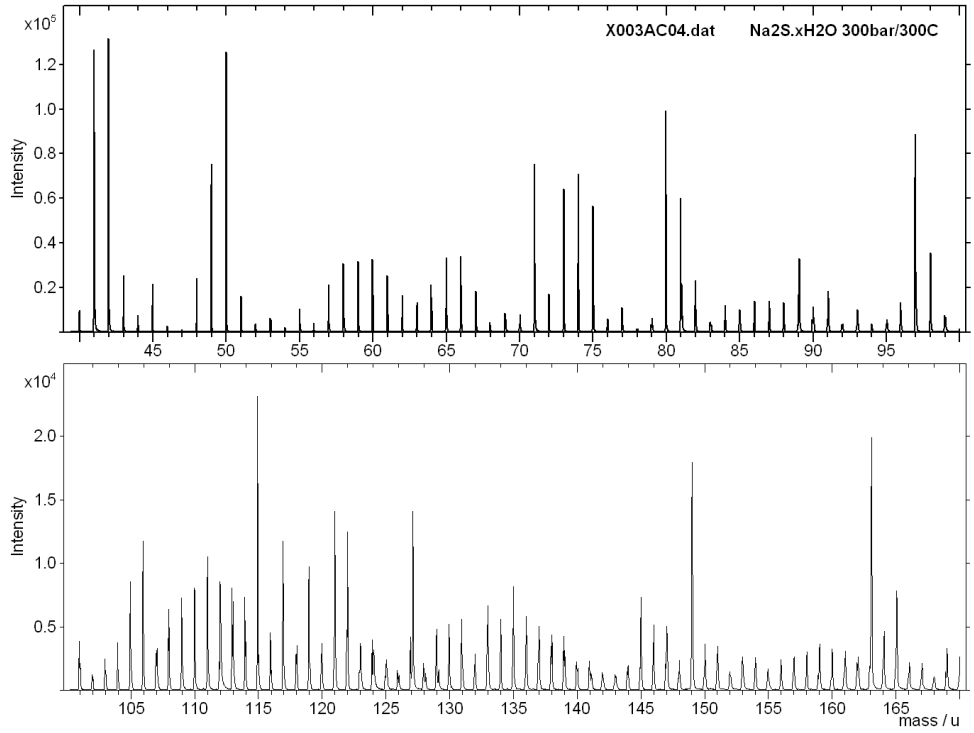

Figure S20: ToF-SIMS spectrum of sample 18 (300 °C/300 bar with Na2S.xH2O) after washings to remove unreacted sulfur.

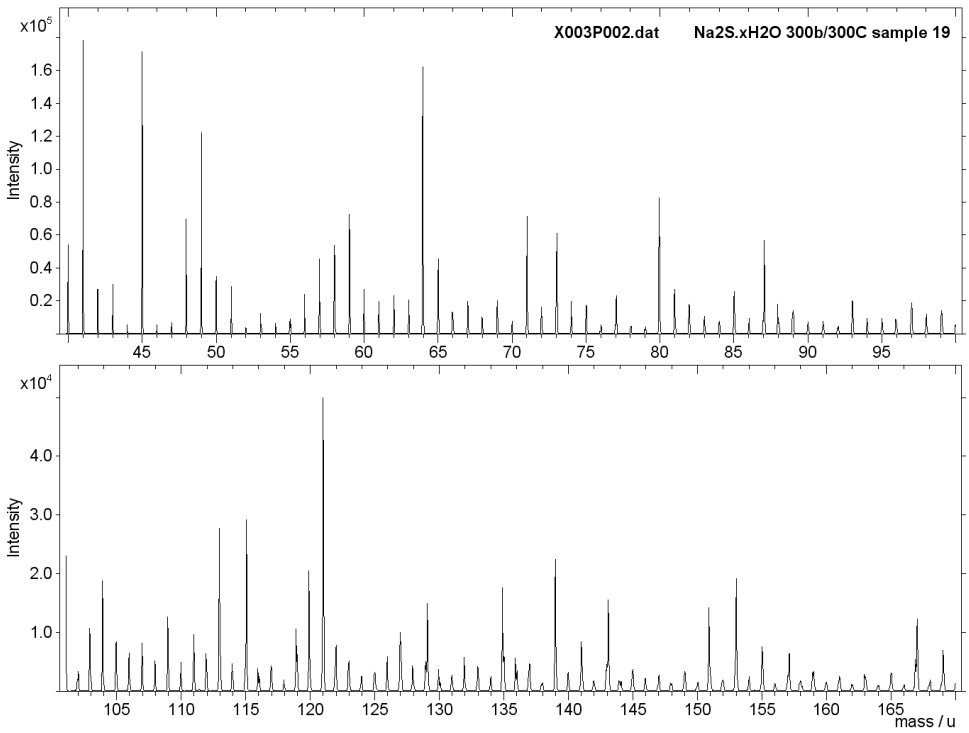

Figure S21: ToF-SIMS spectrum of sample 19 (300 °C/300 bar with Na2S.xH2O). This sample was not washed before analysis.

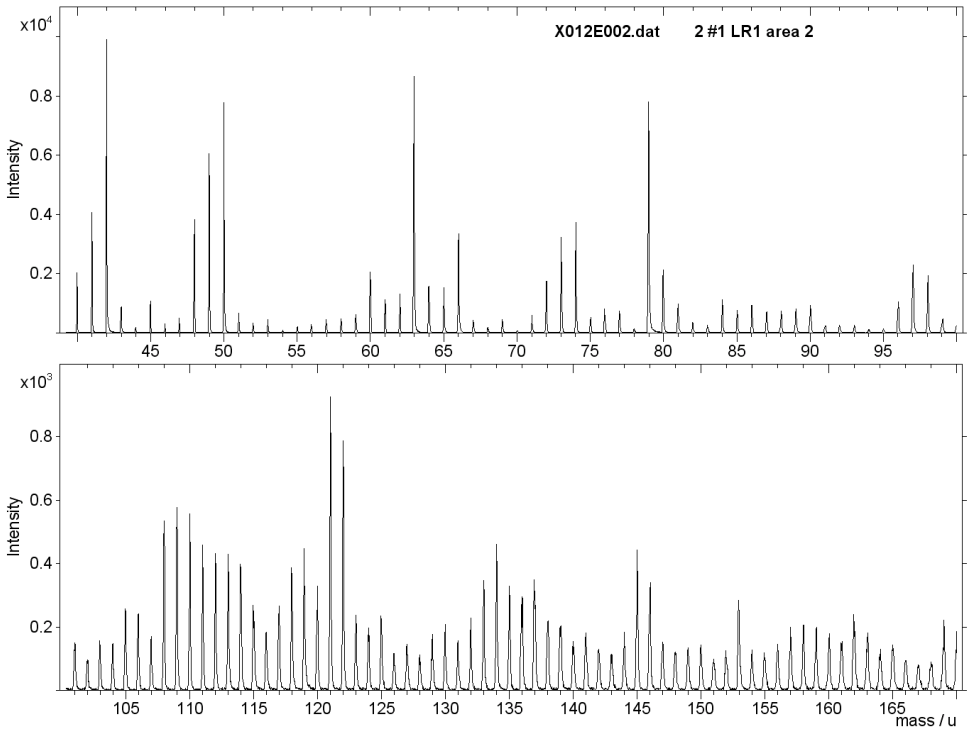

Figure S22: ToF-SIMS spectrum of fossil sample LR1.

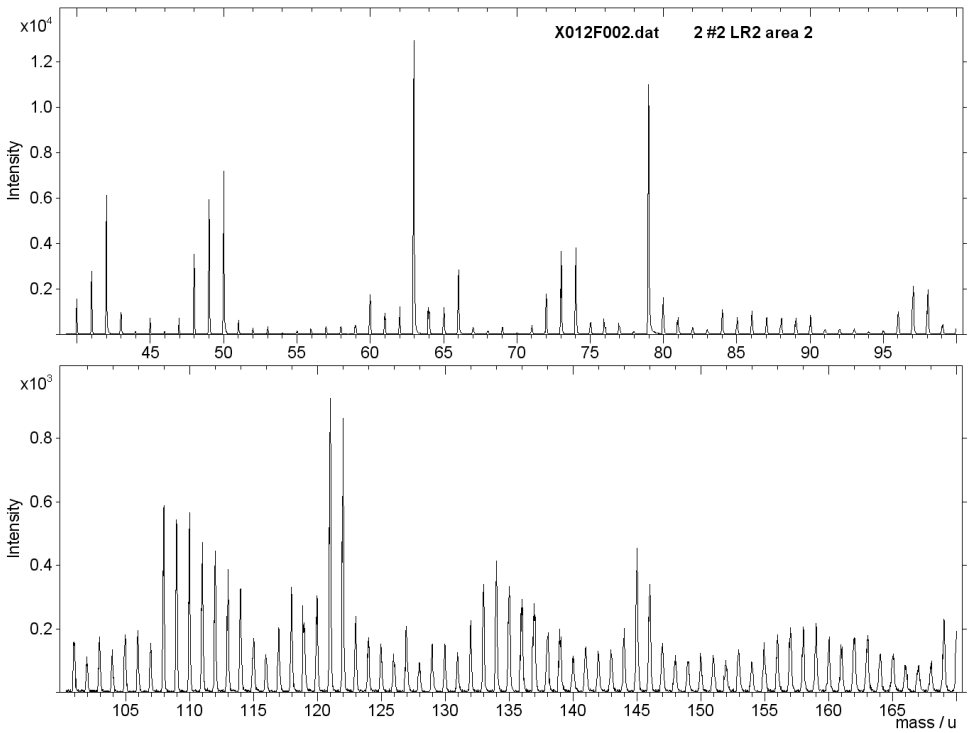

Figure S23: ToF-SIMS spectrum of fossil sample LR2.

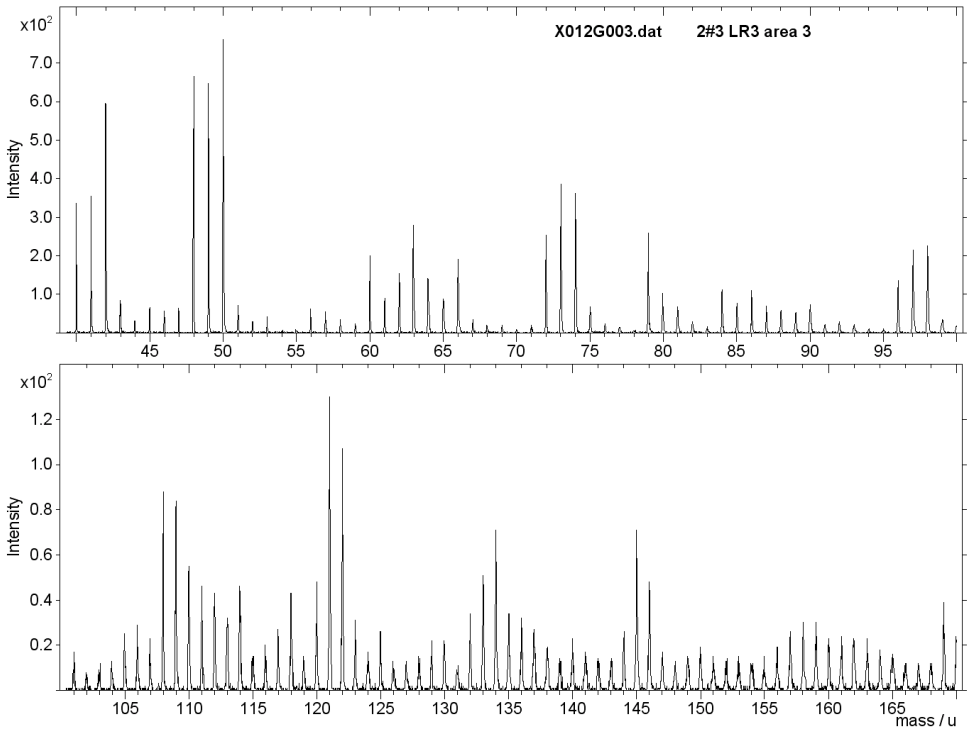

Figure S24: ToF-SIMS spectrum of fossil sample LR3.

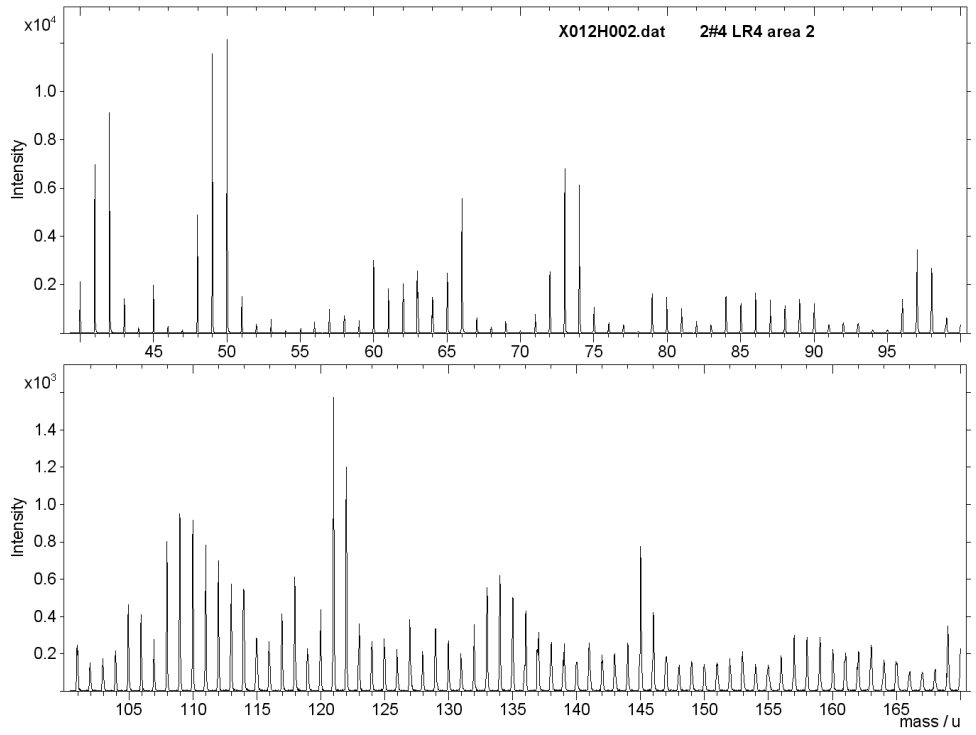

Figure S25: ToF-SIMS spectrum of fossil sample LR4.

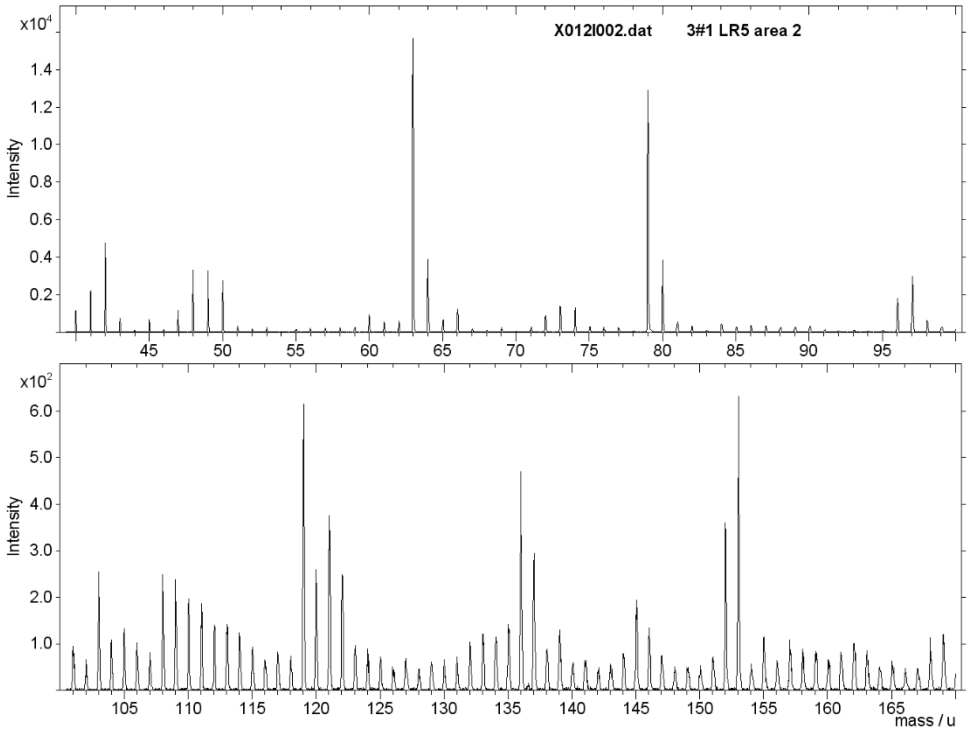

Figure S26: ToF-SIMS spectrum of fossil sample LR5.

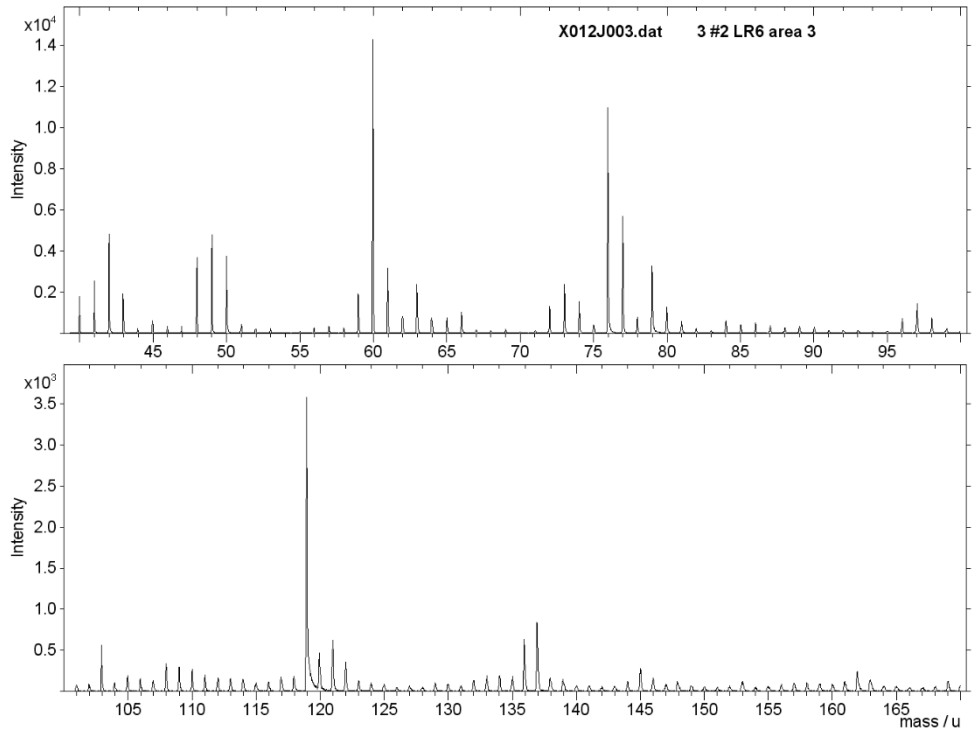

Figure S27: ToF-SIMS spectrum of fossil sample LR6.

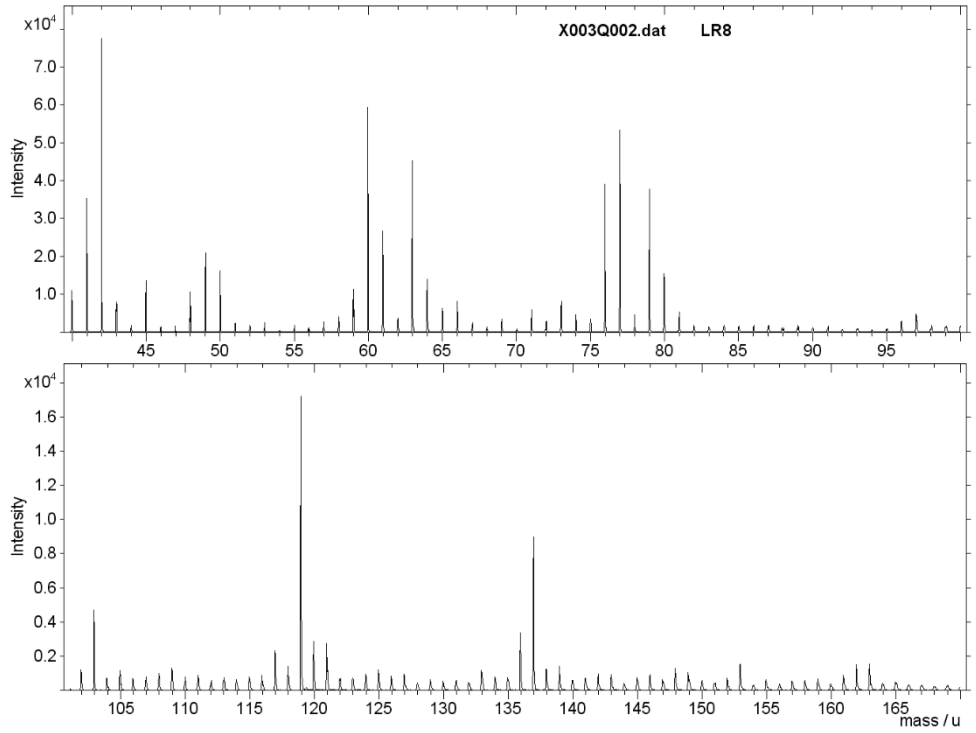

Figure S28: ToF-SIMS spectrum of fossil sample LR8.

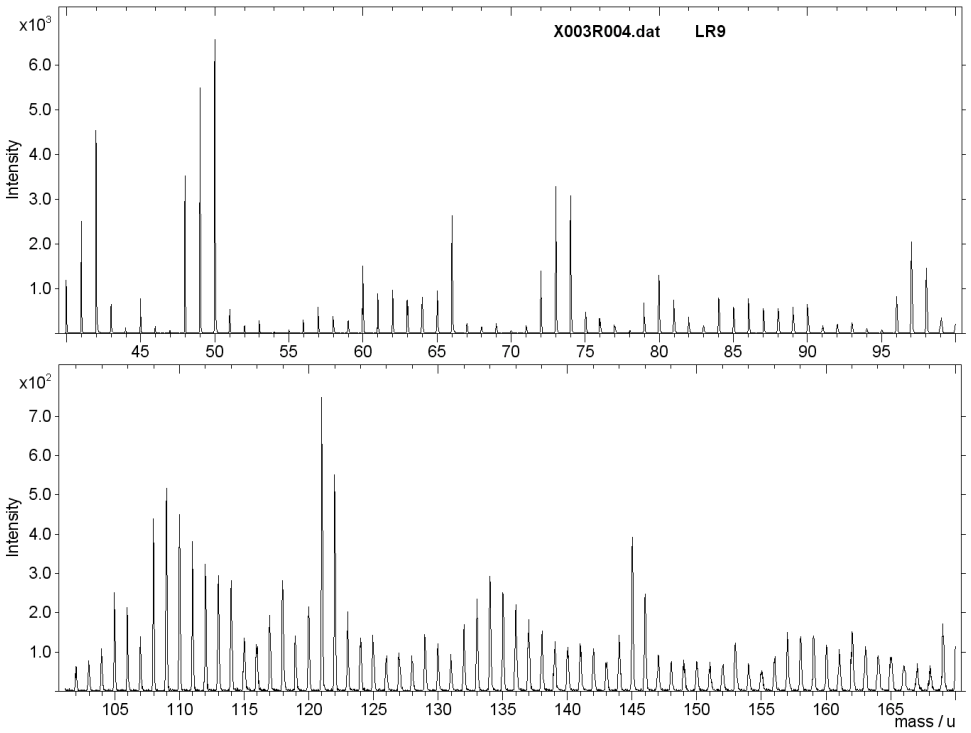

Figure S29: ToF-SIMS spectrum of fossil sample LR9.

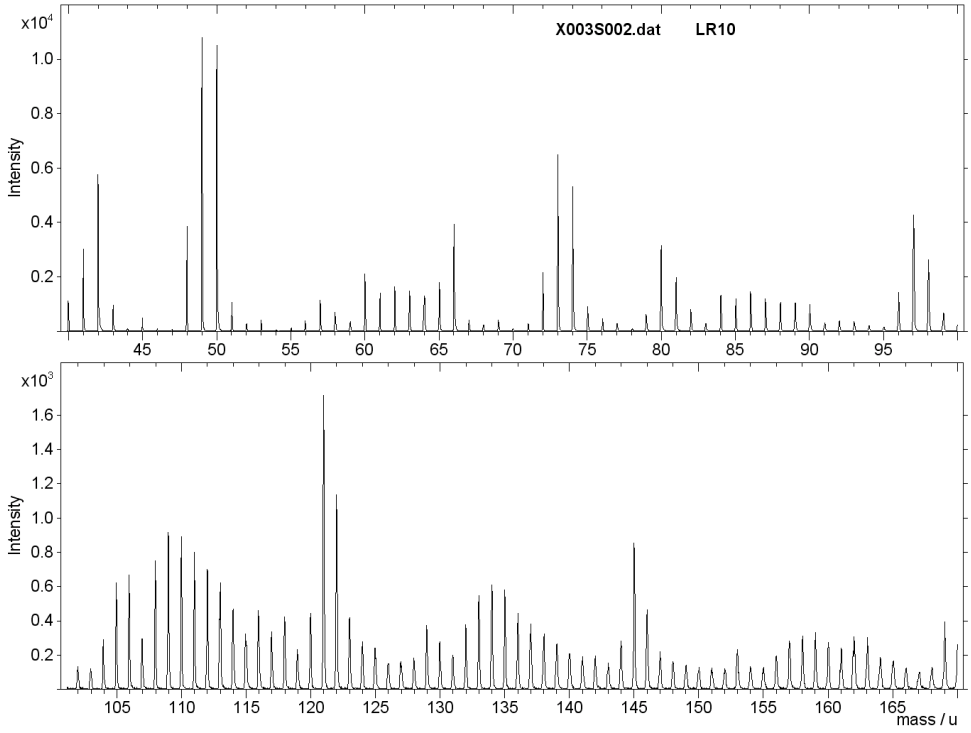

Figure S30: ToF-SIMS spectrum of fossil sample LR10.

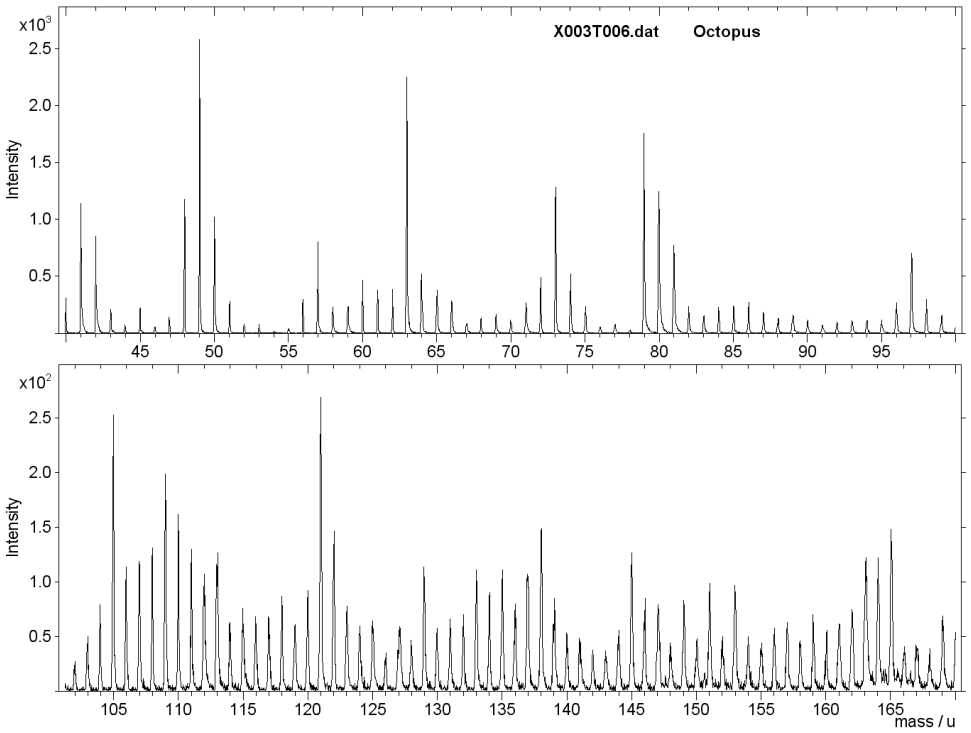

Figure S31: ToF-SIMS spectrum of fossil sample "Octopus".

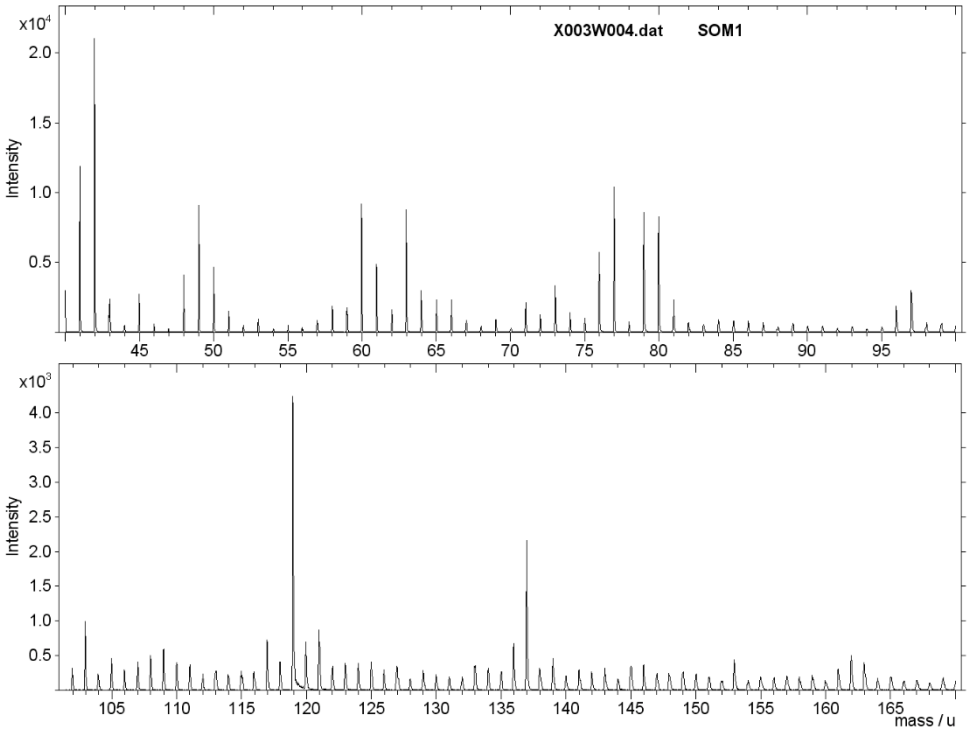

Figure S32: ToF-SIMS spectrum of fossil sample SOM1.

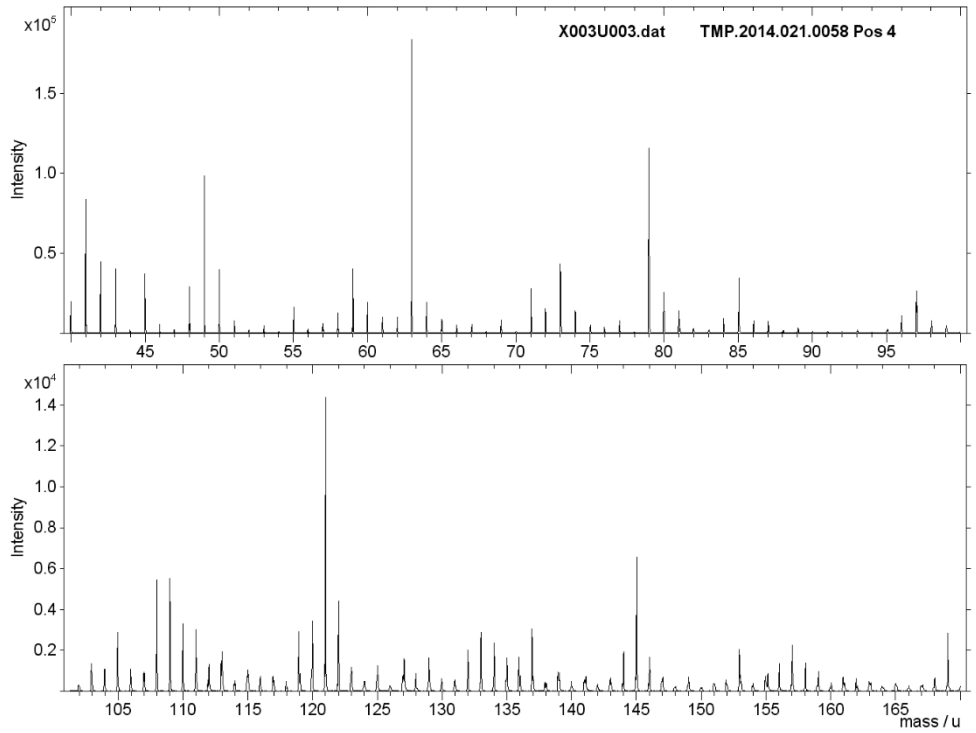

Figure S33: ToF-SIMS spectrum of fossil sample TMP 2014.021.0058.

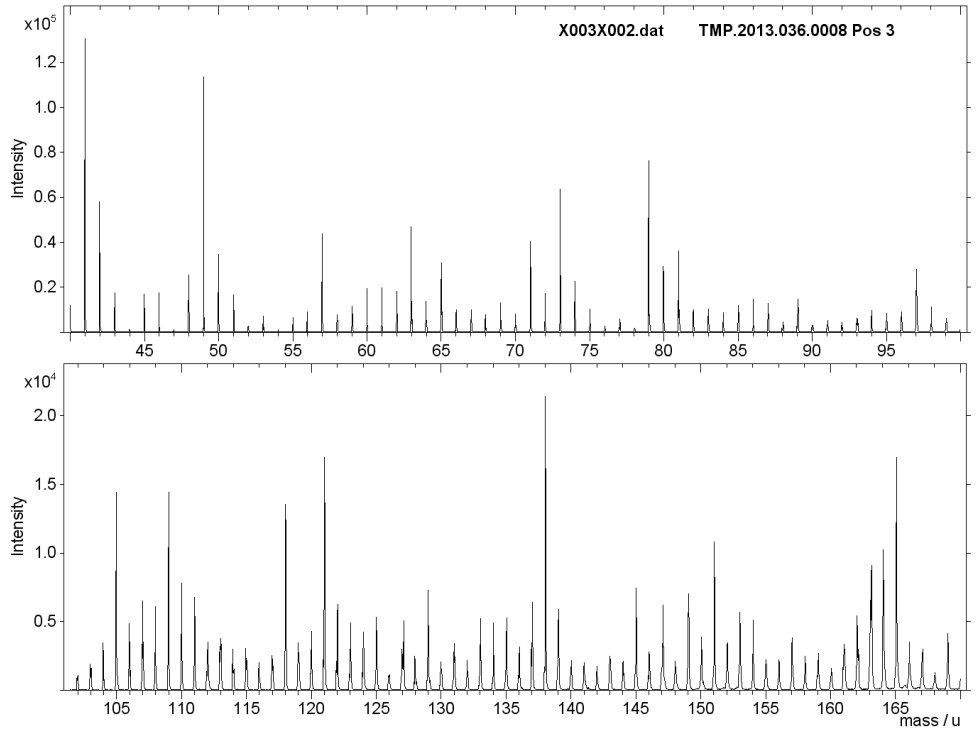

Figure S34: ToF-SIMS spectrum of fossil sample TMP 2013.036.0008.

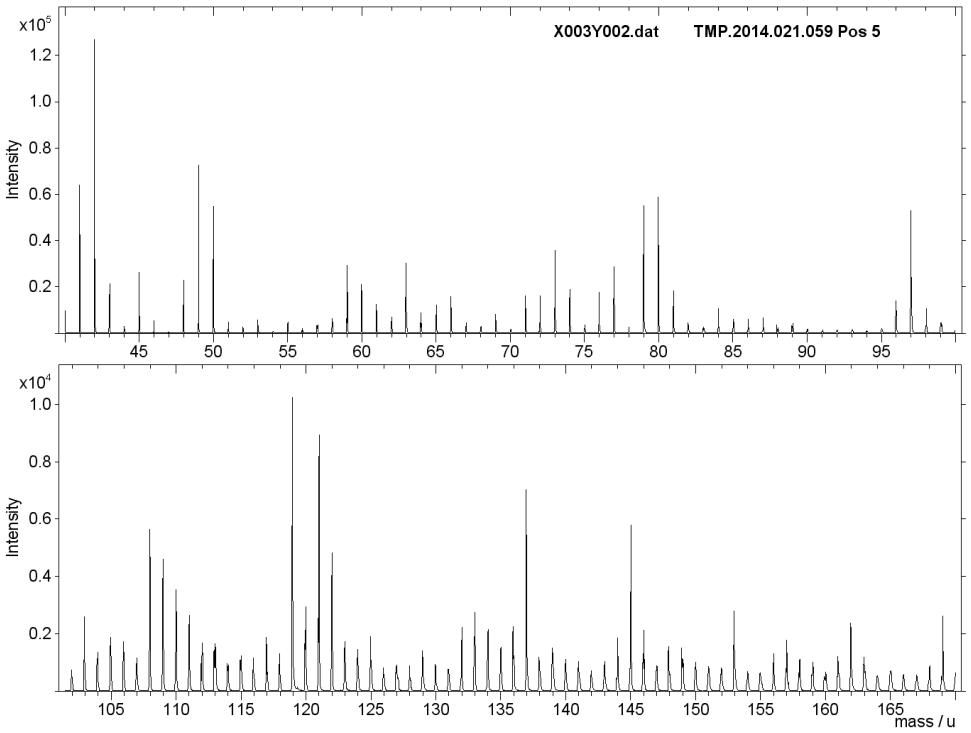

Figure S35: ToF-SIMS spectrum of fossil sample TMP 2014.021.0059.

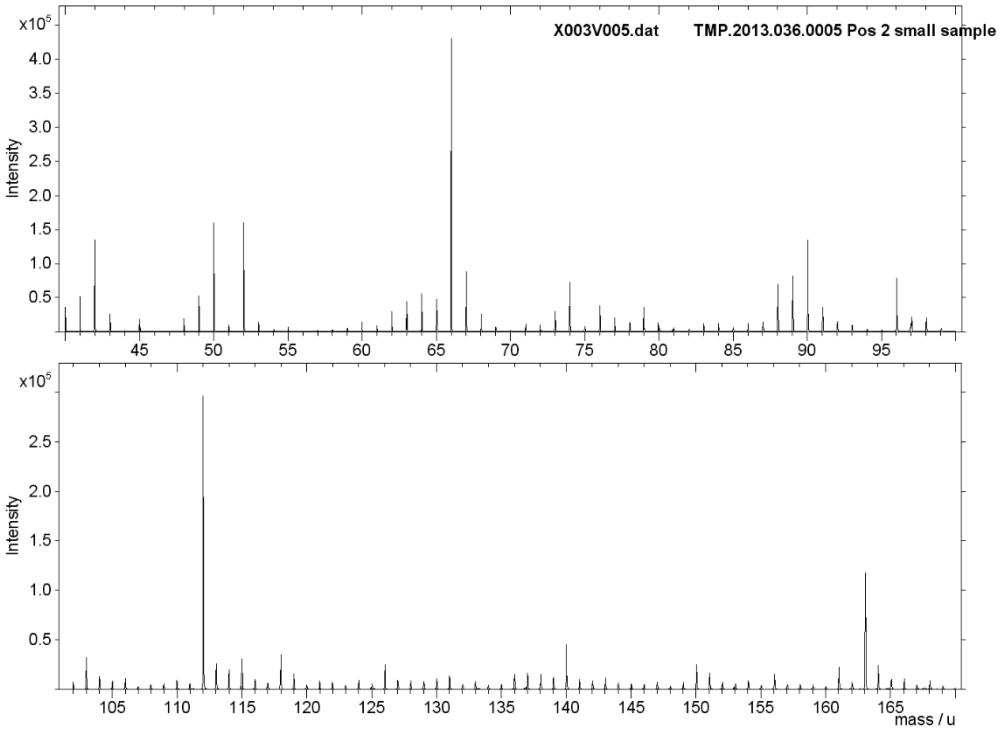

Figure S36: ToF-SIMS spectrum of fossil sample TMP 2013.036.0005.

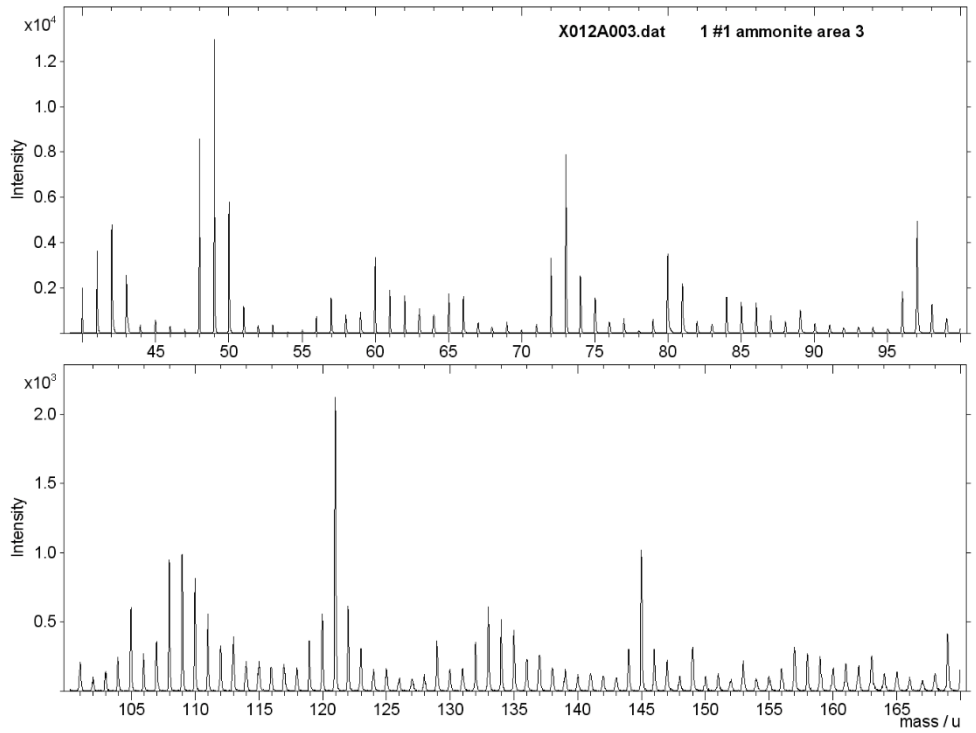

Figure S37: ToF-SIMS spectrum of fossil sample K1.

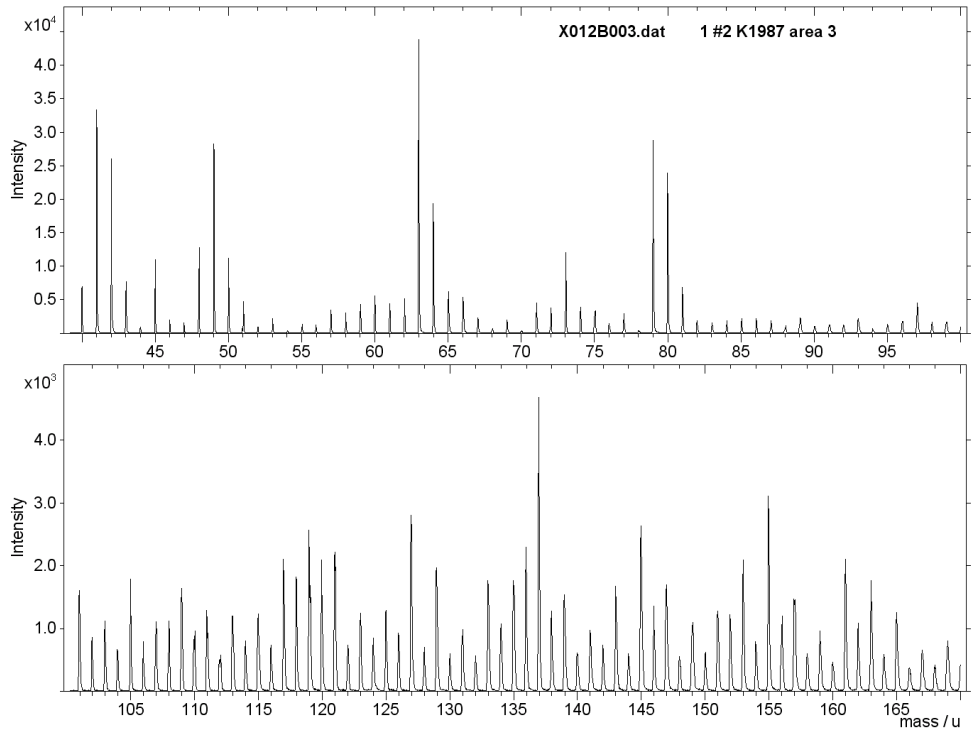

Figure S38: ToF-SIMS spectrum of fossil sample K1987.

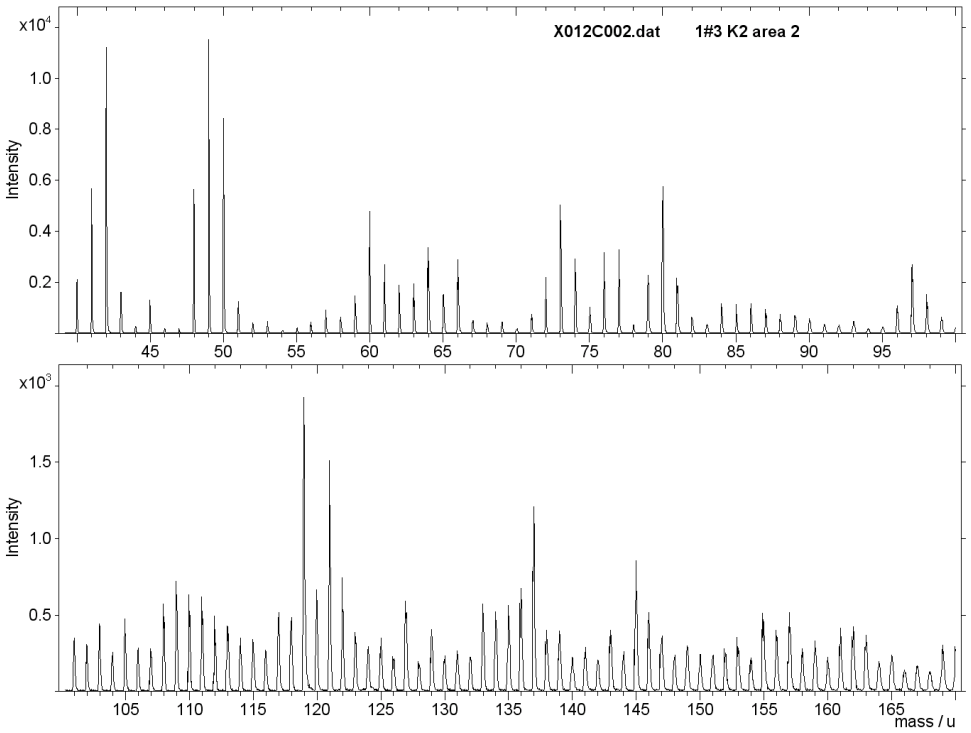

Figure S39: ToF-SIMS spectrum of fossil sample K2.

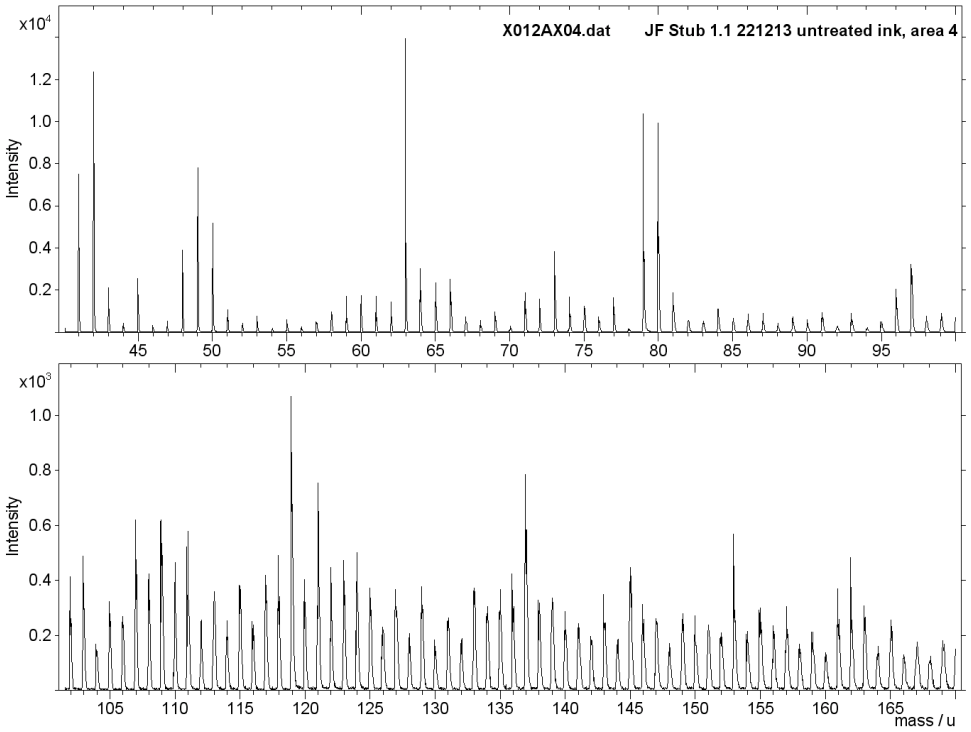

Figure S40: ToF-SIMS spectrum of fossil sample YPM 221213.

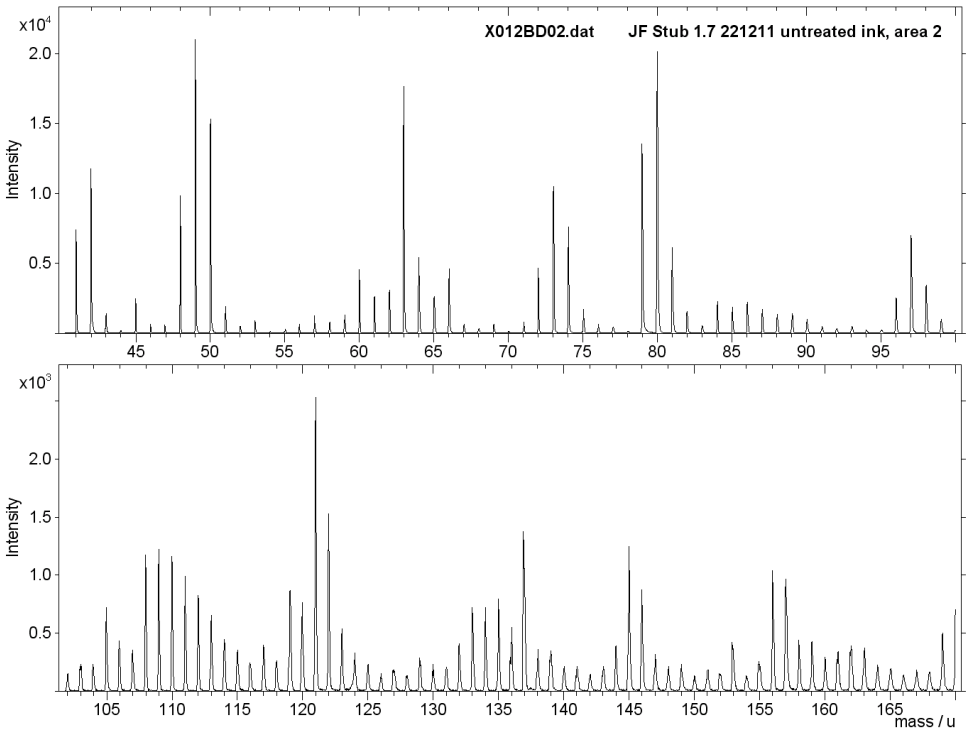

Figure S 41: ToF-SIMS spectrum of fossil sample YPM 221211.

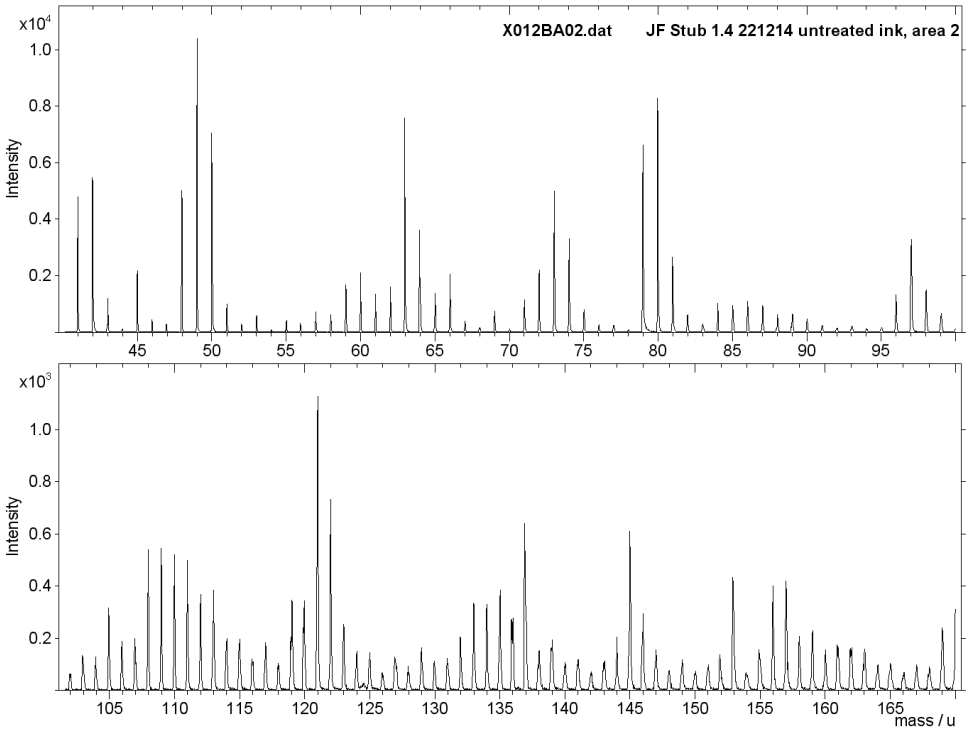

Figure S42: ToF-SIMS spectrum of fossil sample YPM 221214.

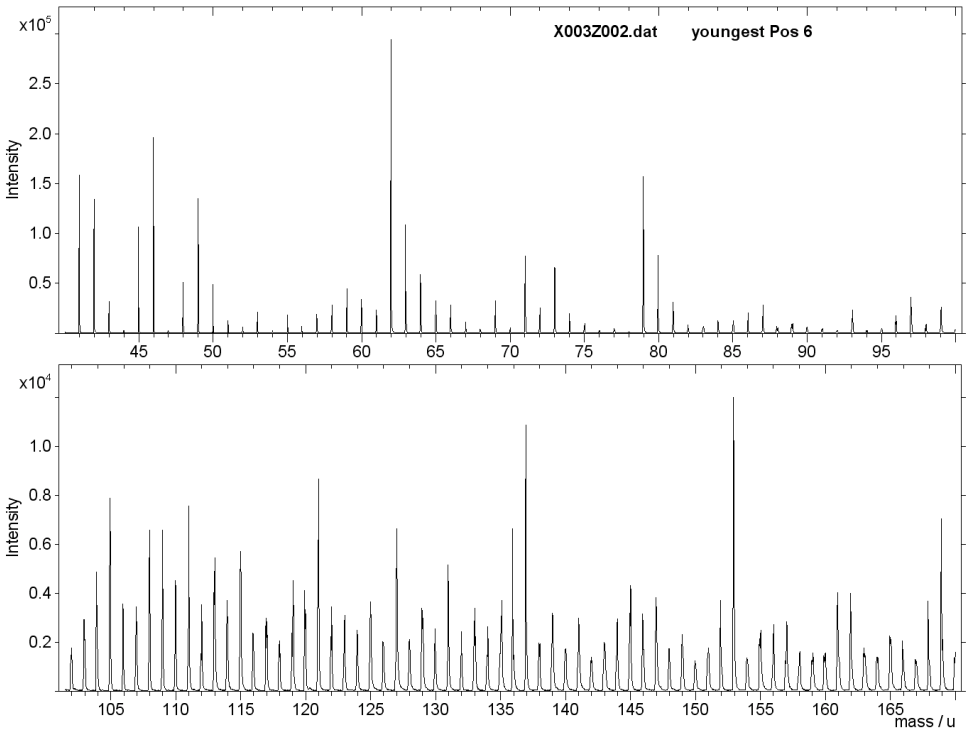

Figure S43: ToF-SIMS spectrum of fossil sample SNM Z20058

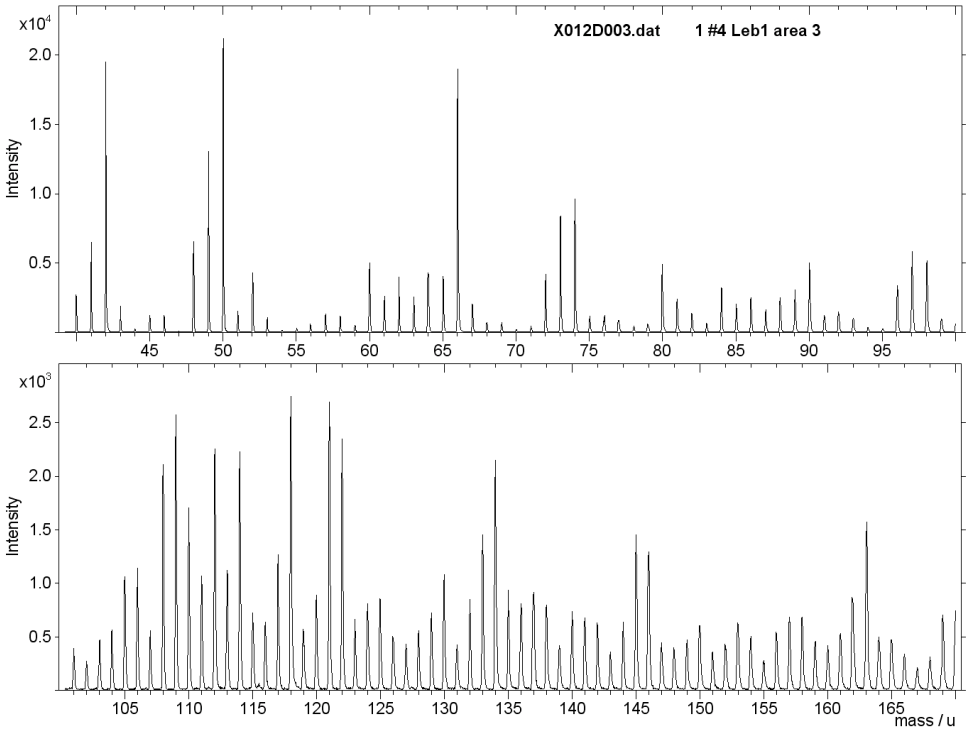

Figure S44: ToF-SIMS spectrum of fossil sample Leb1.

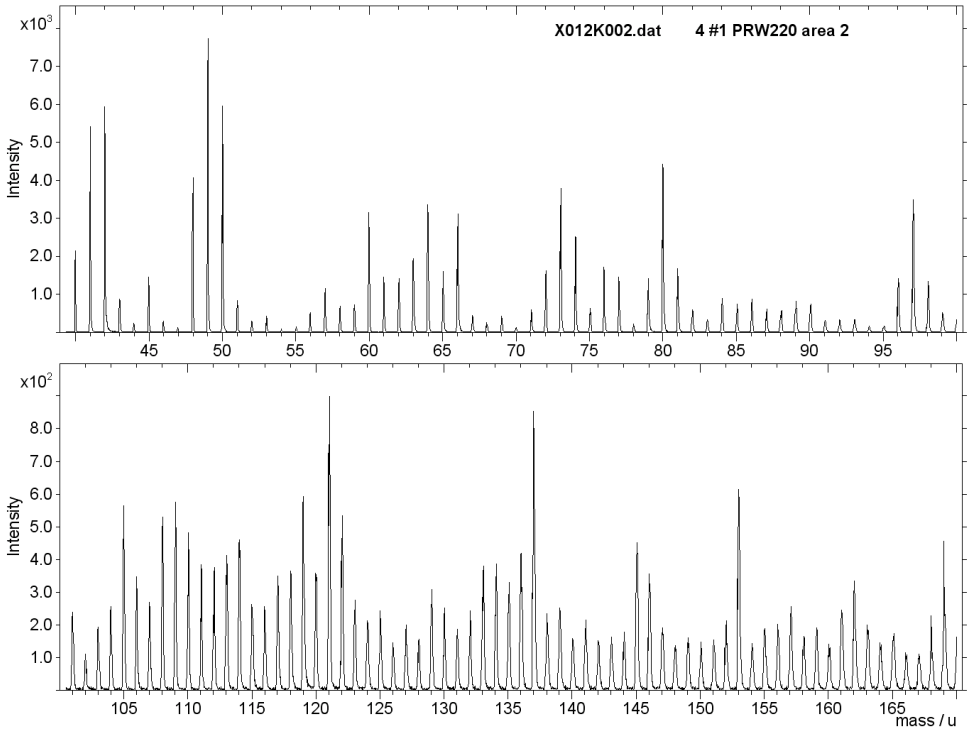

Figure S45: ToF-SIMS spectrum of fossil sample PRW 220.

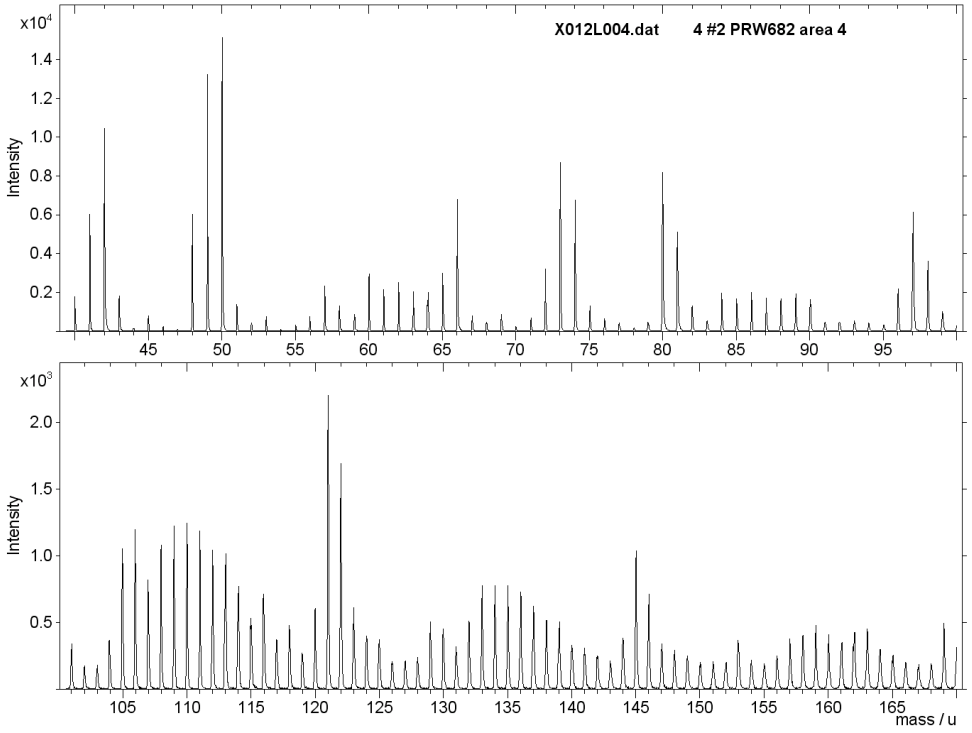

Figure S46: ToF-SIMS spectrum of fossil sample PRW 682.

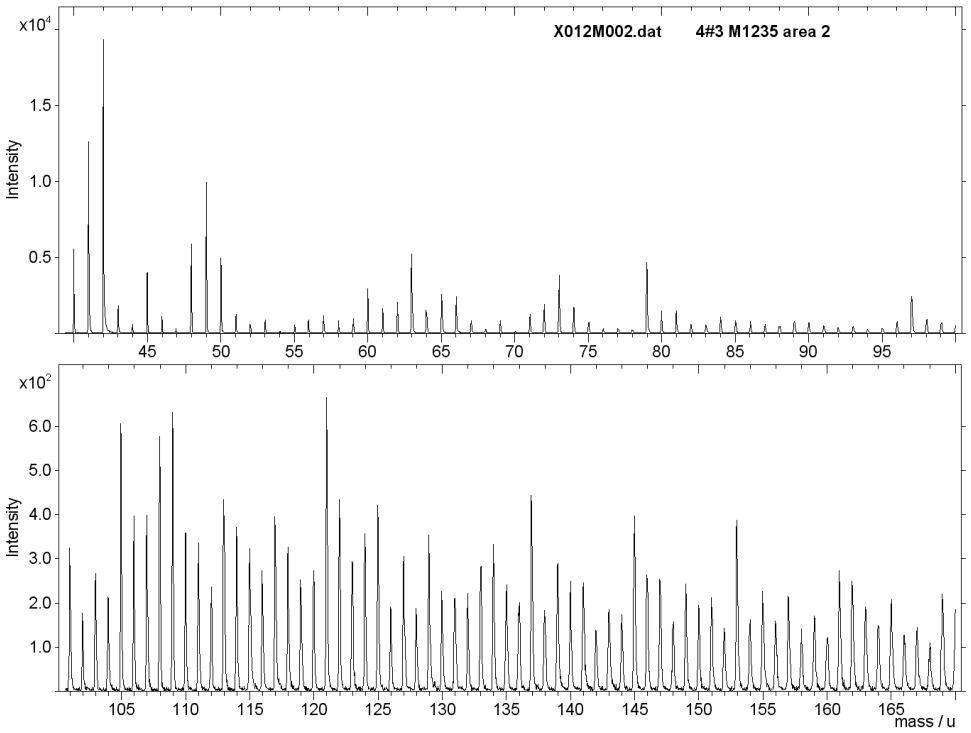

Figure S47: ToF-SIMS spectrum of fossil sample BRLSI M1235A.

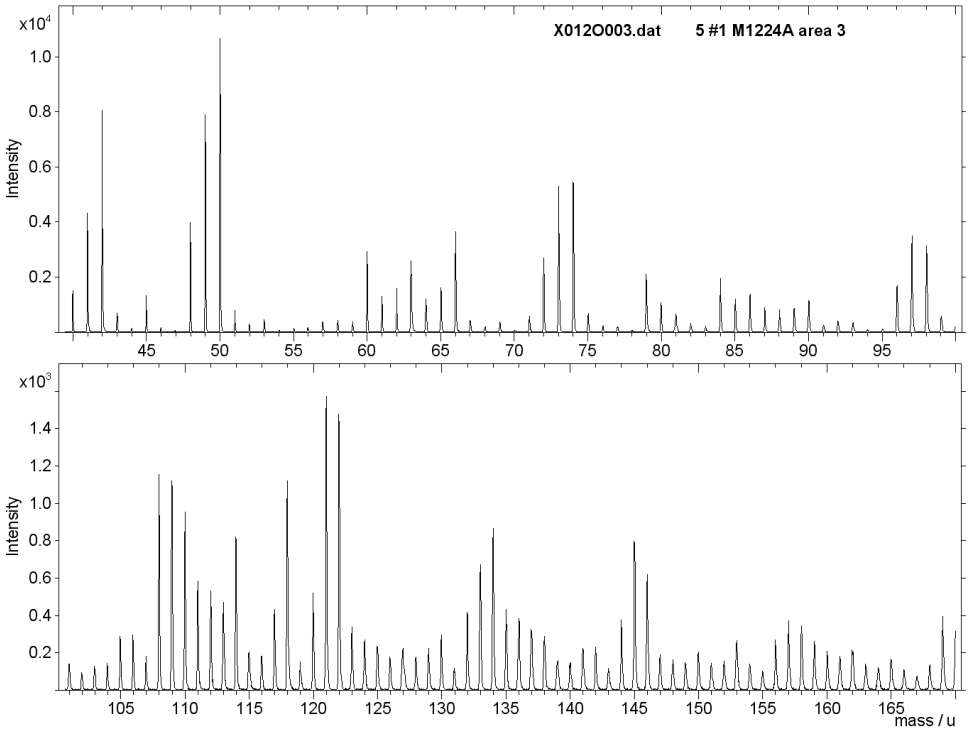

Figure S48: ToF-SIMS spectrum of fossil sample BRLSI M1224A.

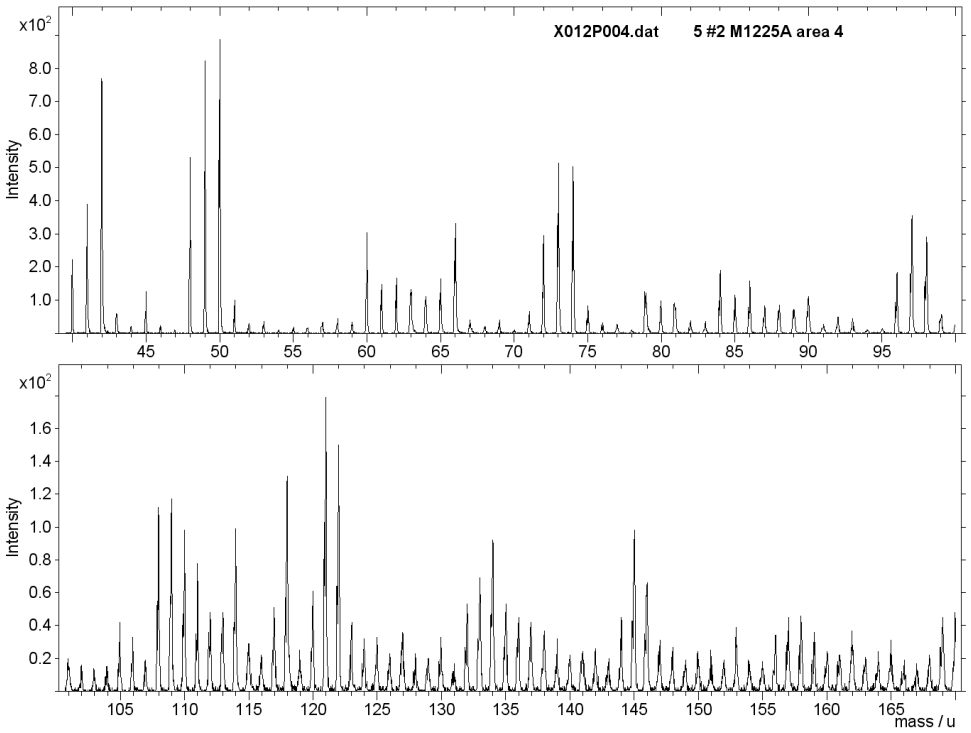

Figure S49: ToF-SIMS spectrum of fossil sample BRLSI M1225A.

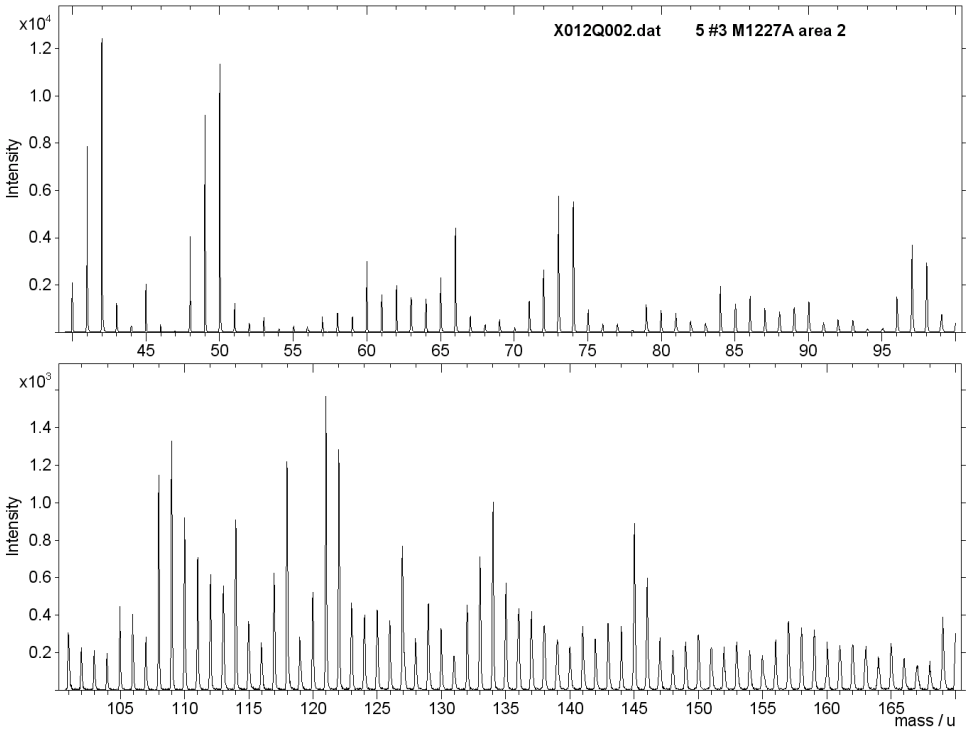

Figure S50: ToF-SIMS spectrum of fossil sample BRLSI M1227A.

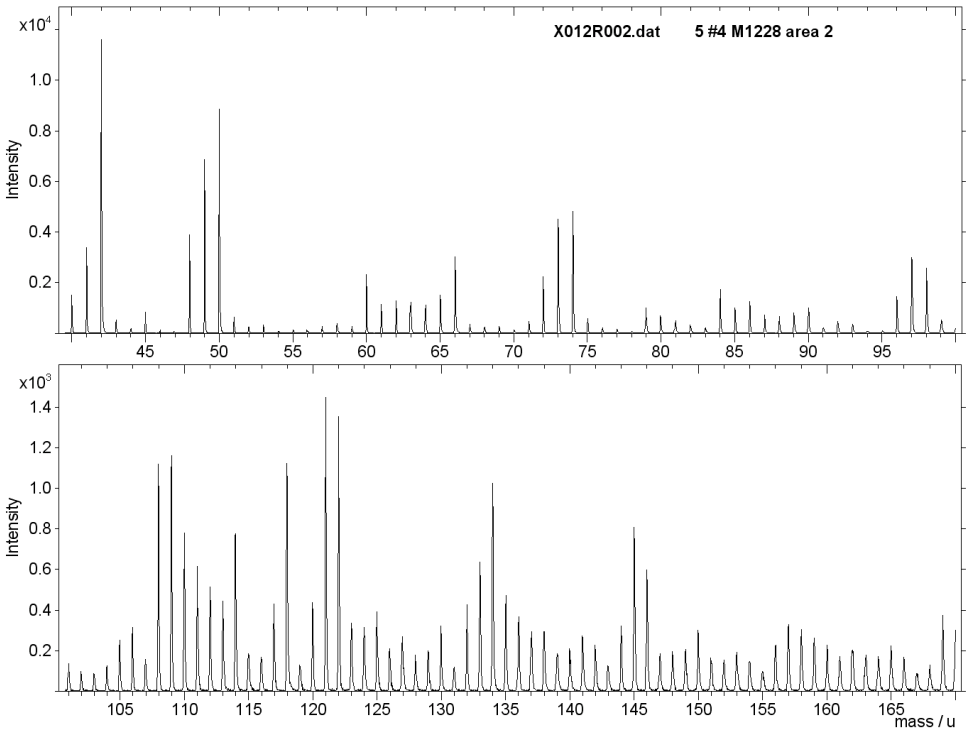

Figure S51: ToF-SIMS spectrum of fossil sample BRLSI M1228.

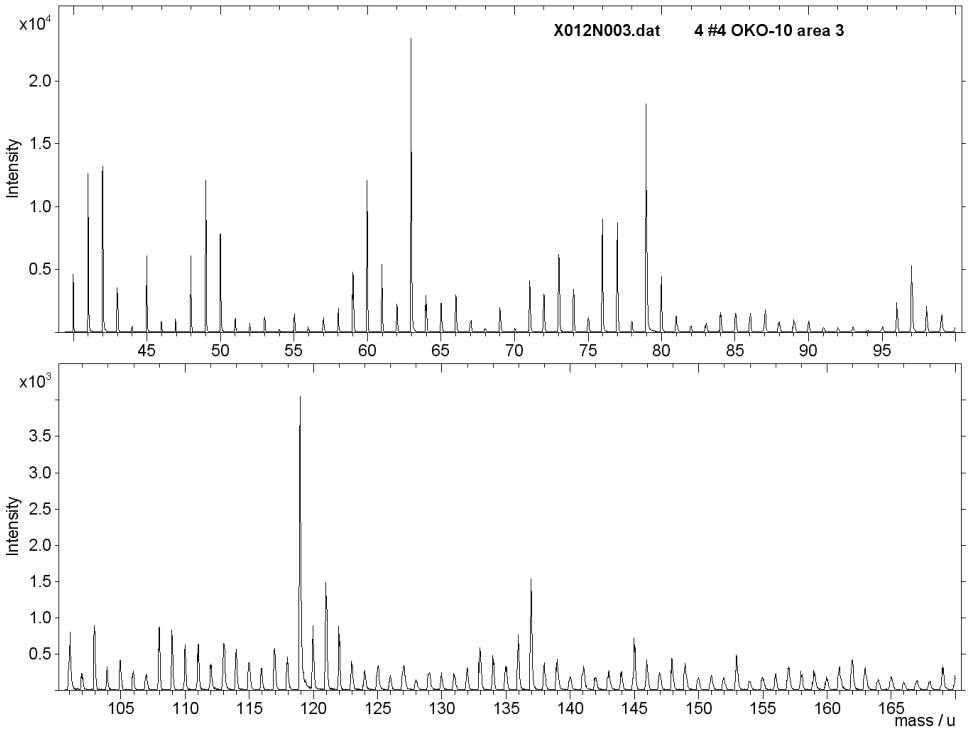

Figure S52: ToF-SIMS spectrum of fossil sample OK D-10.

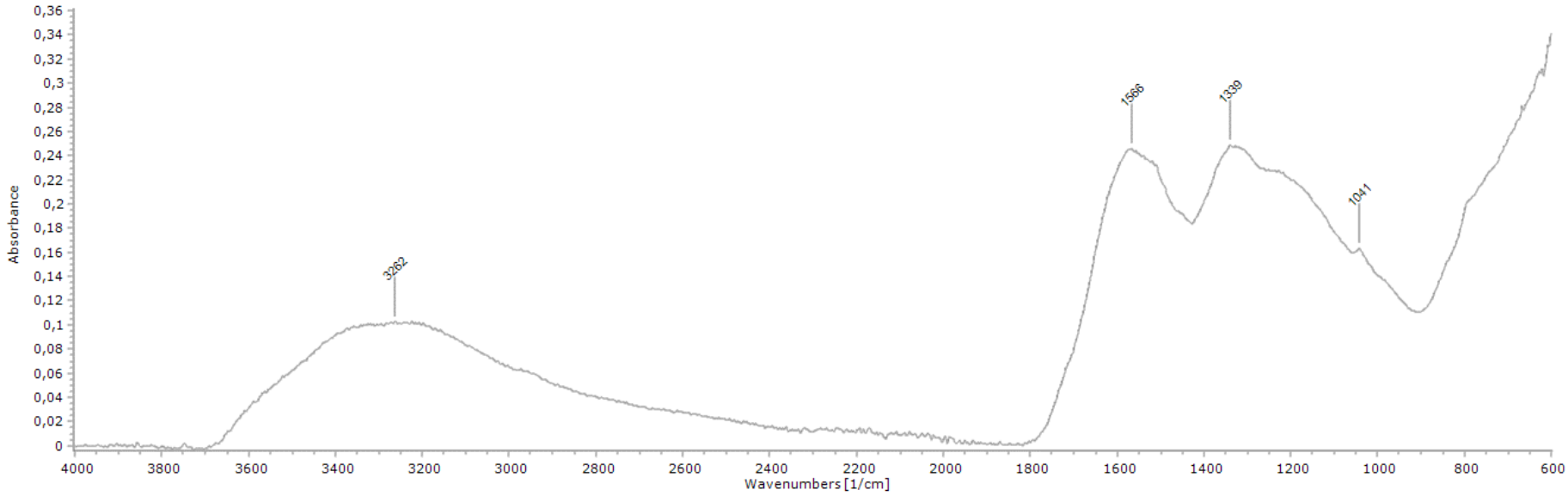

Figure S53: FTIR spectrum of purified cephalopod ink (Fresh).

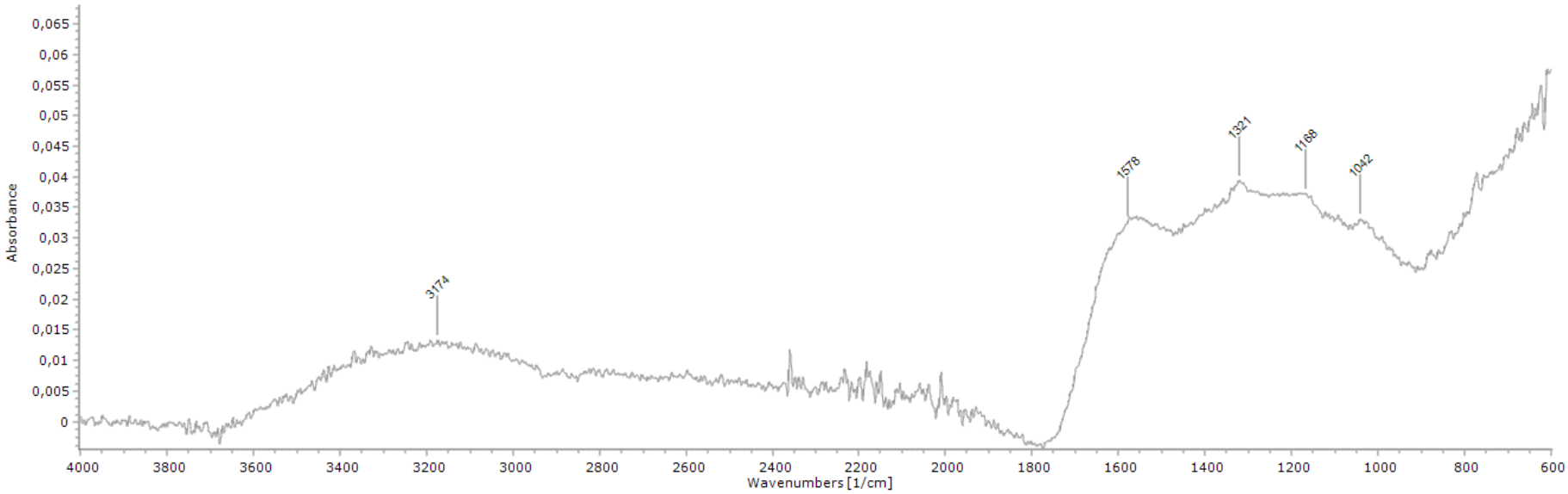

Figure S54: FTIR spectrum of matured sample 1 (200 °C/200 bar).

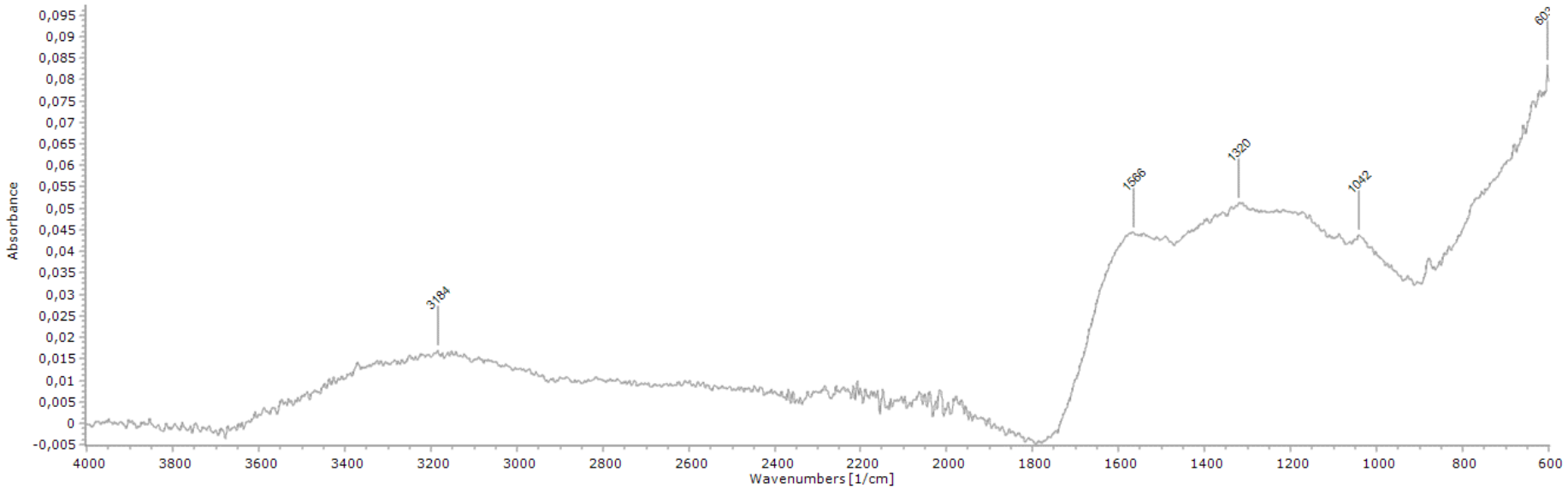

Figure S55: FTIR spectrum of matured sample 2 (200 °C/200 bar).

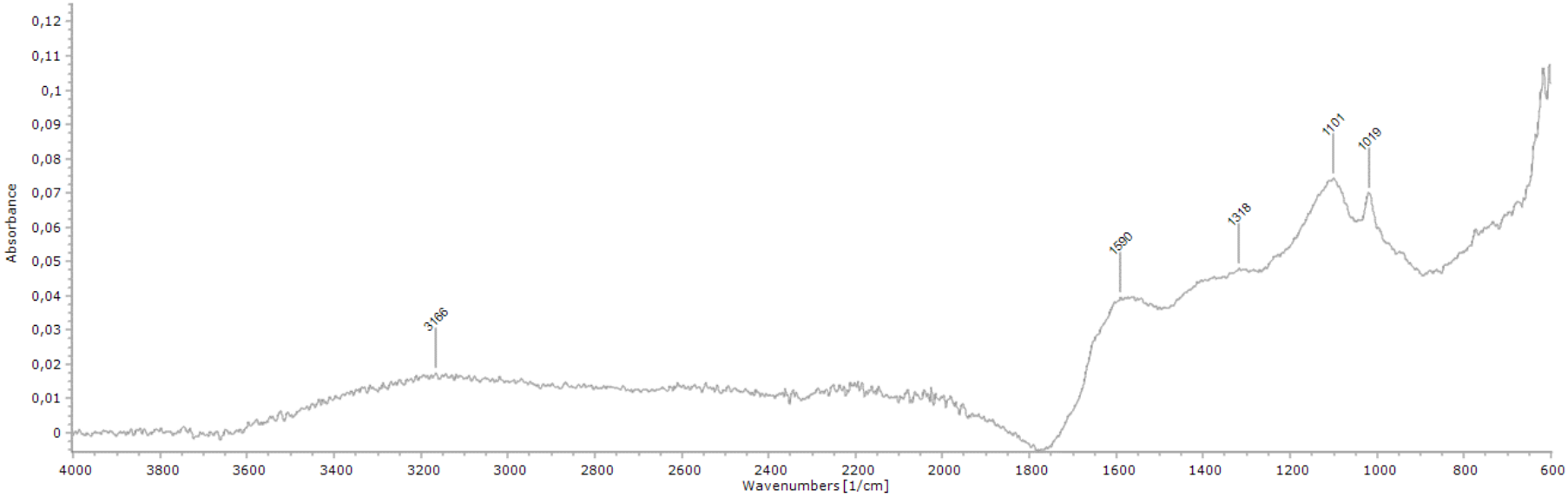

Figure S56: FTIR spectrum of matured sample 3 (200 °C/200 bar with elemental sulfur (S_8)).

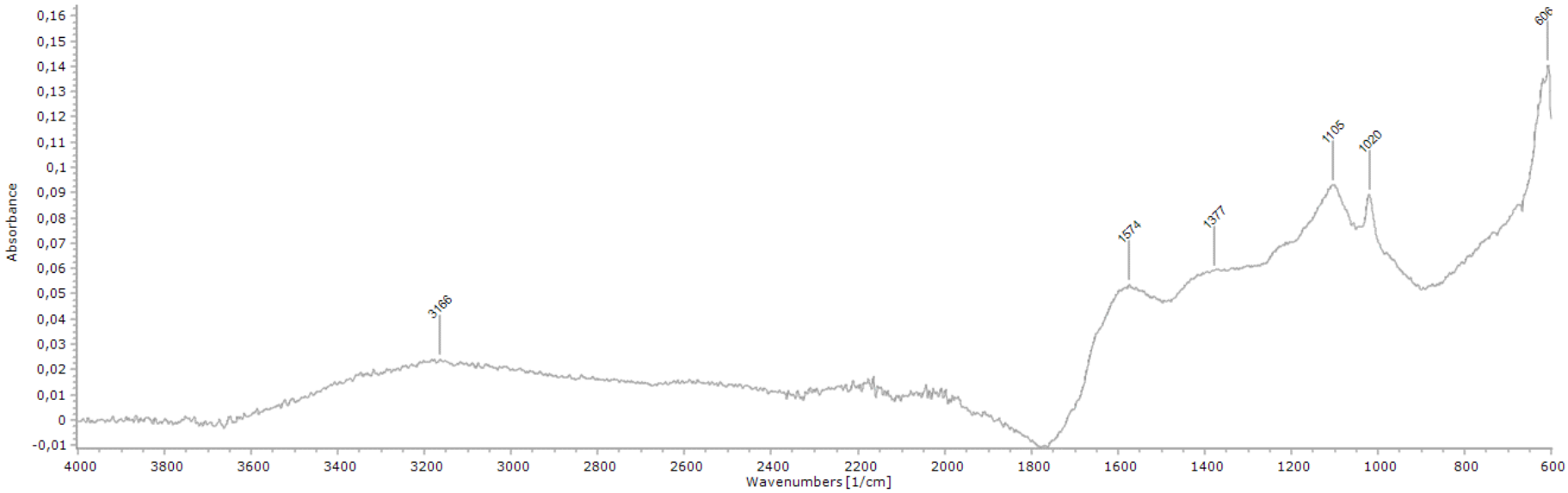

Figure S57: FTIR spectrum of matured sample 4 (200 °C/200 bar with elemental sulfur (S_8)).

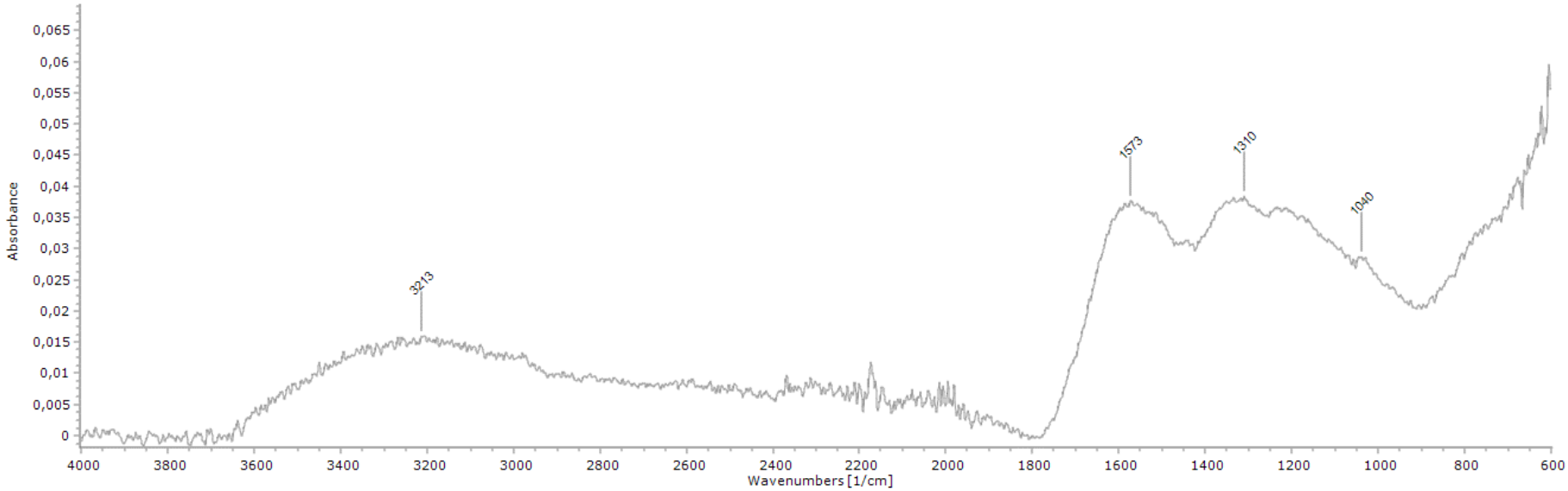

Figure S58: FTIR spectrum of matured sample 5 (100 °C/100 bar with elemental sulfur (S_8)).

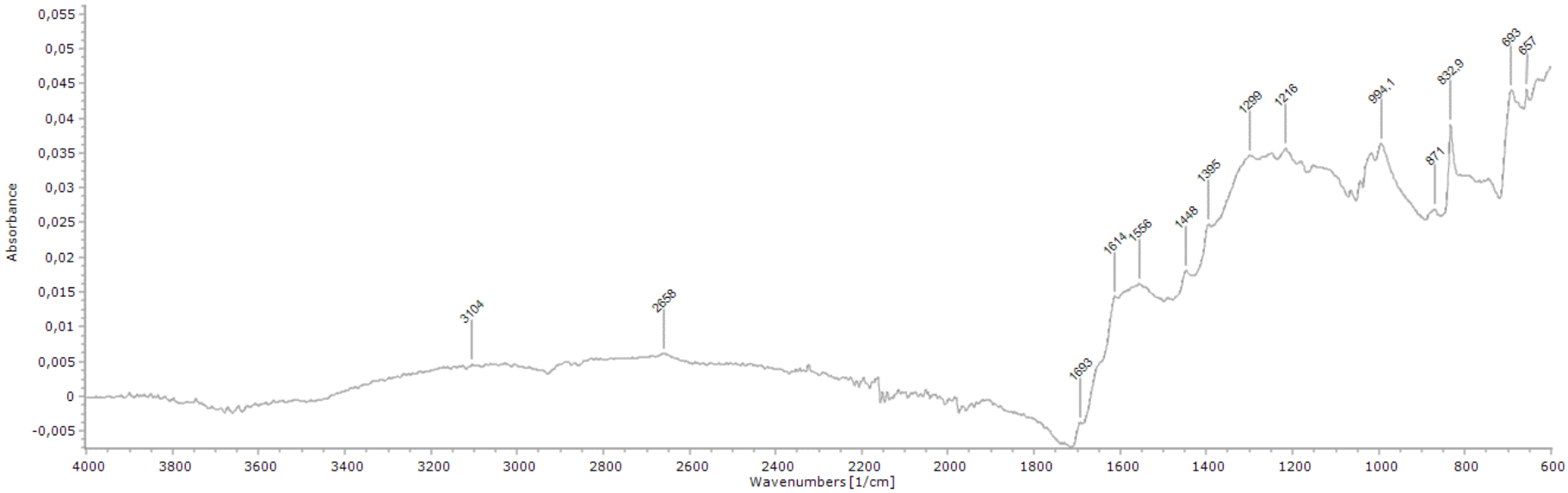

Figure S59: FTIR spectrum of matured sample 6 (300 °C /300 bar with elemental sulfur (S_8)).

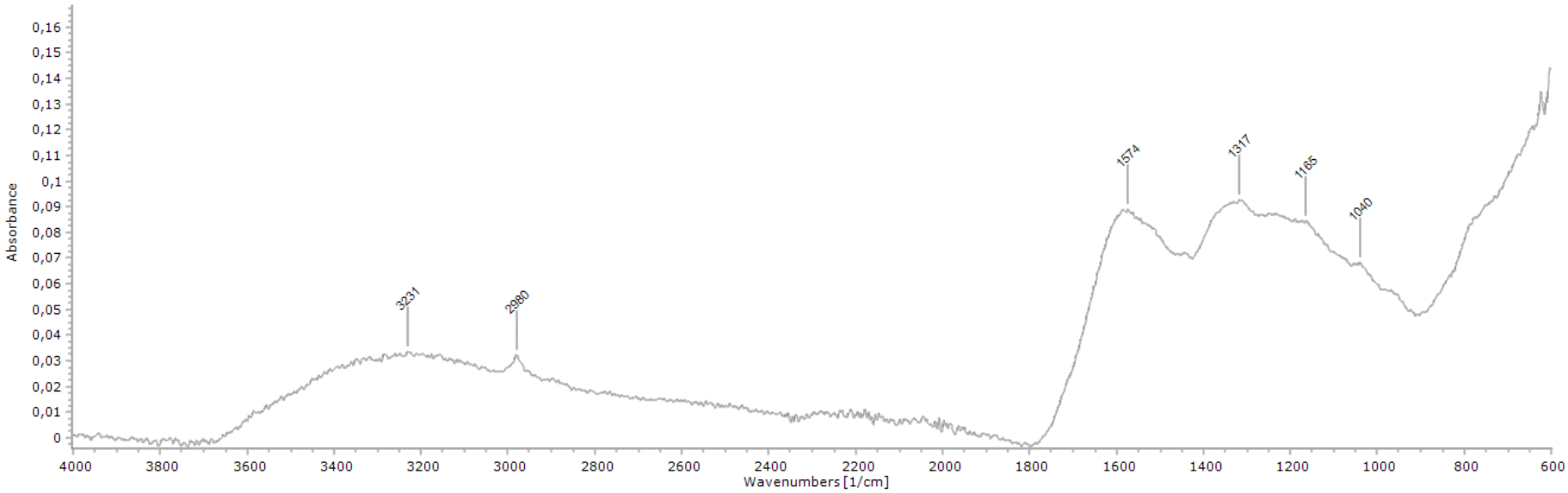

Figure S60: FTIR spectrum of matured sample 7 (100 °C /100 bar).

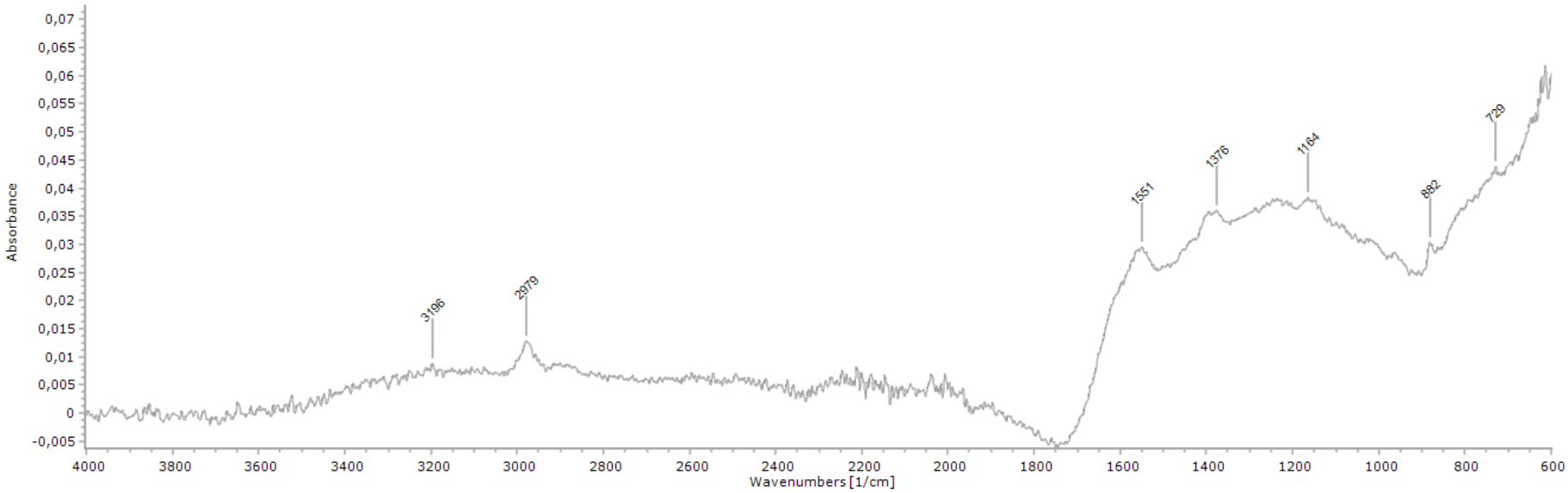

Figure S61: FTIR spectrum of matured sample 8 (300 °C/300 bar).

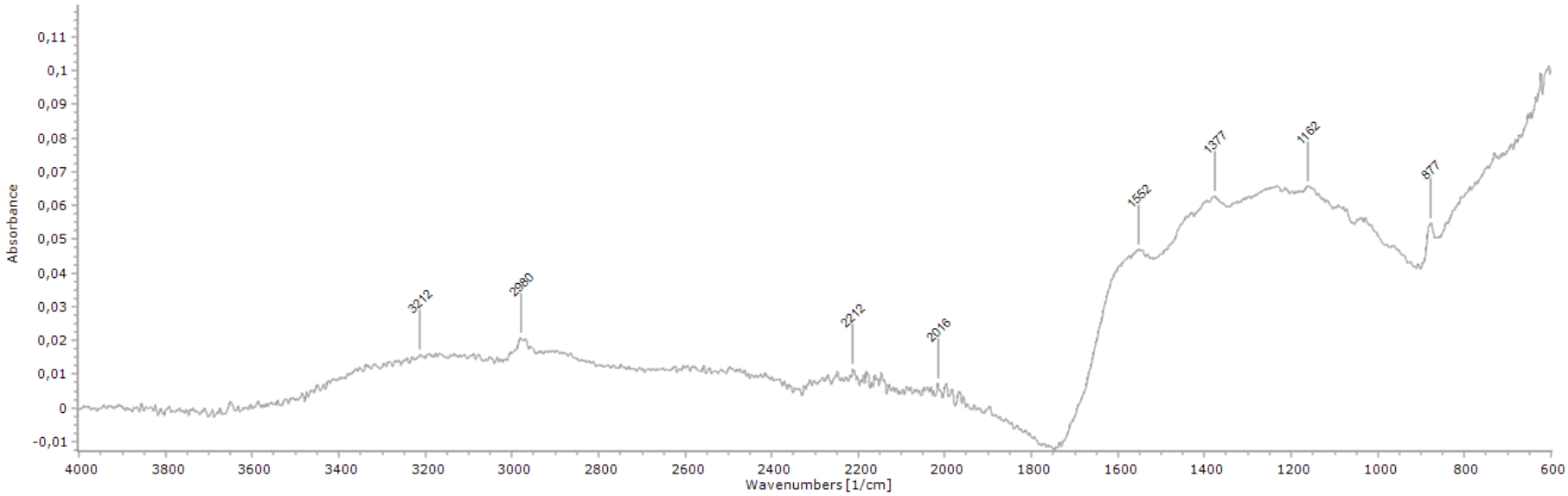

Figure S62: FTIR spectrum of matured sample 10 (300 °C/300 bar).

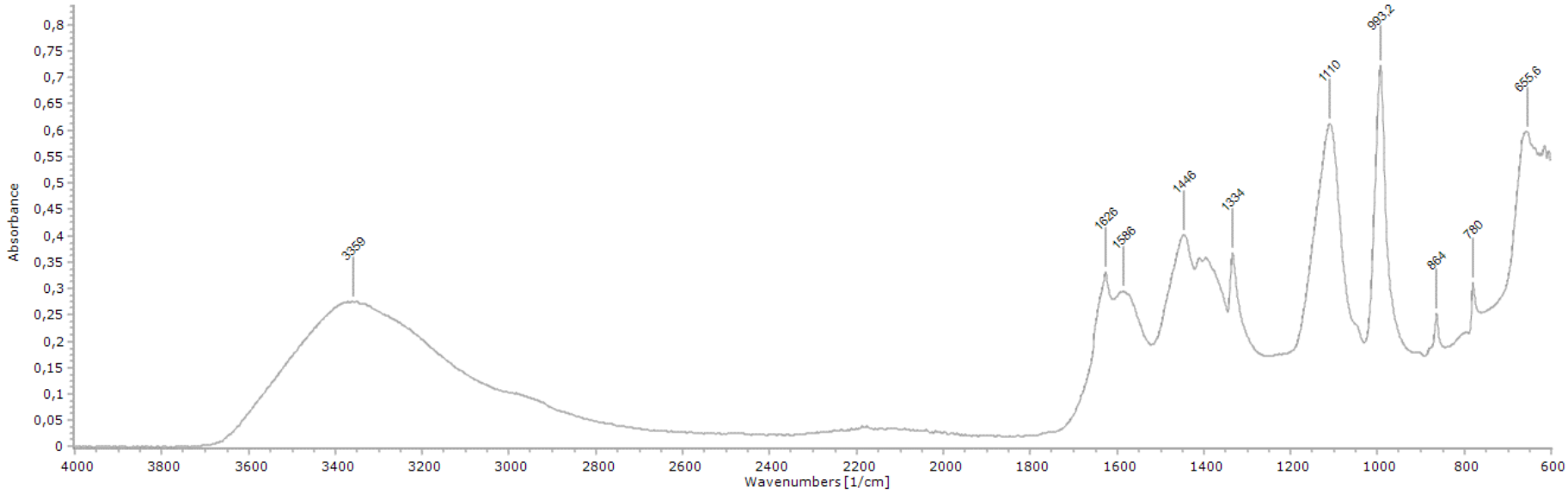

Figure S63: FTIR spectrum of matured sample 11 (100 °C/100 bar with sodium sulfide ($Na_2S.xH_2O$)).

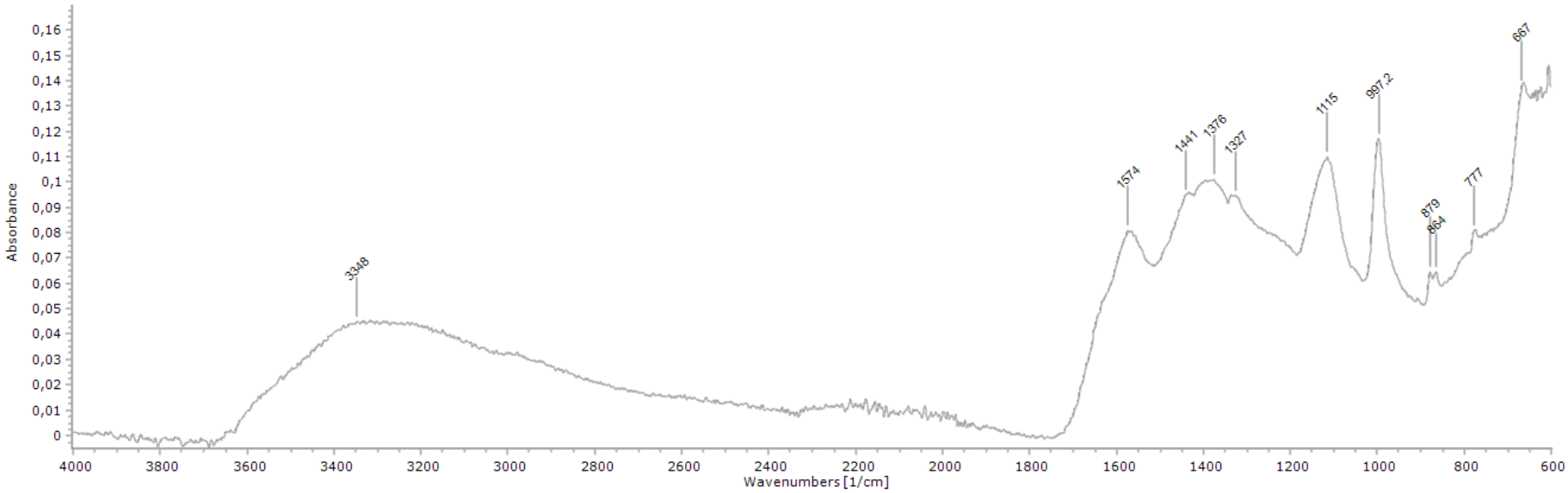

Figure S64: FTIR spectrum of matured sample 12 (100 °C/100 bar with sodium sulfide ($Na_2S.xH_2O$)).

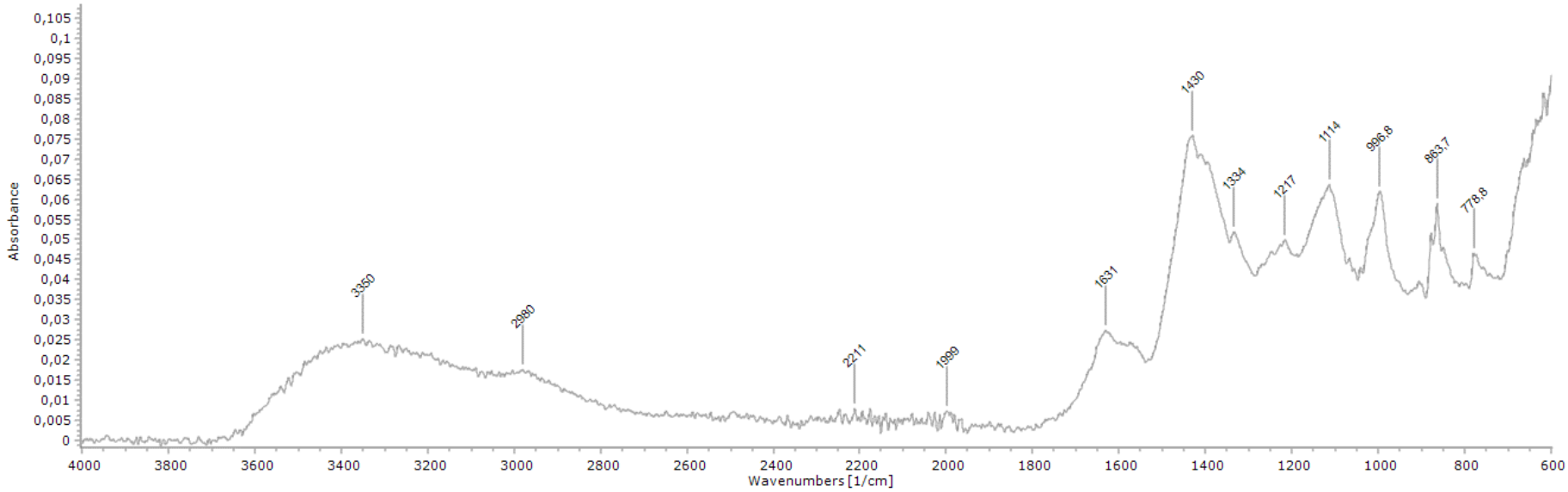

Figure S65: FTIR spectrum of matured sample 13 (200 °C/200bar with $Na_2S.xH_2O$)).

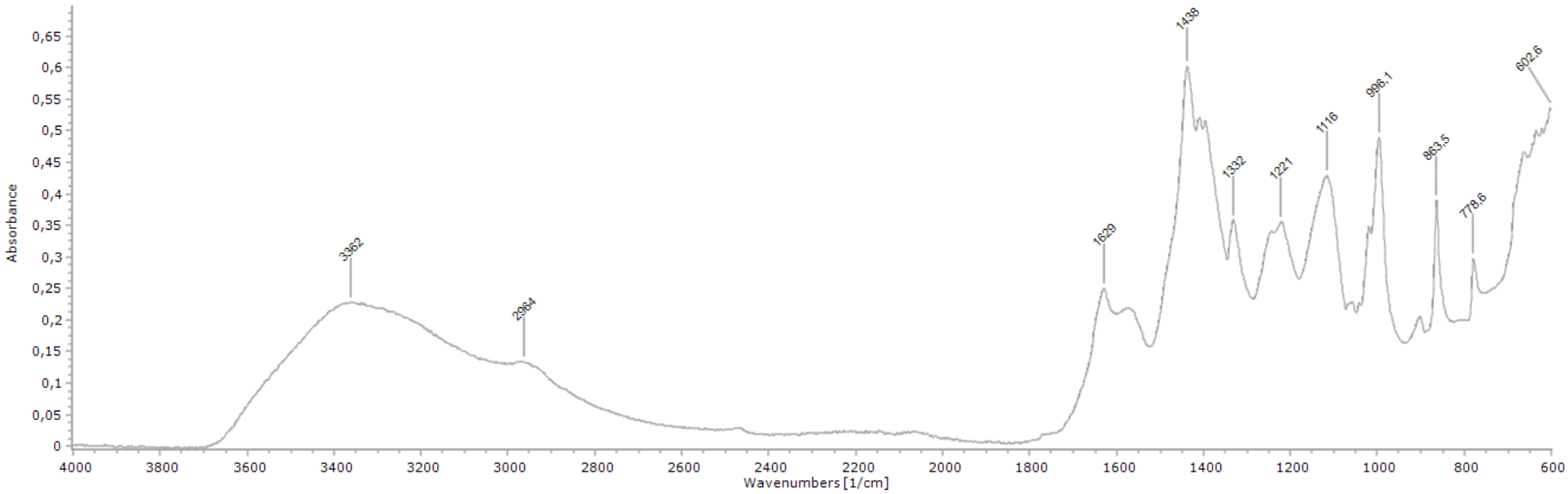

Figure S66: FTIR spectrum of matured sample 14 (200 °C/200bar with $Na_2S.xH_2O$)).

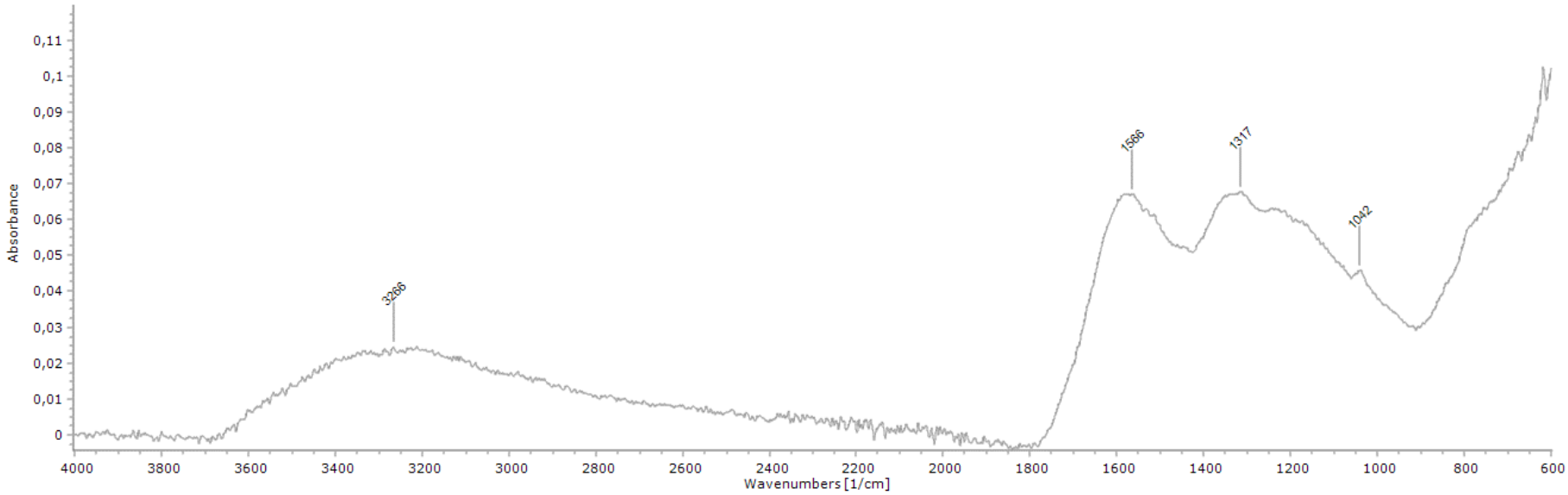

Figure S67: FTIR spectrum of matured sample 17 (100 °C /100 bar).

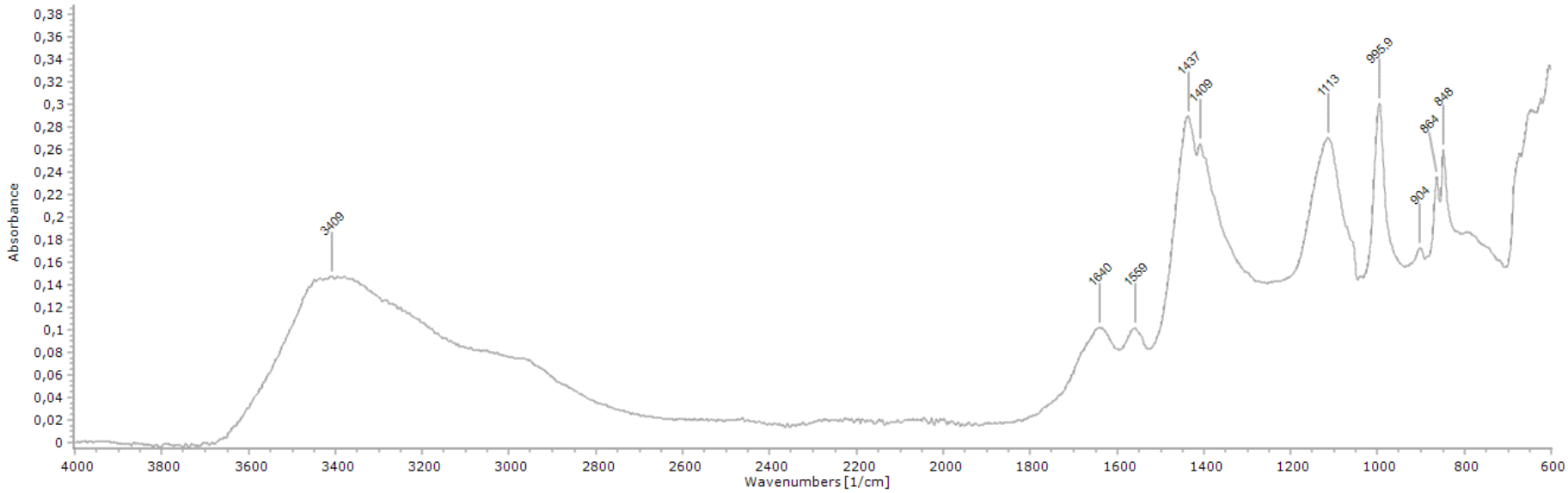

Figure S68: FTIR spectrum of matured sample 18 (300 °C /300 bar with sodium sulfide ($Na_2S.xH_2O$)).

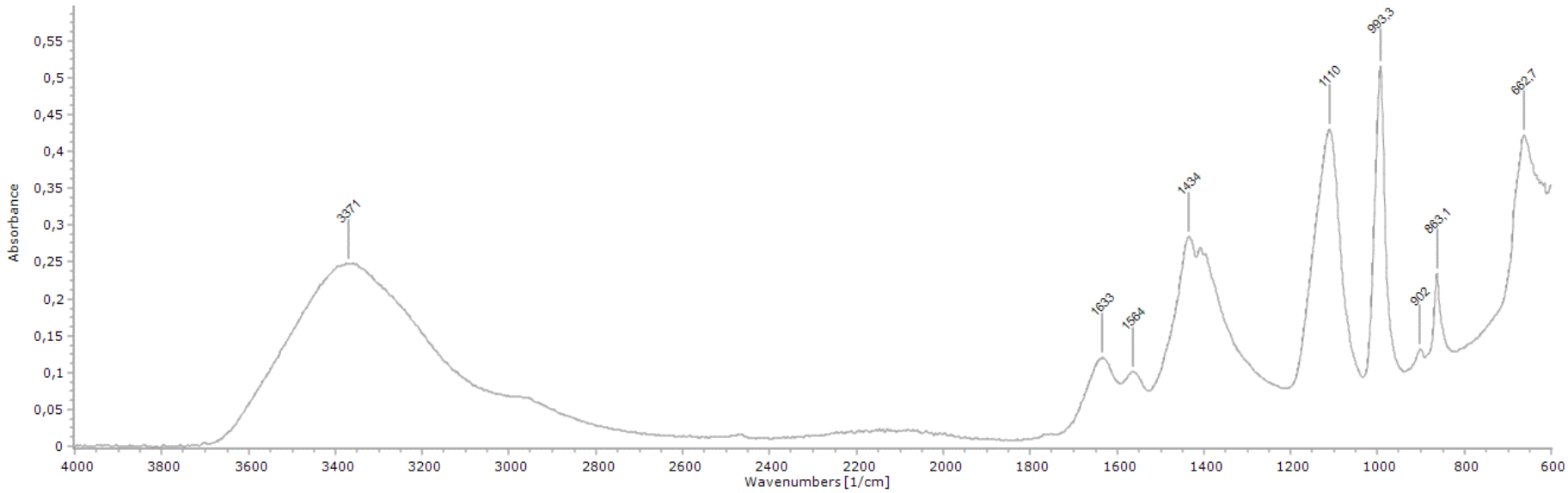

Figure S69: FTIR spectrum of matured sample 19 (300 ºC/300 bar with sodium sulfide ($Na_2S.xH_2O$)).

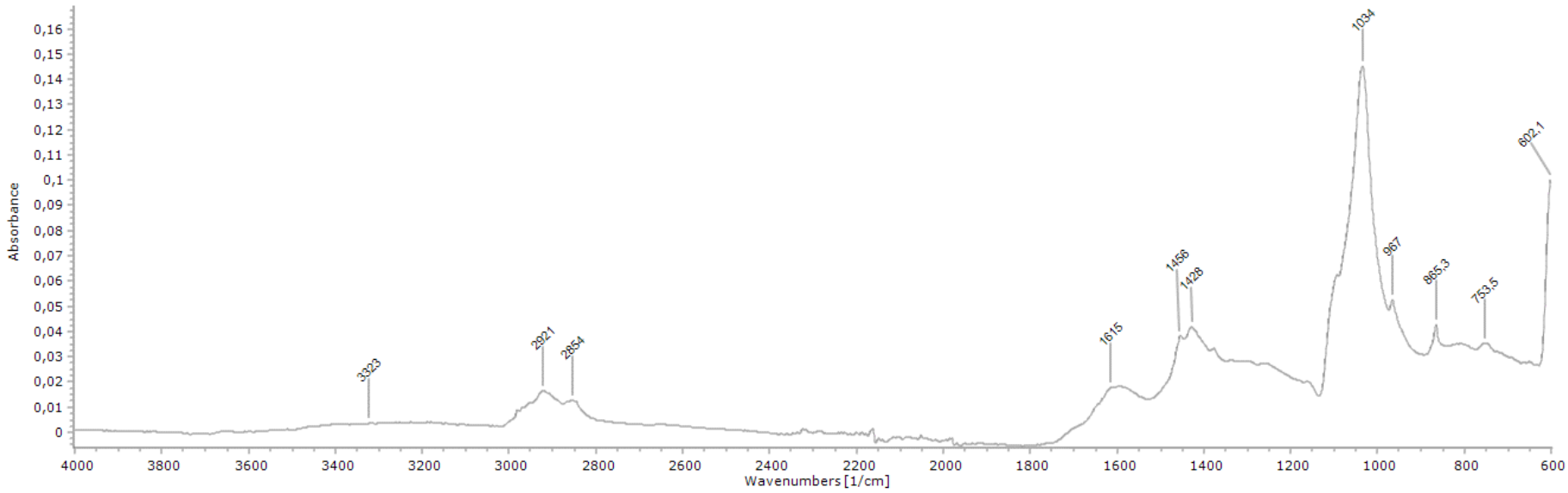

Figure S70: FTIR spectrum of fossil sample YPM 221211.

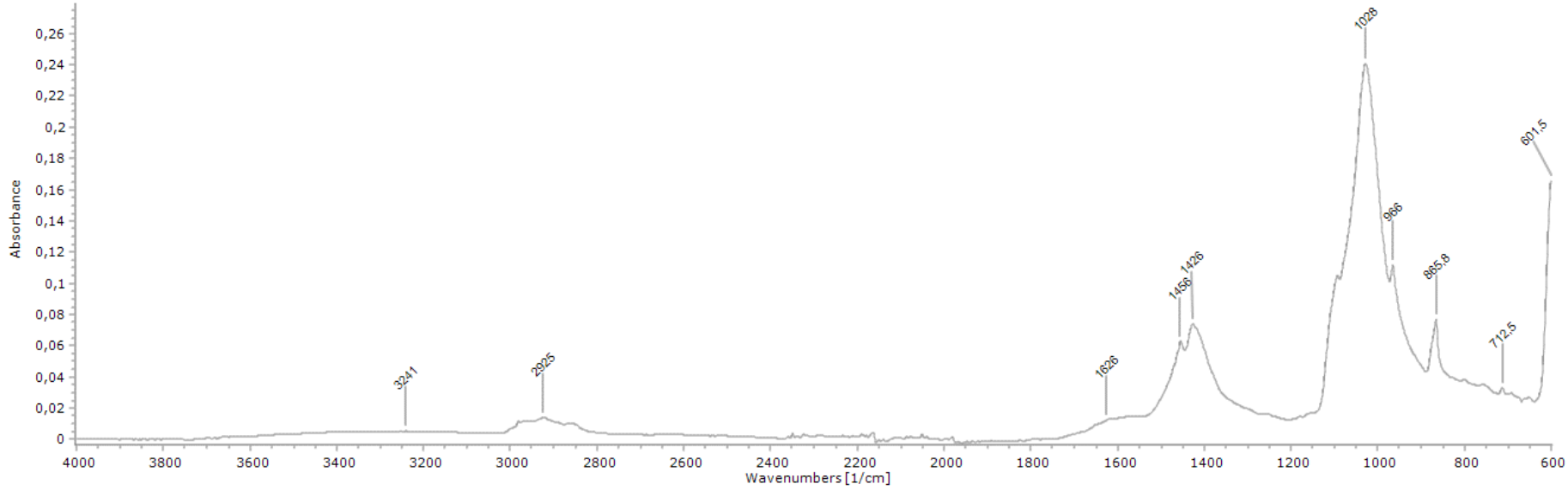

Figure S71: FTIR spectrum of fossil sample YPM 221213.

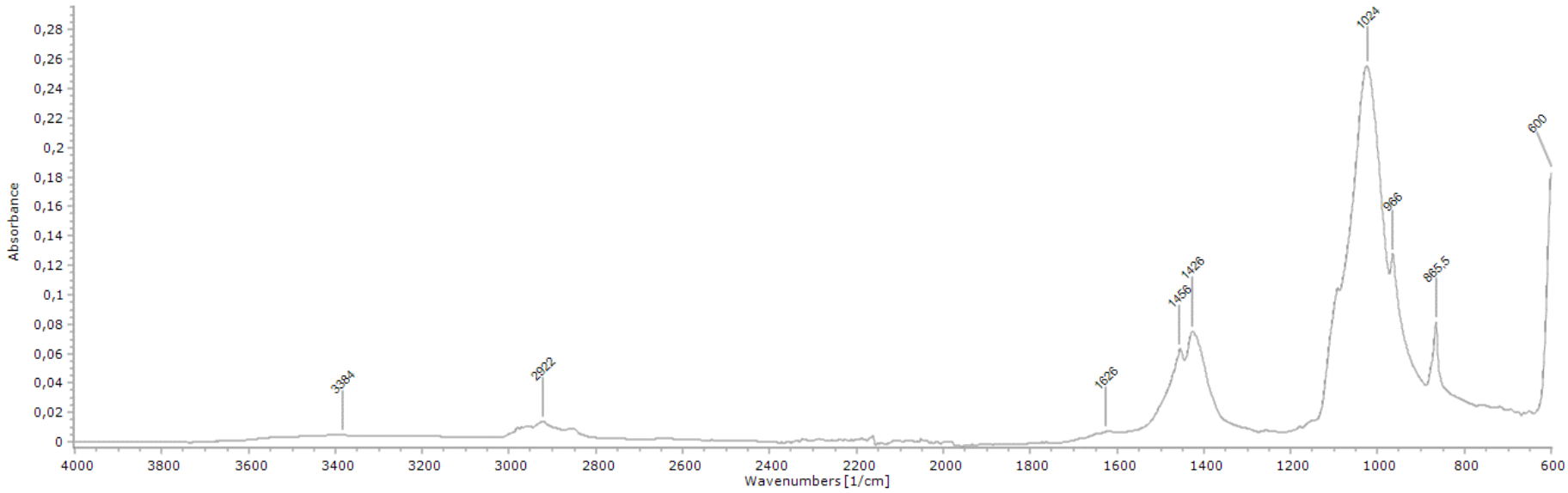

Figure S72: FTIR spectrum of fossil sample YPM 221214.

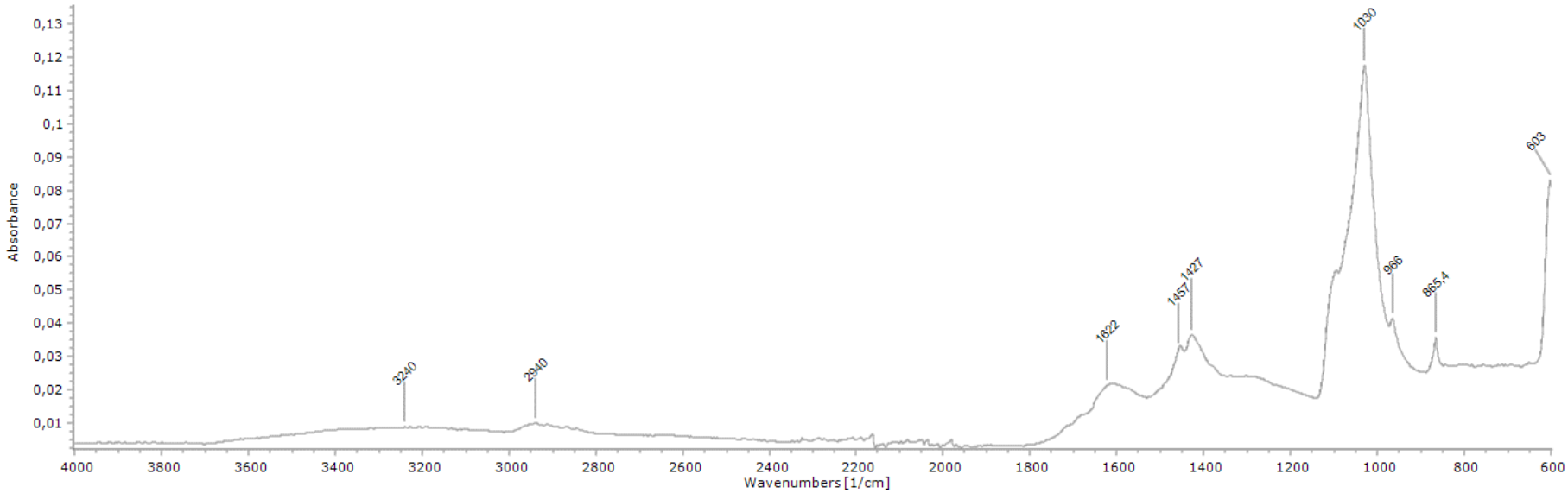

Figure S73: FTIR spectrum of fossil sample K2.

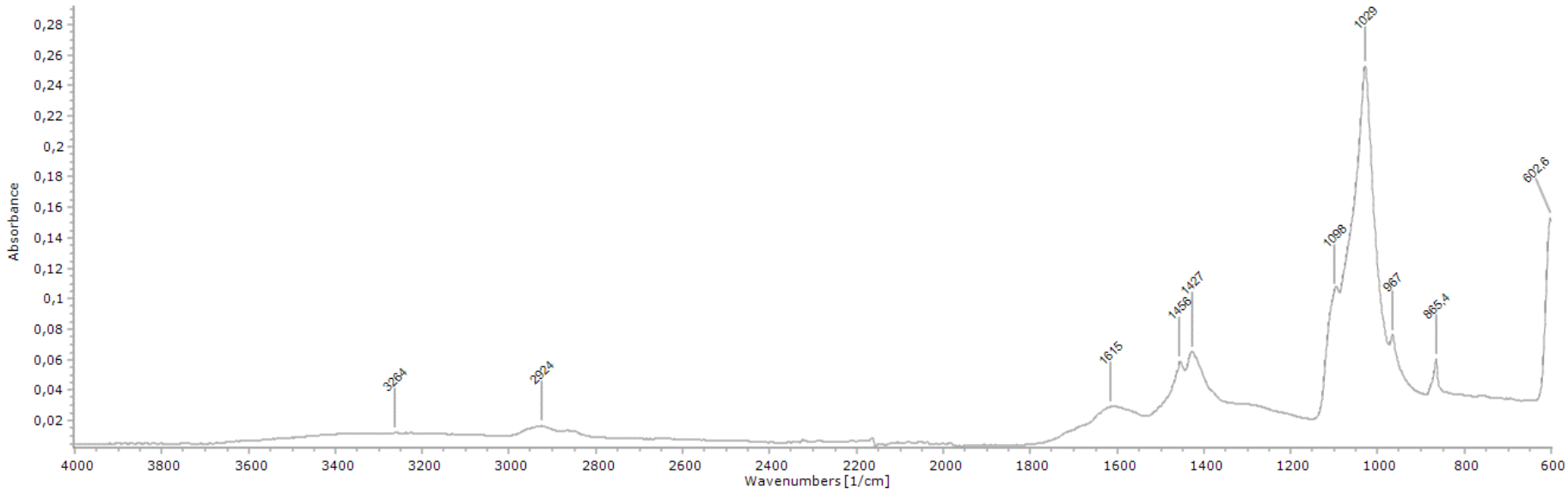

Figure S74: FTIR spectrum of fossil sample K1987.

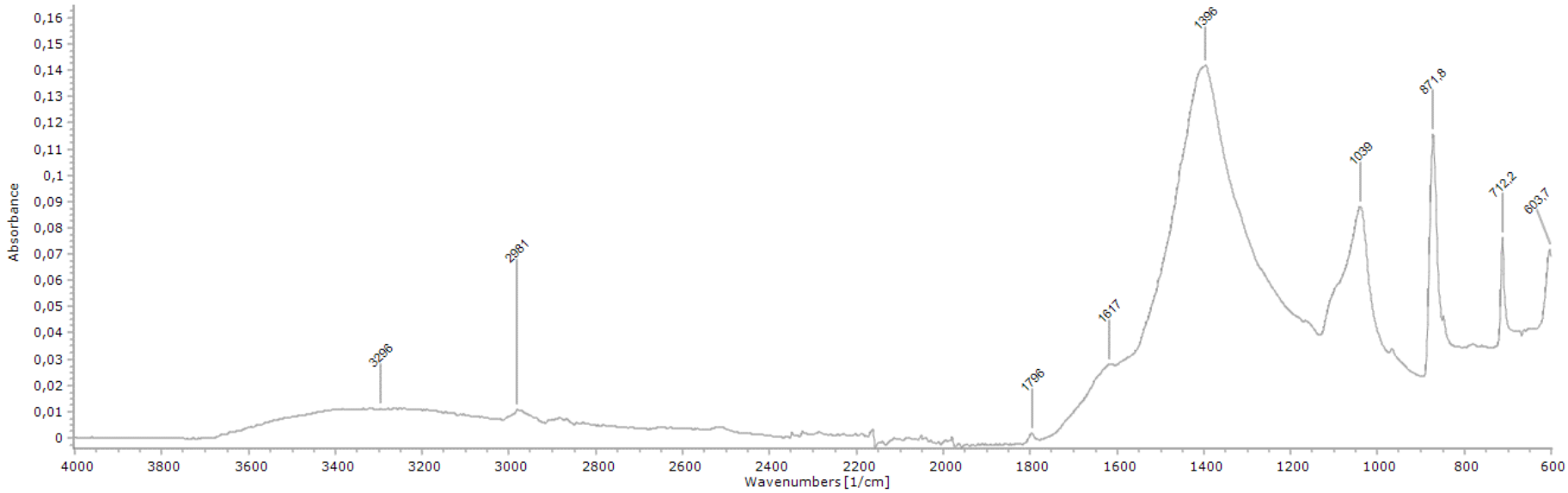

Figure S75: FTIR spectrum of fossil sample LR1.

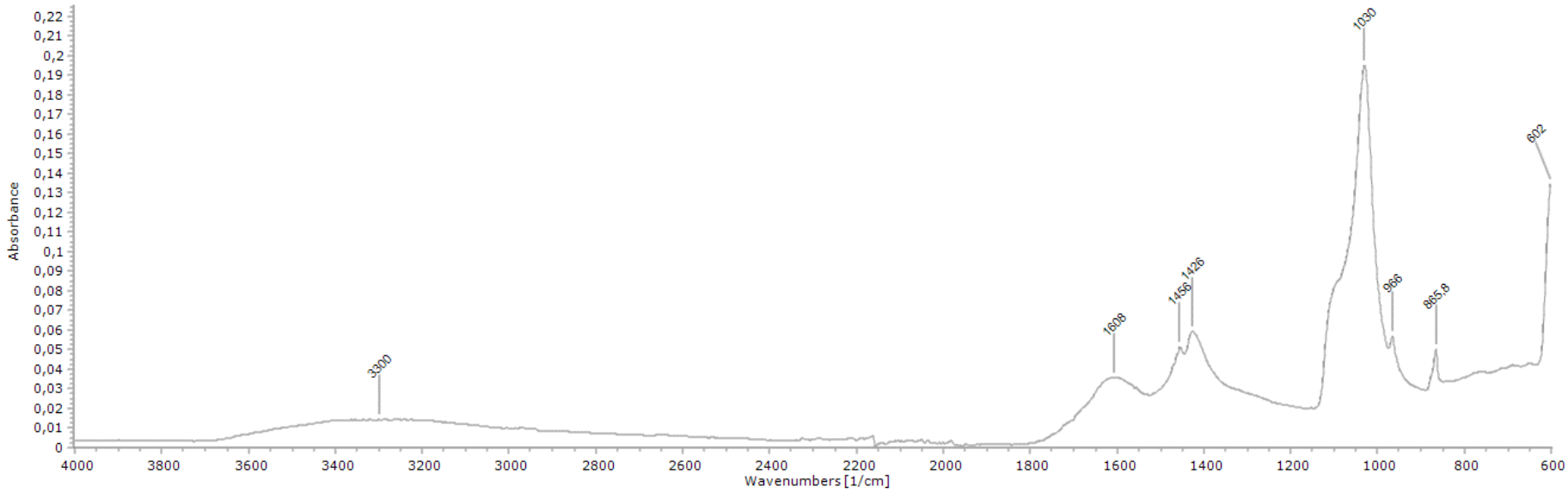

Figure S76: FTIR spectrum of fossil sample LR2.

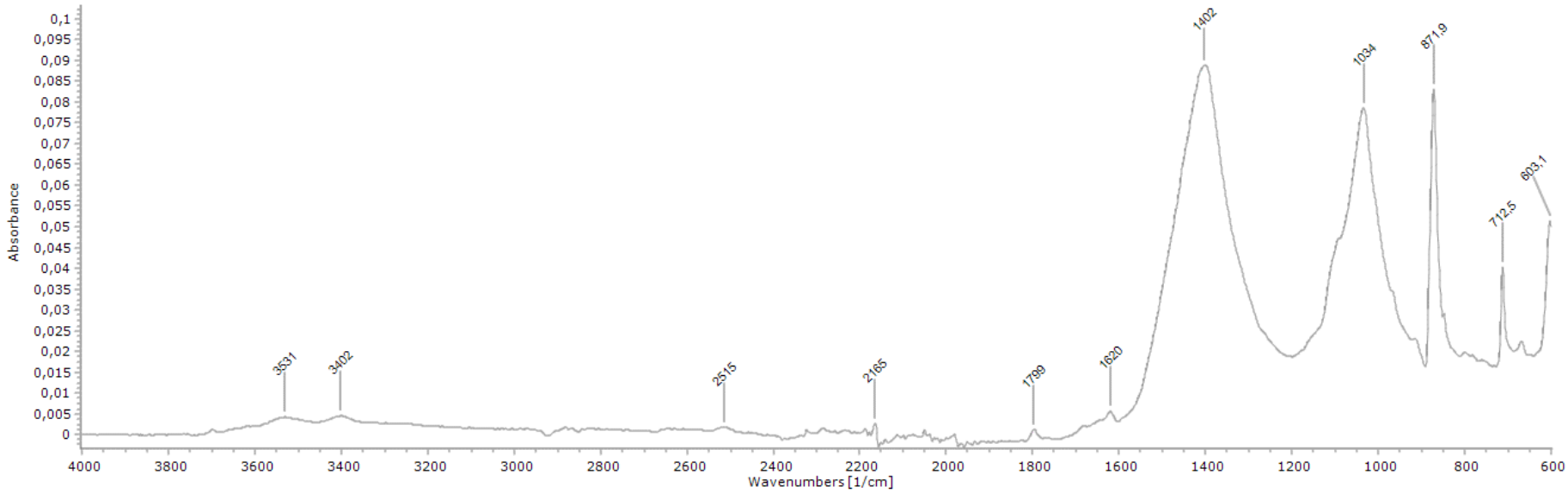

Figure S77: FTIR spectra of fossil sample LR3b.

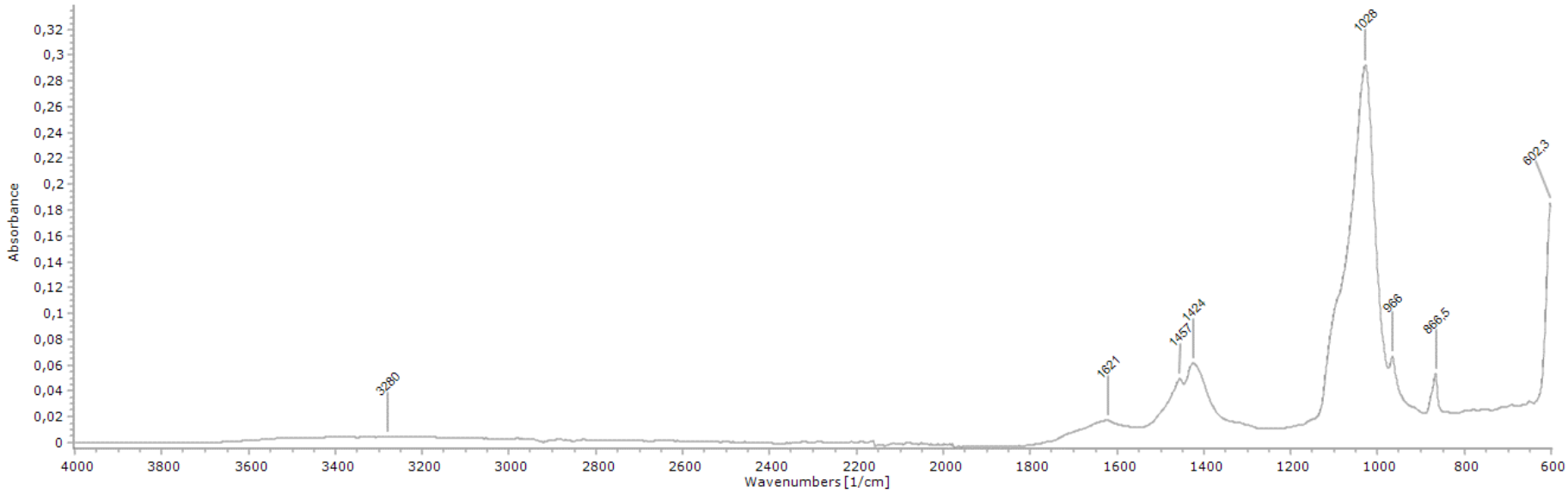

Figure S78: FTIR spectrum of fossil sample LR4.

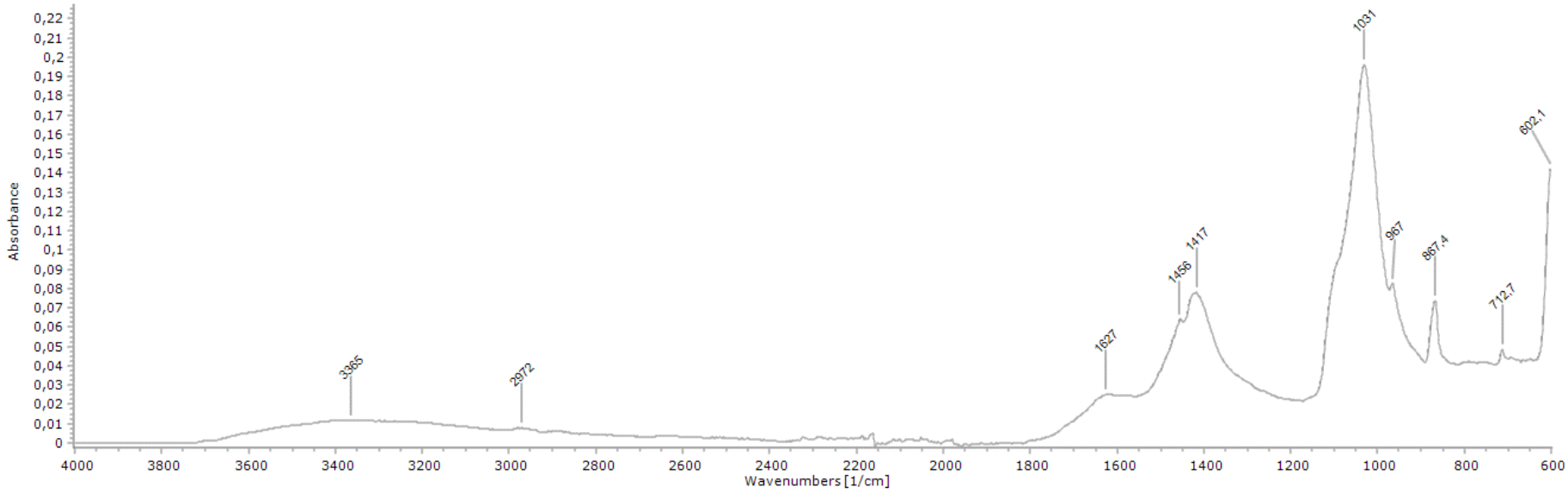

Figure S79: FTIR spectrum of fossil sample LR5.

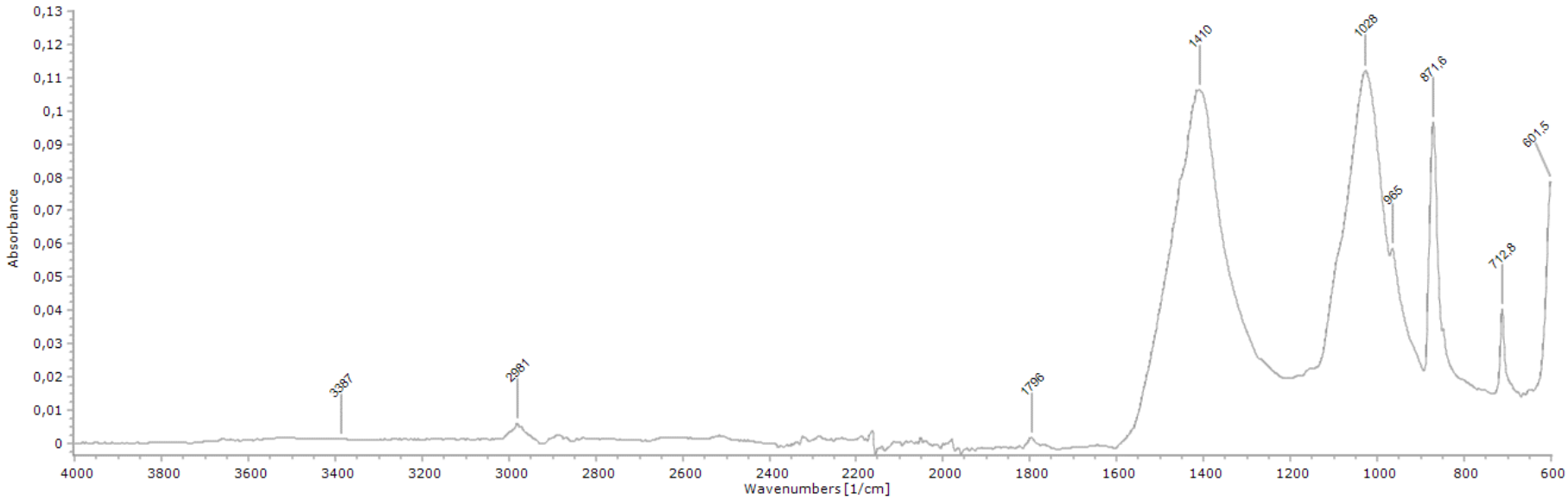

Figure S80: FTIR spectrum of fossil sample LR6.

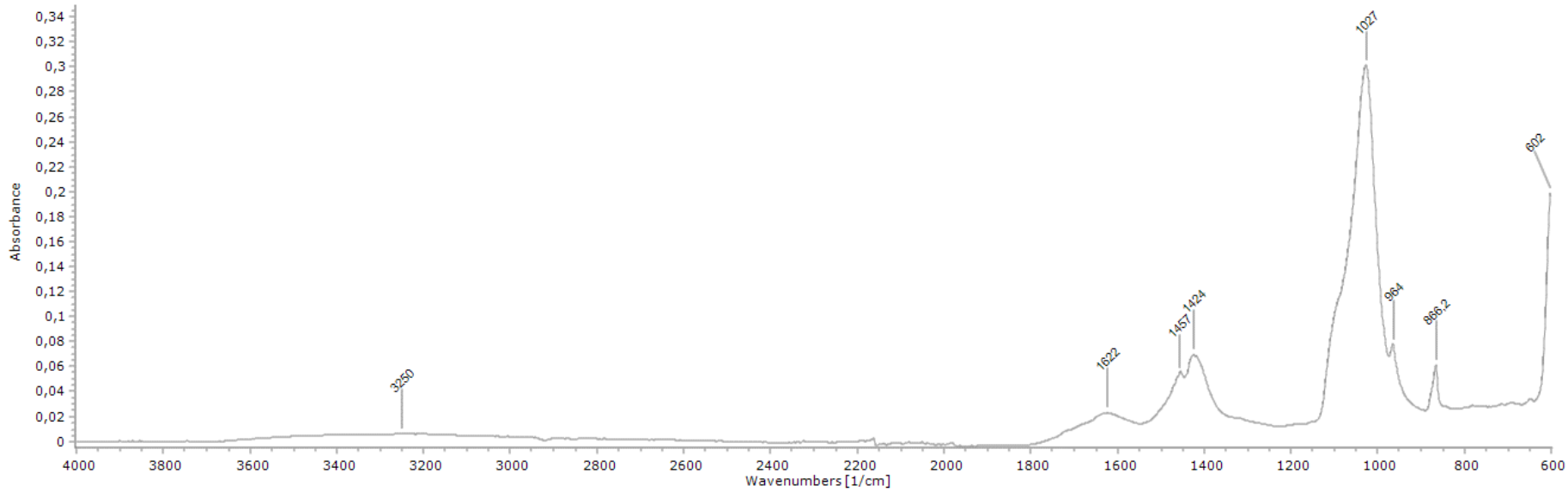

Figure S81: FTIR spectrum of fossil sample LR7.

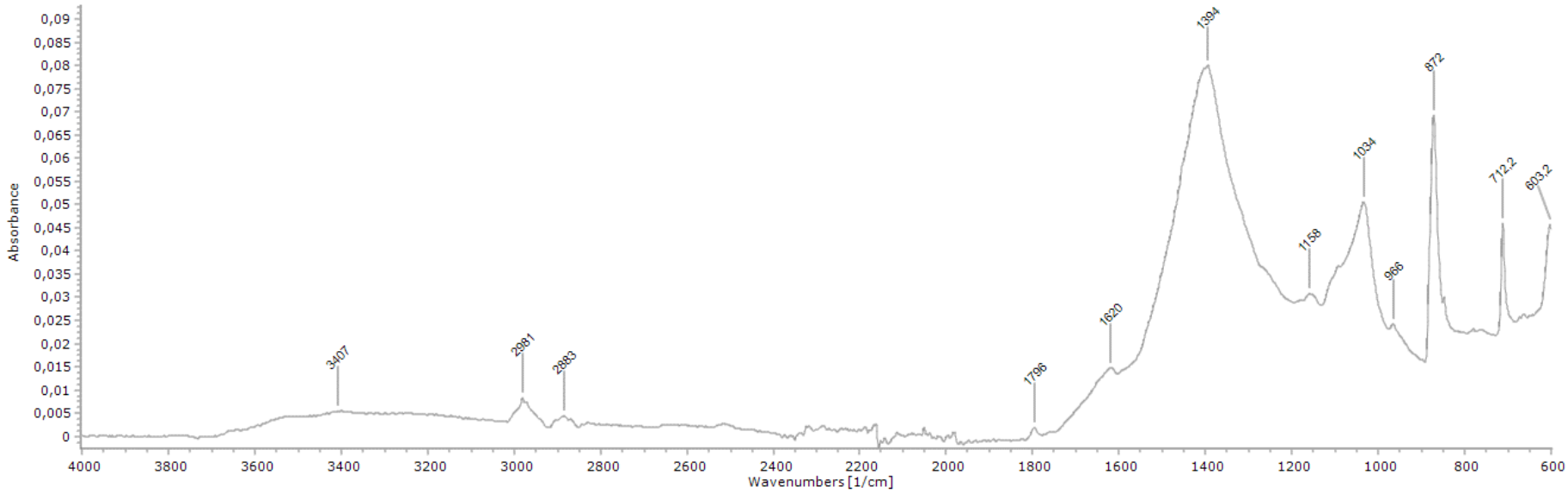

Figure S82: FTIR spectrum of fossil sample LR9.

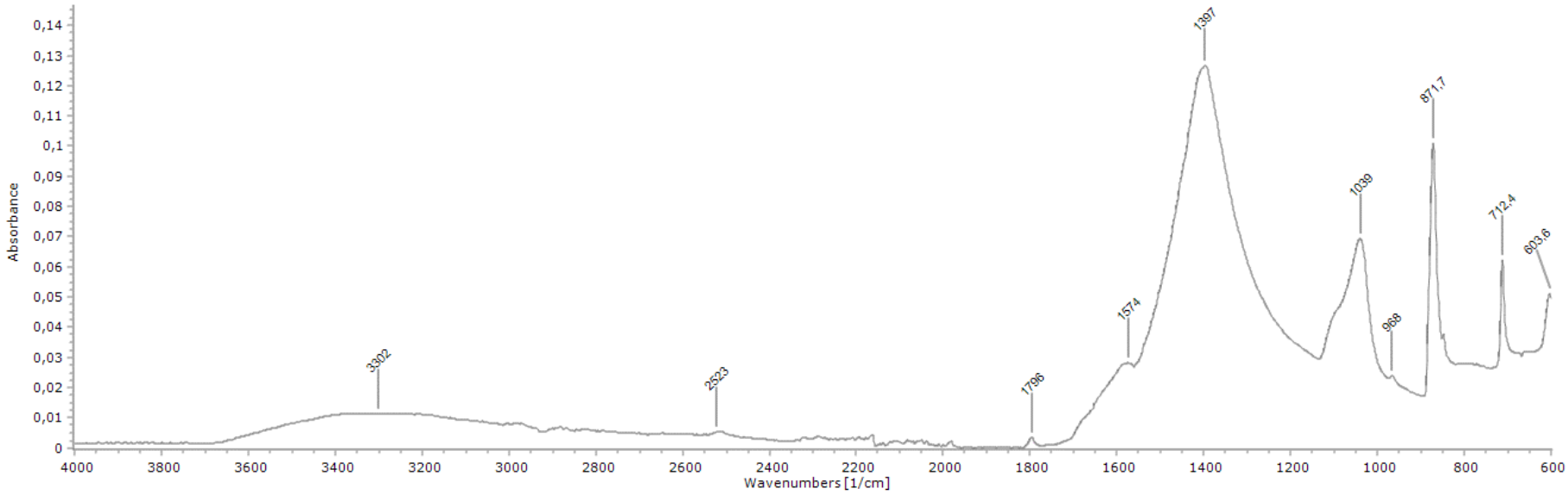

Figure S83: FTIR spectrum of fossil sample BRLSI M1224A.

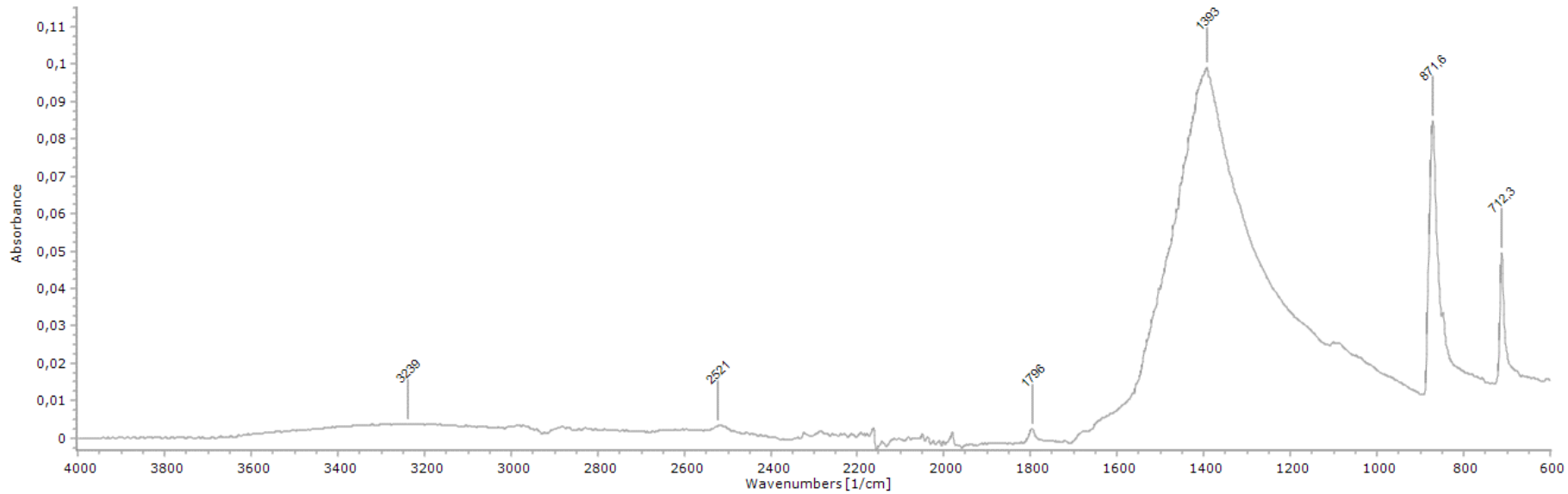

Figure S84: FTIR spectrum of fossil sample BRLSI M1227A.

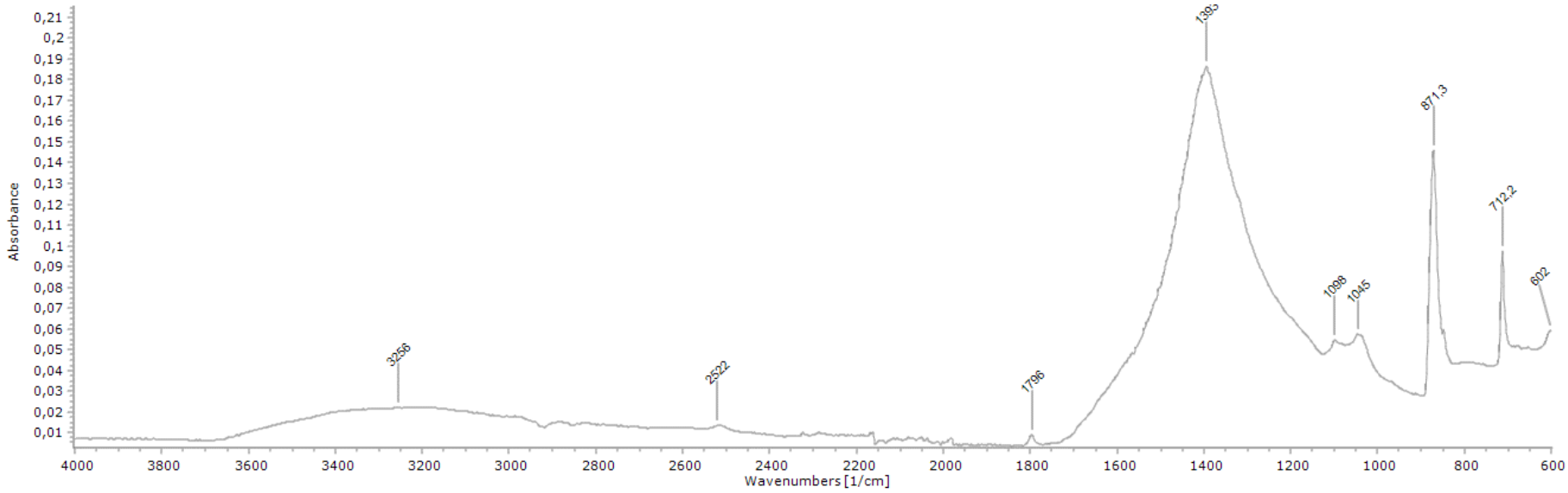

Figure S85: FTIR spectrum of fossil sample BRLSI M1228.

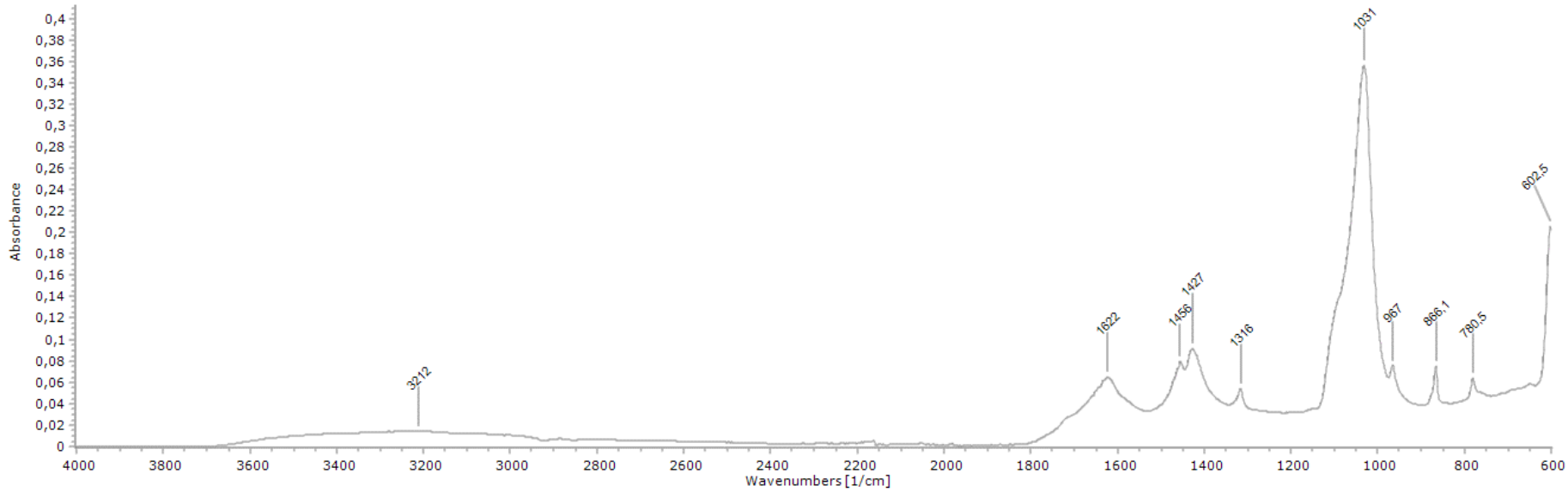

Figure S86: FTIR spectrum of fossil sample BRLSI M1235A.

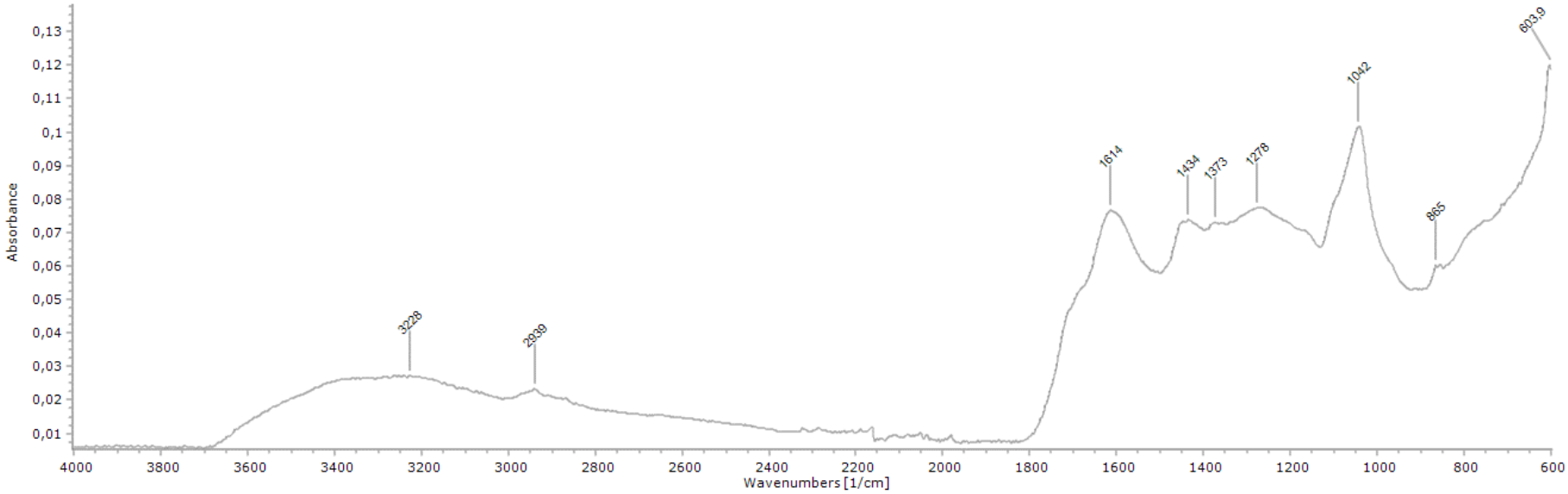

Figure S87: FTIR spectrum of fossil sample PRW 682.

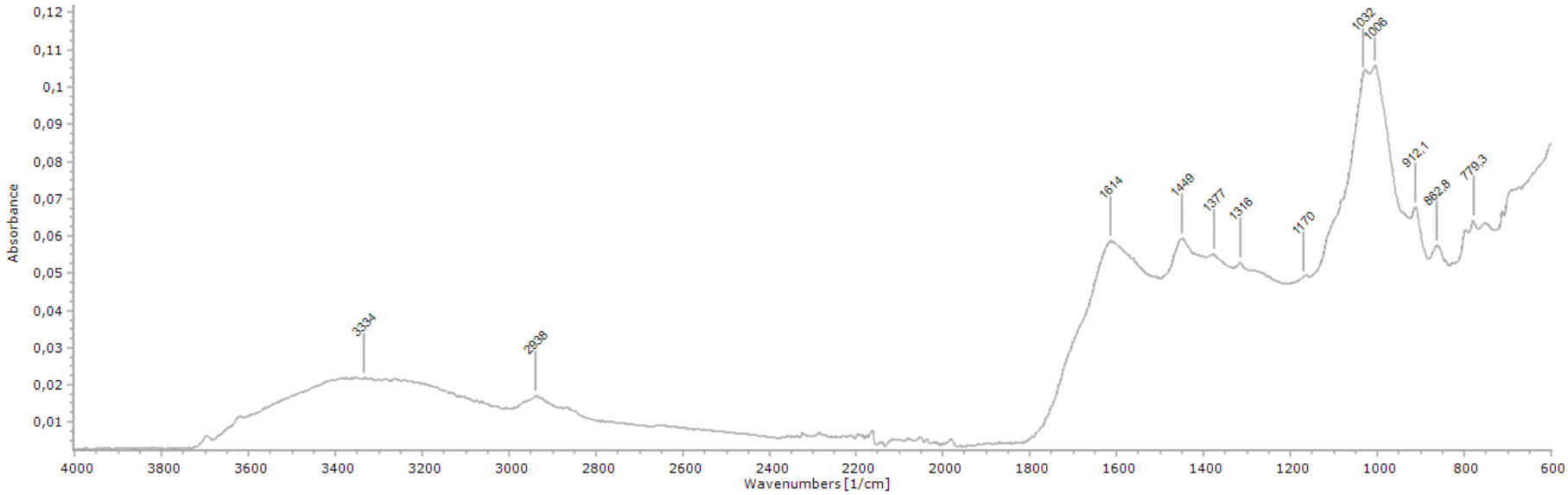

Figure S88: FTIR spectrum of fossil sample PRW 220.

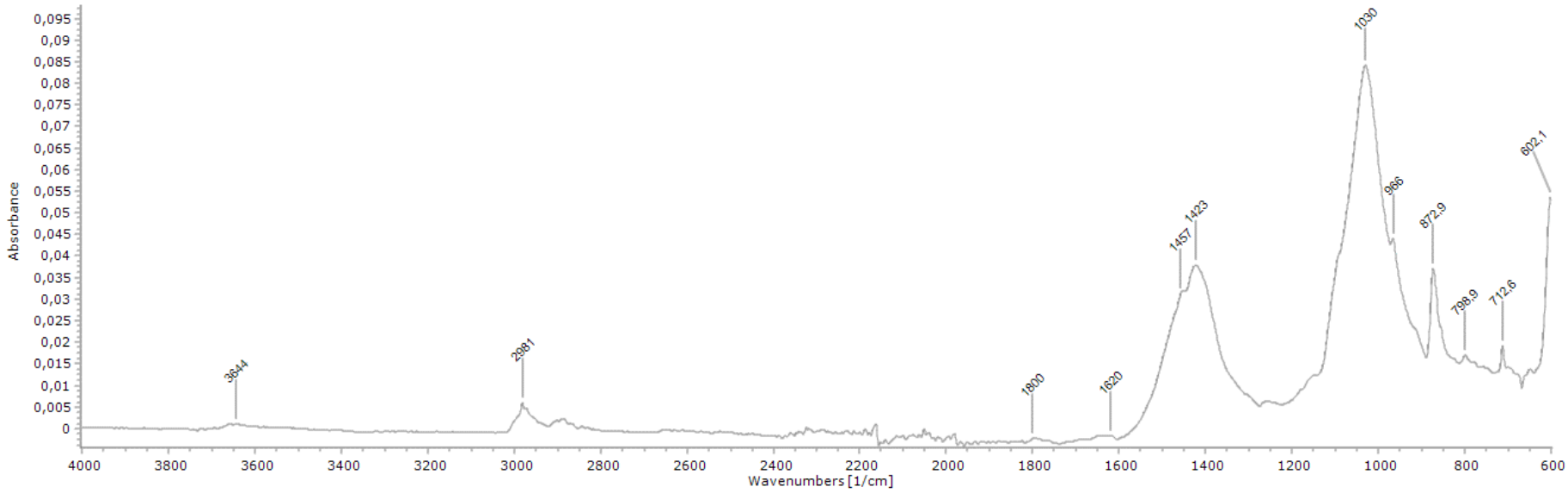

Figure S89: FTIR spectrum of fossil sample SOM1.

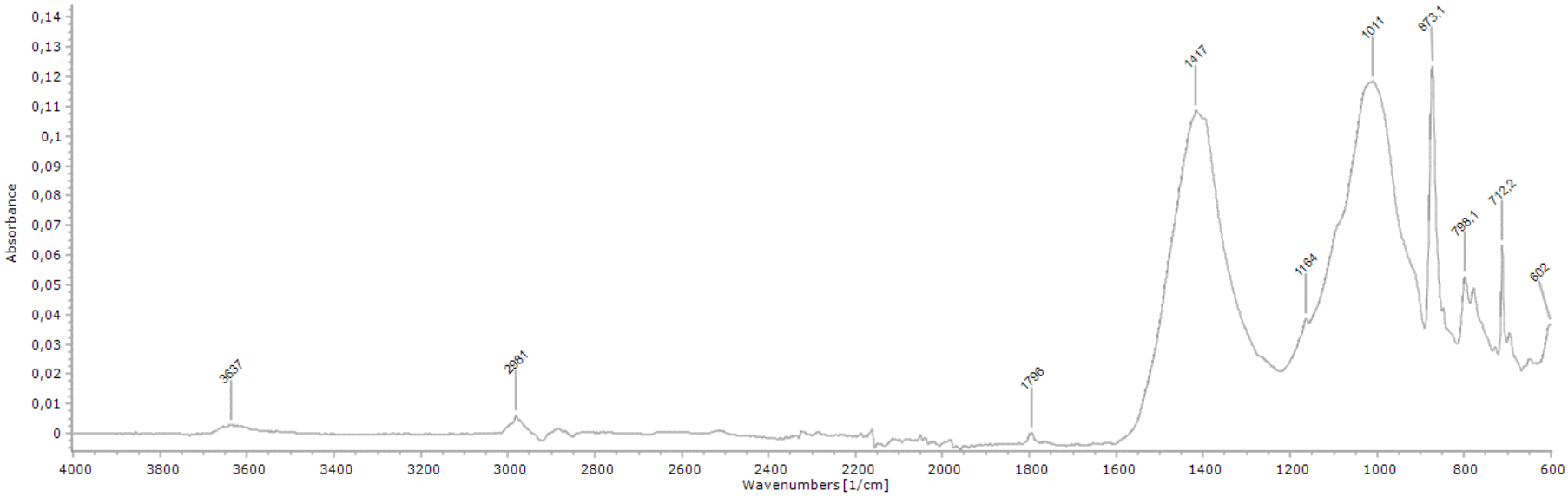

Figure S90: FTIR spectrum of fossil sample TMP 2013.036.0005

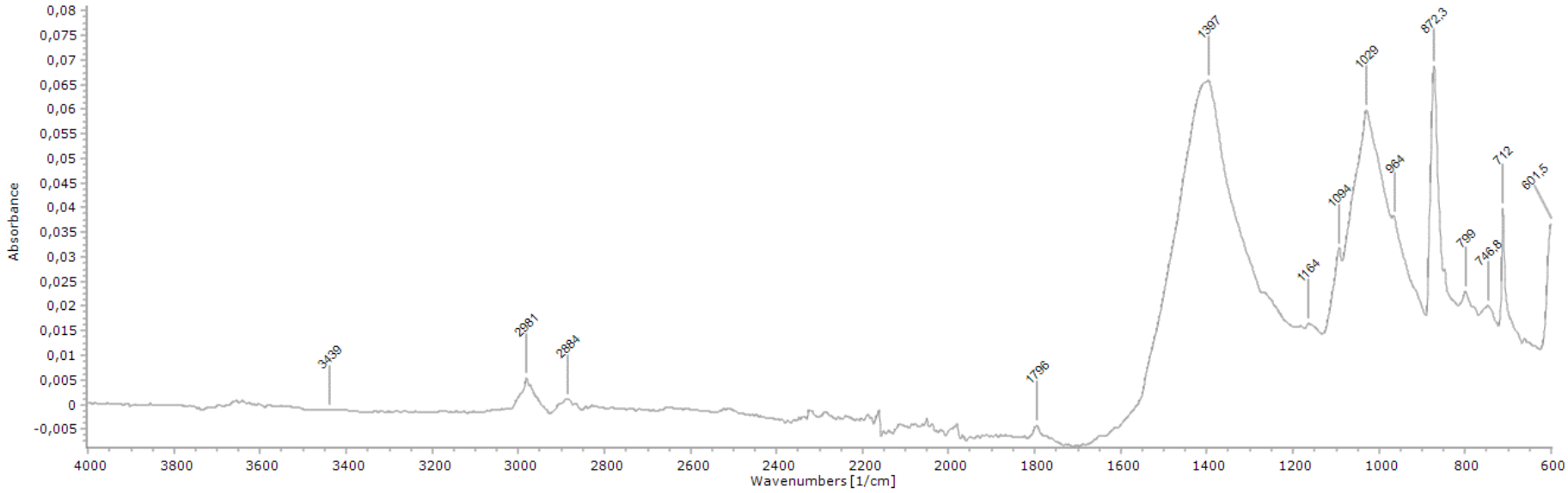

Figure S91: FTIR spectrum of fossil sample TMP 2013.036.0008.

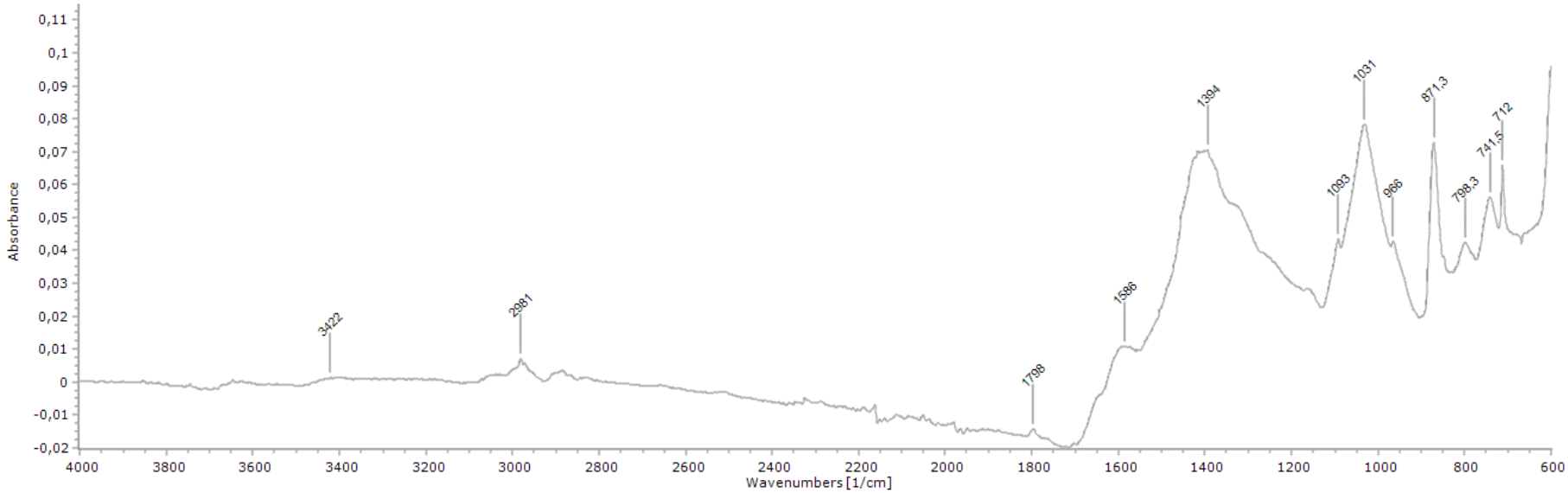

Figure S93: FTIR spectrum of fossil sample TMP2014.021.0059.

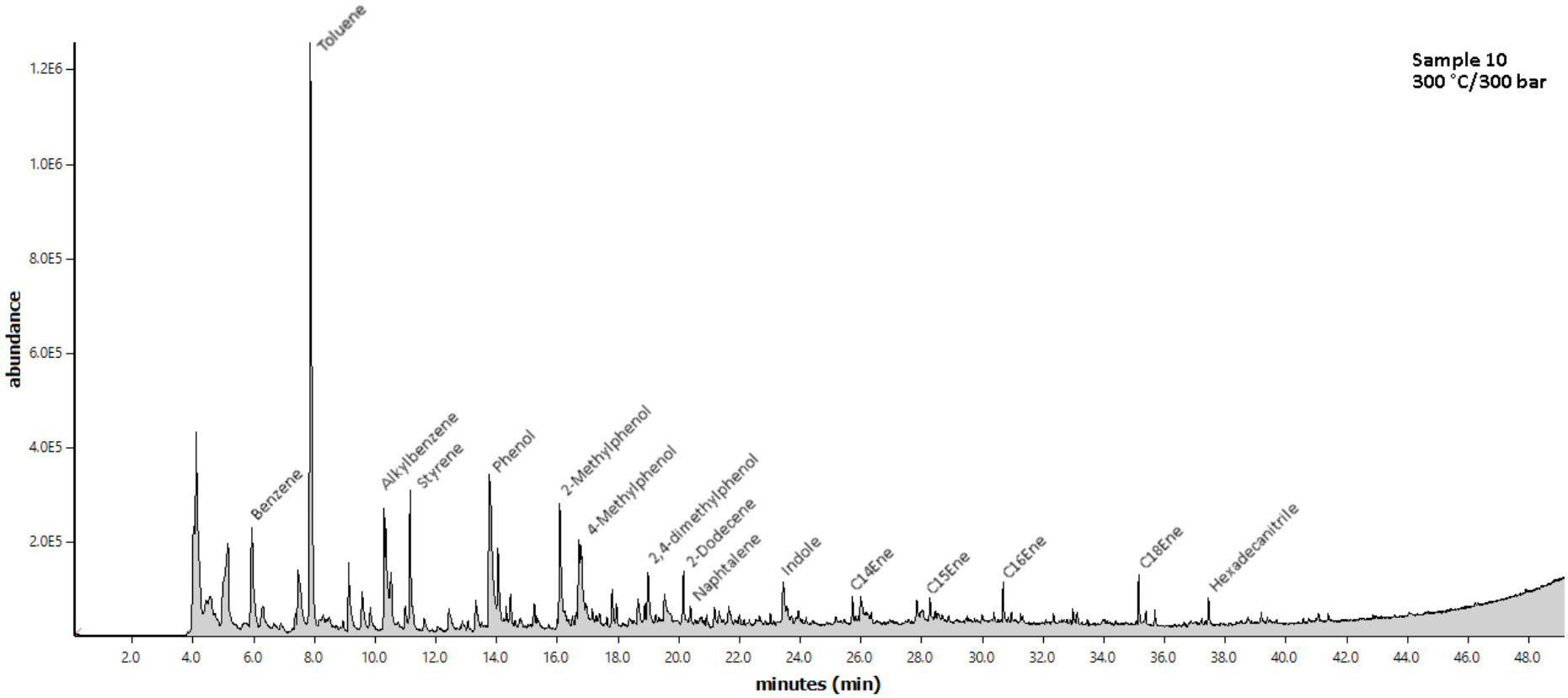

Figure S94: Py-GC/MS chromatogram of sample 10 (300 °C/300 bar) with major pyrolysis products identified.

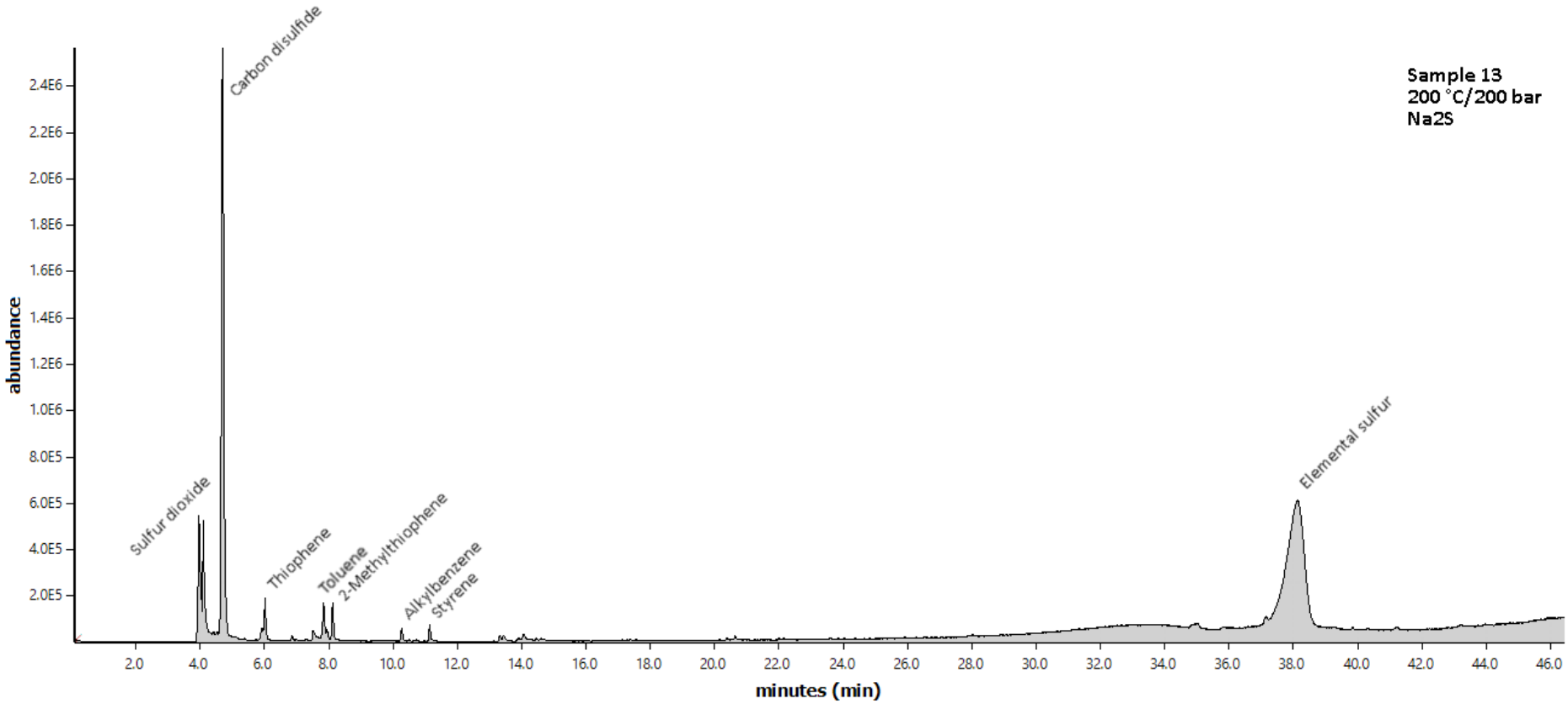

Figure S95: Py-GC/MS chromatogram of sample 13 (200 °C/200 bar with $Na_2S.xH_2O$) with major pyrolysis products identified. Sample was not cleaned before analysis.

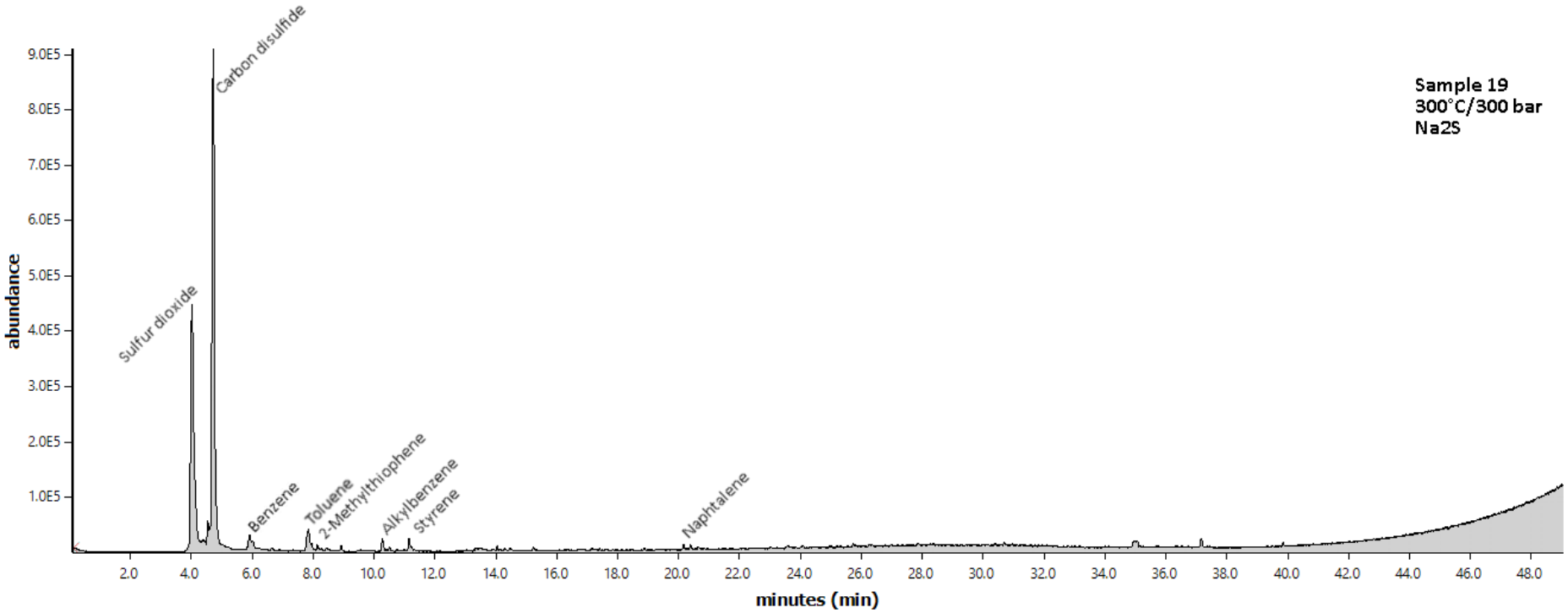

Figure S96: Py-GC/MS chromatogram of sample 19 (300 °C/300 bar with $Na_2S.xH_2O$) with major pyrolysis products identified. Sample was not cleaned before analysis.

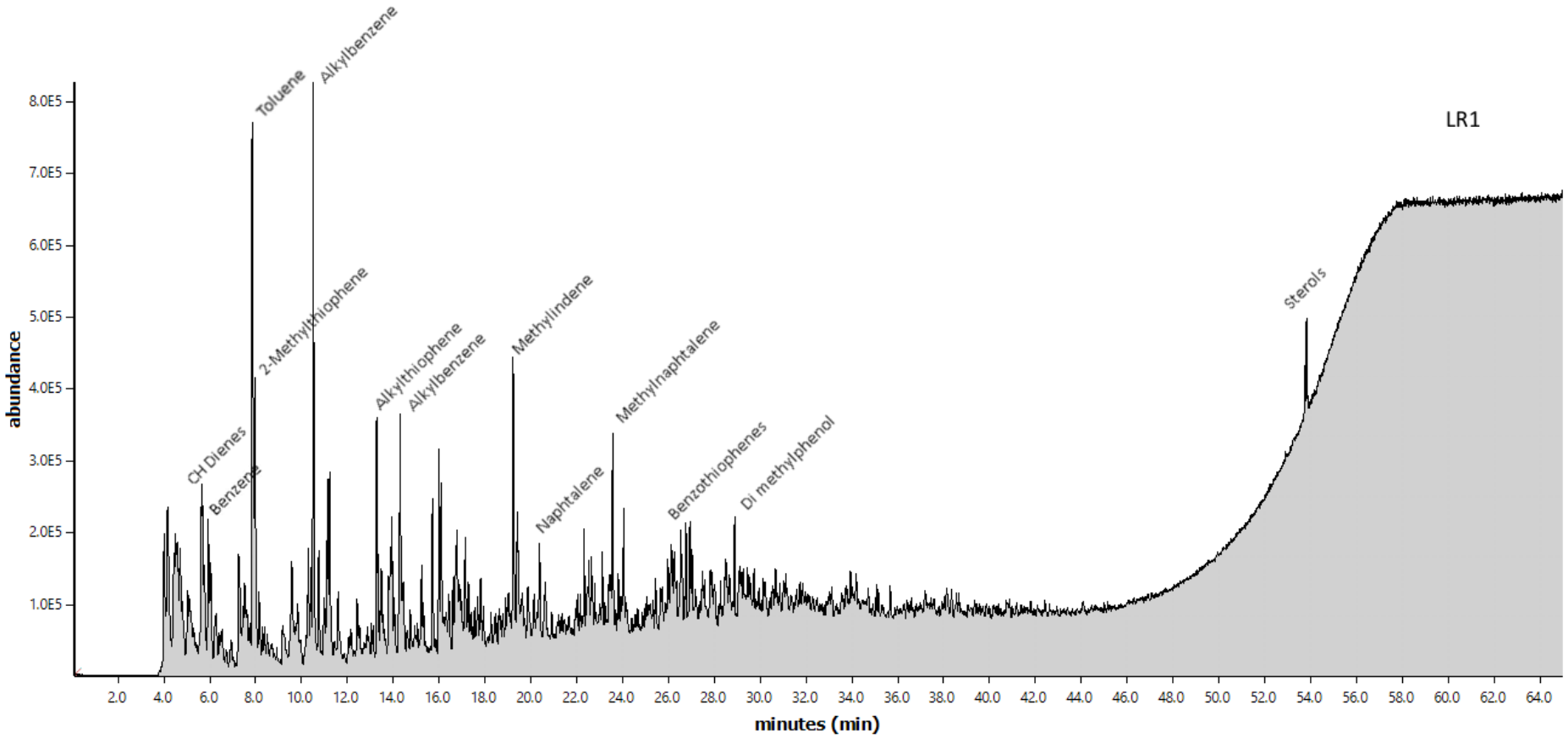

Figure S97: Py-GC/MS chromatogram of fossil sample LR1 with major pyrolysis products identified.

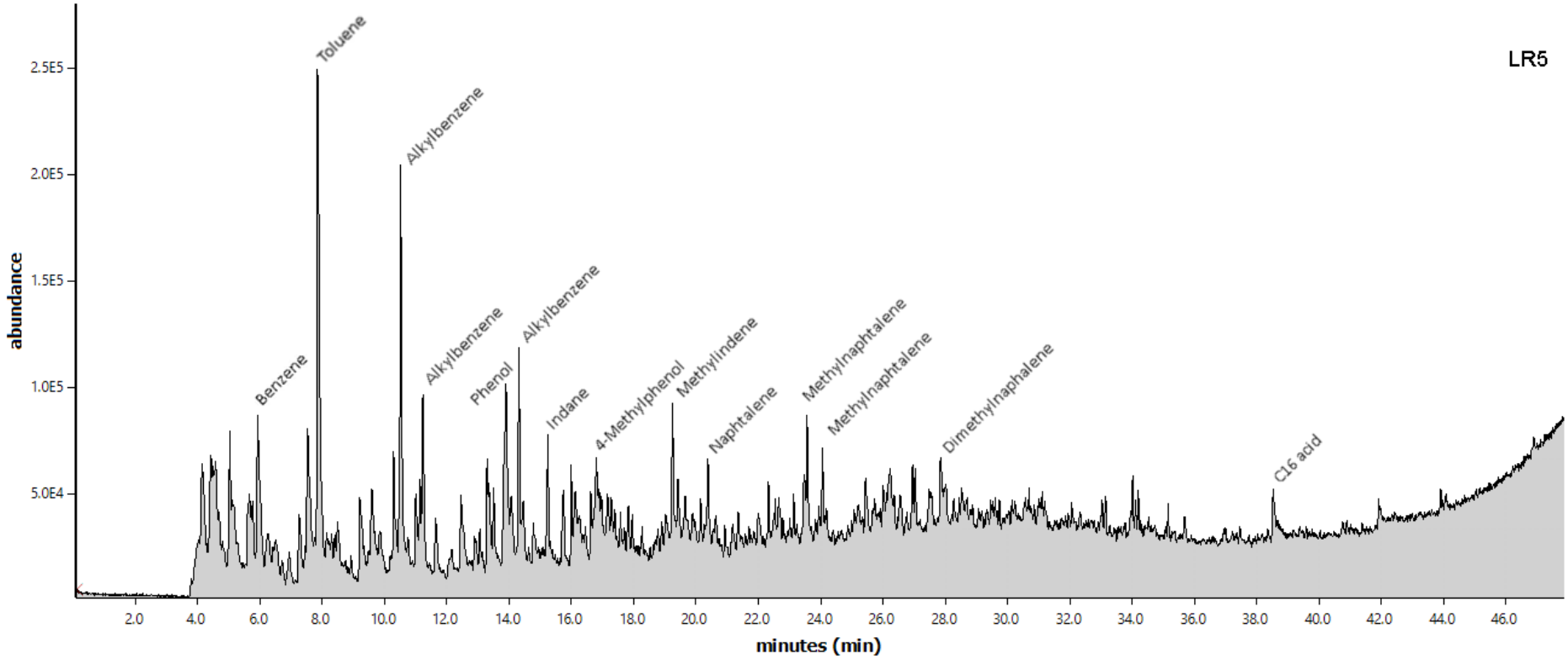

Figure S98: Py-GC/MS chromatogram of fossil sample LR5 with major pyrolysis products identified.